Joana Sofia Campos Figueiredo

Smart Wearable Orthosis to Assist

Impaired Human Walking

Smart Wearable Orthosis to Assist
Impaired Human Walking

Joana Sofia Campos Figueiredo

UMinho | 2019

julho de 2019

Universidade do Minho

Escola de Engenharia

Joana Sofia Campos Figueiredo

Smart Wearable Orthosis to Assist

Impaired Human Walking

Tese de Doutoramento

Programa Doutoral em Engenharia Biomédica

Trabalho realizado sob a orientação do(a)

Professora Doutora Cristina P. Santos

Universidade do Minho

Doutor Juan C. Moreno

Consejo Superior de Investigaciones Científicas

julho de 2019

DIREITOS DE AUTOR E CONDIÇÕES DE UTILIZAÇÃO DO TRABALHO POR TERCEIROS

Este é um trabalho académico que pode ser utilizado por terceiros desde que respeitadas as regras e boas práticas internacionalmente aceites, no que concerne aos direitos de autor e direitos conexos.

Assim, o presente trabalho pode ser utilizado nos termos previstos na licença abaixo indicada.

Caso o utilizador necessite de permissão para poder fazer um uso do trabalho em condições não previstas no licenciamento indicado, deverá contactar o autor, através do RepositóriUM da Universidade do Minho.

Acknowledgments

Special thanks I owe to my family, without your support, none of this would be possible. To my mother, for her unconditional love and affection and all shared strength and encouragement. Thank you for your patience and care even under my absence along these four years. I am grateful to my siblings, grandmother, and godfather for supporting me and always cheer me up, especially at moments of great discouragement. Thank you, sister, for living and striving this adventure so close.

I want to thank you to my advisors. Professor Cristina, I am eternally grateful for your support, encouragement, guidance, and friendship. I am grateful for respecting my opinions, for the given opportunity to investigate my research interests as a team. In the beginning, it was only me, you, and the idea. After so many tears and effort, we got the SmartOs. It was much more than a Ph.D.; it was a project of life.

Juan, thank you for guidance and for showing me how much fascinating is the rehabilitation field. It motivated my decision four years ago. Thanks for the opportunity to work at CSIC.

I also would like to thank Doctor Ana Catarina and Doctor Fátima Pereira for your clinical support and so helpful collaboration. Thank all stroke patients who kindly participated in the preliminary studies. I also want to thank you to *Fundação para a Ciência e Tecnologia*, for granted scholarship SFRH/BD/108309/2015.

My best regards to my friends and colleagues of BiRD Lab, for their help in this achievement, patience in my stressful moments, and the good times we spent together. A special thanks to all who accepted to work in SmartOs, by your trust, knowledge, willingness, and effort. I am thankful for all your support, Guillermo.

Thank you to all my friends. Raquel, Pedro Nuno, Catarina, André, Lili, Cátia, Barbosa, thank you for the encouragement and suggestions you gave me, free advice, and enjoying moments.

And last, my kinder thanks to a special friend, who helped me in the most challenging moments, by the transmitted enthusiasm and energy to achieve this thesis and the SmartOs. Thank you, Simão.

<div align="right">To all,</div>

<div align="right">who always believe and contribute to my dreams</div>

"If your actions inspire others to dream more, learn more, do more, and become more, you are a leader".

STATEMENT OF INTEGRITY

I hereby declare having conducted this academic work with integrity. I confirm that I have not used plagiarism or any form of undue use of information or falsification of results along the process leading to its elaboration.

I further declare that I have fully acknowledged the Code of Ethical Conduct of the University of Minho.

Ortótese Inteligente e Vestível para Assistir a Marcha Humana Debilitada

Resumo

O acidente vascular cerebral (AVC) é a terceira principal causa de incapacidade motora adulta. A reabilitação da marcha com um treino repetitivo e orientado ao doente, possível com ortóteses ativas (OAs), potencia a recuperação da mobilidade. Contudo, é necessário ajustar a reabilitação da marcha às atuais necessidades do sujeito, bem como integrar sensores vestíveis nas OAs para avaliar objetivamente a marcha.

Esta tese visa o desenvolvimento do SmartOs, um sistema ortótico ativo, modular, e vestível, com o intuito de providenciar um treino de marcha repetitivo e orientado às necessidades de doentes com AVC, e de avaliar a locomoção do doente por meio de dados cinemáticos e musculares. Esta tese inclui cinco fases de investigação.

Primeiro, foi desenvolvida uma estrutura modular para integrar, de forma inovadora e eficaz, sistemas sensoriais, ferramentas de análise da marcha, e estratégias de controlo nas OAs. Segundo, foi desenvolvido um laboratório portátil de análise de marcha com quatro sistemas sensoriais, passíveis de serem utilizados em *stand-alone* ou combinados com sistemas externos. O benchmarking com sistemas comerciais demonstrou a potencialidade destes sistemas sensoriais para a avaliação objetiva da locomoção. Terceiro, foi desenvolvida uma máquina de estados com limites adaptativos para a deteção de eventos da marcha, a qual demonstrou ser adequada como *benchmarking* para avaliação de eventos humanos da marcha. Quarto, foi criada uma ferramenta de *machine learning* para o reconhecimento e previsão de modos de locomoção e transições. Esta ferramenta destaca-se pela classificação precisa de direções e terrenos com uso exclusivo de dados cinemáticos. Por último, foi desenvolvida uma arquitetura de controlo hierárquica com quatro estratégias de controlo. As estratégias de trajetória orientada ao sujeito e impedância adaptativa fornecem um treino de marcha repetitivo e *assist-as-needed*, respetivamente. As estratégias baseadas na eletromiografia e na interação homem-OA contribuem para o fortalecimento muscular.

Em suma, os resultados indicam que o SmartOs está funcional para futura aplicação em ambiente clínico quer como uma solução de assistência personalizada, quer como uma ferramenta de avaliação da marcha de doentes com AVC.

Palavras-chave: assistência e reabilitação da marcha, estratégias de assistência, ortóteses ativas, reconhecimento de intenção, sensores vestíveis

Smart Wearable Orthosis to Assist Impaired Human Walking

Abstract

Stroke is the third leading cause of adult long-term motor disability. Gait rehabilitation approaching user-oriented and repetitive gait training has the potential for long-term mobility recovery. Active orthoses (AO) can tackle these rehabilitation abilities. More research is needed to foster gait rehabilitation oriented to the current user's needs and to integrate wearable sensors into AOs for objective gait assessment.

This thesis aims the development of SmartOs, a smart, modular, wearable active lower limb orthotic system, to foster user-oriented and repetitive gait training in impaired gait due to stroke and to evaluate human motor condition using kinematic and muscular gait measures. This work includes five research stages.

First, a modular framework was implemented to integrate into an innovative and effective manner, wearable sensor systems, gait analysis tools, and control strategies into AOs. Second, a wearable motion lab including four wearable sensor systems, with an open-architecture for both stand-alone or third-party systems use, was successfully developed. The benchmarking analysis with commercial systems outlined that the sensor systems are purposeful for objective evaluation of the user's motor condition. Third, a gait event detection tool through a finite state machine with an adaptive threshold-based structure was developed for detecting gait events in daily locomotion. Results show that the tool is suitable as a benchmark for detecting human gait events. Fourth, a machine learning-based recognition and prediction tool was achieved to classify locomotion modes and transitions. This tool advances the state-of-the-art by demonstrating that the exclusive use of kinematic data successfully classifies different walking directions and terrains. The last research stage made the SmartOs a multi-functional system through a hierarchical control architecture with four assistive control strategies. The user-oriented trajectory and adaptive impedance controls foster repetitive and assist-as-needed gait training, respectively. Both the EMG-based and user-orthosis interaction based control contribute to muscle strengthening.

Findings indicate that SmartOs is functionally operative for a future clinical application as a personalized assistive and gait assessment solution of stroke survivors.

Keywords: active orthoses, assistive control strategies, gait rehabilitation and assistance, motion intention recognition, wearable sensors

Table of Contents

List of Figures

List of Tables

List of Abbreviations

AOs	Active Orthoses
ADC	Analog-to-digital converter
ANOVA	Analysis of variance
AFO	Ankle-Foot Orthosis
ANN	Artificial Neural Network
AAN	Assist-As-Needed
CMEMS	Center for MicroElectroMechanical Systems
CCU	Central Controller Unit
CSIC	*Consejo Superior de Investigaciones Científicas*
CAN	Control Area Network
XApEn	Cross-Approximate Entropy
DC	Direct current
EMG	Electromyography
FEL	Feedback Error Learning
FSM	Finite State Machine
FF	Foot Flat
FSRs	Force Sensitive Resistors
HAL	Hardware Abstraction Layer
HS	Heel Strike
HO	Heel-Off
HMM	Hidden Markov model
IMUs	Inertial Measurement Units
I^2C	Inter-Integrated Circuit
ICF	International Classification of Functioning, Disability and Health
KNN	*k*-Nearest Neighbors
KAFO	Knee-Ankle Foot Orthosis
LW	Level-Ground Walking
LED	Light Emitting Diode
LDA	Linear Discriminant Analysis
LM	Locomotion Mode
LMT	Locomotion Mode Transition
LLOS	Low-Level Orthotic System
MCC	Mathew's Correlation Coefficient
MMST	Middle Mid-Stance
MMSW	Middle Mid-Swing
mRMR	Minimum-Redundancy Maximum-Relevancy

NRMSE	Normalized Root Mean Square Error
PAFO	Powered Ankle-Foot Orthosis
PKO	Powered Knee Orthosis
PCA	Principal Component Analysis
PID	Proportional Integral Derivative
RF	Radiofrequency
RA	Ramp Ascent
RD	Ramp Descent
ROM	Range of Motion
RQ	Research Question
RMSE	Root Mean Square Error
SPI	Serial Peripheral Interface
SEA	Series Elastic Actuator
SmartOs	Smart, Wearable Active Lower Limb Orthotic System
SCI	Spinal Cord Injury
SA	Stair Ascent
SD	Stair Descent
SO	Step Over Obstacle
SVM	Support Vector Machine
PRISMA	Systematic Reviews and Meta-Analyzes
TS	Terminal Swing
3D	Three-Dimensional
TO	Toe-Off
UART	Universal Asynchronous Receiver/Transmitter
USB	Universal Serial Bus
WBS	Wearable Biofeedback System
WML	Wearable Motion LAB

Chapter 1 - Introduction

This Ph.D. thesis presents the research and development activities carried out during the past four years in the scope of the Doctoral Program in Biomedical Engineering at the University of Minho. The research activities were mainly performed in Biomedical Robotic Devices Lab included in the Center for MicroElectroMechanical Systems (CMEMS), a research center of Department of Industrial Electronics from the University of Minho. Part of the research was also developed in Neural Rehabilitation Group at *Consejo Superior de Investigaciones Científicas* (CSIC) in Madrid, Spain.

The developed biomedical research is inserted into SmartOs project - Smart control of a stand-alone active orthotic system. It proposes a personalized robotic technology combined with a toxin-based intervention for long-term recovering of the functional motor abilities of stroke survivors. SmartOs aims the development of a smart wearable orthotic system by combining an active lower limb orthosis to assist as need during task-oriented gait training, with a wearable motion lab for monitoring the user's motion. This Ph.D. thesis addressed the first development initiatives of the SmartOs project, which is in a development stage and preliminary validation.

The research activities completed in this Ph.D. thesis address the field of neurorehabilitation robotics with a focus on human gait analysis and assistive control strategies towards personalized gait rehabilitation and assistance in post-stroke conditions using wearable active orthotic devices.

1.1.Motivation and Research Scope

Walking is the most daily performed human gait task, and it plays a relevant contribution to the user's active wellbeing. It consists of a repetitive sequence of lower limb motions to move the body forward, maintaining postural stability [1], [2]. Neurological diseases, muscular deformities, and peripheral injuries can compromise healthy human walking. The impaired gait sequels tend to increase with the actual aging tendency. Currently, 21.3% of the Portuguese population is older adults [3]. In 2060, 30% of Europeans (172 million) will be over 65 years old (currently 17%).

According to the World Health Organisation, every year, 15 million people suffer a **stroke** (20,000 in Portugal) [4]. Stroke is the third leading cause of motor disability [5]. This neurological disease is responsible for **long-term motor disability**; 70% of stroke survivors exhibit motor impairments and remain permanently disabled [6]. Gait after stroke is often characterized by an asymmetrical pattern, neuromotor impairment such as drop foot. About 35% of stroke victims present lower limb spasticity [6], which has an incidence rate of 57.8 cases per million inhabitants in Portugal [7]. Spastic gait may limit the biomechanical and functional motor ability at different daily tasks (e.g., walking, sitting, standing, jumping, climbing, and turnings). The limited mobility commonly results on the dependence on others (i.e., social assistance), social and work exclusion, early retirement (10% in the working-age), and costly medical assistance. Stroke sequels represent a significant burden on health and social resources, growing steadily in Europe due to demographic changes, costing around 1 million euros per year in 2020 [8].

Emerging therapies are necessary to help and improve the quality of life of the individuals that face permanent motor disabilities. Clinicians have been recommending the **physical rehabilitation** as the more appropriate strategy for the long-term biomechanical and functional gait recovery of neurologically injured individuals, such as stroke survivors [9]. An appropriate gait rehabilitation comprises **user-oriented** (i.e., according to the user's driven requirements and needs), **task-oriented** and **repetitive gait training**, and the **encouragement of the user's participation** in the therapy.

Various physical rehabilitation interventions have been proposed [9]–[12]. In particular, gait rehabilitation driven by wearable assistive lower limb devices such as **active orthoses** (AOs) are becoming a prominent assistive and augmented intervention [13]. They are capable of acting in parallel with the human limb for fostering a user-oriented, task-oriented, and

repetitive gait therapy while achieving a continuous **objective assessment of the end-users motor condition** [14]. Moreover, AOs can improve current treatments due to its ability to adapt the mechanical assistance according to real-time evaluation of the user's needs, addressing an **assist-as-needed** (AAN) **approach** [15]. One major milestone was the development of AAN strategies, in which a robotic assistive device only supplies as much assistance as necessary for patients to accomplish a movement.

It is expected that the high degree of physical training with specific and repetitive motion tasks fostered by AOs evokes brain plasticity, providing biomechanical advantages and a functional compensation. This will improve the overall patient's functional ambulation, movement coordination, abnormal gait pattern prevention, muscular strength, balance control, energetic efficiency locomotion, and general wellbeing [13]. Using AOs may enhance the cognitive abilities, which in turns, may increase the user's confidence and raise their levels of activity and independence. Additionally, AOs can be designed to encourage the user's participation in the therapy; thus, accelerating the motor learning process [15].

The current need for physical therapy is expected to remain strong into the foreseeable future, given the likely high prevalence of impaired gait and the reduced number of physical therapists. Wearable assistive devices, such as AOs, may tackle these needs. They will contribute as a complementary rehabilitation tool to conventional physical therapy to strengthen the long-term motor recovery and actuate in daily assistance to offer the patients an adequate level of independence. Further, as AOs are challenged to emulate the skills of a trained therapist, they may relieve and reinforce the repetitive and heavy work of physical therapists [16], [17].

1.2.Problem Statement

To date, available AO-based rehabilitation interventions are not satisfying and present **poor usability and clinical evidence** with pathological end-users. Despite the technological efforts on AOs [18]–[22], they are still not able to foster assistance oriented to the current user's needs, motor tasks, and timely adaptive for dynamic daily environments nor to encourage the user's participation.

The clinical evidence of AOs' effectiveness in gait rehabilitation has been limited to short-term clinical trials involving a reduced number of pathological end-users. There is no sufficient

clinical evidence of the AOs' potential to recover functional motor ability in daily performed tasks. It is imperative to develop a significative evaluation on the usability and cognitive and physical recovery effectiveness of AO-based rehabilitation and assistance.

Quantitative gait analysis is also a required topic for the clinical domain to objectively assess the efficiency of AOs and to provide reliable, objective measures to support the clinical-based motor diagnosis. Nowadays, prescription of rehabilitation interventions are not standardized and often depend on clinicians' experience and subjective measures [23], [24]. More efforts toward objective and easy to apply methodologies for assessing the motor function and unified method to evaluate the effectiveness of AO-based therapy are needed.

More research is needed to boost the achievements expected with AO-based gait rehabilitation and assistance, as follows. First, to develop **adaptive and compliant assistive control strategies** for timely and effective assistance's adjustment according to the user's needs. Second, bioinspired control architectures, following organization principles of the human motion-control system, started to emerge and constitute a relevant aspect for tackling the current gap on AAN strategies [9]. For that matter, it is imperative that the control architecture of AOs endows assistive control strategies, whose assistance is driven by gait tools able to detect current gait event and to recognize the user's motion intention and motor disability level [9], [14]. The control architecture also has to be synchronized with easily wearable sensor systems for objective gait monitoring and user's needs evaluation [25], [26].

Research should transform the AOs into **multi-functional assistive devices**, able to provide different assistive strategies and functionalities for post-stroke gait rehabilitation. Recent studies suggest parameterizing the joints trajectories according to the users' body conditions and gait phases, instead of imposing predefined trajectories as currently applied. This oriented assistive control strategy will contribute to improving the user's comfort and movement coordination [27], [28].

Considering the potentialities of the AAN gait training, current research directions [11], [29] also sought to adapt the impedance behavior of the **human-AO interaction** by proposing adaptive impedance control strategies. However, to achieve an AAN strategy, the dynamic parameters of the human-AO interaction need to be tuned accordantly to the gait cycle and speed [30]. Furthermore, active and natural interaction between user and AO is crucial for promoting motor recovery and increasing brain plasticity [28]. The combination of user-oriented assistive control strategies with biofeedback systems is an unsolved but necessary

challenge to manage the human-robot interaction in free-living scenarios synergistically. This combination can accelerate the motor learning process and boost the overall motor recovery [11], [31].

Moreover, the electromyography-based control strategy is raising as one interesting strategy to take into account the user's motion intention encoded in electromyography (EMG) signals while encouraging the user's participation to provide a functional gait training [32], [33].

Post-stroke gait impairments are usually related to one or several gait phases. Consequently, AOs should not only assist as much as needed but also assist when needed, i.e., to assist in part of a gait cycle related to the target impairment employing gait-phase-based control strategy [34]. It is necessary to develop time-effective, versatile computational tools able to detect the overall human **gait events in both controlled and real-life situations** using wearable sensors [35]–[40]. Furthermore, by analyzing the existing state-of-the-art [41]–[43], there is still a set of challenges to be pursued in the user's motion intention recognition; to develop an user-independent and more versatile tool for predicting and recognizing several **daily locomotion modes and locomotion mode transitions.**

Considering these shortcomings, future designs in AOs towards the direct interaction among gait analysis tools, multiple sensors, and actuation, biofeedback, monitoring, and power supply systems, while meeting the needs of effective assistive control strategies and prioritizing safety mechanisms [9], [16], [44]–[46]. This multiple system integration will increase the complexity of wearable AOs for ambulatory and user-oriented applications, demanding the development of interoperable, deterministic, modular frameworks.

This thesis considered the listed research challenges to bring new insights and innovative research directions into the development of a wearable assistive orthotic system for fostering user-oriented and repetitive gait training while fostering an objective gait monitoring.

1.3.Goal and Research Questions

The ultimate goal of this Ph.D. thesis is the development of a **smart, modular, wearable active lower limb orthotic system,** named as SmartOs system, to foster **user-oriented and repetitive gait training** in impaired gait due to stroke and to **evaluate human motor condition** using real-time and objective kinematic and muscular gait measures.

In the scope of this thesis, SmartOs system includes two **wearable AOs** for knee and ankle assistance, synergistically interconnected with a **wearable motion lab**. This innovative combination allows tailoring in real-time the assistance according to the specific ambulatory response of the user. AOs incorporate a **hierarchical control architecture** bioinspired on the principles and organization of the human motion-control system to tackle an AAN approach. The robotic assistance is based on the user's motion intention and gait phase, both decoded by **gait analysis tools**, which fuse biomechanical and muscular information from wearable motion lab. The interconnection of sensor feedback, analysis and motor control describes the smart nature of the SmartOs system for personalized gait rehabilitation and assistance. The control architecture incorporates different **user-oriented assistive control strategies** that will constitute an innovation action within the healthcare domain.

Furthermore, this thesis develops a modular, real-time, interoperable, power- and time-effective framework to be easily extendable, enabling the inclusion of other modules such as further AOs, sensor and biofeedback systems, assistive control strategies, and gait analysis tools. The development of a modular wearable robotic technology follows a **user-centered design approach** to maximize the user's acceptability and usability and provide a reliable and safe rehabilitation solution.

To achieve these ultimate goals, it is necessary to pursue the following objectives.

- **Objective 1**: **To review related studies to post-stroke gait analysis and gait rehabilitation using wearable assistive orthoses**. First, to identify the key outcome measures and motion capture systems applied in post-stroke gait rehabilitation based on lower-limb orthotic assistance. Second, to review the clinical evidence and methodologies for the orthotic-based gait training. Gathered knowledge guided the designing of clinical protocols for SmartOs-based gait training with neurologically impaired subjects. The third literature analysis focuses on wearable AOs to identify the leading technologies involved, the main clinical achievements and discusses on AOs' potential and challenges for gait rehabilitation. This review will serve as a base for the design of the SmartOs system. Chapter 2 presents these three surveys.

  Furthermore, critical reviews on gait event detection, user's motion intention recognition, and assistive control strategies are addressed in Chapter 5, Chapter 6, and Chapter 7, respectively, to identify the research directions that SmartOs should approach in

these topics. This objective led to one published journal paper [47] and two journal papers under review.

- **Objective 2: To set functionalities and conceptual design of SmartOs and to develop modular, real-time, power- and time-effective framework** to enable the SmartOs system integration and expandability for further sensor and actuation systems, assistive control strategies, and gait analysis tools. Chapter 3 addresses this objective that resulted in two conference papers [48], [49] and two journal paper under review.

- **Objective 3: To design, develop, and validate the wearable motion lab and gait analysis tools** for monitoring and assessing the post-stroke gait progression using biomechanical and muscular measures and metrics. Wearable motion lab aims to include a set of self-calibrated, stand-alone, low-cost, wearable sensor systems to measure in real-time the user's motor condition. The sensor information will be the base for implementing gait analysis tools to detect gait event, to recognize and predict the intended motion, and to feed the closed-loop control architecture. Chapter 4 tackles this objective. It led to one conference publication [50], one journal paper under review, and one journal paper under elaboration.

- **Objective 4: To design, develop, and validate an adaptive, time-effective, real-time gait tool for human gait event detection** using a minimal number of wearable sensors in an attempt to be easily reproducible under different contexts. The detected gait events will be the base for gait cycle-based assistive control strategies and to compute spatiotemporal metrics as relevant features for the user's motion intention recognition tool. Chapter 5 addresses this objective. It led to one conference publication [51] and one journal publication [52].

- **Objective 5: To design, develop, and validate an automatic, user-independent machine learning-based tool for user's motion intention recognition and prediction** of different daily locomotion modes and locomotion mode transitions, based on the minimal kinematical data to improve the SmartOs usability. The classification of the user's motion intention will contribute to timely tuning the assistance provided by AOs according to the user's motion intention and to generate smooth transitions. Chapter 6

approaches this objective. It led to two conference publications [53], [54] and one journal paper under review.

- **Objective 6: To design, develop, and validate a hierarchical, closed-loop, control architecture with a set of user-oriented assistive control strategies**, such as user-oriented trajectory control, adaptive impedance control, EMG-based control, to both attain to different user's needs and to become SmartOs a multi-functional assistive system suitable for distinct kinds of therapies. Additionally, this goal aims to explore more time-effective low-level tracking controls. Chapter 7 addresses this objective, which led to four conferences publications [48], [55]–[57] and one paper under elaboration.

The proposed ideas describe the transdisciplinary research adopted in this thesis that will contribute in the near future to use SmartOs as a robotic assistive technology for personalized and repetitive gait rehabilitation to gaining functional autonomy and improving the quality of life of the stroke survivors.

The following research questions (RQs) are proposed and expected to be answered:

- **RQ1:** Which are the key outcome measures to evaluate the functional motor recovery of stroke survivors upon orthotic-based gait rehabilitation? This RQ is related to Objective 1 and is answered in Chapter 2.

- **RQ2:** What are the main assistive potentialities and scientific challenges to consider in the design of a wearable active orthotic system for robotic-based gait rehabilitation? This RQ is related to Objective 1 and is answered in Chapter 2.

- **RQ3:** Can a single kinematic measure enable a time-effective detection of several gait events under distinct walking conditions? This RQ is related to Objective 4 and is answered in Chapter 5.

- **RQ4:** Is it possible to recognize and predict daily performed locomotion modes and locomotion mode transitions using a machine learning tool that exclusively deploys kinematic data? This RQ is related to Objective 5 and is answered in Chapter 6.

- **RQ5**: Which set of assistive control strategies will yield a multi-functional assistive system addressing different gait therapies? This RQ is related to Objective 6 and is answered in Chapter 7.

- **RQ6:** Can feedback error learning control, a low-level controller, provide proper real-time performance to an active assistive lower-limb device? This RQ is related to Objective 6 and is answered in Chapter 7.

1.4. Contribution to knowledge

This thesis contributes with a smart, wearable orthotic system, SmartOs, able to act and cooperate closely with human beings. This technological solution includes wearable active lower limb orthoses interconnected with a wearable motion lab and assistive control strategies with impact in both rehabilitation and diagnostic domains.

The main contributions outlined of this Ph.D. thesis are, as follows.

- **A systematic review on clinical methodologie**s and **key outcome measures** applied in post-stroke gait rehabilitation using orthotic assistance (Chapter 2).

- **A descriptive review** highlighting the **technical and clinical challenges** and **potentialities** in wearable lower limb **AOs** (described in Chapter 2).

- **Smart, wearable lower limb active orthotic system** - SmartOs system - with a modular, deterministic, power- and time-effective framework, following a user-centered design approach (described in Chapter 3).

- **Multi-modular wearable motion lab** synchronizing a set of stand-alone, self-calibrated, wearable sensor systems, namely an inertial sensor system (InertialLAB) and a wireless instrumented shoe system (GaitShoe) to obtain quantitative lower limb kinematic measures, and an EMG system and a muscular contraction-based force sensor system (MuscLAB) to monitor muscular measures. These are economic sensor systems with extendable potentials for versatile human motion and posture analysis for both healthy and pathological subjects (Chapter 4).

- **Time-effective, versatile, real-time tool able to detect six gait events** through a finite state machine with adaptive thresholds (described in Chapter 5).

- Evidence highlighting the **effectiveness of foot angular** velocity signal at the sagittal plane for **gait event detection** in controlled and non-controlled gait conditions, varying

variations of gait speed and slopes, climbing staircases, and attending to inter-subject and inter-step variability (described in Chapter 5).

- **Automatic, user-independent, more versatile recognition and prediction machine-learning tool** using wearable kinematic sensors for classifying several daily performed locomotion modes while covering different walking directions (forward, back, clockwise, and counter-clockwise) with variations in gait speed and terrains (flat, ascending and descending stairs and ramp, stepping over obstacles). The tool also classifies transitions, with one gait step before their occurrence, from/to those terrains using the user's self-selected lower limb (described in Chapter 6).

- Findings supporting the potential of only using the **trunk and lower limb kinematic data** to recognize and predict **daily performed locomotion modes and locomotion mode transitions** (described in Chapter 6).

- **Time-effective and adaptive low-level control, the Feedback Error Learning control**, innovatively explored in wearable lower limb orthotic devices, providing small steady-state errors, the ability for disturbance compensation and adaptiveness to the user-AO interaction (described in Chapter 7).

- **Four user-oriented assistive control strategies to foster user-oriented gait training** while considering the user's effort, intention, and participation. These strategies constitute four different operation modes of AOs to approach distinct kinds of gait therapies, as follows (described in Chapter 7). First, the **user-oriented trajectory control** enables a user-oriented repetitive gait training, longer than the manual therapists' assistance, enhancing motor coordination. Second, the **adaptive impedance control** provides an AAN gait training through stiffness adjustment with variable challenging therapy strengthening muscle strength. The inclusion of an user-oriented trajectory into the impedance control also enables the user to recover his/her natural gait pattern. Third, the **EMG-based control** and **user-orthosis interaction based control** favour high-challenging motor therapies, contributing to high-level of muscle strengthening. However, the EMG-based control strategy is more suitable for subjects with a high-to-moderate level of impaired gait function since it requires lower physical effort from the user than the user-orthosis interaction-based strategy.

Under an assistive point of view, SmartOs contributes to a multi-functional orthotic system by enabling the physical therapist to challenge the patient with different gait speeds and therapies with variable physical effort and user's participation. Moreover, it decreases the burden of physical therapist work and tracks in real-time the user's motion state. The wearable motion lab provides biomechanical and muscular gait measures that will support the clinical-based diagnosis with more accurate information. This objective evaluation will also contribute to fine-tuning treatments to the patient's specific needs. In the future, it is expected that SmartOs contributes to long-term functional, biomechanical, and energetic-efficient motor recovery of stroke survivors.

During this thesis, scientific and technical support was provided to master students of different fields of engineering, contributing to five Master Dissertations on Industrial Electronics and Computers, one Master Dissertation on Informatics Engineering, one Master Dissertation on Biomedical Engineering, and three academic projects of the Master on Industrial Electronics and Computers. These Master Students contributed to the work herein presented. Moreover, three Master Dissertation on Biomedical Engineering and one Master Dissertations on Industrial Electronics and Computers are currently under co-guidance.

Furthermore, the work developed in this thesis played an important role in the scientific research and development of SmartOs project and in actively specifying two accepted grant proposals, as follows.

- SmartOs: Smart control of a stand-alone active orthotic system, project approved under Individual National Grant Proposal - *Projetos de Investigação Científica e Desenvolvimento Tecnológico* - with Cristina P. Santos as Principal Investigator. Currently supported by FEDER Funds through the *Programa Operacional Regional do Norte* and national funds from FCT.
- SmartOs: Smart control of a stand-alone active orthotic system project accepted under Copromotion National Grant Proposal - *Projetos de Investigação e Desenvolvimento Tecnológico em Copromoção, P2020* - with Orthos XXI as the leader company and Cristina P. Santos as Principal Investigator of the research center.

Lastly, this thesis contributed to the following prize awards:

- Best oral presentation and paper for the work entitled "EMG-based Motion Intention Recognition for Controlling a Powered Knee Orthosis", received at *19th IEEE International Conference on Autonomous Robot Systems and Competitions* (ICARSC), Porto, 2019.

- Finalist at Healthy category of *SantaCasa Challenge-Social Innovation* with SmartOs project, recognized by *Santa Casa Misericórdia de Lisboa*, Lisboa, 2018.

- 1st Prize at *Prémio Engenheiro Jaime Filipe* with SmartOs project, recognized by *Instituto Nacional para a Reabilitação*, Lisboa, 2017.

1.5. Publications

The work here described allowed the publication of the following journal articles, conference papers, and a book chapter. The contribution to the conference papers as the second author relies on the conceptual design of the proposed solution or innovation, performing the experimental validation, and supporting the paper elaboration and review.

Journal Articles

- **Joana Figueiredo**, Simão Carvalho, Diogo Gonçalves, Juan C. Moreno, Cristina P. Santos, "Machine Learning-Based Framework for Daily Locomotion and Transition Recognition and Prediction: A Kinematic-Based Approach", IEEE Journal of Biomedical and Health Informatics, 2019 (submitted, under review) [IF = 4.2; Q1-Electrical and Electronic Engineering, Q1-Health Information Management].

- **Joana Figueiredo,** Pedro Nuno, Paulo Félix, Juan C. Moreno and Cristina P. Santos, "Smart, Wearable, Active Orthotic System – SmartOs: A Gait Rehabilitation and Analysis Framework", Journal of Medical Systems, 2019 (submitted, under review) [IF = 2.4; Q1- Healthy Informatics, Q1-Health Information Management, Q1-Computer Science Applications, Q1-Medicine].

- **Joana Figueiredo**, Simão P. Carvalho, João Paulo Vilas-Boas, Juan C. Moreno, Cristina P. Santos, "Wearable Inertial Sensor System Towards Human Kinematic Gait Analysis: Benchmarking Analysis to MVN BIOMECH", Journal of Biomechanics, 2019 (submitted,

under review) [IF = 2.57; Q1- Biomedical Engineering, Q1-Rehabilitation, Q1-Orthopedics and Sports Medicine].

- **Joana Figueiredo**, Ana C. Matias, Fátima Pereira, Juan C. Moreno, Cristina P. Santos, "Lower limb spastic gait management by combining botulinum toxin with orthotic therapy: A systematic review", *Physical Therapy*, 2018 (submitted, under review) [IF = 3.04; Q1- Physical therapy, Sports Therapy and Rehabilitation].

- **Joana Figueiredo**, Ana C. Matias, Fátima Pereira, Juan C. Moreno, Cristina P. Santos, "Outcome measures and motion capture systems for assessing lower limb orthosis-based interventions after stroke: A systematic review", *Disability and Rehabilitation: Assistive Technology*, 2018 (submitted, under review) [IF = 1.1; Q2-Biomedical Engineering, Q2- Physical therapy, Sports Therapy and Rehabilitation, Q2-Rehabilitation].

- **Joana Figueiredo**, Paulo Félix, Juan C. Moreno, Cristina P. Santos, "Gait Event Detection in Controlled and Real-life Situations: Repeated Measures from Healthy Subjects", *IEEE Transactions on Neural Systems & Rehabilitation Engineering*, vol. 26, 2018. DOI: 10.1109/TNSRE.2018.2868094. [IF = 3.47; Q1- Biomedical Engineering, Q1-Computer Science Applications, Q1-Medicine].

- **Joana Figueiredo**, Cristina P. Santos, Juan C. Moreno, "Automatic Recognition of Gait Patterns in Human Motor Disorders using Machine Learning: A Review", *Medical Engineering & Physics*, vol. 53, pp:1-12, 2018. DOI: 10.1016/j.medengphy.2017.12.006. [IF = 1.78; Q2- Biomedical Engineering, Q2-Biophysics].

Conference Papers

- Pedro Nuno Fernandes, **Joana Figueiredo,** Luis Moreira, Paulo Félix, Ana Correia, Juan C. Moreno, Cristina P. Santos, "EMG-based Motion Intention Recognition for Controlling a Powered Knee Orthosis", *19th IEEE International Conference on Autonomous Robot Systems and Competitions* (ICARSC), Porto, 2019.

- Simão Carvalho, **Joana Figueiredo**, Cristina P. Santos, "Environment-Aware Locomotion Mode Transition Prediction System", *19th IEEE International Conference on Autonomous Robot Systems and Competitions* (ICARSC), Porto, 2019.

- Pedro Nuno Fernandes, **Joana Figueiredo**, Juan C. Moreno and Cristina P. Santos, "Feedback-Error Learning for Gait Rehabilitation Using a Powered Knee Orthosis: First Advances", *IEEE 6th Portuguese Meeting on Bioengineering* (ENBENG), Lisbon, 2019.

- Cristiana Pinheiro, Daniel Sanz-Merodio, **Joana Figueiredo**, Cristina P. Santos, Elena Garcia, "Kinematic and kinetic study of sit-to-stand and stand-to-sit movements towards a human-like skeletal model", *IEEE 6th Portuguese Meeting on Bioengineering* (ENBENG), Lisbon, 2019.

- J. M. Lopes, Daniel Sanz-Merodio, **Joana Figueiredo**, Cristina P. Santos, Elena Garcia, "Three-Link Inverted Pendulum for Human Balance Analysis: A Preliminary Study", *IEEE 6th Portuguese Meeting on Bioengineering* (ENBENG), Lisbon, 2019.

- Luís Moreira, Daniel Sanz-Merodio, **Joana Figueiredo**, Cristina P. Santos, Elena Garcia, "The Study of Gait Cycle Stability Using a Five-Link Inverted Pendulum Model: First Developments", *IEEE 6th Portuguese Meeting on Bioengineering* (ENBENG), Lisbon, 2019.

- **Joana Figueiredo**, Paulo Félix, Cristina P. Santos, Juan C. Moreno, "Real-Time human gait segmentation based on adaptive tool using single-axis wearable gyroscope", *IX Congreso Iberoamericano de Tecnologías de Apoyo a la Discapacidad* (IBERDISCAP), Bogotá, 2017.

- **Joana Figueiredo**, Paulo Félix, Cristina P. Santos, Juan C. Moreno, "Towards Human-Knee Orthosis Interaction Based on Adaptive Impedance Control Through Stiffness Adjustment", *15th IEEE Conference on Rehabilitation Robotics* (ICORR), London 2017.

- **Joana Figueiredo**, Diogo Gonçalves, Juan C. Moreno, Cristina P. Santos, "Automatic and Real-time Locomotion Mode Recognition of a Humanoid Robot", *20th International Conference on Climbing and Walking Robots and Support Technologies for Mobile Machines* (CLAWAR), Porto, 2017.

- Paulo Félix, **Joana Figueiredo**, Cristina P. Santos, Juan C. Moreno, "Adaptive real-time tool for human gait event detection using a wearable gyroscope", *20th International Conference on Climbing and Walking Robots and Support Technologies for Mobile Machines* (CLAWAR), Porto, 2017.

- **Joana Figueiredo,** César Ferreira, Luis Costa, João Sepúlveda, Luis P. Reis, Juan C. Moreno, Cristina P. Santos, "Instrumented Insole System for Ambulatory and Robotic Walking Assistance: First Advances", IEEE International Conference on Autonomous

Robot Systems and Competitions (ICARSC), Coimbra, 2017. DOI: 10.1109/IC-ARSC.2017.7964062.

- Paulo Félix, **Joana Figueiredo**, Cristina P. Santos, Juan C. Moreno, "Electronic Design and Validation of Powered Knee Orthosis System with Wearable Sensors", *IEEE International Conference on Autonomous Robot Systems and Competitions* (ICARSC). Coimbra, 2017. DOI: 10.1109/ICARSC.2017.7964061

- **Joana Figueiredo**, Cristina P. Santos, Juan C. Moreno, "Assistive Locomotion Strategies for Active Lower Limb Devices", *IEEE 5th Portuguese Meeting on Bioengineering* (ENBENG), 2017. DOI: 10.1109/ENBENG.2017.7889473.

- Paulo Félix, **Joana Figueiredo**, Cristina P. Santos, Juan C. Moreno, "Powered knee orthosis for human gait rehabilitation: First advances", *IEEE 5th Portuguese Meeting on Bioengineering* (ENBENG), Coimbra, 2017. DOI: 10.1109/ENBENG.2017.7889427.

Book Chapter

- Juan C. Moreno, **Joana Figueiredo**, José L. Pons, "Exoskeletons for lower-limb rehabilitation", Chapter 7 in *Rehabilitation Robotics: Technology and Application, Elsevier,* 2018.

1.6. Thesis outline

This thesis is organized into eight chapters, as illustrated in Figure 1.1.

Chapter 2 is a comprehensive review on wearable lower limb orthotic devices, disclosing the main reasons and advantages of their application in post-stroke gait rehabilitation and assistance, the clinical methodologies and outcome measures applied in passive orthosis and representative technical advancements in AOs.

Chapter 3 introduces the main functionalities and conceptual design of SmartOs system and the development of the modular, interoperable, power- and time-effective framework for integrating modules of SmartOs.

Chapter 4 presents the design and development of the hardware and software interfaces of each wearable sensor system that formed the Wearable Motion Lab. The chapter provides the experimental validation of each sensor system considering a benchmarking analysis with commercial well-established solutions.
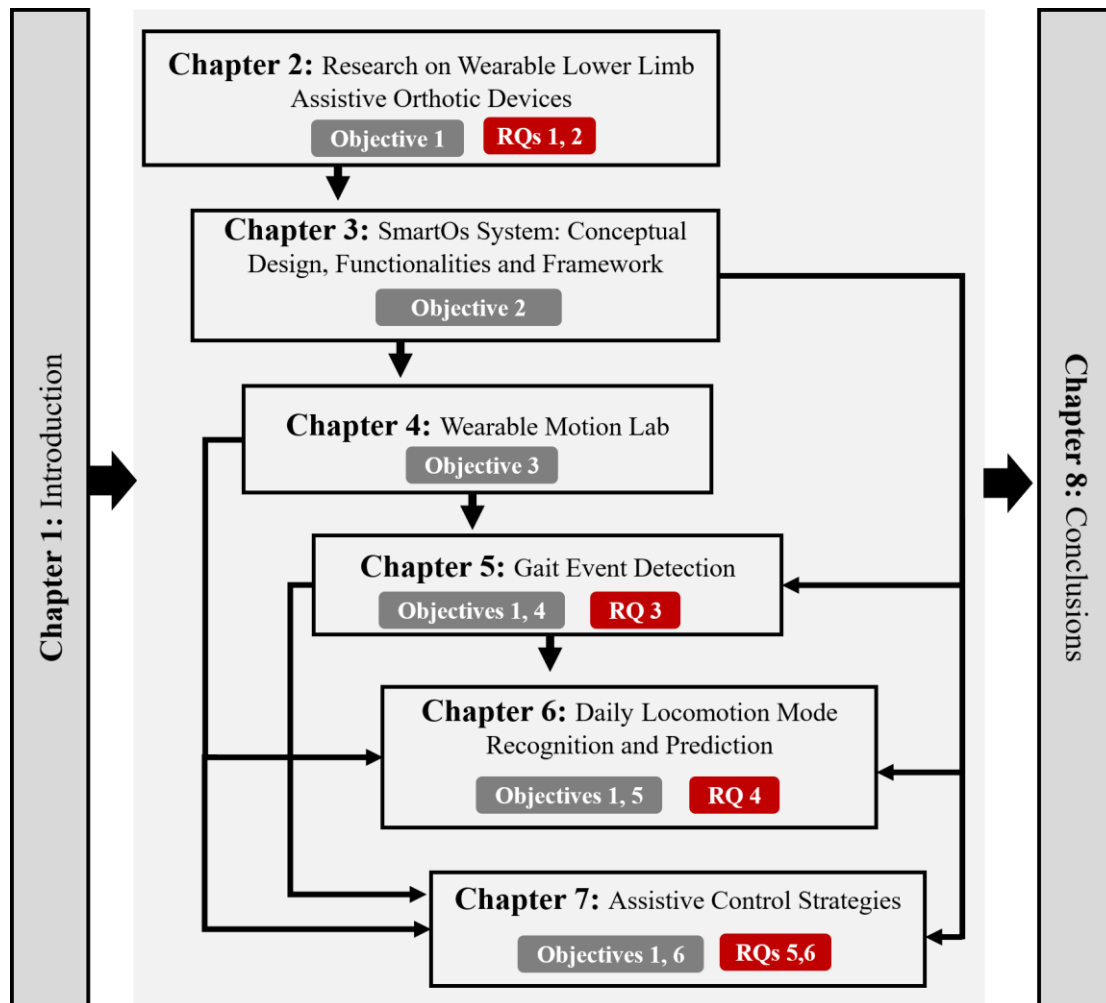
Figure 1.1- Graphical diagram of thesis organization.

Chapter 5 describes the development of a novel, real-time gait event detection able to detect up to six gait events tool using minimal sensor kinematic information. It also investigates the real-time effectiveness of the tool by including repeated healthy gait patterns collected in controlled and non-controlled gait conditions.

Chapter 6 proposes a machine learning-based framework to find an accurate and general motion intention recognition and prediction tool. It also explores the feasibility of only using kinematic data for daily locomotion mode recognition and prediction.

Chapter 7 presents the hierarchical control architecture, detailing the methodologies, the effectiveness from experimental evidence, and clinical potentialities of each assistive control strategy. This chapter also provides a critical analysis of the most effective low-level controller for SmartOs system.

Chapter 8 presents a summary of the thesis' key findings and contributions, together with directions for future research and technical improvement opportunities.

Chapter 2 – Research on Wearable Lower Limb Assistive Orthotic Devices

This chapter aims to review wearable lower limb assistive orthotic devices, disclosing the main reasons and advantages of their application in post-stroke gait rehabilitation and assistance and representative advancements in the technology involved.

The chapter starts with an introductory insight on stroke sequels and highlighting the impact of involving and complementing the conventional therapies with robotic-aid therapies, namely wearable assistive orthotic devices.

Subsequently, this chapter presents three literature surveys. The first survey covers a systematic review focused on the outcome measures and motion capture systems applied in post-stroke gait rehabilitation using lower-limb orthotic devices. The second systematic survey aims to review the clinical evidence and the key methodologies for the orthotic-based gait training. The third literature analysis focuses on wearable AOs to identify the leading technologies involved and discusses on AOs' potential in the rehabilitation domain. Each survey raises the limitations presented in the associated field. This critical analysis will allow identifying the scientific challenges in post-stroke gait rehabilitation with wearable AOs, aiming to face them with the proposed SmartOs system.

2.1.Introductory Insight

Stroke is one of the leading causes of motor disability in adults, where stroke survivors might live with life-changing neurological consequences. It can lead to an **impaired biomechanical** performance (e.g., decreased gait speed, step length, and ankle dorsiflexion), asymmetric gait pattern, postural instability, and **abnormal motor conditions** (e.g., *equinus* foot, drop foot, and spastic gait) [7], [58]. Focal spasticity at plantar flexors is the main cause associated to *equinus* foot [59]–[61]. The stroke victims also report **difficulty to perform daily functional tasks** (e.g., walking, sitting, standing, jumping, climbing, and turnings) leading to dependence on others (i.e., social assistance), and costly medical assistance.

Individuals that have suffered neurological diseases, such as stroke, often require physical rehabilitation interventions to improve their motor ability and ambulation. Various lower limb rehabilitation interventions have been proposed, such as (i) walking aids as canes and wheeled walkers, (ii) manual training assisted by therapists, (iii) treadmill with partial body weight support, (iv) functional electrical stimulation, and (v) wearable assistive devices, namely orthoses and exoskeletons [9]–[12], [62]. The walking aids consist of a simple rehabilitation not oriented for the user's motor condition and generally prescribed for people with low levels of mobility impairment [9], [63]. Gait training realized by therapists requires exhaustive manual assistance that may promote asymmetric rehabilitation. The gait training's duration is limited by the therapist's fatigue and subjectively determined by the therapist's experience [10].

On the other hand, previous studies [11], [14], [64]–[67] have reported that the arrangement of body weight support-based treadmill systems with a static lower limb assistive device (e.g., Lokomat and LOwer-extremity Powered ExoSkeleton) leads to positive rehabilitation effects, even for spastic gait in opposition to the manual training [11]. Nevertheless, the static lower limb assistive systems present a limited rehabilitation to the clinical setting for relatively brief training sessions, and to less-challenging locomotor tasks [12], [68].

Physical rehabilitation interventions that evoke brain plasticity and involve user-oriented, task-oriented and repetitive gait training and encourage the user's participation in the therapy are challenging and needed [9]. Both functional electrical stimulation as neuroprosthetic devices and wearable assistive robotic devices, as exoskeletons and AOs, may achieve such rehabilitation.

In last years, an exponential increase of researches on the lower limb exoskeletons and AOs have been shown as they are becoming a prominent physical rehabilitation intervention for fostering a user-oriented, task-oriented and repetitive gait rehabilitation in neurological conditions. This mechanic-based assistance, with similar physical principles to the ones in the conventional physical rehabilitation, does not constitute a physical burden for therapists and enable a practical use for the daily living assistance while meeting the requirements for an objective gait assessment [14].

Both exoskeletons and AOs are defined as active/powered mechanical devices with an anthropomorphic nature to fit the human body tightly and to work according to the human's motions [16]. In general, an exoskeleton is used to augment the strength and endurance of the movements of an able-bodied user [16], [69]. **AO** is an assistive device applied to **restore or modify the structural and motor function** of the neuromuscular and skeletal system to achieve an overall recovery of the ambulatory ability of a person exhibiting impaired gait function due to neurologic or/and motor diseases/injuries [16], [69]. The development of an AO is generally more difficult and challenging than the one addressed for an exoskeleton since AO faces the daunting issue that the specific nature of a disability is widely variable between patients [16]. However, the term "exoskeleton is also used to refer to assistive devices when they encompass the majority of the lower limbs" [16]. AOs have been designed only to assist actively the motion of specific lower limb joint, mainly the knee and ankle joints, or a motor condition [13], [16].

The investigation carried out in this Ph.D. thesis was centered on wearable lower limb assistive orthotic devices, instead of static devices, for two reasons. First, there is evidence that rehabilitation with functional and daily performed activities, only ensured by wearable devices, outcomes a more effective and lasting functional motor recovery. Second, current tendencies suggest the application of wearable orthotic devices has the advantage to assist the users in accomplishing their desired activities [69], [70].

Due to the potential advantages of wearable AOs, it is crucial to present and discuss the current state of this research area. Sub-Chapter 2.4 presents a review of the available technological designs of AOs, analyzing their application purposes and scenarios, and clinical evidence. It also provides a critical analysis of the state-of-the-art disclosing future technical and clinical challenges and new expected functionalities.

Moreover, it is crucial to find unified measures that investigate post-stroke rehabilitation to pave the way for further clinical research on AOs. Research should first identify the key outcome measures and set benchmarks to objectively evaluate the clinical evidence in the post-stroke rehabilitation based on wearable assistive devices. Such analysis is presented in Sub-Chapter 2.2 in the format of a systematic review.

Lastly, the investigation should look for standardization of clinical protocols to contribute to AOs' prescription. Nonetheless, it was observed a brief clinical evaluation of AOs in post-stroke rehabilitation, which in turns, also showed a lack of standardized clinical methodologies in research with AOs. Sub-Chapter 2.3 presents a systematic review of the clinical protocols and key methods to consider in post-stroke clinical interventions involving wearable assistive devices.

Although the exclusive inclusion of passive orthosis in the two systematic analyses, the reviewed knowledge may be transferred to better design the clinical protocols in AO research. Note that passive devices assist or passively control the motion of the lower limb joints during gait with direct physical resistance [17].

2.2. A Systematic Review of Outcome Measures for Post-stroke Clinical Assessment

As with all available orthotic-based rehabilitation programs, the inclusion of outcome measures has gained importance through the years, driven primarily by the need for the evidence-based practice [71]. The outcome measures in post-stroke rehabilitation can be classified according to the World Health Organization's International Classification of Functioning, Disability and Health (ICF) into three categories, namely: body structure/impairment, activities, and participation [72], to approach a unified assessment.

Although numerous outcome measures for post-stroke motor function exist, it is not clear which most accurately measure meaningful changes upon orthotic-based interventions. Additionally, the analysis of motion capture systems applied for measuring the outcome measures in clinical interventions has not received attention. This systematic review aims to analyze the outcome measures used in orthotic-based gait rehabilitation of post-stroke patients towards identifying the key outcomes, the most applied motion capture systems and the standard timing for assessment. This review sought to answer the following research

questions: (i) Which are the most measured outcomes?; and, (ii) Are the motion capture systems used in post-stroke gait analysis wearable systems?.

2.2.1.Methods

This work follows the Preferred Reporting Items for Systematic Reviews and Meta-Analyzes (PRISMA) guidelines [73] to ensure transparency of the review. The literature search was conducted until November 2017 in Web of Science, Scopus, MEDLINE, and Physiotherapy Evidence Database using the following search strategy: ["stroke"] AND ["lower limb orthosis" OR "ankle orthosis" OR "knee orthosis"] AND ["rehabilitation" OR "assistance" OR "gait training"] AND ["outcomes" OR "gait measurements" OR "therapeutic scales" OR "clinical measures" OR "clinical scales" OR "assessment" OR "measures"]. The search was limited to titles, keywords, and abstracts.

The papers identified in this initial search were evaluated based on the following inclusion criteria: (i) included participants in an acute or chronic stage of stroke; (ii) investigated the rehabilitation effects using quantitative or participation measures; (iii) prescribed passive or active wearable lower limb orthoses; and (iv) conducted randomized controlled clinical trials. Articles were excluded if they: (i) used non-portable system associated with the orthotic device; and (ii) prescribed other treatment approaches besides the orthotic therapy namely, functional electrical stimulation and brain computational interface. The methodologic quality of each included study was assessed using the Cochrane risk-of-bias tool [74].

2.2.2.Results and Discussion

Figure 2.1 summarizes the literature search process of this review. From this analysis, 18 studies were included. The ankle-foot orthosis (AFO), mostly the conventional AFO configuration (i.e., polymeric, non-articulated posterior leaf-spring AFO), was prescribed in 16 randomized trials (88.9%) whereas only two studies [75], [76] used the knee orthosis. From the full-text article analysis, we verified that studies including active orthotic devices [19], [77]–[81] did not accomplish randomized clinical trials, as such, they were not included in this analysis.

The included studies, as demonstrated in Appendix A.1, successfully performed the generation of the allocation sequence (100% lower risk of bias). They also present a low risk of bias through incomplete data and selective reporting. However, studies assessment quality may be affected by detection bias since a significant portion of the studies (83.3%) did not provide

any information relating to whether the intended blinding of outcome assessors was conducted or effective. Another factor that may affect the quality of the reported findings is the high risk of attrition bias observed in 27.8% of studies due to the handling of incomplete outcomes.
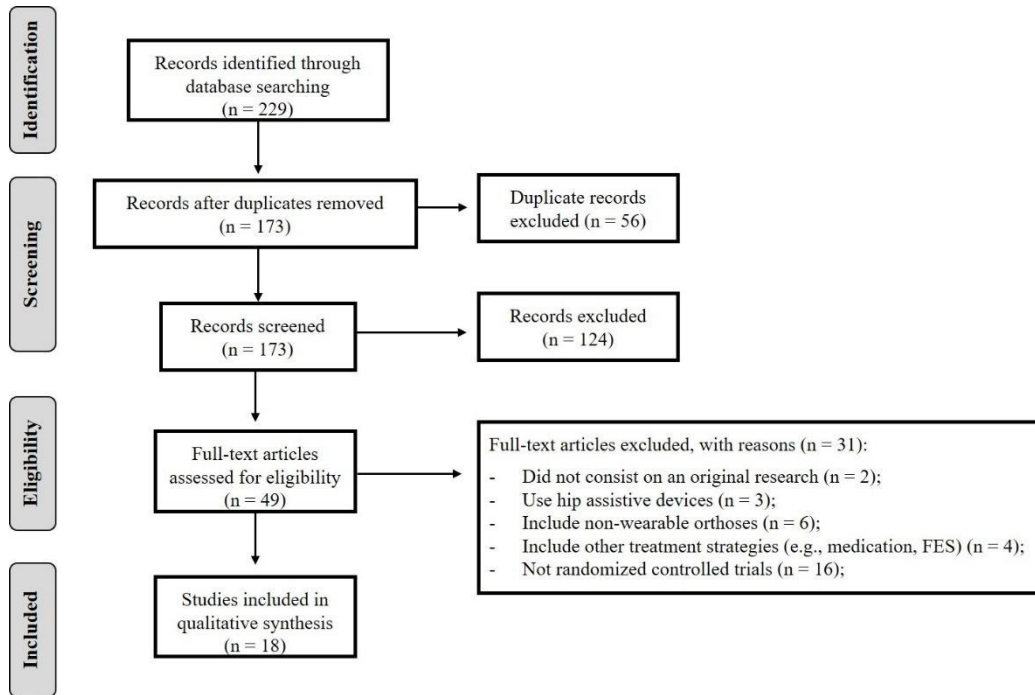
Figure 2.1- Flow chart of the literature search process.

The literature analysis found 39 outcome measures for assessing the orthosis-based gait rehabilitation applied to 387 post-stroke survivors in the chronic or acute stage. This analysis observed heterogeneity in the assessment protocol for selecting the outcome measures and timings for assessment when considering similar assessment goals. Such heterogeneity was also reported in previous systematic analyses [82]–[84]. Appendix B lists the information extracted from 18 studies as well as the ICF category per outcome measure. The research questions were tackled according to this information as follows.

Which are the most measured outcomes?

There is evidence to apply outcome measures from the Activity ICF category, including **biomechanical** (such as spatiotemporal, kinematic, and kinetic measures), **functional and balance outcome measures**, for assessing the post-stroke orthosis-based gait rehabilitation.

This review demonstrated that the spatiotemporal measures, namely gait speed [75], [85]–[92], step length [75], [85]–[89], [91], [93], cadence [75], [86], [91], [93], and stride duration

[75], [87], [89], [92], [93]) were the most monitored outcome measures. Gait speed was pointed out as the primary outcome given its contribution for measuring the increased motor function upon the orthotic-based intervention [86]. Lower limb kinematics, including flexion/extension of hip, knee and ankle at different stages of the gait cycle, and range of motion (ROM) of these joints, were the second most measured outcomes [85], [86], [88]–[91], [93], [94] followed by functional metrics (mainly, Time-Up-Go Test, 10 Meter Walking Test, and Berg Balance Scale [75], [76], [95]–[98]).

On the other hand, the impairment (mainly, Modified Ashworth Scale to assess the spasticity level [88], [89], [96]) and body function outcome measures (such as electromyography measures of tibialis anterior [75], [90], [93], *biceps femoris* [93], and rectus femoris muscles [93]), both belonging to Body Structure ICF category, were the quantitative outcome measures less inspected.

Furthermore, only four clinical trials investigated the applicability and usability of the orthotic-based gait rehabilitation for daily use through Participation outcome measures [75], [86], [88], [99], using satisfaction questionnaires [75], perceived exertion scale [99], and EuroQol EQ-5D-5L29 quality of life questionnaire [86], [88]. A systematic review centered on assessing satisfaction with orthoses reported that objective measures continue to be more discerning than patient self-reports [100].

Are the motion capture systems used in post-stroke gait analysis wearable systems?

Non-wearable motion capture systems recorded most of the outcome measures. These systems are not able to analyze consecutive gait cycles nor the gait recovery in daily locomotion activities [101], [102]. The studies used non-portable motion capture systems to monitor the Activity outcome measures such as the force platforms (AMTI BP400600 platform [86], GAITRite [87], Kistler platform (Switzerland) [91], pedar® platform [92] to measure the spatiotemporal outcomes), optical motion systems (Vicon system (Oxford Metrics, UK) and ELITE (BTS Bioengineering, Italy) to track spatiotemporal parameters and kinematic parameters), and balance platforms (Biodex system [97]).

On the other hand, muscular activity outcomes were measured by wearable EMG systems, such as telemetric EMG device (Zebris Medical GmbH, Germany) [75], wireless EMG (BTS FREEEMG 300) [93], and the Myopac EMG unit (Myopac) [90].

2.2.3. Clinical Highlights and Future Directions

There is evidence for assessing the effectiveness of **orthosis-based gait rehabilitation after stroke through Activity outcome measures, primarily the gait speed.** Non-wearable motion capture systems have mostly recorded these outcomes. The widespread use of Activity outcome measures suggests that post-stroke rehabilitation mainly approaches the functional ability or difficulty that an individual might experience in completing a given daily motor activity. Participation outcome measures may introduce complementary information to the objective outcome measures. This clinical highlight may guide the clinical assessment in AO-based gait rehabilitation, as the SmartOs.

To progress the evidence regarding orthotic-based rehabilitation in post-stroke conditions, future researches are recommended to (i) approach a transparent declaration of blinded outcome assessment, (ii) fully describe the methodologies used to collect outcome measures, (iii) endow wearable motion systems, and (iv) include baseline and follow-up outcome completeness to enable critical and reliable appraisal of the viability of the rehabilitation treatment fostered by the lower limb orthosis. Furthermore, clinical studies involving active wearable orthotic systems should follow a randomized trial approach, a relevant methodological procedure in clinical trials. The heterogeneity found in this analysis highlights the need for some agreement on assessing post-stroke rehabilitation towards a unified clinical methodology.

2.3. A Systematic Review of Clinical Protocol and Evidence on Post-Stroke Rehabilitation using Wearable Passive Orthoses

Given the prevalence and wide diversity of wearable orthotic devices in the health care system, it is still needed to set clinical methodologic guidelines and benchmarks for the research in orthotic-based rehabilitation in terms of clinical protocol design (e.g., physical activities, and frequency and duration of therapy) and clinical evidence analysis.

This systematic review aims to analyze the clinical protocol and key methodologies in post-stroke orthotic-based rehabilitation and the clinical effects. For this purpose, this systematic review seeks to answer the following questions: (i) What are the main inclusion and exclusion criteria?; (ii) Which are the key methodologies for designing the clinical protocol in the orthosis-related studies?; (iii) Which are clinical interventions endowed in orthosis-related studies?; and, (iv) What is the clinical evidence of passive orthosis in post-stroke gait recovery?.

2.3.1.Methods

This work follows the PRISMA guidelines [73]. A comprehensive literature search was carried out until January 2017 through the databases Web of Science, Scopus, MEDLINE, and Physiotherapy Evidence Database. The keywords explored during the electronic search, through AND and OR operators, are: ["stroke"] AND ["lower limb orthosis" OR "ankle orthosis" OR "knee orthosis"] AND ["rehabilitation" OR "assistance" OR "gait training"] AND ["effects" OR "evidence"] AND ["protocol" OR "experiment" OR "clinical test"]. The search for such keywords was limited to titles, abstracts, and keywords.

The studies identified in this initial search were evaluated based on the main following inclusion criteria: (i) assessed the effect of the wearable ankle or knee orthosis in rehabilitation; (ii) involved at least 5 participants in an acute or chronic stage of stroke; and, (iii) described the experimental design included randomized trials. Articles were excluded if they: (i) used non-portable orthotic devices; and (iii) prescribed other treatment approaches besides the orthotic therapy. The Cochrane risk-of-bias tool [74] was employed to assess the methodological quality of the included studies in terms of sources bias.

2.3.2.Results and Discussion

Figure 2.2 illustrates the literature search process of this review. From the specified search strategy and after removal of duplicates using Mendeley, 20 randomized studies were analyzed, which involved 1154 post-stroke patients. This review does not investigate clinical remarks regarding AO-based rehabilitation given the lack of randomized clinical methodology and the inclusion of a few participants (less than 3).

Concerning the methodological quality of the included studies (presented in Appendix A.2), there is a low risk of selection bias (100% of random sequence and 75% allocation concealment) and outcomes reporting bias (100%). On the other hand, there is an unclear risk of bias related to the blinding of participants, personnel and outcome assessors. Another factor that may affect the quality of the reported findings is the high risk of attrition bias observed in 35% of studies due to the handling of incomplete outcomes.

The research questions were tackled according to the information extracted from 20 studies (listed in Appendix C) as follows.
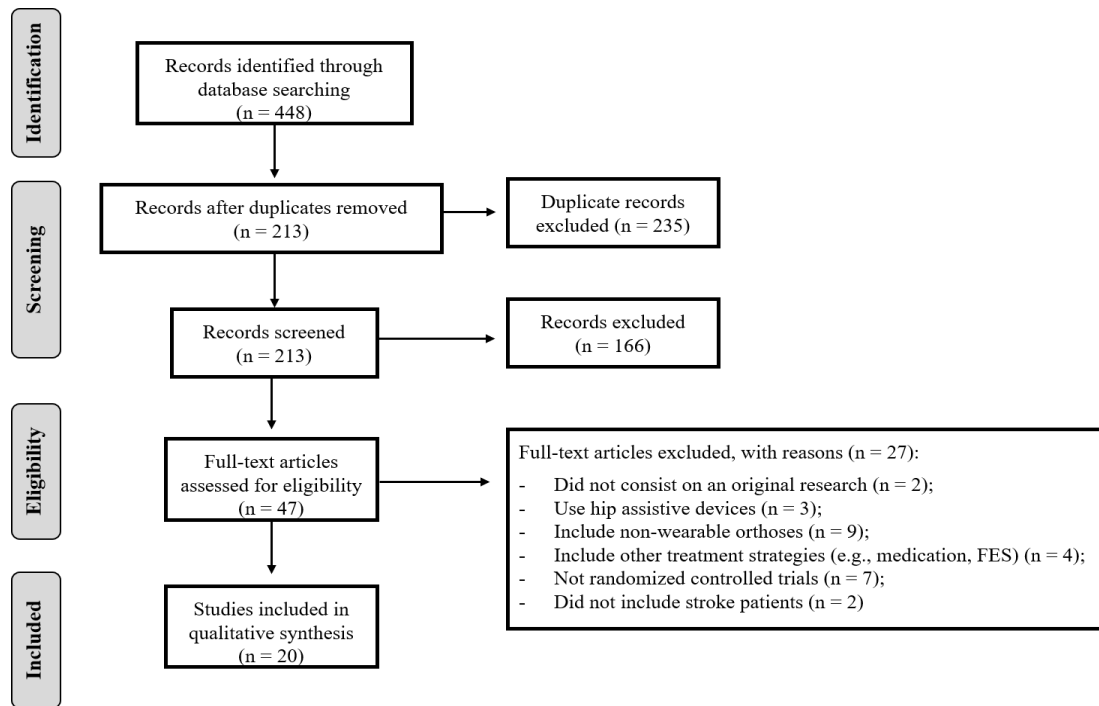
Figure 2.2- Flow chart of the literature search process.

What are the main inclusion and exclusion criteria?

Diverse inclusion and exclusion criteria were observed according to the rehabilitation goal. Nonetheless, the main inclusion criteria were: (i) suffered a single unilateral ischemic or hemorrhagic stroke [95], [98], [103] at least 6 months ago [86], [99], [103]–[107]; (ii) presented hemiplegia [75], [86], [95], [96], [104], [105], [108]; (iii) able to walk with the AFO or knee ankle foot orthosis (KAFO) safely, (iv) had not undergone any surgical procedures in recent months; and, (v) patients over 18 years old [85], [86], [94], [95], [98], [104]–[106]. Moreover, the participants should present a cognitive level sufficient to give informed consent, as also cognitive, visual, hearing, cardiac, and respiratory functions should be appropriate such that the patient is able to understand and follow the protocols [87], [94], [95], [98], [106], [109].

The studies excluded patients that presented additional orthopaedic or neurological deficits to the paretic or non-paretic limbs [75], [87], [98], [109], and morbid obesity that might impair the locomotion [107].

Which are the key methodologies for designing the clinical protocol in the orthosis-related studies?

Findings suggest that the design of the clinical protocol should approach the following methodologies. First, carry out **randomized trials** for enhancing the statistic quality and

properness of the clinical evidence. Second, before performing the clinical trials, the researchers or therapist must concede a **familiarization period** (ranging from 5 days to 2 weeks) to the participants that did not usually wear the prescribed orthosis such that they become familiar with the device and thus do not mis-analyze the adaptation period. Third, use of **footwear** during the assessments with and without orthosis to allow a more reliable comparison between the presence and absence of orthotic assistance, discarding the eventual corrective effect of footwear [86], [97], [103], [105], [106], [108], [110]–[112].

Which are clinical interventions endowed in the orthosis-related studies?

There is evidence that **functional tests** were the most endowed clinical interventions to investigate the functional locomotor recovery of post-stroke patients upon orthotic-based rehabilitation. In overall, the post-stroke participants underwent functional tests, such as **10 Meter Walking** [75], [85]–[87], [94], [95], [98], [99], [103]–[105], [108], [113], [114]; **Timed Up Go** [95], [96], [98], [99], [103], [106], [113]; **Timed Up and Down Stairs** [96], [98], [103], [106]; and, **Berg Balance Scale** [95], [113]. Participants could rest, generally, from 2 to 10 minutes between each trial [87], [96], [104], [105], [108].

Each session usually lasted from **30 to 60 minutes. There is no consensus for the repeatability** of the clinical intervention. It can present a short-term duration for 6 trials [85], [94], [104], [105] or can last for variable long-term periods: 8-week [75], 12-week [98], [107], [114], 24-week [99], [115], and 30-week [113].

What is the clinical evidence of passive orthosis in post-stroke gait recovery?

This systematic review found that the clinical evidence of post-stroke rehabilitation based on orthotic devices depend on the patient's disability level, the timing for prescribing orthosis and its configuration, and the underwent clinical intervention.

A dynamic KAFO [104] used for six trials and a hinged soft KAFO [75] applied for four weeks decreased knee hyperextension during the stance phase (i.e., reduces the *genu recurvatum*) [75], [104]. The dynamic KAFO increased gait speed and stride length [104].

The short-term and long-term therapy with AFOs improved (i) walking speed [85]–[87], [96], [103], [104], [109], [114], [116]; (ii) step length of the paretic limb [85]–[87], [105], [116]; (iii) peak ankle dorsiflexion at swing phase [94], [105], [114], and peak keen flexion [85], [114]. These kinematic achievements were related to the correction of foot-drop and *equinus* foot. Furthermore, AFO-based rehabilitation slightly enhanced motor ability regarding Timed Up

and Down [86], [95], [96], [103], Timed Up and Down Stairs [96], [103], and 10 Meter Walking Test [95], [114] and postural balance in Berg Balance Scale [86], [95]–[97].

2.3.3.Clinical Highlights and Future Directions

Orthotic-based gait rehabilitation may depend on the design of the clinical protocol, duration of the gait training, and the wearable orthosis configuration. An early prescription of an orthotic device can lead to more efficient locomotion recovery compare to a delayed one. Passive wearable orthoses can rectify abnormal motor conditions and lead to beneficial effects on the spatiotemporal outcomes. Nonetheless, the **functional motor ability recovery** upon passive orthosis-based rehabilitation **was not prominent** nor was the main clinical achievement. Metallic and rigid orthoses are less recommended to achieve an overall functional motor recovery.

Future researches are recommended to describe the clinical protocol following methodologic guidelines entirely, to investigate the long-term effects, and to endow clinical interventions with motor activities daily performed. Clinical studies involving wearable AOs should follow a randomized trial approach and engage further participants for a significative analysis of their clinical evidence, mainly for functional motor recovery.

2.4. Wearable Active Orthotic Devices: A Descriptive Review on Potentialities, Current Solutions, and Challenges

Although passive orthotic devices are often prescribed to improve gait deficiencies, they do not include active elements to accommodate for changing walking conditions or functional tasks [17], neither to face the intra- and inter-subject variable nature of motor disability [16]. On the other hand, technological directions on wearable AOs have pursued personalized, user-oriented, task-oriented and repetitive gait training focused on restoring function locomotor ability to perform daily motion activities [14].

2.4.1.Wearable AOs Potentialities

Wearable AOs are becoming an increasingly prominent clinical intervention to provide a **long-term functional motor recovery** through the replacing or restoring of a portion of the mechanical work performed by the biological muscle-tendons acting at the joints during locomotion [117]. They are challenged to partly emulate the skills of a trained therapist and to

actively and safely assist the human legged mobility following an AAN approach while enabling a **natural and compliant interaction** with the biological muscle-tendons [16], [17], [118] and a **continuous gait monitoring** [9], [119]. AAN physical rehabilitation paradigm means to assist the participant only as much as is needed to accomplish the desired motion activity [120].

AOs have been designed to exhibit a set of features, advanced regarding passive orthotic devices, such as: (i) provide an intensive and repetitive therapeutic training according to a real-time evaluation of the user's needs and disability level [9], [121]; (ii) tailor the mechanical assistance to accommodate different motor activities of higher metabolic energy consumption and gait speed variations [121]; (iii) incorporate the patient-active mode by taking into account the participant's active intention and the voluntary efforts [31], [120]; (iv) encourage the **user's participation** in the therapy since his/her active and high-intensity physical participation may facilitate the motor learning process and, thus, accelerating and enhancing the gait recovery [11], [15], [31], [118], [122]; and (v) adapt the mechanical assistance ensuring a compliant human-AO interaction through the real-time adjustment of the human-AO dynamics [123].

2.4.2. Current Wearable AOs

Advances in actuation, energy storage, miniaturized sensing, and embedded computational technology have led to the development of wearable assistive robotic devices [9]. This descriptive review was limited to wearable AOs that provide some means of augmenting power and oriented assistance of lower limb joints. AOs endowing active components that merely lock and unlock joints of an orthosis or those are not portable and do not stand-alone mechanically (e.g., treadmill-based devices, and AOs using tethered sources for power or computing) are not discussed. When compared to tethered assistive devices, the wearable AOs that could be worn during untethered functional locomotor activities, focusing on specific daily activities, which may benefit rehabilitation with the more considerable evidence and largest effect sizes [76].

Table 2.1 describes the wearable AOs (Figure 2.3) with focus on the actuation and sensor systems, the current development stage, application and clinical studies carried out. To date, **wearable AOs are mostly in a scientific development stage** with a limited commercial offer by Ottobock© [124]. The application of AOs with mechanical assistance at hip and knee joints

was divergence, including various locomotor system diseases, such as spinal cord injury (SCI), stroke, and poliomyelitis; whereas, ankle AOs were mainly applied to prevent drop-foot gait.

The issue of portability is one of the significant factors that limit the application of AOs outside of clinical therapy. The AOs' mass is a relevant feature for increasing the AOs' usability and affordability as well as the user's acceptance. From the results extracted, it was verified a variable body mass; Arizona Univ. AAFO weights 1.75 kg [18], [19]; the Univ. of Illinois Active AFO weights 1 kg plus the mass of the power supply system [20]; the body mass of most of the AOs varies from 2 to 3 kg [21], [22], [78], [125]; the mass of the knee AOs rounds 3.7 kg [76], [126], [127]; Achilles mass is 6.7 kg [128]; and, the heavier system has 12 kg [129].
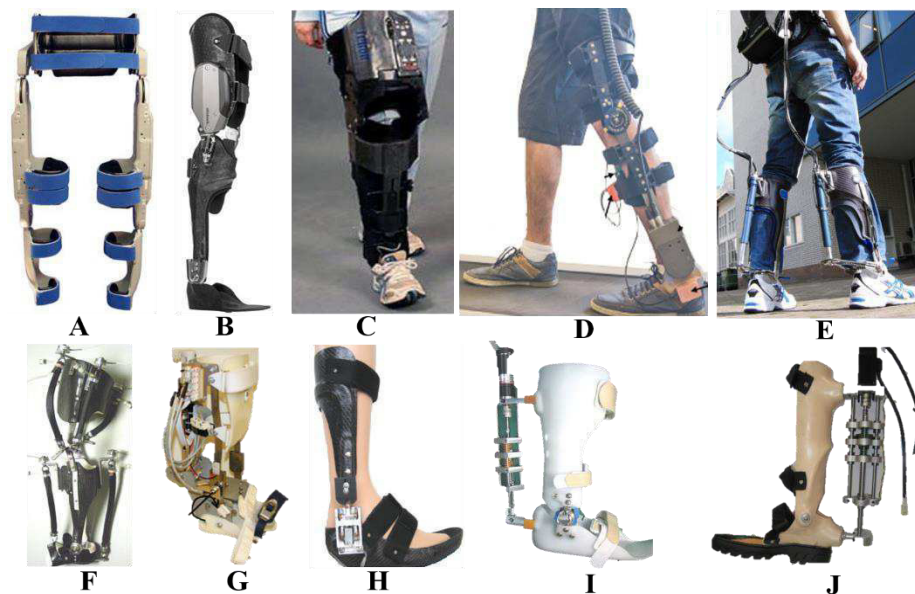
Figure 2.3- Wearable AOs. A:Vanderbilt Powered Orthosis [129]; B: C-Brace KAFO [124]; D: Tibion PK100 Knee orthosis [127]; E: LISSI Active AFO [130]; F:Achilles [128]; G:Michigan Active AFO [21], [131]; H:Arizona State Univ. AAFO [18], [19]; I:Univ. of Illinois Active AFO [20]; J:Yonsei University Active AFO [78].

Independently of the application, the design considerations for wearable AOs must account for compact, lightweight, time-effective actuation systems to provide net power to move the joints, and sensor systems and a control architecture to define the needed assistance to be applied to move the weakened limbs in desired gait patterns [120], [132]. Figure 2.4 shows the on-body location of the actuation system and sensor systems of the reviewed wearable AOs in this survey.

Table 2.1- Wearable AOs: actuation system, sensor system, application, development stage, and developed clinical studies.

Wearable AO	Actuation System				Sensor system		Application [Stage] [Total Mass]	Clinical Study	
	Actuator	Actuated joint			Sensor (Location)	Measurement Goal		Participants	Effectiveness
		Hip	Knee	Ankle					
Vanderbilt Powered Orthosis [129]	Electric	A	A	-	Potentiometer (Actuator)	Hip and knee angle	SCI [RS] [12 kg]	1 paraplegic male subject (35 years; 1.85 m, 73 kg) with T10 complete SCI	-High degree of step-to-step repeatability of hip and knee trajectories - Increased gait speed
					Accelerometer (Thigh)	NI			
C-Brace KAFO [124]	Electric	-	A	P	IMU (Knee)	Knee orientation Gait event detection	Poliomyelitis, Incomplete SCI (lesion between L1 and L5). No spasticity. [CA] [NI]	NI	NI
SCKAFO [126]	Electric	-	A	P	Load cell (Feet)	Gait initiation	Poliomyelitis [RS] [3.6 kg]	1 male subject with poliomyelitis (54-years; 1.68 m; 68 kg)	- Facilitated controlled knee flexion/extension -Gait pattern closer to the normal gait
Tibion PK100 Knee orthosis [127]	Electric	-	A	-	Force sensor (Feet)	Gait event detection	Post-stroke [RS] [3.7 kg]	3 post-stroke patients in chronic stage	-Improved sit-to-stand - Improved gait speed after a 4 week-training
					Encoder (Actuator)	Knee angle			
Tibion Knee orthosis [76]	Electric	-	A	-	Force sensor (Feet)	Gait event detection	Post-stroke [RS] [3.7 kg]	3 chronic stroke survivors (2 males, 1 female; 54.7 ± 15.9 years; 1.67 ± 0.9 m; 97.5 ± 5.97 kg)	Improved balance (12.6% for BBS), and functional mobility (12.0% for 6MWT and 16.7% for Emory Functional Ambulation)
					Encoder (Actuator)	Knee angle			
					EMG (Tibialis-anterior and gastrocnemius)	Tibialis-anterior and gastrocnemius muscular activity			
					Force sensor (Feet)	Gait event detection			
					Encoder (Actuator)	Ankle angle			
Univ. of Illinois Active AFO [20]	Pneumatic	-	-	A	Force sensor (Feet)	Gait event detection	Drop foot [RS] [1 kg plus power supply]	-	-

Wearable AO	Actuation System				Sensor system		Application [Stage] [Total Mass]	Clinical Study	
	Actuator	Actuated joint			Sensor (Location)	Measurement Goal		Participants	Effectiveness
		Hip	Knee	Ankle					
LISSI Active AFO [130]	Electric	-	P	A	IMU (Ankle)	Ankle angle	Drop foot [RS] [NI]	-	-
					EMG (Tibialis-anterior and gastrocnemius)	Tibialis-anterior and gastrocnemius muscular activity			
					Force sensor (Feet)	Gait event detection			
					Encoder (Actuator)	Ankle angle			
Univ. of Illinois Active AFO [133]	Pneumatic	-	-	A	Angle sensor (Ankle)	Gait event detection	Drop foot [RS] [NI]	1 plantarflexor impaired male subject (51years; 1.75 m; 86 kg) and 1 dorsiflexor impaired female subject (37 years; 1.57 m; 62 kg)	Active AFO: - provides functional assistance during gait and increased stance times -prevented the drop foot and maintained toe clearance during swing.
					Force sensor (Feet)				
Michigan Active AFO [21], [131]*	Pneumatic	-	A	A	EMG sensors (soleus, tibialis anterior, vastus lateralis, medial hamstrings)	EMG-based control	Neurologically injured patients [RS] [2.9 ± 1.3 kg]	-	-
					Load Cell (Actuator)	Actuator's force			
IPEC AFO [134]	Pneumatic	-	-	A	Potentiometer (Actuator)	Ankle angle	Drop foot [RS] [NI]	1 SCI subject	Prevented toe-drag during the swing phase
					Encoder (Actuator)	Ankle angle			
					Force sensors (Feet)	Gait event detection			
SMAFO [135]	Pneumatic compliant**	-	-	A	Encoder (Actuator)	Ankle angle	Drop foot [RS] [NI]	1 subject with right drop foot (80 kg)	Prevented the drop foot
					Force sensors (Feet)	-Gait event detection -Ankle torque			

Wearable AO	Actuation System				Sensor system		Application [Stage] [Total Mass]	Clinical Study	
	Actuator	Actuated joint			Sensor (Location)	Measurement Goal		Participants	Effectiveness
		Hip	Knee	Ankle					
Achilles [128]	SEA	-	-	A	Encoder (Actuator)	Ankle angle	Drop foot [RS] [6.7 kg]	-	-
MIT Active AFO [22]*	SEA	-	-	A	Potentiometer (Actuator)	Ankle angle	Drop foot [RS] [2.6 kg plus power supply]	2 male subjects with unilateral drop foot (62 years; 1.79 - 1.77m; 79 - 95 kg)	AO with variable-impedance: - provides more benefits for the treatment of drop foot compared to passive orthoses; -Kinematic pattern closer to healthy gait.
					Force sensor (Feet)	Gait event detection			
Arizona State Univ. AAFO [18], [19]	SEA	-	-	A	Encoder (Actuator)	Ankle angle	Post-stroke [RS] [1.75 kg]	3 stroke survivors (2 male, 1 female; 52±6.93 years; 84.67 ±7.3kg; 1.71±16.6 m)	-Increased cadence, ankle range of motion and push-off power; - Key ankle gait metrics closer to healthy values.
					Force sensors (Feet)	Gait event detection			
Yonsei University Active AFO [78]	SEA	-	-	A	Force sensors (Feet)	Gait event detection	Drop foot [RS] [2.8 kg]	3 male hemiplegic patients with drop foot (51±2.3 years, 1.64±4.2 m, 63.5±5.7 kg)	-Prevents drop foot; -Prevents toe drag; -Higher improvement in step length and gait speed than passive AFO
Univ. of Medical Sciences Active AFO [80]	SEA	-	-	A	Foot-switches (Feet)	Gait event detection, gait speed, stride duration	Post-stroke [RS] [NI]	1 post-stroke patient in the chronic stage (45 years, 1.78 m, 83 kg)	-Increased stride length, moments of the joints; - Improved standing and walking abilities compared to the passive orthosis
					Encoder (Actuator)	Ankle angle			

P – Passive; A – Active; '-' Not addressed; CA – Commercially Available; RS – Research Stage; NI: not indicated; *- Unclear the presence of tethered components

** Pneumatic compliant: Pneumatic stiffness adjustment

BBS: Berg balance scale; 6MWT: six-minute walk test.
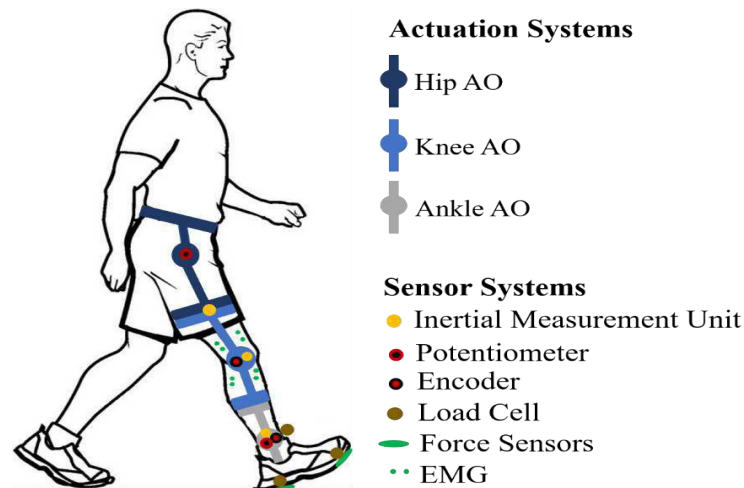
Figure 2.4- Overview of the on-body location of the actuation system and sensor systems considering the reviewed wearable AOs in Table 2.1.

Actuation Systems

The design principles of the actuation system, such as output force/torque, efficiency, and portability, has a crucial significance for the wearable AOs since they generally determine their performance. Actuation systems, such as electric motors, pneumatic muscle actuators, and series elastic actuator (SEA) were applied to move the AO by converting a source of energy into mechanical motion. Table 2.1 shows that the application of pneumatic and SEA actuators in wearable AOs centered on ankle assistance; whereas the electric actuators presented a more versatile lower-limb application. Further, some AOs combine passive and active mechanical joints, both approaching the sagittal plane. This literature analysis indicates that actual wearable AOs do not endow hydraulic actuators.

Electric actuators convert the electrical energy into mechanical torque. For most gait-related applications, they integrate an electric motor (e.g., direct current (DC) motors) and a harmonic drive to achieve the desired torques and control the provided torque and speed [136], [137]. As described in Table 2.1, electric actuators are the elected actuators for most wearable AOs, including the commercial AO. They are easily controllable and meet the criteria of necessary power with compact and portable solutions for wearable devices. Their main drawback is the low power-to-weight ratio, being essential to connect them to harmonic drive gears. Novel lightweight electric actuators are needed.

Pneumatic actuators include variable volume pressure chambers to convert a pressurized gas into mechanical torque. They provide a set of inherent benefits over electric ones, such as high force-to-weight ratio without the need of gearboxes, faster response time, smooth

actuation, and enable backdrivability [69], [137], [138]. Nevertheless, the control is more complex, and electric actuators are 92% more power efficient for robot-assisted walking applications [69]. Furthermore, this actuation technology showed to be bulky and is commonly associated with tethered systems [139]–[141].

Alternative **compliant actuation systems** to these conventional technologies are under investigation, such as **SEA**. SEA combine compliant structures (e.g., a spring) in the electro-mechanical actuators to convert compression of springs into mechanical torque [17], [69], [137]. SEA has essential features for wearable AOs since it can exhibit low impedance, low friction, shock tolerance, acceptable dynamic range, and may enable the user to feel more comfortable assistance [80]. Nonetheless, the use of these actuators in wearable AOs faces a limitation about the spring constant of the elastic element that is fixed, i.e., limited bandwidth [18], [22]. Research on compact and highly efficient mechanisms that allow varying the stiffness of series elastic components, a compromise between minimal endpoint impedance and high force control bandwidth, is needed.

Table 2.2 summarizes the advantages and disadvantages of each actuator.

Table 2.2-Advantages and disadvantages of actuators. Information obtained from [17], [69], [137].

Actuator	Advantage	Disadvantage
Electric	- Easily controllable - Power efficient - Portable	- Heavy - Requires gear reduction to achieve the desired torque - Noisy
Pneumatic	- Silent - Precise - Resistant to rough environments -High ratio actuator power to weight - High efficiency	- Low control bandwidth - Big dimensions (bulky) - Power lost in pressure drops - Issues on internal friction and leakage, intrinsic noise
SEA	- High force fidelity - Low impedance - Low friction	- Limited bandwidth (constant spring) - Stability limitations

Sensor systems

Active assistive devices rely on sensor systems' feedback to control the system according to the motion activity and to determine the assistance required by the user. The integration of the sensors on AOs has been limited to control purposes, including **encoders** [18], [80], [127], [130], [134], [135], **potentiometers** [22], [129], [134] and **Inertial Measurement Units** (IMUs) [124] for angle and angular speed estimation, and **load cells** [21], [125], [126] for motor

torque estimation and user-AO interaction torque estimation. To supplement the information available from AOs, **EMG sensors** [117], [142] for muscle activity analysis, and **force sensors** such as foot-switches and force sensitive resistors (FSRs) [20], [22], [78], [80], [127], [130], [132], [134], [135], for gait event detection, have been placed on the user's body. There is a common use of wearable sensors in wearable AOs.

Clinical Evidence

Preliminary, **short-term clinical trials** with neurological patients have been carried out to investigate the clinical effectiveness of wearable AOs. They involved patients with sequelae of SCI [129], [134] and poliomyelitis [126], stroke survivors in the chronic stage [18], [19], [76], [80], [127], and subjects with drop foot gait [22], [78], [135].

The studies had **small sample sizes**, varying from 1 to 3 participants, which may limit the effectiveness and robustness of their study findings. Inspection of the protocol designs across studies revealed **non-detailed clinical protocols** on clinical interventions and outcome measures, and there are considerable variations in the duration and frequency of sessions performed. The most applied outcome measures used to assess the capabilities of an AO for gait rehabilitation (to re-train the user's walking capability) and gait assistance (to bring the patient's walking ability closer to that of healthy subjects) are: walking speed, ROM, gait symmetry, and step cadence [143].

The **effectiveness of AO-based therapy is an open matter of research** [143]. The Tibion knee orthosis improved gait function in stroke survivors in terms of increased gait speed, sit-to-stand activity, balance, and functional walking ability [76], [127]. The gait training delivered by active AFOs, with actuation systems based on pneumatic and SEA, successfully prevented drop foot gait and maintained toe clearance during swing [22], [78], [133]–[135]. Consequently, these active AFOs augmented push-off power [18], [19] and increased stance timing [133], stride length [80], and cadence [18], [19]. Furthermore, the active AFO-based improvements in walking ability were more apparent and closer to healthy gait than the ones achieved by the passive orthoses [18], [19], [22], [78], [80].

In overall, the findings of these pilot clinical studies support that the motor learning boosted by the AO-based repetitive gait training has the potential to augment and extend the **effect sizes of the functional motor recovery** when compared to the passive orthosis.

2.4.3.Discussion on Technological and Clinical Challenges

To date, AOs proposed in the scientific field are still not able to foster personalized, user-oriented assistance and timely adaptive for dynamic daily environments nor to encourage the user's participation. Current technological challenges in wearable AOs include the integration of following technologies: (i) polyvalent, time-effective **assistive control strategies** tailored accordantly to the **current user's needs** and user-AO interface sensing to deliver a personalized assistance, (ii) unobtrusive **wearable biofeedback system** approaching less-cognitive effort to actively **encourage the user's participation**, (iii) **wearable sensor systems** and easy to apply gait analysis methodologies for the **real-time monitoring of the user's needs** evaluation and neuro-mechanical user's motor condition, and (iv) tools for the **recognition of user's motion intention** and current patient's disability level. Moreover, the approaches for modeling the human-AO interaction is not yet taking into account the symbiotic interaction between the user and the AO, a critical factor for ensuring compliant and efficient assistive control strategies [69].

These challenges are key innovation points that will be addressed by SmartOs system towards a repetitive, user-oriented gait therapy [14], [118]. For this matter, SmartOs aims to combine in an interoperable manner wearable sensor systems, biofeedback systems, and gait analysis tools into an AO such that it has the ability to adapt the delivered mechanical work according to a real-time evaluation of the user's needs while encouraging the user's participation in the therapy.

Despite much progress in robotic technologies, there is still needed to develop **lightweight**, **compact AOs** with a unique mechanical design, that reduces its mass and overall dimensions for lower metabolic expenditure and AOs with lightweight, compliant, low-power, easily controllable actuation systems that behaviours like human joints [10]. Computational mechanisms for AOs' mass compensation are proposed in SmartOs to be more compatible with the user's minimal metabolic requirements.

The challenges in sensor systems go through the development and integration of modular wearable time-effective sensor systems, easily flexible to incorporate a wide range of sensors, in a way that they provide quantitative and repeatable long-term assessments. To accomplish the AAN approach, current directions suggest that AOs should have a close-communication with sensor systems to enable the evaluation of the therapy in free-living environments [25],

[26], [144]. To address the previous two challenges, SmartOs pursues the development of a wearable motion lab with a set of modular sensor systems for the biomechanical and muscular motion analysis. It will enable the real-time, ambulatory monitoring of the neuro-biomechanical user's motor condition and decoding the user intended movement.

Studies have demonstrated that biofeedback systems can complement gait training in post-stroke conventional therapy by enhancing balance, gait symmetry, and weight bearing [145]–[147]. Nonetheless, the integration of wearable biofeedback systems (not limited to non-ambulatory rehabilitation as explored in [148]) with wearable AOs still has to be approached for encouraging and motivating the patient to improve gait pattern. SmartOs aims to tackle this problematic.

The increased complexity of AOs, given the combination of sensors, actuation, and biofeedback systems, control strategies, and computational tools for gait analysis, demands the development of frameworks with features such as modularity, interoperability, scalability, determinism, and effective response. Moreover, the design of **bioinspired control architectures**, following design principles based on human motor control, started to emerge [9]. The design of the framework and control architecture of SmartOs follows these technological challenges while guaranteeing users' safety.

C-Brace [124] is the closest solution of a personalized gait training therapy, by endowing technologies able to assess the user's motor condition and to determine how many assistance is needed. However, C-Brace does not apply methodologies to stimulate the user's participation in the motor activities as it is not indicated for patients with spasticity, a motor condition commonly observed after a stroke [149]. There a common limitation for the application of AOs in the presence of **spasticity** (Miller, Zimmermann, & Herbert, 2016). SmartOs proposes innovative initiatives on the **combined use of pharmacologic interventions with AOs in spastic gait recovery**, which is boosted by task-specific therapy and stretching during daily activities [11], [31], [68].

Recent tendencies have suggested the application of soft robotic devices that use soft materials such as textiles and elastomers to assist in a more comfortable, unobtrusive, and compliant means [7]. Nevertheless, further technological advances are needed since current soft robots include an off-board actuation unit comprising the ambulatory assistance [7], [150], or they require that the user wears the actuation system via a heavy backpack frame with a mass of 10.64 kg [151].

There are a set of challenges to be tackled regarding the short-term clinical trials with AOs performed with a limited number of participants. First, more controlled clinical research considering **randomized trials** is needed to determine AOs' clinical effectiveness and usefulness, which would also strengthen the literature in general support of AOs use for functional gait rehabilitation [152].

Second, there is a lack of the clinical evidence of AOs for the functional motor recovery, reducing the metabolic cost of the user, and the average muscular generated torques by the user. A literature review previously underlined the need for a standardized methodology to benchmark the AOs ability for gait rehabilitation and assistance [143]. Future clinical protocols should include a **significant number of participants**, who will undergo **repetitive functional tests and locomotor activities daily performed**, and consider **quantitative outcome measures**, such as Activity and Impairment ICF outcomes, and the patients and clinicians' perception through Participation outcome measures.

Third, clinical trials comprising **long-term evaluation** with several follow-up assessment timings are needed to investigate the long-term motor recovery. A long-term benchmark analysis with passive devices and other conventional rehabilitation therapies is an avenue to be approached considering homogenous control and study groups involving a significant number of participants.

Fourth, more research is needed to investigate (i) the **adaptation of the user** to powered assistance and (ii) the **interaction of the device with the user's body**, considering the physical interaction (i.e., how the lower limbs successful accomplish the desired motion) and neural interaction (i.e., how the nervous system will respond to the provided assistance) [143].

Further clinical challenges cover a significative evaluation regarding the usability, and the possible cognitive and physical burden regarding the AOs' use on daily living environments. The delineated clinical trials for SmartOs followed these challenges to achieve long-term, high-quality research towards gaining higher levels of clinical evidence of AOs' use and effects. Such clinical step may support the clinical decision for a more informed prescription of physical rehabilitation therapy.

2.5.Conclusions

Wearable AOs are promisor assistive devices to meet the requirements of a suitable physical rehabilitation intervention including a user-oriented, task-oriented, and repetitive gait rehabilitation in neurological conditions while enabling an objective gait assessment. Advances in these assistive devices may offer great potential for post-stroke gait rehabilitation, contributing to transformative changes in functional motor ability to perform daily locomotor activities, biomechanical performance, and boost cognitive motor control ability.

This literature research identified a set of technological and scientific challenges in wearable AOs, such as mechanical designs, actuation systems, sensor systems, assistive control strategies to strengthen their position as personalized rehabilitation or gait analysis tool. The survey allowed to conclude that the AO should endow a modular, time-effective framework able to combine, in an interoperable manner, wearable sensor systems, and biofeedback systems into an AO. Furthermore, real-time, robust gait analysis tools for recognizing user's motion intention and disability level have to been introduced into control architectures of AOs, considering the current directions for bioinspired and AAN control architectures. The AO design has to be fully wearable, lightweight, comfortable, and tightly shape the user's body. Additionally, there is an actual needed for personalized, long-term training solutions to treat spastic gait condition.

Lastly, there are still missing clinical studies considering a significant number of participants with stroke sequels. More efforts are needed towards a unified clinical methodology approaching functional motor exercises and using objective metrics to assess the long-term effectiveness of AO-based gait therapy. The gathered information in Chapter 2.2 and Chapter 2.3 may guide the designing of the clinical protocols attending to the actual demand for a benchmark scheme.

The design and development of SmartOs system, presented in Chapter 3, pursue to consider the highlighted scientific challenges and know-how. Continuous user involvement is essential in the design and development of personalized solutions, as proposed by SmartOs, ensuring that they match user needs and desires, as well as capabilities.

Chapter 3 – SmartOs System: Conceptual Design, Functionalities and Framework

This chapter describes the conceptual design and functionalities of SmartOs system, considering the gathered knowledge in Chapter 2. This information enabled to identify all SmartOs' modules for designing the modular framework in an interoperable and time-effective manner. Moreover, this chapter presents the performance evaluation of the modular framework considering a technical validation of the developed hardware and software interfaces.

3.1. Introductory Insight

Current technological and scientific directions on wearable AOs include the integration of wearable sensor and biofeedback systems and assistive control strategies driven by gait analysis tools for recognizing user's motion intention and motor disability [14]. SmartOs system addressed these directions. It includes wearable AOs linked to a full-lower limb Wearable Motion Lab (with biomechanical and muscular sensors) and a Wearable Biofeedback System. This innovative combination is advantageous over the state-of-the-art, and turns SmartOs an affordable system that can be applied for gait rehabilitation and ambulatory gait analysis.

For this purpose, a modular framework was designed and developed to approach a time-effective and robust integration of the identified SmartOs' modules. Further the SmartOs system integration, the framework allows the SmartOs system expandability for further gait analysis tools, assistive strategies, and sensor, biofeedback and actuation systems. The framework followed the bioinspired principles of a hierarchical control architecture to timely tune the assistive level delivered by AOs according to the evaluation of the user's needs, motion intentions and user-AOs interaction tracked in real-time by the Wearable Motion Lab and decoded by the Gait Analysis Tools. Finally, the framework includes mobile and desktop applications for the intuitive configuration of the SmartOs' modules and functionalities and visual monitoring of the user-AOs motion, respectively.

3.2. Conceptual Design and Functionalities

SmartOs is a new **multi-functional**, **modular, wearable active orthotic assistive system** able to act and cooperate closely with human beings to approach AAN rehabilitation. Consequently, the design of SmartOs followed the functional and technical **end-users driven requirements** to increase the user's acceptability and to foster a reliable and safe gait rehabilitation. End-users and clinicians have been involved in consolidating a set of requirements that has triggered and fine-tuned the development of SmartOs.

The clinical initiatives of SmartOs approach (i) task-oriented and repetitive gait training according to the user's needs; (ii) long-term biomechanical, energetic-efficient and functional motor recovery; (iii) abnormal gait pattern correction, in particular, drop foot gait; (iv) encouraging the user's active participation in the gait training and thus accelerating gait recovery and likely enabling a cognitive ability improvement; and, (iv) objective gait analysis of the user's motor condition by tracking biomechanical and muscular information. Figure 3.1 presents the conceptual design of SmartOs, highlighting the included modules to fulfil these clinical functionalities.
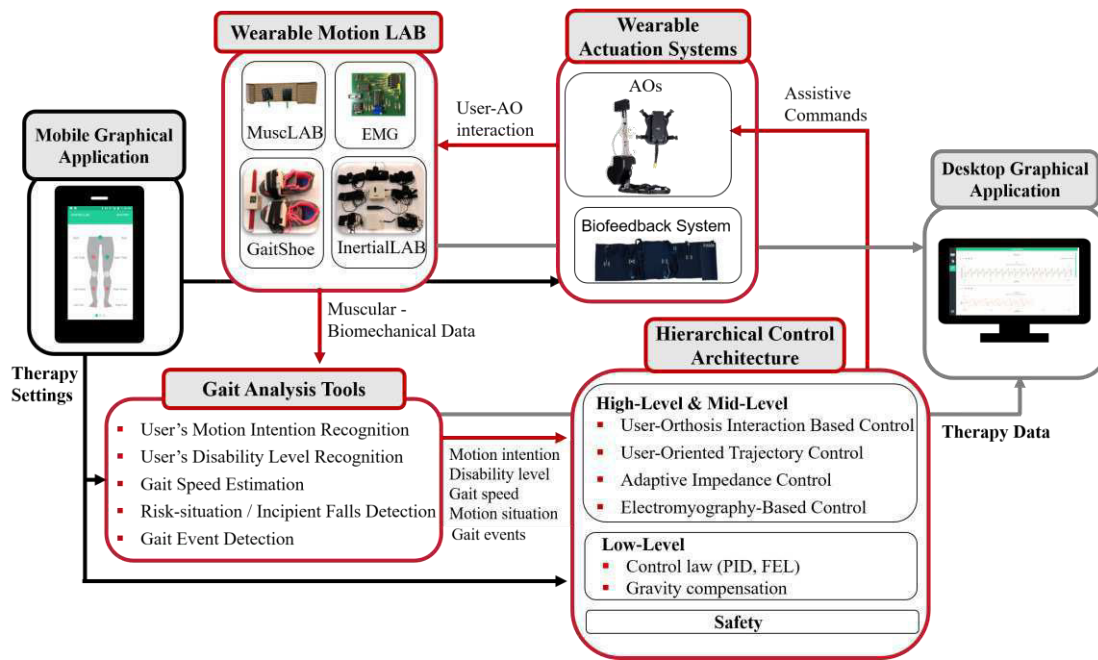
Figure 3.1- SmartOs conceptual design.

Wearable Motion Lab includes a set of stand-alone, low-cost, self-calibrated wearable sensor systems, detailed described in Chapter 4, to monitor the immediate user's muscular-biomechanical data during daily performed locomotor tasks. The sensors' information allows tailoring in real-time the personalized therapies according to the specific user's motor condition and is the base for the implementation of the gait analysis tools, as summarizes Table 3.1.

Table 3.1-Application of sensor data monitored by the Wearable Motion LAB in the Gait Analysis tools

Wearable Motion LAB		Gait Analysis Tool
Sensor system	*Sensor Data*	
GaitShoe	Force-ground contacts	Gait event detection
	Foot's kinematics (angle, angular speed, acceleration)	Gait speed estimation
		Joint angle estimation
		User's disability level recognition
MuscLAB Surface EMG	Lower limb muscles' activation	User's disability level recognition
InertialLAB	Kinematics (angle, angular speed, acceleration) of lower limb joints (ankle, knee, hip) and segments (foot, shank, thigh, trunk)	Joint angle estimation
		User's disability level recognition
		User's motion intention recognition
		Risk/incipient falls detection

SmartOs incorporates a set of automatic, time-effective **Gait Analysis Tools** to detect gait events (described in Chapter 5), to recognize user's motion intention (described in Chapter 6) and disability level, and to detect incipient falls and other risk situations. These gait tools are processed into the **Hierarchical Control Architecture**, detailed presented in Chapter 8, to

generate user-oriented assistive commands. This architecture also endows safety mechanisms to safeguard the joint integrity, which may interrupt the assistance as and when needed. Furthermore, SmartOs embodies two sources of **Wearable Actuation Systems**, the AOs and the wearable biofeedback system, and two user-friendly **Graphical Applications**, described below.

3.2.1.Wearable Actuation Systems

Currently, SmartOs's framework integrates **two AOs**, the ankle (PAFO) and knee (PKO) right-side modules of the lower-limb H2-exoskeleton (Technaid S.L., Spain). Figure 3.2.A illustrates the two AOs that only assistance in the sagittal plane for **gait speed** ranging from **0.5 to 1.6 km/h**. Each AO has the following embedded sensors: (i) precision **potentiometer** (resolution of 0.5°), the angle position sensor; (ii) **strain gauges** (four strain gauges connected in a full Wheatstone bridge, resolution of 1 Nm), the user-AO interaction torque sensor; and, (iii) **hall effect sensor**, used to track the motor's angular speed, the motor's current and torque. PAFO also integrates two **FSRs** at the heel and toe to measure the ground reaction force. Moreover, three **IMUs** (MPU-6050, InvenSense, USA) were integrated into AOs for gravity compensation and gait event analysis.

The actuation system consists of an **electrical actuator** (flat brushless DC motor EC60-100 W, Maxon) coupled to a **gearbox,** the CSD20-160-2A strain wave gear (Harmonic Drive), with a ratio of 160:1, providing an average **torque of 35 Nm** and peak torques of 180 Nm. The brushless DC motor was selected given its advantages in the DC motors category for wearable applications, including higher efficiency, more torque density, reduced noise, and reduced electromagnetic interference. The mechanical structure is made of stainless steel and type 7005 aluminum. More technical details regarding the AOs can be found in [48], [154].

The Control Area Network (CAN) was used to establish the communication among the AOs and the Hierarchical Control Architecture, given its strict determinism, data collision avoidance, optimized data transfer, and multiple-access points that allow new AOs to be easily connected to the physical layer [153].

Additionally, SmartOs includes a **Wearable Biofeedback System** with a minimum-to-null cognitive and physical effort for fostering time-discrete vibrotactile/tactile and visual stimuli. **Vibrotactile and visual stimuli** have been explored. The wearable vibrotactile stimuli-based waistband (actuation system formed by a coin eccentric rotating mass vibrotactile motor and

DRV2605 haptic drivers (Adafruit®, USA)) will provide time-discrete vibrotactile stimuli in the lower trunk (at navel and spine zones) and paretic limb. For visual stimuli, the ORA-2 augmented reality glasses (Optinvent, France) is being used.

❶ STM32F4-Discovery	Ⓐ CAN Cable	❶ Vibrotactile system	
❷ Electronic board of battery	Ⓑ Potentiometer	❷ ORA-2 Smart Glasses	
❸ LiFePO4 battery	Ⓒ Motor & Gearbox		
❹ AO: PAFO & PKO	Ⓓ Strain Gauge		
	Ⓔ Embedded IMU		
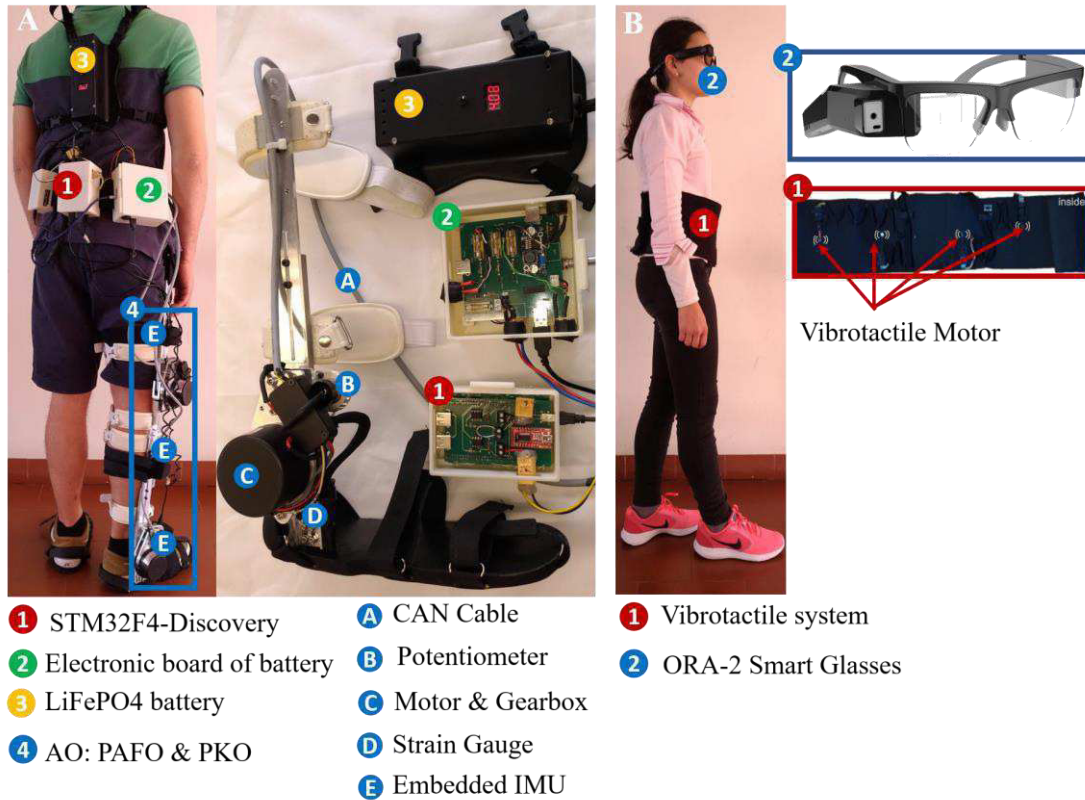
Figure 3.2- Wearable Actuation System: **A:** Wearable AOs. **B:** Wearable Biofeedback System.

3.2.2.Graphical Applications

Two user-friendly graphical applications (Figure 3.3) were designed and developed to enable the **intuitive use** and full abstraction from low-level interfaces and technical aspects of the SmartOs' modules in both laboratory and clinical context. The applications, integrated into SmartOs via wireless technology, were designed to be intuitive in terms of usability considering the **therapist and technical as possible users**. Furthermore, the applications enable easy integration of any new modules or settings.
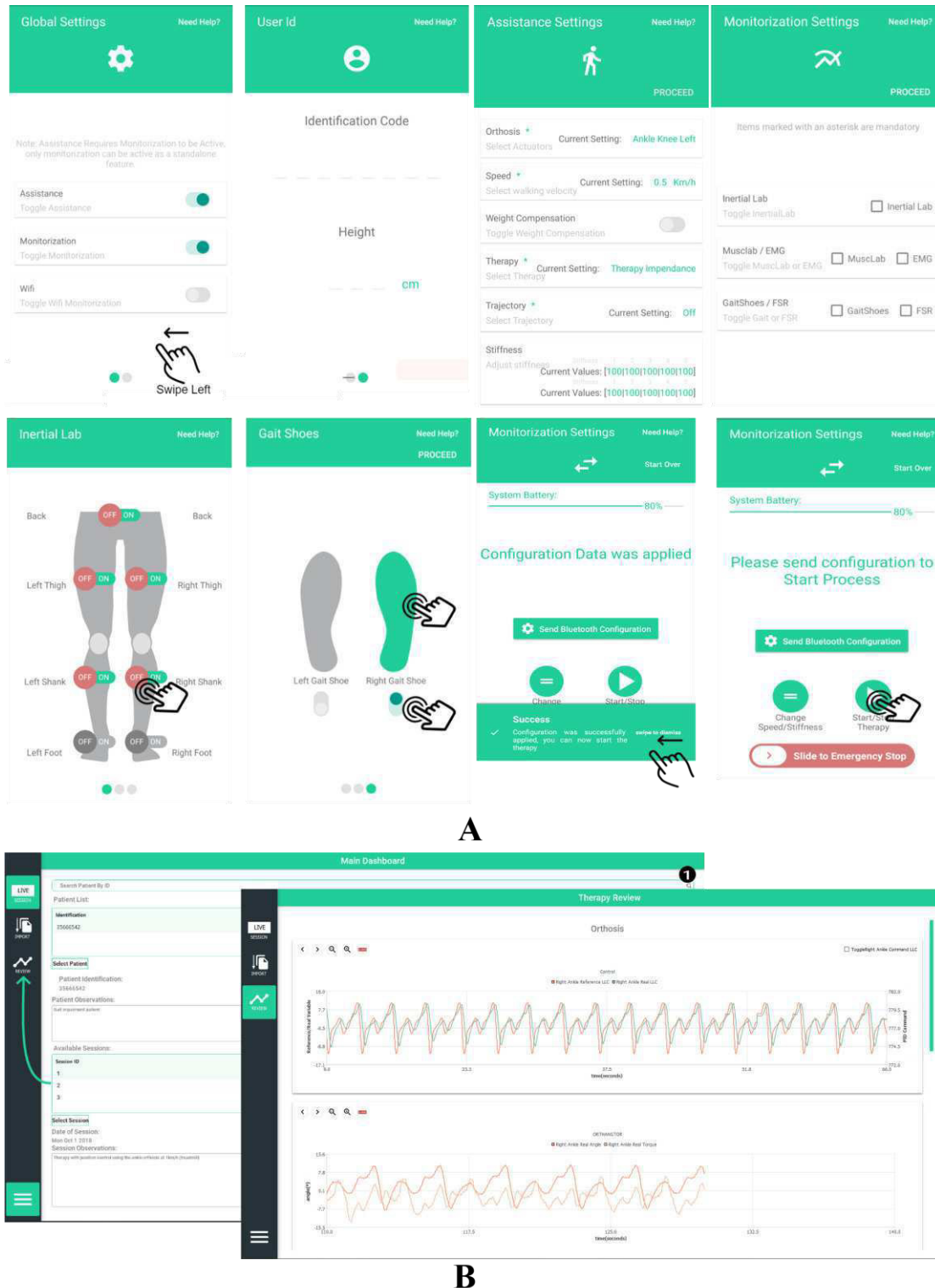
Figure 3.3- Main menus of Graphical Applications. **A**: Mobile Graphical Application. **B**: Desktop Graphical Application.

The **Mobile Graphical Application** enables the intuitive set-up of all SmartOs' modules, allows the **system's configuration to different subjects and therapies,** and provides the system's status for end-users. This application fulfills requirements such as (i) streamlined and

guided interaction for a fast, natural, walk-through navigation, and (ii) use of explicit graphical components for being more easily user's understandable. It was developed in Android operating system (tested in multiple devices, ranging from Android 5.0 to 8.1.) following configurations dependencies and with a protection layer such that the therapies are configured without allowing invalid functional configurations that might compromise the physical integrity of both the user and system. All messages are transmitted via Bluetooth protocol to the central controller unit of SmartOs. Each application's layout was made up of Widgets declared in Android XML vocabulary. Figure 3.3.A presents a set of menus available in this application.

The **Desktop Graphical Application** (Figure 3.3.B) was developed using Qt platform. It focuses on **real-time monitoring** at 100 Hz of all data generated along with therapy in a dashboard design tailored to the user. Additionally, it manages all collected data over therapy session and user's information for **logging** in JavaScript Object Notation (JSON) format into a **local database**, the SQLite. This application was designed considering minimal input from the user, automatic displaying, and human-readable visualization graphical tools. The WiFi protocol was used to establish communication with the central controller unit of SmartOs.

Both applications were scored with **"Good" to "Excellent"** range of **intuitiveness** and **ease of use** and navigation according to the System Usability Scale questionnaire by eight non-technical users. More results are presented in [155].

3.3. Modular Framework for SmartOs' Modules Integration

In this thesis, it was designed, developed, and validated a modular, real-time, interoperable, power- and time-effective, fully wearable framework to enable an effective and safety integration and interaction of SmartOs modules.

3.3.1. Framework Requirements

The framework should consider the ambulatory functionality of SmartOs, which opens a set of new requirements as follows. First, the framework should embody **wearable modules** to be usable by end-users with different heights, body mass, and morphologies. Second, it is desirable that the framework is power-effective using a wearable power supply unit able to supply at least eight hours for prolonged recording sessions. Third, the framework should be **modular** in terms of hardware and software interfaces to facilitate the integration of more stand-alone modules and functionalities. Fourth, the framework should provide a **time-**

effective communication between all modules and include software interfaces capable of hitting all real-time deadlines with small latency (determinism). Additionally, the framework should be **hierarchically structured** and should respect the distinct real-time constraints of the hierarchical control architecture. This lead to the development of the framework with a non-centralized architecture.

Furthermore, the framework should include a **central storage unit for data logging**. Lastly, it should provide intuitive interaction with SmartOs' functionalities and modules and visual feedback regarding therapy progress. The integration of mobile and desktop graphical application allows fulfilling these two requirements.

3.3.2. Framework with Non-centralized Architecture

The framework was designed following a **non-centralized architecture,** including different development boards for managing the SmartOs' modules. This architecture includes a single **Central Controller Unit** (CCU) for running Gait Analysis Tools, high-level controllers of Hierarchical Control Architecture, and the external communication with the Graphical Applications. Moreover, the architecture includes development boards with less-computational performance, namely: (i) **Low-Level Orthotic System** (LLOS) that handles the AOs, the low- and mid-level controllers of Hierarchical Control Architecture, and embedded IMU sensors; (ii) **Wearable Motion LAB** (WML) that manages the Wearable Motion Lab, namely InertialLAB, GaitShoe, MuscLAB and EMG system; and (iii) **Wearable Biofeedback System** (WBS) that handles the biofeedback systems. The interfaces of WBS are out of the scope of this thesis.

Figure 3.4.A presents the developed non-centralized architecture. The separation of the low-level from the high-level modules favours the management of the SmartOs' performance by not affecting the hard-real-time requirements of the low-level modules. Also, a hierarchical safety mechanism can be easily controlled in case of a system failure at any part of the SmartOs' framework. Moreover, this approach emphasizes the expandability of the framework.
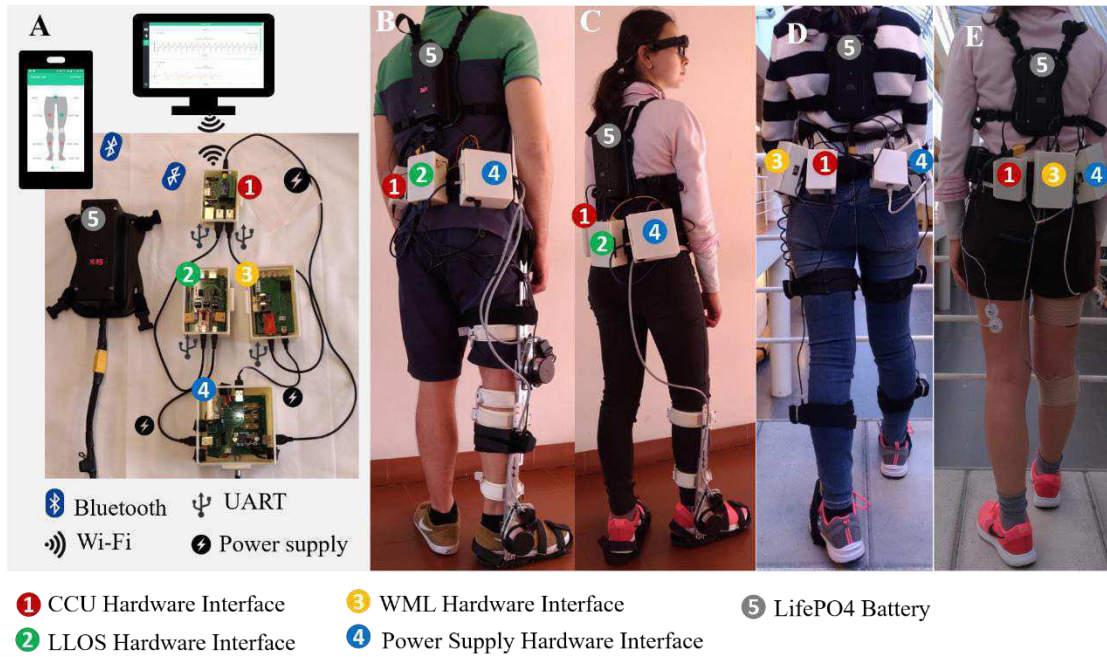
Figure 3.4- **A**: Representation of SmartOs non-centralized architecture and interfaces for SmartOs integration. **B**: LLOS interfaces for AOs and embedded sensors. **C**: WBS interfaces. **D**: WML interfaces including GaitShoe and InertialLAB. **E**: WML interfaces including MuscLAB and EMG system.

3.3.3.Framework: Hardware Interfaces

This subchapter provides an overview of the hardware interfaces developed for integrating SmartOs' modules. The **CCU** includes a **Raspberry Pi 3** (Raspberry Pi Foundation, UK), a single-board computer with a quad-core processing unit (1.2 GHz, 64 bit CPU) and 1 GB of RAM. The built-in wireless LAN and Bluetooth connectivity were used for communicating with desktop and mobile graphical applications, respectively. Three universal serial bus (USB) ports embedded in the board were used for serial port communication with LLOS, WML, and WBS. The available peripherals for SmartOs' modules communication together with the high-speed capabilities and low-dimensionality (56x85x16 mm) made the Raspberry Pi 3 suitable for CCU.

The **LLOS'** hardware interface (Figure 3.4.B, 65x96x31 mm) integrates a **CAN interface** (using XT90 connector) and **inter-integrated circuit** (I^2C) **interface** (using USB connector) to interface with the AOs and IMUs (MPU-6050, InvenSense, USA), respectively.

The **WML** (Figure 3.4.C and D, 65x100x34 mm) includes the **I^2C interface** (using ethernet connector) for communication with the InertialLAB, the **serial peripheral interface** (SPI) to control the radiofrequency (RF) module (NRF24L01+) for wireless communication with GaitShoe, and **analog-to-digital converter** (ADC) **interface** (using 2-pin connector) for MuscLAB and EMG system. LLOS and WML include a Universal Asynchronous Receiver/Transmitter

49

(UART) interface (set at 230400 bps) in the direct memory access mode for high-performance communication with the CCU using USB converter (FT232RL FTDI) given its easy plug-in with the USB ports of Raspberry Pi 3.

The hardware interfaces of LLOS and WML are handled by the **wearable STM32F4-Discovery development board** (STMicroelectronics, Switzerland) a power-cost effective solution centralized on the STM32F407VGT microcontroller (ARM® Cortex®-M4 32-bit core), running at 168 MHz. SmartOs' framework takes advantage of features of this board, such as high-speed embedded memories (flash memory up to 1 Mbyte and SRAM up to 192 Kbytes), a number of I/Os and peripherals with standard communication interfaces (CAN, SPI and I^{2}C). Lastly, this development board presents an acceptable dimensionality (80x100x25 mm) for wearable applications as this one.

The **power supply system** (Figure 3.4.A) includes a lithium iron phosphate battery (LifePO4, 22.4 VDC, 12 Ah), which enables at least 8 hours of autonomy, and a hardware interface to power up all SmartOs' modules with 5 V. The battery's body mass (781 g) and dimensions (161x49x47 mm) are acceptable to be used on the user's back.

3.3.4. Framework: Software interfaces

This sub-chapter discloses a general overview of the framework software interfaces. A more detailed description is provided in Appendix D.

A specific SmartOs' communication protocol with a standardized message structure was defined to (i) establish the communication with/from CCU; (ii) exchange data between the SmartOs' modules with efficiency; (iii) allow for easier integration of any new module; and, (iv) facilitate the detection and reporting of errors and warnings. Three types of SmartOs messages were specified: (i) **command messages** to set-up any configurable aspect of the SmartOs' modules; (ii) **data messages** containing data from the sensors, controls, and/or gait analysis tools; and, (iii) **status messages** briefing about the executed commands, including success messages, error messages, and current status of SmartOs (e.g., battery level). The command messages follow a top-down approach from the mobile graphical application to CCU, and from this to the LLOS and WML, as illustrated in Figure 3.5. On the other hand, status and data messages have a bottom-up approach, except for some LLOS configurations for specific assistive control strategies.

The **CCU** interfaces all SmartOs' modules and graphical applications and executes the high-level methods on Ubuntu Mate OS. Given the complexity of distributed systems, the CCU was implemented in C++ language, which allows: (i) object-oriented programming; (ii) complete control over memory management; and (iii) scalability to expand the system following a modular and standard software design. The POSIX Pthread Libraries were used.

The software architecture of CCU (depicted in Figure 3.5) was organized into five main software modules (classes), namely ***ExternalDevice*** (communication with external devices to CCU), ***CentralController*** (setup, start and stop all configurable modules), ***HLController*** (manages and executes high-level controllers), ***SmartGaitAnalysis*** (handles and executes gait analysis tools), and ***Log*** (data logging in JSON file and Desktop Graphical Application).
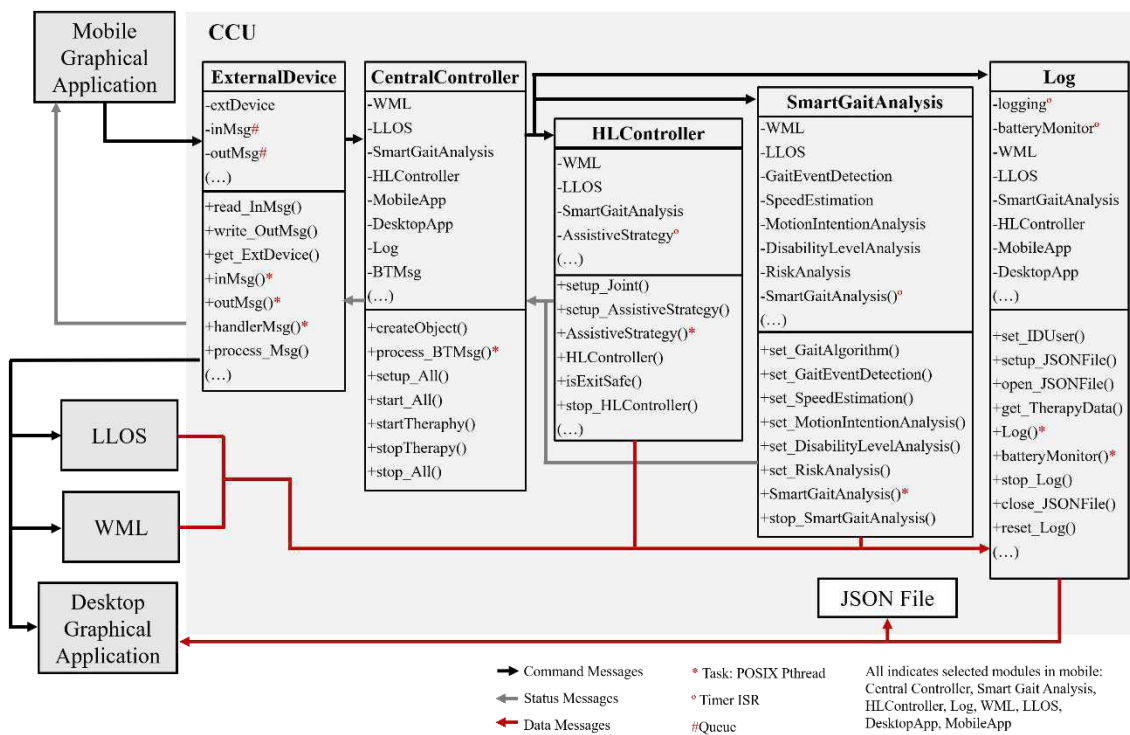
Figure 3.5- Software architecture of CCU. Diagram of main classes in CCU and flow of SmartOs' messages between CCU and its external devices.

For the **software architecture of LLOS and WML** (Figure 3.6), the programming language selected was C language. The middleware layer of this architecture incorporates the freeRTOS real-time operating system and hardware abstraction layer (HAL) libraries, namely STM32Fx HAL drivers (e.g., CAN, ADC, I^{2}C, and SPI drivers). The freeRTOS provides the facilities for multitasking, concurrent programming towards the development of an effective framework and a set of libraries that allow easy definition and use of tasks, queues, and semaphores.
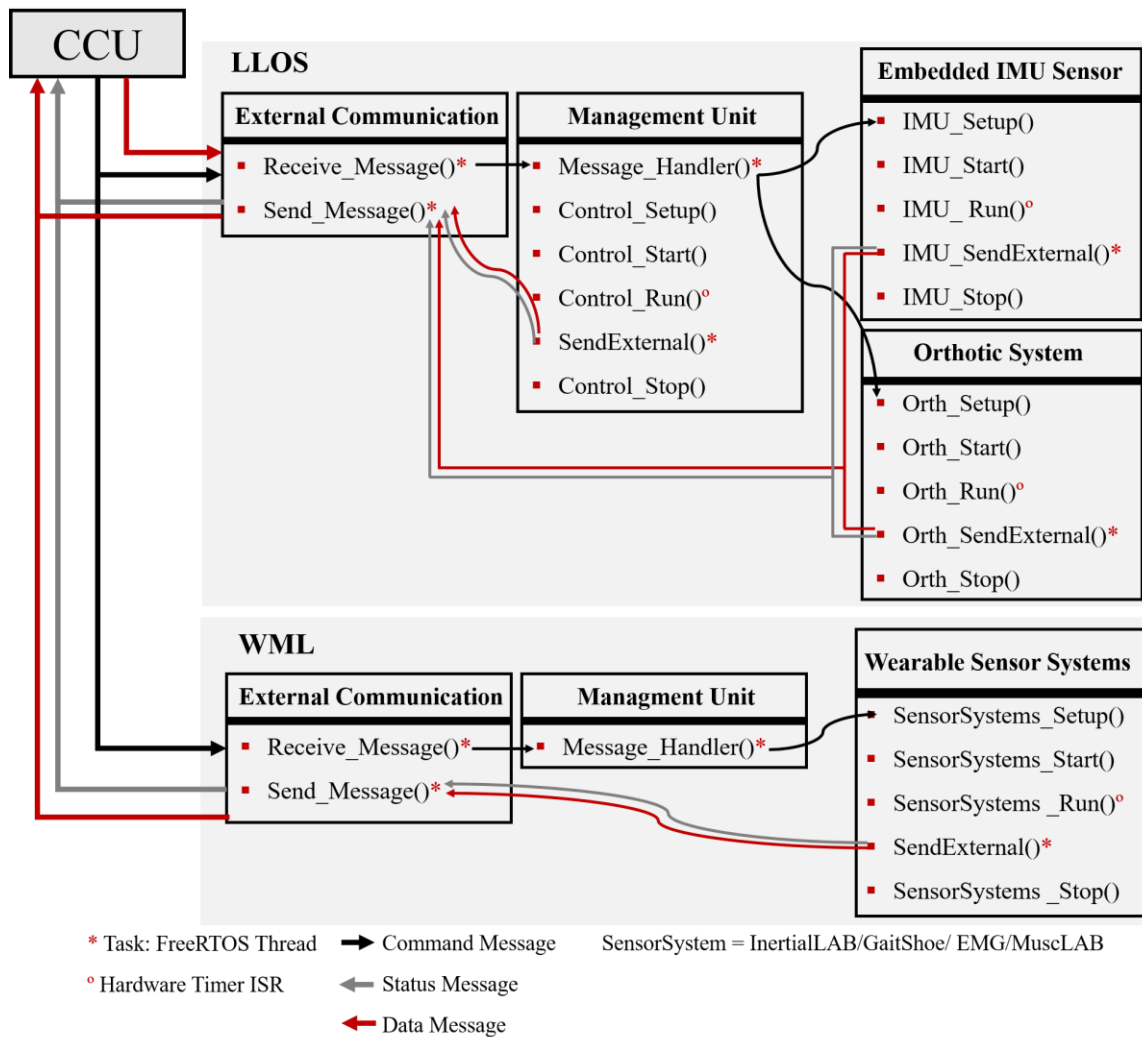
Figure 3.6- Software architecture of LLOS and WML and flow of SmartOs messages.

The software architecture of LLOS and WML endows four and three main software modules, respectively, as follows. ***External Communication*** handlers the communication from/to CCU; ***Management Unit*** handles command messages and, in the LLOS, it executes the mid- and low-level controls; ***Embedded IMU sensor*** manages the sensor data acquisition and processing from IMUs; ***Orthotic system*** setups, starts and stops AOs; and, ***Wearable Sensor System*** setups, starts and stops all wearable sensor systems and manages sensor data acquisition and processing. The priority of the real-time software interfaces was adjusted such that the hardware timers were configured to meet the time requirements of LLOS and WML.

The real-time processes of the CCU, WML, and LLOS are executed to meet the time requirements listed in Table 3.2. The data acquisition and processing of InertialLAB, GaitShoe, MuscLAB, and embedded IMUs of LLOS are executed every 10 ms (100 Hz), attending to the fact that the high energy frequencies of human biomechanical gait data ranging from 0.25 to 25

Hz [156]. On the other hand, we set the data acquisition and processing of the EMG system (WML) to 1 kHz since the bandwidth of EMG measures may reach up to 500 Hz [157].

All data messages are exchanged every 10 ms, except the data messages from CCU to LLOS, that contain data of high-level controllers timing-specified according to the gait speed. Additionally, the mid-level control loop runs at 100 Hz attending to the usually applied frequency for gait application [156]; whereas the low-level control loop runs at 1 kHz, a frequency ten times higher than the mid-level controller, to minimize the delayed actuator response. Finally, all status and command messages present an asynchronous operating rate given their singular occurrence during the therapy configuration or random occurrence during real-time therapy.

Table 3.2- SmartOs' time requirements for real-time therapy.

SmartOs Modules	Software Modules	Software Routine	Required Time (ms)
LLOS	Embedded IMU Sensor	IMU_Run	10.0
		IMU_SendExternal	10.0
	Orthotic system	Orth_Run	10.0
		Orth_SendExternal	10.0
	Management Unit	Control_Run*	1.0
		Control_SendExternal	10.0
WML	Wearable Sensor System	InertialLAB_Run	10.0
		InertialLAB_SendExternal	10.0
		GaitShoe_Run	10.0
		GaitShoe_SendExternal	10.0
		EMG_Run	1.0
		EMG_SendExternal	10.0
CCU	HLController	AssistiveStrategy (Data Messages, CCU → LLOS)**	51; 58; 65; 72
	Log	Log (Data Messages, CCU → Desktop Application)	10.0
	ExternalDevice	handlerMsg (Data Messages, CCU ↔ Mobile Application)	Asynchronous

*The hard-real-time conditions are presented since *Control_Run* includes the mid-level and low-level controllers running at 10 ms and 1 ms, respectively.

** Timing-specified according to the gait speed

3.3.5. Framework: Performance Evaluation

The performance of the framework was inspected through a technical validation concerning computational and energetic effectiveness. This evaluation aims to verify whether the

proposed non-centralized architecture comprises the real-time computational and energetic performance of SmartOs system since the use of several development boards may introduce some latency and may increase power consumption.

Validation Setup

The validation was performed along 50 gait cycles with the experimental setup defined for the LLOS and WML modules, as follows. For LLOS, the setup included the (i) PAFO configured with user-oriented trajectory control strategy (described in Chapter 7.4) at the maximum gait speed (1.6 km/h), (ii) right foot IMU running the gait event detection tool (described in Chapter 5), (iii) two IMUs executing the gravitational compensation (described in Chapter 7.2.3). The setup of WML included the InertialLAB, GaitShoe, and EMG system. As the use of EMG system and MuscLAB is mutually exclusively in SmartOs system, the WML's validation involved the EMG system given its higher computational demanding when compared to MuscLAB.

The validation duration (50 gait cycles) was set to consider a sufficiently long period to investigate the variability of the framework along the gait cycle, instantaneous effects, and the ramp-up time.

Data Collection and Performance Metric

During the validation, **power consumption measures**, involving current consumption and power consumption, and **computational time measures**, including (i) call periods of the timers (all routines named as *Run*) and tasks (all routines named as *SendExternal*), and (ii) latency of tasks and timers, were collected for a posterior analysis. A current sensor (INA219) was connected to the development boards of LLOS and WML by I^{2}C interface to measure the current and power consumed by the LLOS and WML during the experiment. The computational time measures were collected by setting the available timers to 1 μs, so the call periods and latency of *Run* and *SendExternal* procedures of LLOS and WML could be validated. This approach was preferred to available time measurement tools to add the less overhead possible to the real-hard time processes of LLOS and WML.

The mean, standard deviation, maximum, and minimum values of the collected computational and consumption measures were computed to evaluate the framework performance under real-time conditions. The standard deviation metrics enables to analyze the framework performance's variability along the gait cycle, whereas the maximum and minimum values

were determined to investigate the occurrence of instantaneous effects. Moreover, the root mean square error (RMSE) of all call periods was determined considering the measured call period and the defined call period (listed in Table 3.2).

Results and Discussion

Table 3.3 and Table 3.4 present the results of the computational performance of LLOS and WML, respectively. This evaluation only considered the timers and tasks evocated repeatedly in real-time to investigate the effects of a non-centralized architecture during real-time therapy.

By analyzing Table 3.3, lower RMSE values (0.005 < RMSE < 0.289 ms) related to the call period measures were reported, indicating that the time requirements of LLOS (listed in Table 3.2) were met. Further, there is variability in the call period times along the gait cycle, as shown by maximum and minimum values presented in Table 3.3. This variability was more evident during the system initialization. The time variability was mostly observed for *SendExternal* task when compared to the respective *Run* routine likely due to highest execution priority of *Run* routines than *SendExternal* tasks.

Table 3.3- Computational performance evaluation of LLOS. Mean, standard deviation (STD), maximum (Max), and minimum (Min) time values, and RSME of the call period of tasks and timers of LLOS.

Software Module	Software Routine	Measure				
		Description	*Mean ± STD (ms)*	*Max (ms)*	*Min (ms)*	*RMSE (ms)*
Embedded IMU Sensor	*IMU_Run*	Call period	9.999 ± 0.005	10.189	9.963	0.005
		Latency	1.585 ± 0.016	1.686	1.499	-
		Acq_Proc Latency	1.575 ± 0.016	1.622	1.490	-
	IMU_SendExternal	Call period	9.998 ± 0.035	10.459	9.560	0.035
		Latency	0.088 ±0.039	0.415	0.007	-
Orthotic system	*Orth_Run*	Call period	9.999 ± 0.011	10.310	9.942	0.011
		Latency	0.009 ± 0.0004	0.015	0.009	-
	Orth_SendExternal	Call period	9.998 ± 0.053	10.406	9.565	0.053
		Latency	0.021 ±0.03	0.370	0.011	-
Management Unit	*Control_Run*	Call period	0.999 ± 0.0005	1.010	0.993	0.0005
		Latency	0.219 ± 0.013	0.255	0.008	-
		ML_LL Latency	0.079 ± 0.062	0.255	0.003	-
	Control_ SendExternal	Call period	9.998 ± 0.289	10.738	8.213	0.289
		Latency	0.081 ± 0.243	0.311	0.015	-

Figure 3.7 presents a graphical distribution of the LLOS' computational performance as an instance of the higher-complexity moments of LLOS along the gait cycle.
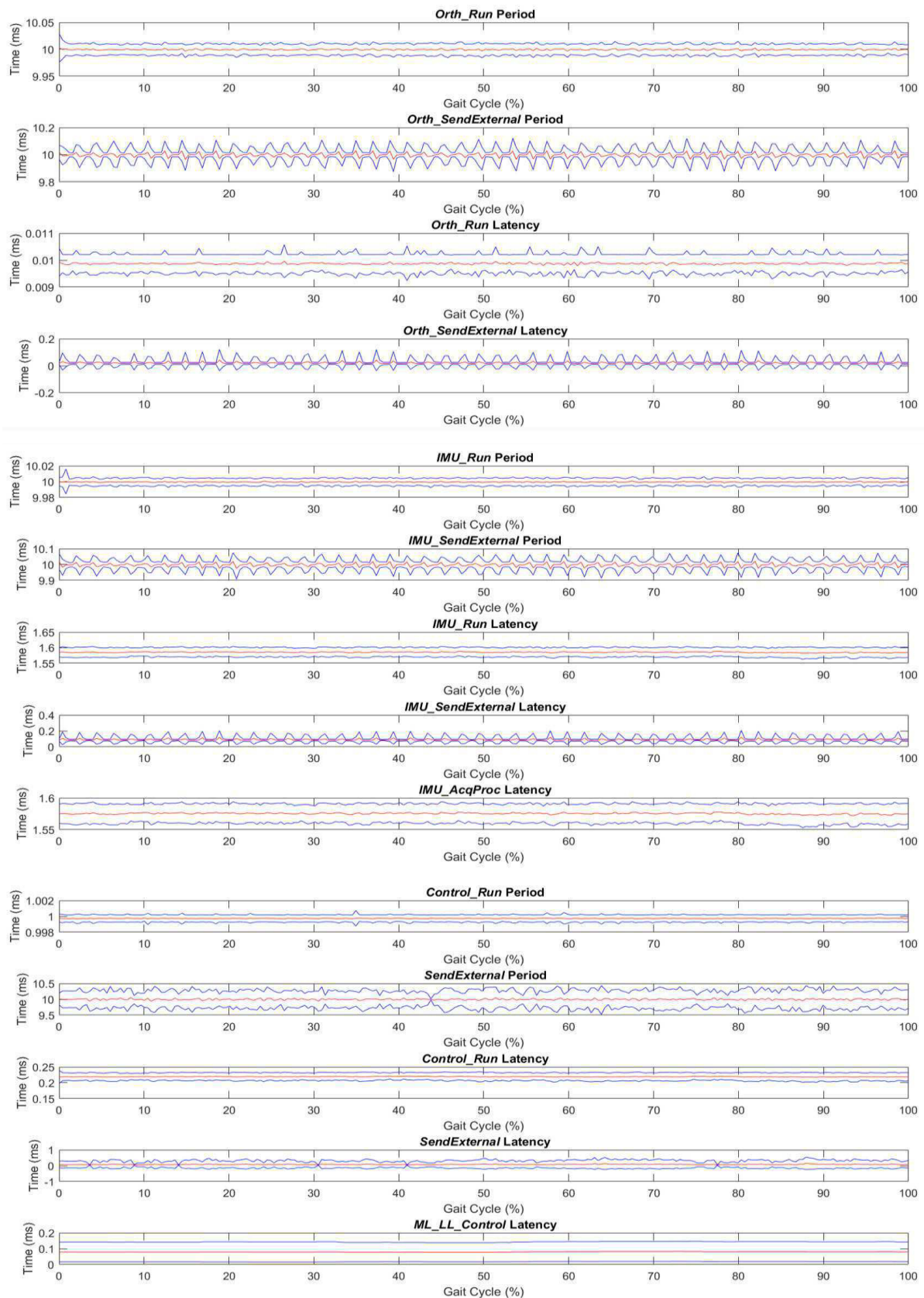
Figure 3.7- Graphical distribution of the LLOS' computational performance. Mean and standard deviation values marked at red and blue, respectively.

The latencies obtained for tasks and timers are relatively lower than the respective call periods. This finding indicates that (i) the time execution of the software interfaces of LLOS is lower than the available time, (ii) non-hierarchical architecture does not compromise LLOS performance, and (iii) there is room to add more mid- and low-level controls or embedded sensors to the LLOS. The latency of *IMU_Run* (1.585 ± 0.016 ms) was mainly responsible for IMU data acquisition and processing (*Acq_Proc* Latency = 1.575 ± 0.016 ms). On the other hand, the latency of executing the mid- and low-level controls (0.079 ± 0.062 ms) is half of the one spent in *Control_Run* (0.219 ± 0.013 ms).

Moreover, a latency of 0.243 ms was observed for the command messages send from high-level control (running in CCU) to mid-level (executed in LLOS) given the non-centralized architecture. However, the **introduced latency** due to the non-centralized architecture **did not compromise the time requirements** of high- and mid-level controls (both configured to be executed every 10 ms).

Regarding the WML, the low RMSE values (0.0006 < RMSE < 0.008 ms) obtained during experimental validation indicate that the developed interfaces of WML met the defined time requirements. The results presented in Table 3.4 also show the existence of variability in the call period times along the gait cycle, mostly for *SendExternal* tasks given their lowest execution priority when compared to *Run* routines. Note that for *Run* routines, the maximum call period times never overcome the defined time requirements.

InertialLAB was the sensor system with higher latency for Run routines likely due to higher complexity for data processing (described in Chapter 4.2). The **latencies** obtained for tasks and timers are relatively lower than the own call periods suggesting that (i) the time execution of the software interfaces of WML **does not compromise the WML performance**, and (ii) there is still room to add sensor systems to the WML.

In overall, the computational evaluation points out that the **STM32F4-Discovery** development board provides the resources required for **computational effectiveness of LLOS and WML**, as well as enables the **inclusion of further modules**. Additionally, the developed software interfaces were capable of hitting all real-time deadlines with small latency (determinism).

Table 3.4- Computational performance evaluation of WML. Mean, standard deviation (STD), maximum (Max), and minimum (Min) time values, and RSME of the call period of tasks and timers of WML.

Software Routine	Measure				
	Description	*Mean ± STD (ms)*	*Max (ms)*	*Min (ms)*	*RMSE (ms)*
InertialLAB_Run	Call period	9.999 ± 0.0005	10.0	9.999	0.0006
	Latency	2.751 ± 0.004	3.039	2.725	-
	Acq_Proc Latency	2.740 ± 0.004	3.029	2.714	-
InertialLAB_SendExternal	Call period	9.999 ± 0.008	10.596	9.971	0.008
	Latency	0.013 ± 0.002	0.015	0.0	-
GaitShoe_Run	Call period	9.999 ± 0.0005	10.0	9.999	0.0006
	Latency	0.154 ± 0.0003	0.154	0.153	-
	Acq_Proc Latency	0.144 ± 0.0005	0.144	0.143	-
GaitShoe_SendExternal	Call period	9.999 ± 0.003	10.068	9.996	0.003
	Latency	0.009 ± 0.002	0.033	0.007	-
EMG_Run	Call period	0.999 ± 0.0004	1.0	0.999	0.0007
	Latency	0.133 ± 0.0005	0.133	0.132	-
	Acq_Proc Latency	0.122 ± 0.0004	0.123	0.122	-
EMG_SendExternal	Call period	9.999 ± 0.0005	10.0	9.999	0.0006
	Latency	0.054 ± 0.002	0.095	0.051	-

Table 3.5 presents the power consumption evaluation of LLOS and WML during 50 gait cycles. Both current consumption and power consumption were higher for WML than LLOS given the higher number of sensor systems, peripherals and development board's resources activated in WML. The variability of power consumption along the experiment was more pronounced for LLOS than WML.

Moreover, the results presented in Table 3.5 report that the inclusion of further development boards, for achieving the non-centralized architecture, **increases the current consumption** (around 100 mA). Nonetheless, this increment **was not sufficiently high to comprise the energetic performance of the SmartOs system** since the total current consumption (around 100 mA) is quite inferior to the capacity of the SmartOs' power supply system (12 Ah).

Table 3.5- Power consumption evaluation of LLOS and WML. Mean, standard deviation (STD), maximum (Max), and minimum (Min) values of the current and power consumed.

	Current Consumption (mA)			Power Consumption (mW)		
	Mean ± STD	*Max*	*Min*	*Mean ± STD*	*Max*	*Min*
LLOS	22.72 ± 1.5	23.9	17.2	66.76 ± 4.4	70	51
WML	76.18 ± 0.04	76.3	76	222.99 ± 0.03	223	221

3.4. Conclusions

For achieving the gait rehabilitation and analysis challenges proposed for SmartOs system, a modular, real-time, power- and time-effective framework was developed. It was designed following a user-centered design approach given the relevance of continuous user involvement in the development of personalized solutions, such as SmartOs. All interfaces of the framework are wearable.

Overall, the developed hardware and software interfaces of the framework shown to be **time- and power-effective**. The technical validation, in real-time conditions, emphasized that the increased latency and power consumption, as a result of the non-centralized architecture, did not compromise the framework performance. This finding indicates that the hierarchical interaction between AOs with the wearable sensor systems (described in Chapter 4), gait analysis tools (Chapter 5 and Chapter 6), and assistive control strategies (presented in Chapter 7), was successfully achieved through a non-centralized architecture. Moreover, there is still room to **expand the SmartOs system with other stand-alone modules** to attempt to the user's requirements as needed.

Lastly, the integration of the mobile and desktop graphical applications allows an intuitive interaction with SmartOs' functionalities and modules and visual feedback regarding therapy progress.

Chapter 4 – Wearable Motion Lab

This chapter starts with an introductory insight into the relevance of human gait analysis and the use of wearable sensors for this application. It presents the Wearable Motion Lab, outlining the hardware and software developed for the InertialLAB, GaitShoe, MuscLAB, and EMG system. Moreover, it describes the gait analysis tools implemented in each sensor system to monitor relevant biomechanical and muscular measures and metrics for the post-stroke gait rehabilitation assessment. The chapter ends with a concluding analysis of performance and challenges of Wearable Motion Lab.

4.1. Introductory Insight

Human gait analysis has the potential to be applied as an automatic and objective assessment tool of human gait condition. Clinical gait analysis may contribute (i) to better understand the etiology of gait abnormalities supporting the clinical-based diagnosis with objective and timeless information, (ii) to foster better treatment decisions, (iii) to recognize walking risk situations, and (iv) to improve clinical follow-up [158], [159]. Furthermore, real-time gait analysis may be applied in the design of personalized gait therapies by tuning the assistance according to the patient-specific needs [101], [159]–[162], and eventually at home for monitoring the quality of walk (to forecast any forthcoming abnormality of user's gait).

In the context of gait rehabilitation, human gait analysis may involve the systematic study and monitoring of distinct biomechanical information such as spatiotemporal, kinematic, and kinetic gait data, and physiologic parameters such as muscular activity [1].

Most commonly, the human gait analysis is conducted in a **motion analysis laboratory** with expensive but highly accurate sensor systems, such as optical motion systems and force plat-forms. Nevertheless, these motion capture systems are non-portable [39], only operating in controlled environments and reducing equal access to healthcare [163]. Consequently, they do not analyze consecutive gait cycles for long-term mobility scenarios [101].

Current challenges include the development of **wearable motion labs** with cost-effective, robust, unobtrusive, easily wearable sensor systems for all-day and any-place real-time gait monitoring without interfering with the user's movement [26], [158]. Technological advances have made these sensors smaller, lighter, cheaper, and with low-power consumption, making them suitable for long-term and outdoor ambulatory applications [39].

Diverse wearable sensor systems have been developed to enable the evaluation of the hu-man biomechanical and muscular status in a free-living environment, such as (i) **force-based systems** to monitor the feet contacts on the ground (i.e., the gait events) for a posterior de-termination of temporal parameters, (ii) **inertial sensor-based systems** to monitor the lower limb kinematics, and (iii) **EMG sensor systems** to track muscular activation for a posterior muscle weakness evaluation.

This chapter presents a **Wearable Motion Lab** given the potentialities of human gait anal-ysis, mainly for personalized AO-based gait rehabilitation purposes. The Wearable Motion Lab integrates a set of **stand-alone, self-calibrated, low-cost, ergonomic, wearable sensor sys-tems** to measure in real-time the user's motor condition. In particular, it includes an inertial sensor-based system (**InertialLAB**) and a wireless instrumented shoe system (**GaitShoe**) to track lower limb biomechanical measures, and an **EMG system** and a muscular contraction-based force sensor system (**MuscLAB**) to monitor muscular measures.

The design of these wearable sensor systems addressed five **main requirements**. First, the hardware systems should embed compact, low-cost, and efficient electronic components to produce a cost-effective wearable system. Second, the sensor system should incorporate an easy-wearing system to cover 10th-to-90th percentile of the male/female population (height ranging from 1.50 m to 1.90 m and body mass ranging from 45 kg to 100 kg). Third, software routines should follow a modular, open-architecture to provide real-time kinematic and

muscular information to third-party systems. Fourth, the sensor system should endow a prompt calibration routine with a minimum-to-null effort. Lastly, the system's autonomy should last for at least eight hours for accommodating prolonged recording sessions.

4.2. InertialLAB

4.2.1. Critical Analysis of Related Work

Research contributions related to the ambulatory human gait analysis may involve inertial sensor-based systems with IMUs [158]. The IMU-based systems proposed in the research community have to deal with three main challenges as follows: (i) automatic, user-independent calibration to avoid the use of time-consuming calibration methods [164], [165]; (ii) reliable computational tools, eventually combined with biomechanical models, for the real-time angle estimation [166]; and (iii) technical matters to deal with sensor's misalignments [167], [168]. Moreover, there is an emergent need to make the IMU-based systems easily calibrated solutions [25], [26], [144].

On the other hand, commercial IMU-based solutions such as MVN BIOMECH (Xsens, Netherlands), RIABLO (CoReHab, Italy), G-walk (BTS Bioengineering Corp., Italy) (i) are high-cost systems, (ii) usually require non-wearable processing units to run the joint angle estimation, (iii) do not directly and easily provide the real-time biomechanical data to third-party devices or algorithms (for instance, human motion intention recognition tools), and (iv) do not offer a fully wearable integration into further sensor and actuation systems.

4.2.2. Methods

A **cost-effective wearable inertial sensor system**, the InertialLAB, was developed for real-time tracking of three-dimensional (3D) **angular velocity and 3D-acceleration** up to 6 lower limbs and trunk segment, and **joint angles** in the sagittal plane up to 6 lower limb joints.

As a gait analysis tool, InertialLAB includes a low computational joint angle estimation method to enable its execution in a wearable board for a more practical ambulatory analysis. The joint angle estimation was implemented at a relatively high sampling frequency (≤ 200 Hz) to meet the computational requirements of high-performance tools, such as the motion intention recognition and control architectures [9].

Hardware-in-the-loop

Figure 4.1.A illustrates the hardware architecture of InertialLAB. It is scalable as desired **up to seven IMUs**, placed on the **back**, **thigh**, **shank**, and **foot** segments, as suggested by [169], [170]. The **MPU-6050** (InvenSense, USA), that combines a 3-axis MEMS accelerometer (± 8 g) and a 3-axis MEMS gyroscope (± 2000 º/s), was selected given its small size (15x20x2 mm) and mass (0.009 kg), and low admissible current consumption (3.8 mA). A magnetometer was not included to avoid the complications related to the magnetic field in rehabilitation scenarios as treadmill [165].

A **multi-channel board** (80x80x25 mm) to enable multi-channel recording (TCA9548A I^{2}C multiplexer) was developed. Each IMU communicates with development board (STM32F407VGT) through I^{2}C protocol (up to 400 kHz) using USB cables in the spiral form to meet the anthropometry requirements and to enable an easy plug and unplug solution.

The **STM32F407VGT development board** (80x100x25 mm) has the resources required for a time-effective (up to 200Hz) acquisition and processing. Additionally, it communicates with an attached USB flash drive (4GB of storage capacity, write speed of 8MB/s) to store the collected data. A standard 2000 mAh power-bank powers InertialLAB. It ensures the autonomy of at least eight hours, considering that the InertialLAB consumption reaches up to 25 mAh.
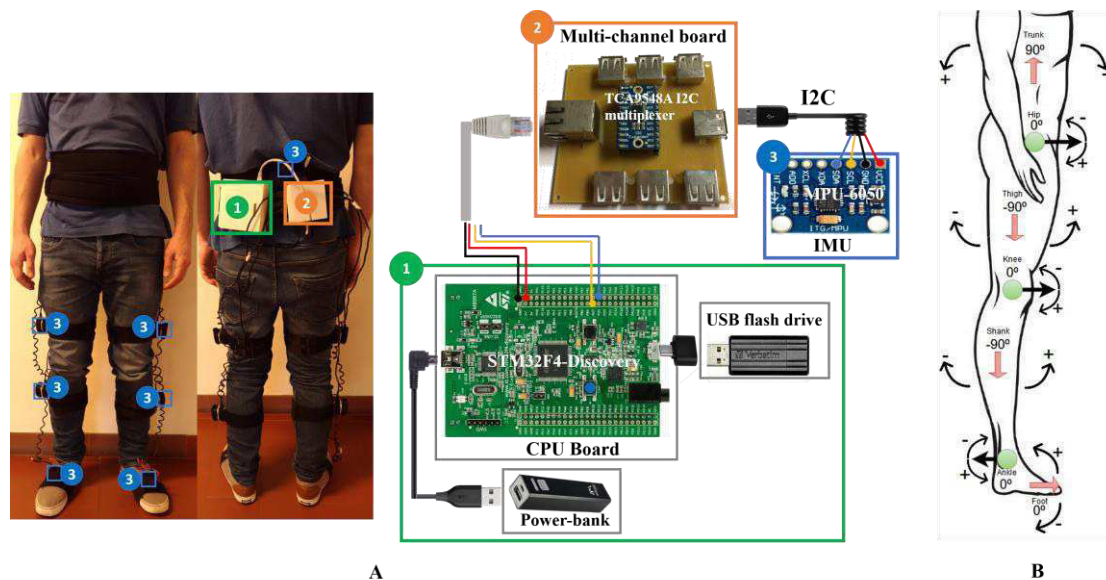
Figure 4.1- **A**: Hardware architecture of InertialLAB. **B**: Orientation of the segment (red arrow and the associated numbers) and joint angles (green circles and the associated numbers) in the stand-up steady-state and direction of the joint rotation.

Each IMU, the development board and multi-channel boards were fixed in 3D printed boxes and attached to the human using adjustable straps (Figure 4.1.A) aiming for easy usability and portability. This approach also minimizes the sensor's relative motion to the human's segments to avoid fluctuations in the IMU measures.

Software-in-the-loop

The software routines may run up to 200 Hz in the STM32F407VGT for real-time monitoring and calibration of kinematic data, and gait analysis tool for segment orientation estimation and joint angle estimation in the sagittal plane (more details in Appendix E.1).

An **automatic, user-independent, on-body calibration** routine was proposed. This calibration takes place on the first 10 s of each trial, simultaneously for all IMUs, while the user is wearing the IMUs in the stand-up steady-state. Equation (4.1) was used to calculate the gyroscope's calibrated value (C_{value}) for each new sample (N_{value}), considering the gyroscope's scale factor (S_{factor}), and the gyroscope offset per axis (O_{gyro}) as the mean of gyroscope's raw values for 10 s [171].

$$C_{value} = \left(N_{value} * S_{factor}\right) - O_{gyro} \qquad (4.1)$$

The calibration of accelerometer consists of its normalization using the positive and negative component of the acceleration vector ($\|\vec{A}\|$), as the maximum and minimum values for the normalization, respectively [171]. Equation (4.2) presents the determination of the norm of the acceleration vector ($\|\vec{A}\|$), considering the acceleration measures of each axis (A_x, A_y, and A_z).

$$\|\vec{A}\| = \sqrt{\left(A_x^2 + A_y^2 + A_z^2\right)} \qquad (4.2)$$

The **segment orientation** was estimated by inertial data fusion-based methods, namely the complementary and Kalman filters [172]. The **complementary filter** was implemented using 0.98 and 0.02 as the gains of the gyroscope and accelerometer contribution, respectively. The gains were found by an empiric trial-error procedure considering a tradeoff of the short-term reliability of gyroscope-based estimation and long-term reliability of accelerometer to minimize the drift that would arise from an entire contribution to the gyroscope. The **Kalman filter** is more complex, more computationally expensive than the complementary filter, but it was

explored given its effective response [172]. After a parameter tuning, the Kalman filter was implemented using the noise covariance matrix Q_k and the measurement covariance matrix R, as described in Equation (4.3).

$$Q_k = \begin{bmatrix} 0.005 & 0 \\ 0 & 0.0003 \end{bmatrix} \tag{4.3a}$$

$$R = \begin{bmatrix} 0.0669 & 0 \\ 0 & 0.039 \end{bmatrix} \tag{4.4b}$$

The gait analysis tool for **joint angle estimation followed a trigonometry-based method** dependent on the segments' orientation values ($\theta_{Trunk}, \theta_{Thigh}, \theta_{Shank}, \theta_{Foot}$) and the assumption that, in the stand-up steady-state, the segment and joint orientations are as described in Figure 4.1.B. Additionally, it was considered that leg segment angles vary from [-270; 180]°, the other segments vary from [-180; 180]°, and the joint angles vary from [-180; 180]°. Taking these aspects into consideration, the hip (θ_{Hip}), knee (θ_{Knee}) and ankle (θ_{Ankle}) angles were estimated using the formulas described in Equation (4.4).

$$\begin{aligned} \theta_{Ankle}(°) &= -90 - \theta_{Shank} + \theta_{Foot} \\ \theta_{Knee}(°) &= \theta_{Thigh} - \theta_{Shank} \\ \theta_{Hip}(°) &= -(\theta_{Trunk} - \theta_{Thigh} - 180) \end{aligned} \tag{4.4}$$

The use of sensor fusion methods for joint angle estimation may be highly sensitive to internal and external sensor errors. Consequently, the effectiveness of empiric models for drift error compensation was explored to be applied in InertialLAB upon joint angle estimation tool. A software tool was implemented to identify a well-fitted, user-independent, joint-dependent **regression model** for improving the joint angle estimations of InertialLAB **to minimize the drift errors**. Different machine learning-based regression models (artificial neural network (ANN), decision tree, and support vector machine) were explored considering the InertialLAB's joint angles and joint angular velocities as inputs and the MVN BIOMECH's joint angles as the target measurements. All variables were normalized using the min-max method within [-1; 1].

After a comparative analysis using 31500 observations in 5-fold cross-validation, the two-layer shallow **ANN** with 5 neurons in the hidden layer was the **best-fitted regression model** to predict the hip, knee and ankle angles ($R^2 = 0.92$, $R^2 = 0.94$, and $R^2 = 0.87$, respectively).

Lastly, a light-based feedback system was developed using the light-emitting diodes (LEDs) available in the development board to inform the user about the InertialLAB's state. The green

LED is on during the calibration routine whereas the blue LED is on during data acquisition and storage. The red LED warns the user for the occurrence of some error.

4.2.3. Experimental Validation

A **benchmarking analysis** of InertialLAB against the **MVN BIOMECH** [173] was performed to assess the operability and effectiveness of InertialLAB in **free-walking conditions**. The MVN BIOMECH was included for two-fold reasons. First, it is a well-established wearable inertial system able to monitor all kinematic data monitored by the InertialLAB (angular velocity, acceleration, and joint angles). Second, it is a wearable solution able to track the human gait in ambulatory scenarios like those explored in this work in opposition to camera-based motion systems. Additionally, literature's results report that MVN BIOMECH quantifies lower-limb joint angles with an excellent validity and fair-to-excellent reliability for overground walking [174], [175] and climbing stairs [175] when compared to camera-based motion systems.

Participants

The benchmarking analysis included 11 able-bodied subjects (7 males and 4 females) who signed a written informed consent to participate in this study. The participants' mean age was 24.53 ± 2.09 years old, with a height of 1.71±0.10 m and body mass of 59.3 ± 17.37 kg.

Protocol and Data Collection

The participants wore their sport-shoes and 7 IMUs in the configuration depicted in Figure 4.2.A. To ensure the repeatability of the sensor's alignment in the leg, the assessor identified and marked the lateral side at the middle of the thigh and shank segments [176]. For the trunk and foot segments, the assessor identified the lower back position (near to the center of mass) aligned with the spinal cord and the instep position aligned with the navicular bone, respectively. The sensors of InertialLAB and MVN BIOMECH were placed on these positions by the assessor, who used the double holder straps of InertialLAB to ensure that its sensors are aligned and fixed over the IMUs of MVN BIOMECH. A hardware-based sync method (TTL sync) synchronized both systems.

Each trial started with the calibration of the MVN BIOMECH in N-pose (stand upright on a horizontal surface with back straight). Then, the participant stayed in the stand-up steady-state for 10 s to calibrate InertialLAB. Subsequently, the participants were asked to randomly perform **3 trials per self-selected gait speeds** (slow, normal, and fast) on a **10 m-flat surface**.

Additionally, the subjects randomly conducted 10 gait trials by ascending and descending on two terrains (a **staircase and a ramp,** Figure 4.2.B), at a self-selected gait speed. The staircase had 8 steps with 17 cm of height, 31 cm of depth and 110 cm width. The ramp was 10 m with 10° inclination. Furthermore, the participants conducted 9 trials with 180° turns as illustrated in Figure 4.2.C.
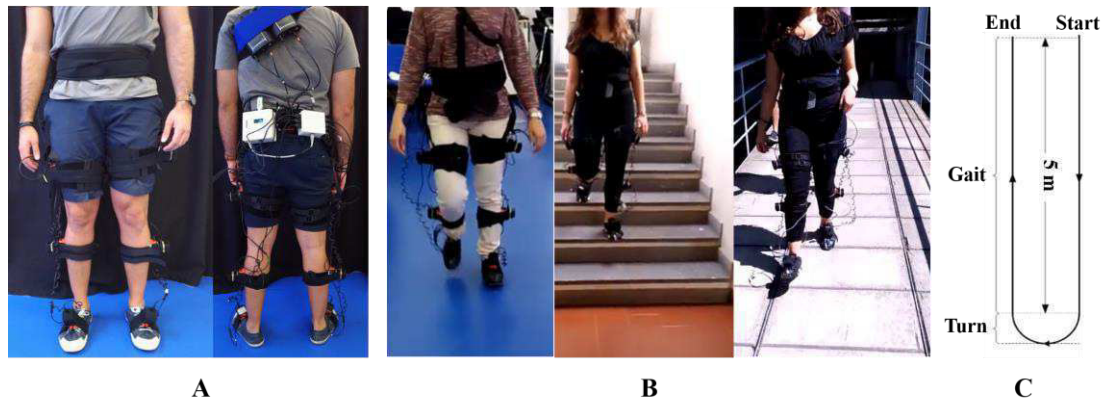
Figure 4.2- **A**: Usability of InertialLAB (black boxes) and MVN BIOMECH (orange boxes). **B**: Ongoing gait trials in flat terrain and staircase. **C**: Turns set-up.

Data Collection and Analysis

The data (3D angular velocity, 3D acceleration, and sagittal joint angles) were collected at 100 Hz, the maximum rate allowed by MVN BIOMECH. The Matlab® (2017b, The Mathworks, USA) was used for the benchmarking analysis of these kinematic measures as follows, without considering the acceleration and deacceleration zone. First, the correlation coefficient (ρ) and cross-approximate entropy (XApEn [177]) were computed for assessing the waveform similarity and dissimilarity/asynchrony, respectively, and the normalized root mean square error (NRMSE) was computed as a magnitude-based deviation measure. Second, the ratio among the InertialLAB' drift error and the MVN BIOMECH's drift error (*Drift Ratio*) was computed to investigate the drift error in the joint angle estimations. The drift error was calculated as the slope of the linear trend of the joint angle signals [164]. For trials including turns, the percentage of the increment of drift with the 180°-turn was computed to compare the drift error before and after the turning. Lastly, Bland-Altman plots were used to assess the effect of regression models for drift error reduction.

4.2.4.Results

The following technical remarks were observed during the experiments. MVN BIOMECH's performance was highly dependent on the calibration's environment. The power supply system of MVN BIOMECH was replaced every 60 min in daily recording sessions; whereas, no charging periods were needed for the InertialLAB. Moreover, from video modeling and analysis tools of an open-source optic tracker, a comparable performance between the complementary filter and Kalman filter (differences were lower than 0.2° with RMSE < 6.5°) was observed for the segment orientation. Thus, the **complementary filter was used for segments' orientation estimation,** given its inherent lower computation load when compared with the Kalman filter. The InertialLAB software routines were executed with a mean computation time of 2.4 ± 0.47 ms, with 95% of the samples computed within 3.1 ms. Furthermore, the IMU placed on the foot was the less effective sensor in magnitude (mean NRMSE < 0.115 and <0.10 of foot IMU and remaining sensors, respectively) and waveform similarity (0.81 < ρ <0.87 for foot IMU and 0.89 < ρ <0.95 for remaining sensors) as the speed increases.

The benchmarking analysis relied on the kinematic data monitored by InertialLAB to evaluate its operability at self-selected gait speeds (slow: 0.83 ± 0.11 m/s, normal: 1.09 ± 0.16 m/s, and fast: 1.59 ± 0.17 m/s) throughout three non-structured terrains (flat, staircase and ramp).

Table 4.1 shows that the **error of the gyroscope** embedded on the InertialLAB **increases with the gait speed**. On the other hand, the InertialLAB's angular velocity signals become more similar (ρ increases) and synchronous (XApEn decreases) to those of MVN BIOMECH as the speed increases. The acceleration signals of InertialLAB presented a similar performance in magnitude (0.114 < NRMSE < 0.117) and waveform correlation (0.721 < ρ < 0.73) when the gait speed varies. Comparing with MVN BIOMECH, the **gyroscope and accelerometer of the InertialLAB performed better in stair ascend and descend**.

Table 4.1- Benchmarking Analysis for 3D Angular Velocity. Mean NRMSE, ρ, XApEn.

Terrain	Speed	NRMSE	ρ	XApEn
Flat	Low	0.08 ± 0.012	0.859 ± 0.062	0.069 ± 0.017
	Normal	0.103 ± 0.017	0.863 ± 0.082	0.052 ± 0.058
	Fast	0.104 ± 0.018	0.871 ± 0.037	0.043 ± 0.079
Ramp ascend	Normal	0.117 ±0.024	0.857 ± 0.078	0.051 ± 0.029
Ramp descend	Normal	0.103 ± 0.026	0.807 ± 0.139	0.057 ± 0.049
Stair ascend	Normal	0.082 ± 0.047	0.925 ± 0.076	0.051 ± 0.032
Stair descend	Normal	0.083 ± 0.037	0.903 ± 0.057	0.062 ± 0.026

The findings stated in Table 4.2 indicate that the waveform similarity between the Inertial-LAB's joint angles and MVN BIOMECH's joint angles increases as the speed increases (ρ increases from 0.899 to 0.909; XApEn reduces from 0.082 to 0.075). The **joint angle signals** of the InertialLAB tracked in **ramp and stairs tend to be more correlated** (increment of mean ρ from 0.898 to 0.944) and less dissimilar (reduction of mean XApEn from 0.082 to 0.051) with the paired joint angles of MVN BIOMECH, as illustrated in Figure 4.3.
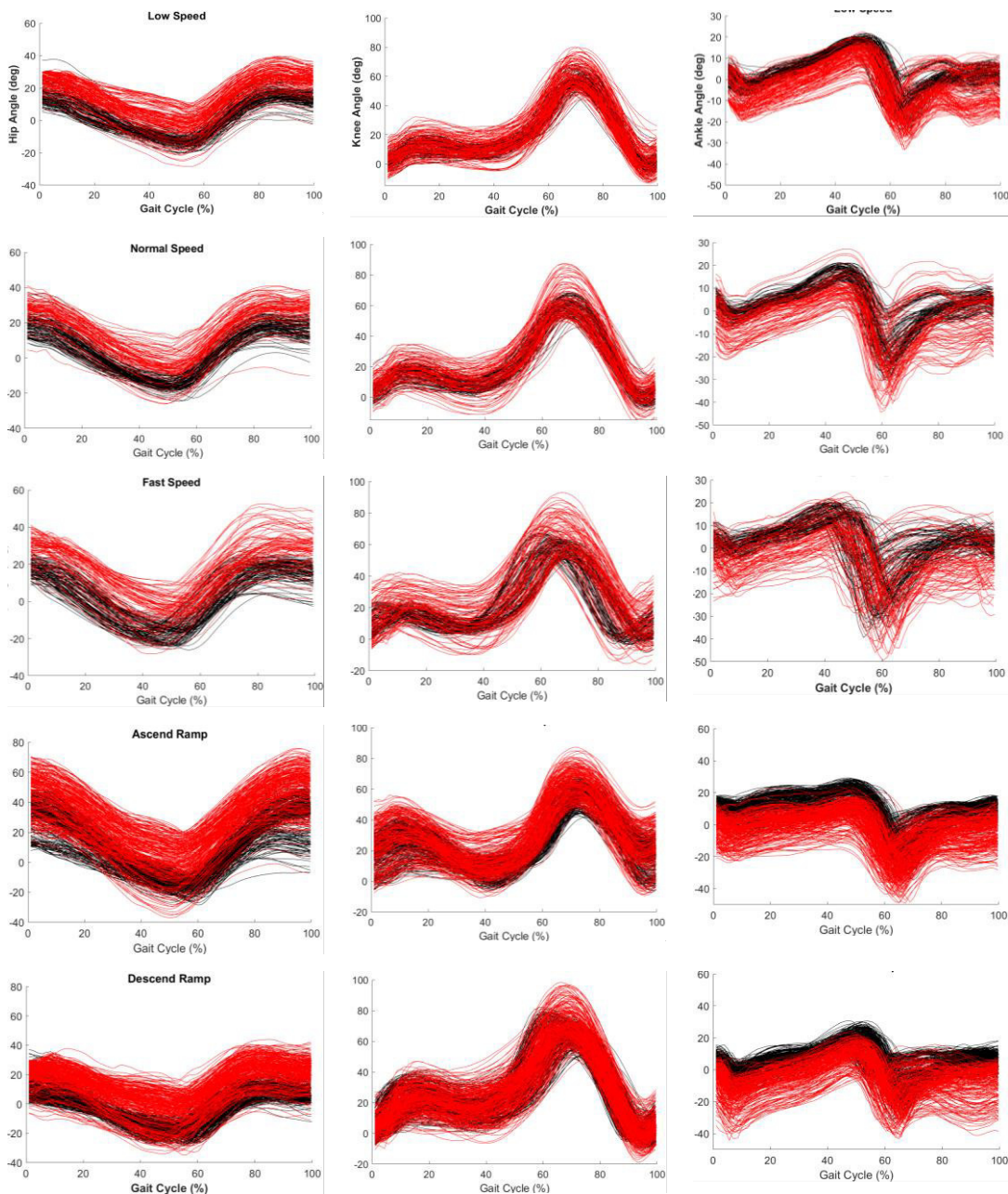
Figure 4.3- Representative time series of hip (1st column), knee (2nd column) and ankle (3rd column) angles in sagittal plane from all subjects wearing the InertialLAB (red) and MVN BIOMECH (black) at low (1st row), normal (2nd row), and fast (3rd row) speed in flat terrain, and at self-selected speed for ascend ramp (4th row), and descend ramp normal (5th row).

However, an offset in the absolute values (drift error) is evident. The **InertialLAB's drift error** was more pronounced in the **ankle joint**, and it tends to **increase with the gait speed** and when walking in a ramp. Moreover, the findings indicate that turns affect the joint angle estimations of both systems, but with double effect in the InertialLAB (drift error increased 59.72% and 27.46% for InertialLAB and MVN BIOMECH, respectively, after turns).

Table 4.2- Benchmarking analysis for the sagittal joint angle. Mean and standard deviation values of NRMSE, ρ, XApEn, Drift Ratio per speed and terrain (RA- ramp ascend, RD-ramp descend, SA-stair ascend, SD-stair descend).

Terrain	Speed	NRMSE	ρ	XApEn	Drift Ratio		
					Hip	Knee	Ankle
Flat	Low	0.066 ± 0.01	0.898 ± 0.042	0.082 ± 0.021	2.7	2.8	3.9
	Normal	0.067 ± 0.008	0.905 ± 0.049	0.080 ± 0.014	3.2	2.5	4.1
	Fast	0.070 ± 0.009	0.909 ± 0.063	0.075 ± 0.012	3.5	3.2	4.9
RA	Normal	0.086 ± 0.012	0.936 ± 0.08	0.051 ±0.020	5.4	4.6	5.5
RD	Normal	0.084 ± 0.011	0.931 ± 0.035	0.053 ± 0.025	6.5	5.6	6.9
SA	Normal	0.098 ± 0.007	0.930 ± 0.013	0.057 ± 0.013	4.7	4.0	4.2
SD	Normal	0.088 ± 0.004	0.944 ± 0.014	0.061 ± 0.027	2.6	2.3	3.7

NRMSE values do not reflect the drift errors of both sensor systems

Furthermore, the Bland-Altman plots illustrated in the top view of Figure 4.4 indicate the presence of a bias in the joint angles estimated from fusion-based methods given the non-zero mean difference values (-4.54, 2.67, and -3.98 for the hip, knee, and ankle, respectively).
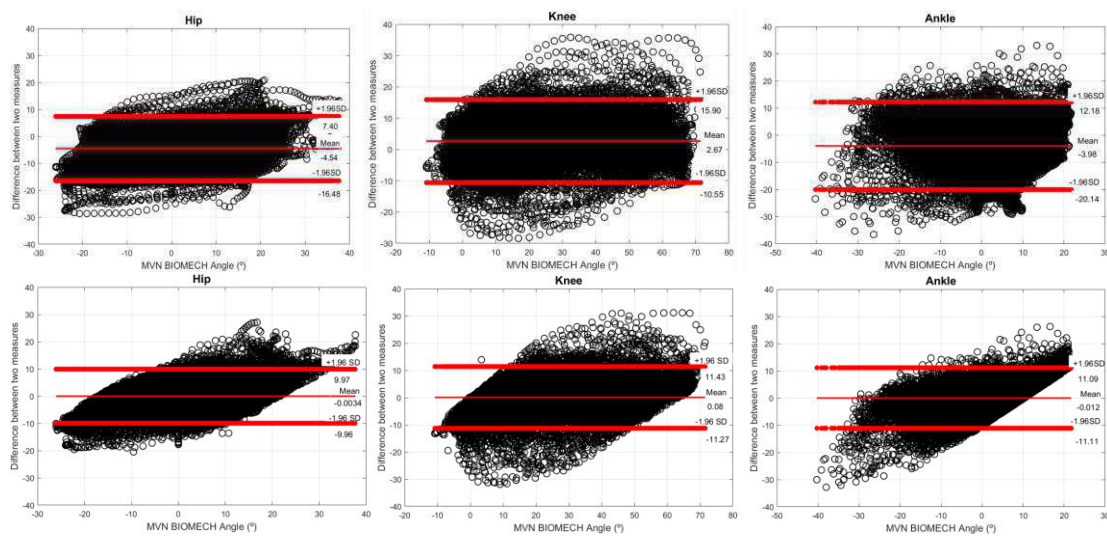
Figure 4.4- Bland-Altman plots of InertialLAB' angle estimations (top view) and the joint angle predictions by the ANN (bottom view) against the angles of MVN BIOMECH. The red horizontal lines represent the mean difference and the 95% limits of agreement (i.e., mean difference ± 1.96 SD of the difference).

In opposition, the mean difference is closer to 0° after ANN regression model application (bottom view of Figure 4.4), suggesting that the bias, such as the drift error, is approximately null for the ANN's joint angle predictions.

4.2.5. Discussion

InertialLAB Design Analysis

Concerning the design, the InertialLAB presents the following contributions. First, the use of an **automatic, user-independent, on-body calibration** in the first 10 s of the data monitoring avoids higher time-consuming calibration methods [164], [178] and demands less effort for the user and assessor. Second, InertialLAB advances similar commercial systems by presenting a **modular and open-architecture** with the possibility of full customization to operate as a stand-alone solution for general human motion analysis or gait phase detection as in [52] and to be directly integrated into third-party systems, particularly in AOs [179]. Such modularity will enable a prompt integration of the software routines into other processing units, limiting the changes to the peripheral devices' configuration routine.

Third, the power supply unit of InertialLAB is more advantageous than the one of MVN BIOMECH regarding the durability and usability (power unit of 20x20x100 mm *vs.* two power units of 60x50x150 mm), which favors its daily application.

Furthermore, the gait analysis tools were executed by a wearable board (80x100x25 mm) when compared to MVN BIOMECH (higher-dimensionality board such as a personal computer) and the one (200x137x55 mm) used in [178]. This allows a more practical application of InertialLAB for **ambulatory gait analysis**.

Kinematic Gait Analysis

The carried out **validation extends the one presented in previous studies** [164], [167], [178] by analyzing the joint angles and also the 3D-angular velocity and 3D-acceleration with gait patterns from non-structured real-world scenarios to better assess the reliability and repeatability of InertialLAB.

The **increased magnitude-based errors** in the gyroscope and accelerometer with **gait speed** may be explained by the increment of the IMUs' attachment instability as speed increases, especially considering the positioning of InertialLAB over MVN BIOMECH. Furthermore, the performance of the IMUs embedded on the InertialLAB was **better in climbing stairs**

than in flat terrain and ramp. Two reasons may explain it. First, it may result from a shorter walked distance in the staircase comparing to other terrains. Second, climbing stairs may deal with a slight impact interaction with the ground, resulting in lower secondary motions of the IMUs than in other terrains.

The proposed **joint angle estimation tool** is fairly simple, but it presents a high waveform similarity when compared with MVN BIOMECH, while considering different terrains (flat, stairs, and ramp). Previous studies [174], [175] reported an excellent waveform similarity (> 0.9) with MVN BIOMECH for walking [174], [175], jumping activity [174] and climbing stairs [175]. Tadano *et al.*[167] have shown high correlations ($\rho > 0.78$) in a 5m-flat surface. The InertialLAB presented a comparable performance in a 10m-flat surface (mean $\rho = 0.905$ for three joints). According to [167] and [174], the high correlation in joint angle time-series ($\rho >$ 0.898 for the three terrains) can be interpreted as a **high reliability and excellent validity** of the InertialLAB, respectively.

There is evidence of the presence of offset-based errors in the InertialLAB's joint angle estimations. Previous works also reported offset-based errors for the lower limb joint angle estimation when using the Kalman filter for short distance trials [164], [167], [178]. Liu *et al.* [164] reported a maximum RMSE of 16.6° for trials with 3 strides; Beravs *et al.* [178] outlined a mean error lower than 5° when one subject walked 30 steps; and Tadano *et al.* [167] found a mean RMSE ranging from 7.88° to 10.14° from a gait analysis along 5 m. On the other hand, the errors reported in the InertialLAB's validation reflect a larger number of heterogenous gait patterns from non-structured and longer trials to investigate the repeatability over time.

The **drift error** was more pronounced in the **ankle joint**, as reported in [167], [174], [178]. Often the most distal segments are the ones that move the most during gait; therefore, they are more susceptible to fluctuations and signal distortions at heel-strike and toe-off timings [167]. With this study, it was verified that the **ANN regression** models may successfully be applied to **minimize the bias in joint angle signals** and to yield signals with excellent validity [174]. It is worth to note that these regression models were tuned to be user-independent and to generalize to speed variations aiming a versatile application of InertialLAB in biomechanical analysis.

The proposed calibration procedure may be affected as follows. The differences in the real joint kinematics and the assumptions considered in the calibration may introduce a fixed bias.

Moreover, the effectiveness of the proposed calibration is affected by incorrect postures during the stand-up steady-state.

4.3. GaitShoe

4.3.1. Critical Analysis of Related Work

Research contributions related to **shoe- or insole-based force sensor systems** usually integrate **FSRs** to measure the foot contacts on the ground and enable gait event detection given their low cost, low-power consumption, high flexibility and thinness to fit over an insole.

Previous studies [25], [180] proposed a flexible insole-based system with thirty-two FSRs [180] and sixty-four pressure-sensitive sensors [25], respectively, to analyze the ground reaction forces. Other researches [26], [181] developed a wireless shoe-based system including four FSRs (placed on the heel, first and fifth metatarsals, and toe) to detect gait events. They also incorporated an **IMU** to determine foot orientation. In Pappas *et al.* [182], three FSRs (placed on the heel, the first and fourth metatarsus of insole) and a gyroscope (placed on the heel of the shoe) were used to measure forces exerted by the foot and the foot's orientation relative to the ground, respectively. However, more research should be developed to (i) augment the linearity and durability of the force-based systems, (ii) **avoid time-consuming calibration procedures**, (iii) to extend the validation to several **daily walking conditions**, and (iv) to provide **real-time spatiotemporal parameters**, such as step length and gait speed [25].

Moreover, a number of commercial wearable force-based systems have been proposed, such as F-Scan system (Tekscan, Boston, USA), In-Shoe (Tekscan, Boston, USA), DynaFoot (TechnoConcept, France), Footswitch insole line (Noraxon™, USA), Footwork insole (amcube, France) using FSRs and pedar® insole (novel.de) using capacitive sensors. These systems record dynamic pressure mapping and spatiotemporal gait parameters. Despite the well-established robustness and usability, these commercial solutions are quite expensive when considering their limited durability and the need for a user-specific insole. Furthermore, they do not provide an **open-architecture** for easy and direct integration into third-party systems, such as further sensors and robotic assistive devices.

4.3.2. Methods

GaitShoe consists of a **wireless, stand-alone, cost-effective, low-power consumption, in-strumented shoe**. This wearable sensor system includes gait analysis tools designed for real-time estimation of **gait speed** and **gait event detection** in walking scenarios, including variable gait speed and terrains at a relatively high sampling frequency (100 Hz).

This sensor system advances the similar commercial systems with modular hardware and software architecture as follows. Except for the instrumented insole, the electronic interfaces of GaitShoe can be migrated to other shoes extending the GaitShoe's application to divergent feet anatomy and without demanding a user-specific system for the gait event analysis.

Hardware-in-the-loop

Figure 4.5 represents a general system architecture of GaitShoe, which extends the instru-mented shoes proposed in [50], and it is based on [144], [181]. GaitShoe includes a flexible **insole-based system with four FSRs** (FlexiForce A201 Sensor, Tekscan^{TM}), strategically placed on the heel, the first and fifth metatarsals, and toe/hallux, and **one IMU** (MPU-6050, Inven-Sense, USA) in the instep of the foot. The number and location of force sensors fulfill a tradeoff between a holistic gait event detection [50], [181] and the minimal computational load of gait analysis.

The selected FSRs are small (9.53 mm of diameter), thin (0.203 mm), flexible, with a suita-ble force sensitivity (from 100 g to 10 kg), low-power consumption (1 mA/cm^2 of applied force), and low-cost sensors. A voltage divider was implemented for FSR data acquisition (Fig-ure 4.5), providing a linear output for the operating conditions.

GaitShoe is formed by two slave interfaces, one per foot, for sensors' data acquisition, user-independent, on-body calibration, data processing, and transmission to a master interface. The master interface is responsible for slave interfaces' synchronization, overall data storage in a micro SD card (8 GB of storage capacity) and data transmission to third-party systems via Bluetooth protocol (HC06 Serial Module). The time-effective data transmission between each slave and the master interface occurs through a bidirectional radio frequency communication protocol (NRF24L01+, Nordic Semiconductor ASA) to augment the system's ergonomy. The NRF24L01+ was selected given its low dimensionality (29x15x1.2 mm), low-power consump-tion (<14 mA), transmission-effectiveness (2 Mbps with communication range < 70m) [183].

The Arduino Nano Atmega328P (running at 16 MHz) was the development board used for slave and master interfaces. It is a small (18x45 mm), mass (7 g), low-power consumption (19 mA) development board, and has the resources required for (i) data acquisition from four FSRs (ADCs interface) and one IMU (I^2C interface), (iii) data transmission (SPI interface for radio frequency modules and micro SD card, and RX/TX interface to connect to the Bluetooth module).

GaitShoe is powered by a standard 2000 mAh power-bank that ensures the autonomy of at least eight hours and presents a suitable capacity-size relation, easily plug and unplug for charging, and intuitive use for the user.

For portability and easy donning and doffing, the hardware systems were fixed into 3D printed boxes. Further, adjustable straps attach the slave interfaces to different shoes' models, and the master interface is used as a watchband.
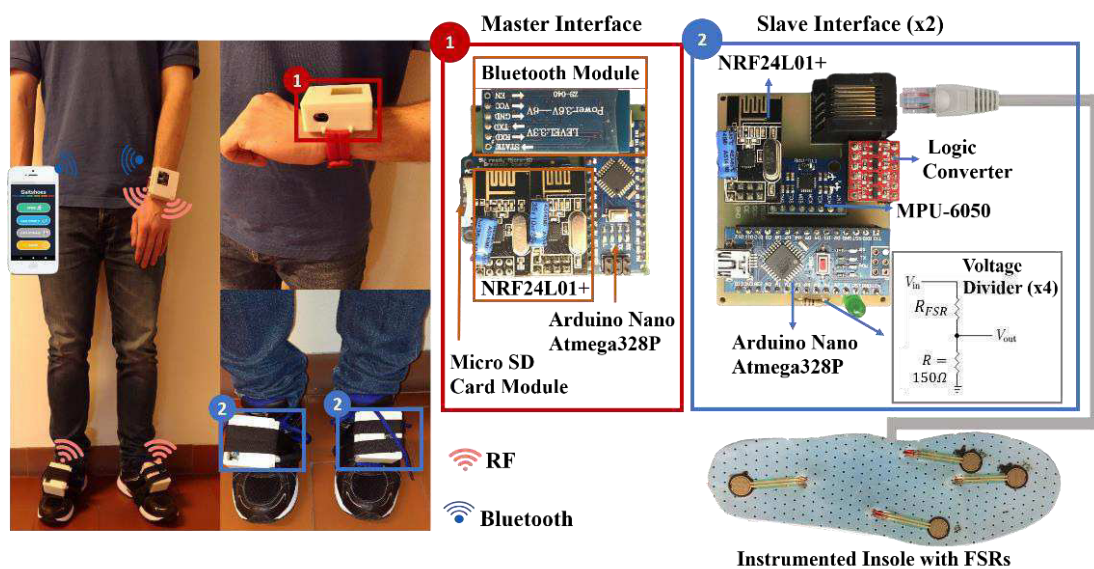
Figure 4.5- GaitShoe: Hardware interfaces and human body positioning.

Software-in-the-loop

This subchapter presents the main software routines of GaitShoe, namely radio frequency communication, automatic calibration, and the gait analysis tools for gait speed estimation and gait event detection. Appendix E.2 describes more details regarding the programs implemented in the master and slave interfaces.

For wireless radio frequency communication, a double-channel communication protocol (losses rate < 0.5%, empirically verified as more robust than single-channel) was implemented

by including two RF modules in the master interface to communicate independently with each slave (each slave has one RF module). The frequency channel (default, 2462 MHz and 2484 MHz) can be changed as needed to ensure the integrity of communication. The maximum packet structure was set to 32 bytes.

GaitShoe endows two **automatic, on-body calibration** approaches for each sensor system that are carried out in the first 10 s of each trial. The IMU was calibrated as described for InertialLAB. The FSRs' calibration aims to deal with FSR measure-dependency on the subject's body mass and the variable sensibility of FSRs over time. Equation (4.5) describes the calibration of a new FSR value (N_{FSR}) considering a ratio between the maximum binary measure of FSR (255) and the maximum force (FSR_MAX) applied by the user on each FSR when he/she is standing-up for 10 s.

$$C_{FSR} = N_{FSR} * \frac{255}{FSR_{MAX}|_{255}} \qquad (4.5)$$

The **gait event detection tool** can segment in real-time up to six gait events: Heel Strike (HS), Foot Flat (FF), Middle Mid-Stance (MMST), Heel-Off (HO), Toe-Off (TO), and Middle Mid-Swing (MMSW). For this purpose, three approaches were implemented in the slave interfaces using (i) the **measures of four FSRs**, (ii) the sagittal axis of the **foot-mounted gyroscope**, and (iii) the **sensor fusion of FSRs' measures and the foot angular velocity**.

First, the **gait event detection-based FSR** endows an adaptive tool that self-tuned the FSR-based thresholds, which are compared to the current FSR's measures through adaptive decision rules implemented by a **finite state machine** (FSM). The tool was proposed in [39] to detect HS, FF, HO, and TO gait events, as illustrated in Figure 4.6.A. Three levels of thresholds (HIGH, MEDIUM, and LOW) were set, tailored in real-time every three consecutive gait cycles, that correspond to 80%, 60%, and 40%, respectively, of the minimum value of the FSRs' maximum values (in the initial conditions those values were found in the calibration routine).

Second, it was implemented an **inertial sensor-based detection** to overcome some of the inherent limitations of force-based sensors [53] and to extend the gait segmentation to the swing phase. This gait event detection tool consists of an FSM based on heuristic decision rules dependent on adaptive thresholds applied to the **foot angular velocity** in the sagittal plane (measured by IMU of GaitShoe). A detailed description of this tool is presented in Chapter 5 and in [52].
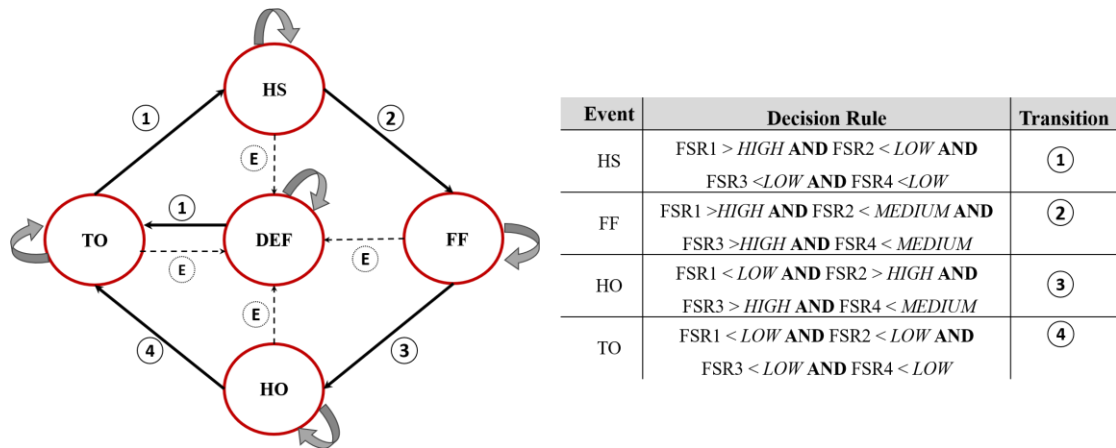
Figure 4.6- Gait event detection-based FSR. **A**: FSM. **B**: Decision, where DEF-default state, FSR1- heel, FSR2- 1st metatarsal, FSR3- 5th metatarsal, FSR4- toe.

Third, the **sensor fusion** of **force-ground contact measures** [50] with **foot angular velocity measures** [52] was implemented. The decision rules of both force-based and gyroscope-based detection were combined with OR condition to detect the HS, FF, MMST, HO, TO events by the first sensor whose algorithm conditions are satisfied. The MMSW event can only be identified by the gyroscope-based tool.

The adaptability conferred to these three computational tools aims to handle the intra- and inter-subjective gait variability and to foster a reliable gait event detection in non-structured environments with variations of gait speeds and ground surfaces.

The gait analysis tool for real-time **gait speed estimation** used the **foot acceleration and angular velocity** (measured by the IMU) and the timing information of the **FF event.** This event was used as the reset integration moment at each gait cycle by considering the zero-velocity update strategy [170]. This approach (i) takes advantage of the gait cyclical properties to mitigate the bias introduced by the integration, and (ii) avoids the subject-specific anthropometric calibration required in the human gait model-based methods, such as the pendulum model [184].

The gait speed tool was organized as follows, as represented in Figure 4.7.A. First, the foot angle in the sagittal plane was estimated by applying the FF reset-based integration of the foot angular velocity in the sagittal plane. Second, the user's foot acceleration components (horizontal (A_x) and vertical (A_z) components) were computed as outlined in Equation (4.6), using the acceleration measures (X-axis (a_x) and Z-axis (a_z)), compensated by the gravity acceleration (g), and the estimated foot angle (θ).

$$A_x = a_x \cos\theta - a_z \sin\theta \qquad (4.6a)$$

$$A_z = a_x \sin\theta + a_z \cos\theta - g \qquad (4.6b)$$

Subsequently, the gait speed was estimated by applying the norm technique to the instantaneous velocity (v_x and v_z components), which were computed by integrating the user's foot acceleration (A_x and A_z components) in the time interval between every FF event, where the initial velocities were set to 0 m/s [185].
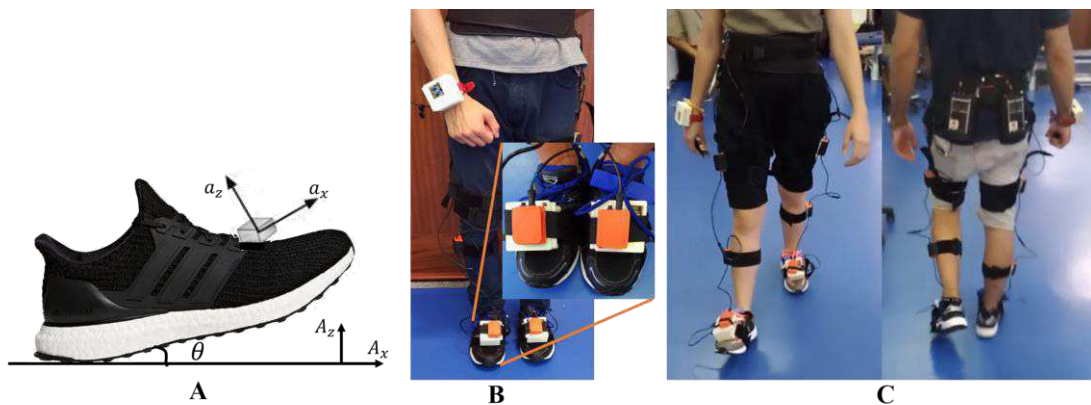
Figure 4.7- A: Representation of IMU placement in shoe. Measured horizontal and vertical accelerations (a_x, a_z) have to be corrected to the floor fixed frame (A_x and A_z) and the effect of gravity eliminated. **B**: User wearing GaitShoe and MVN BIOMECH. **C**: Ongoing tests.

4.3.3.Experimental Validation

An experimental validation was performed to investigate the operability of GaitShoe. A benchmarking analysis against MVN BIOMECH for gait speed was performed considering the reasons stated in Chapter 4.2.3 and the affordability of MVN to measure the gait speed. The validation of the gait event detection tool is presented in Chapter 5.

Participants

This validation involved the same healthy participants described in Chapter 4.2.3. The inclusion criteria were: body mass ranging from 45 to 100 kg; female participant wear 38-39 size sports shoes; and male subject wear 41-43 size sports shoes.

Protocol

The participants wore GaitShoe considering the most appropriate size and the full lower-limb configuration of MVN BIOMECH since this system does not allow a less instrumented configuration for the gait monitoring. The MVN BIOMECH sensors located on the feet were always positioned by the same person, who carefully positioned a visible mark on the GaitShoe cases to ensure the repeatability of the sensor's positioning, as depicted in Figure 4.7.B. A hardware-based sync method (TTL sync) synchronized both systems.

Each trial started with the calibration of the MVN BIOMECH in N-pose. Then, the participant stayed in the stand-up steady-state for 10 s to calibrate GaitShoe. For gait trials, the participants were asked to randomly perform **3 trials per self-selected gait speed** (slow, normal, and fast) in **level-ground** as follows: forward walking on a 10 m flat surface; change the walking direction with a turning motion; and, forward walking to back to the initial position.

Data Collection and Analysis

The estimated gait speed of GaitShoe and MVN BIOMECH was collected at 100 Hz. The data analysis used the Matlab® for computing the RMSE in the averaged gait speed for both systems. Furthermore, statistical analysis with a significance level of 5% was conducted investigating the hypothesis that the average gait speed monitored by both systems was equal. The data analysis did not cover the two first and last gait cycles to eliminate the acceleration and deacceleration periods, respectively.

4.3.4.Results and Discussion

During the experimental validation, the GaitShoe presented some design contributions regarding the MVN BIOMECH. First, the use of a fully **automatic** (without requiring user's demographic data), **shorter calibration**. Second, when comparing to commercial systems, GaitShoe has advantageous relative to the **modular and open-architecture** able to operate as a stand-alone solution and to be directly integrated into third-party systems. Moreover, it enables the use of a single IMU sensor for gait speed analysis; whereas, MVN BIOMECH always requires the usability of the full lower-limb configuration independently of the purpose of the gait analysis. This aspect makes the GaitShoe a more ergonomic system for the ambulatory gait speed analysis.

Table 4.3 presents the averaged results of 1340 gait cycles at a varying self-selected gait speed in ambulatory walking conditions, including turns. The gait speed estimation tool implemented in GaitShoe overestimate the gait speed when compared to MVN BIOMECH's tool for the three self-selected speeds (for instance, for slow self-selected conditions, the MVN BIOMECH and GaitShoe monitored an averaged gait speed of 0.84 and 0.88 m/s, respectively). The **RMSE increases**, varying from 0.065 to 0.19 m/s, as the user's self-selected **gait speed augments**.

Nonetheless, the **differences in the gait speed estimation** of GaitShoe and MVN BIOMECH **were not significant** (*p*-value > 0.264, from the tested hypothesis that the average gait speed monitored by both systems was equal). This finding indicates that it is feasible to develop an accurate, self-contained gait analysis tool into a wearable development board using minimal inertial sensors, eliminating the need for complicated and usually expensive capture systems. Furthermore, the cyclic-based reset method showed to be useful to attenuate the unbounded growth of integral drift errors, as reported in [186].

Table 4.3- Benchmarking analysis of gait speed estimation. Mean and standard deviation (std) of gait speed values monitored by Xsens and GaitShoe, and RMSE.

Self-selected Speed	Speed of MVN BIOMECH (m/s)		Speed GaitShoe (m/s)		*p-value* of equal means	RMSE (m/s)	
	Mean	**Std**	**Mean**	**Std**		**Mean**	**Std**
Slow	0.84	0.085	0.88	0.04	0.264	0.065	0.06
Normal	1.19	0.147	1.23	0.242	0.69	0.16	0.13
Fast	1.82	0.089	1.91	0.26	0.304	0.19	0.16

The outcomes of Table 4.3 indicate that the differences found in the averaged values across the slow (> 0.84 m/s), normal (> 0.19 m/s), and fast (> 1.82 m/s) self-selected speed are as expected. Moreover, the gait speed measures provided by both systems are according to the well-established findings reported by Winter [187] for slow, natural, and fast cadence in healthy conditions.

The accuracy of the proposed gait speed estimation method is critically dependent on (i) the IMU's performance (e.g., offset, sensitivity drift), (ii) time-effective FF gait event detection, (iii) correct foot angle estimation, and (iv) the effects of relative movements between the shoe-mounted IMU case and the human foot. More representative gait patterns collected in inclined surfaces and stairs are needed.

4.4.MuscLAB and EMG System

4.4.1.Introduction

Considering the increased number of people with muscle weakness, the monitoring of muscular activity becomes a necessity [158]. The **surface EMG** is the standard technique for **muscular activity monitoring** by detecting the bioelectrical signal produced during muscle contraction through electrodes placed at specific locations on the surface of the muscle belly. Furthermore, the EMG system may contribute to the development of **EMG-based assistive control strategy** to explore the anticipative nature of EMG measures under gait training.

Different commercial wearable EMG systems have been proposed such as FREEEMG (Bioengineering Corp., Italy), Myopac EMG unit (Myopac), MyoWare (Sparkfun, EUA), Trigno^{TM} wireless EMG (Delsys Inc., USA), and myoMUSCLE (Noraxon^{TM}, USA). However, **surface EMG-based system** requires (i) **careful electrode placement** and excellent contact with a **clean and hairless skin**; (ii) electrodes with a conductive gel, enhances the detection of the electrical activity under the skin, that may cause **skin irritation and discomfort for daily use**; and, (iii) complex signal acquisition and processing. Furthermore, this sensor system is affected by the **user's sweating** that can damage EMG-based muscular measures over time [188].

Although the EMG system usually presents high robustness and reliability, there is a current need for using easily applicable methodologies with a shortened installation and low-effort for the user and therapist [189], [190].

4.4.2.Methods

SmartOs integrates two customized systems, namely wired EMG system and MuscLAB, for monitoring the muscle activity up to **7 muscles** and thus enable an objective user's motor condition analysis.

To achieve a **more ergonomic, cost-effective system for monitoring the muscular activity**, SmartOs proposed a force-based wearable sensor system, the **MuscLAB**. It relies on mechanomyography principle by measuring the muscle activity through variation of the mechanical pressure that the muscle contraction exerts on the force sensor. For this purpose, the force sensors were fixed to a compressible textile band robustly, which in turn, was attached to the surface of the target muscle. The design of MuscLAB is similar to the wearable sensor systems proposed in [191], [192].

EMG system: Hardware and Software-in-the-loop

The raw EMG signal measured from surface electrodes has a peak-to-peak magnitude range from 0 to 10 mV and response frequency limited from 0 to 500 Hz, with dominant frequency from 50 to 150 Hz [157].

Figure 4.8.A shows the wired surface EMG system, highlighting the developed hardware for EMG signal acquisition and processing. Each interface (55 x 53 mm) present the following electronic blocks. The first block includes an **instrumentation amplifier** (INA128p with offset = 50 uV, CMRR =120 dB) to obtain the electric potential of the muscle's activity, with an amplification gain factor of 50 to allow the first stage of signal amplification. The second block includes an active 2nd order bandpass filter (cut-off frequency from 20 to 500 Hz) and a notch filter (cut-off frequency of 50 Hz) to remove the baseline muscular bioelectrical activity and to attenuate the effect of motion artifacts and ambient noise, respectively. An offset voltage adjustment circuit was introduced to adjust the EMG signal for the operating range of the selected ADC interface. Next, an amplifier with a variable gain (through high-precision potentiometer of 1MΩ) was introduced to increase the signal resolution, allowing signal's readability for both healthy and subjects with muscular weakness. The last block introduces gain and limits the output signal from zero to the maximum voltage, using the ADC reference voltage. EMG system is powered by a standard 2000 mAh power-bank that enables autonomy of at least eight hours.
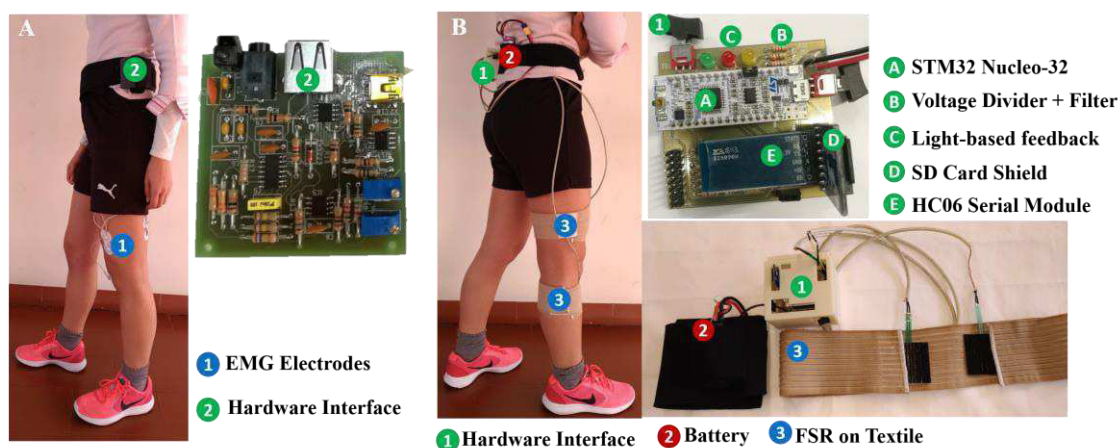
Figure 4.8- A: Wired EMG system: Hardware interfaces and human body positioning. **B:** MuscLAB: Hardware interfaces and human body positioning.

The EMG system was customized to include up to 7 hardware interfaces, which are managed by the STM32F4-Discovery development board able to: (i) conduct digital acquisition of

the EMG signals at 1 kHz using ADC interfaces; (ii) perform an **user-oriented EMG calibration**, when needed; and, (iii) execute **gait analysis tool to compute the EMG envelope**. This tool consists of a digital 2nd order low-pass Butterworth filter with 1.6 Hz of cut-off frequency to compute the EMG envelope. It gives a measure of the power of the signal, namely the most significant amplitude of the EMG signal while producing a waveform that is easily analyzable and useful for real-time control and feedback.

MuscLAB: Hardware and Software-in-the-loop

MuscLAB (Figure 4.8.B) is a **wearable muscular contraction-based force sensor system** designed to include up to **7 FSRs** (406 Square FSR, Interlink Electronics®). These sensors can be integrated easily into user-adjustable and compressible textiles due to their **flexibility** and reduced **thickness** (0.42 mm). Additionally, the selected FSRs present a relative high dimension (38 x 38 mm) to make misplacement and shifting less critical. The hardware interface (53.5 x 58.42 mm), incorporated into wearable 3D printed boxes, includes custom-made boards for force signal acquisition using a voltage divider and processing (1st order low-pass filter, cut-off frequency of 10 Hz).

Additionally, MuscLAB has an STM32 Nucleo-32 development board (STMicroelectronics, running at 72 MHz) that runs up to 100 Hz routines for (i) digital data acquisition using ADC interfaces; (ii) **on-body, automatic calibration**; (iii) data storage in a memory SD card (using SPI interface of STM32); (iv) **computing muscular voluntary contraction**; and, (v) data transmission to third-party systems via Bluetooth (using HC06 Serial Module). A 7.4V/900 mAh LiPo Battery powers the system.

MuscLAB endows an **automatic, on-body calibration tool**, organized into two phases, to remove the possible offset in the FSRs' measures and to deal with user's muscular contraction variability. In the first phase, the tool computes the offset (baseline pressure between the sensor and the muscle) as the mean value of FSR measures during the first 5 s of gait trial when the muscle is relaxed and subtracts it to the subsequent FSR outputs. In the next 10 s, while the subject is moving and contracting his/her muscle, the user-oriented muscle gain is determined as the maximum value of FSR measures during the 10 s. The gain is updated every 10 s. The user-oriented muscle gains are computed to enable a posterior objective evaluation of the muscular strength across gait training sessions.

The FSR signal calibration enables to estimate the **muscular voluntary contraction**, i.e., the most significant component of mechanical muscle contraction, by considering a digital **2ⁿᵈ order low-pass Butterworth filter** with 1.6 Hz of cut-off frequency, as applied for EMG system.

Lastly, MuscLAB endows a light-based feedback system to inform the user about the system's operating state. The green and yellow LEDs are turned on together during the calibration. The green LED alone indicates the real-time monitoring and storage. If the green led turns off, it means an error occurred. The yellow LED alone warns the user for low battery.

4.4.3. Experimental Validation

The experimental validation of both systems involved 8 healthy subjects (3 females and 5 males) who signed a written informed consent to participate in this study. The participants' mean age was 24.32 ± 1.09 years old, with a height of 1.72±0.12 m and body mass of 60.4 ± 19.79 kg. *Gastrocnemius medialis* and tibialis anterior were the muscles chosen, given its relevance in post-stroke gait analysis since stroke survivors commonly present weakness at tibialis anterior and spasticity at *gastrocnemius.*

EMG System: Protocol, Data Collection and Analysis

An assessor carefully followed standard recommendations for surface electrodes assessment [193]. This procedure assures the repeatability of the sensor's placement and minimizes intra-subjects and intra-trials variability. Three surface electrodes were considered. One is a reference electrode that was placed on the center of the knee joint, which is an electrically neutral tissue [194]. The other two electrodes are used to measure the muscle electrical signal and were placed on top of it, separated by about 2 cm from each other [194]. The muscle sites were prepared by removing excess hair, and the skin was cleaned by mildly scrubbing with an alcohol wipe.

The gain of the EMG channels was tuned regarding the level of muscular activity presented in the user's muscles. The participants were asked to perform motions under a treadmill as follows: keep 10 s in the stand-up steady-state pose; walking for around 40 s at a specified speed (1, 2 and 3 km/h); back to stand-up steady-state posture until reach 60 s. Each subject conducted 3 trials per speed. This experimental setup enables both **static and dynamic motion assessments.**

The EMG signal and EMG envelope were collected at 1 kHz. Signal-noise ratio was computed for EMG signal in Matlab® (2017b, The Mathworks, USA) to inspect the effectiveness of the processing blocks of the EMG system.

MuscLAB: Protocol, Data Collection and Analysis

The effectiveness of MuscLAB for monitoring muscle activity was investigated employing a **benchmarking analysis with wireless Trigno^{TM} Avanti Sensors** (Delsys, Natick, USA) during static and dynamic motions. Avanti Sensors are commercial EMG systems commonly applied in the scientific field for muscle activity monitoring.

The sensors were positioned as follows. The Avanti Sensors were placed on the muscle belly considering the electrode placement instructions aforementioned. The FSRs of MuscLAB were placed on muscle point motor (where detectable muscle inflation occurs), strictly to the respective Avanti Sensors. Subsequently, the subjects were asked to sit on a chair to reduce the muscle activation (feet not touching the floor) for conducting the first calibration phase of the MuscLAB.

In **static trials**, the participants conducted isometric contractions repeated 10 times per muscle. For **dynamic motions**, the participants performed 3 trials per self-selected gait speed (slow, normal, and fast) in level-ground to validate the MuscLAB robustness while the subject is moving.

The EMG envelope (100 Hz) was computed using EMGWorks (Delsys' software), and it was compared with muscular voluntary contraction measured by MuscLAB at 100 Hz. For benchmarking analysis, the Pearson Correlation coefficient, signal delay, and NRMSE were computed in Matlab® (2017b, The Mathworks, Natick, USA).

4.4.4.Results and Discussion

EMG System

From the experimental validation, it was verified that the signal never saturates across different walking speeds, such that there is no loss of information. Furthermore, as illustrated in Figure 4.9, the **EMG system performs as expected**. It measured constant electrical muscle activation in steady-state pose (period 1 in Figure 4.9); it can measure the muscular activation correctly in dynamic motions with a repetitive pattern similarly to gait (period 2 in Figure 4.9);

it is able to **discriminate the agonist and antagonist function** among the *gastrocnemius* medialis and tibialis anterior muscles during walking.

The results presented in Table 4.4 indicate that the signal-noise ratio decreases as the gait speed increases, mainly for tibialis anterior muscle (from 19.21 dB to 10.31 dB). This finding suggests that the EMG system must be improved to minimize possible secondary motion artifacts, which may introduce noise in the EMG acquisition. Nonetheless, the achieved signal-noise ratio values are satisfactory considering that the EMG system will be applied for conditions that do not exceed 2 km/h of gait speed.
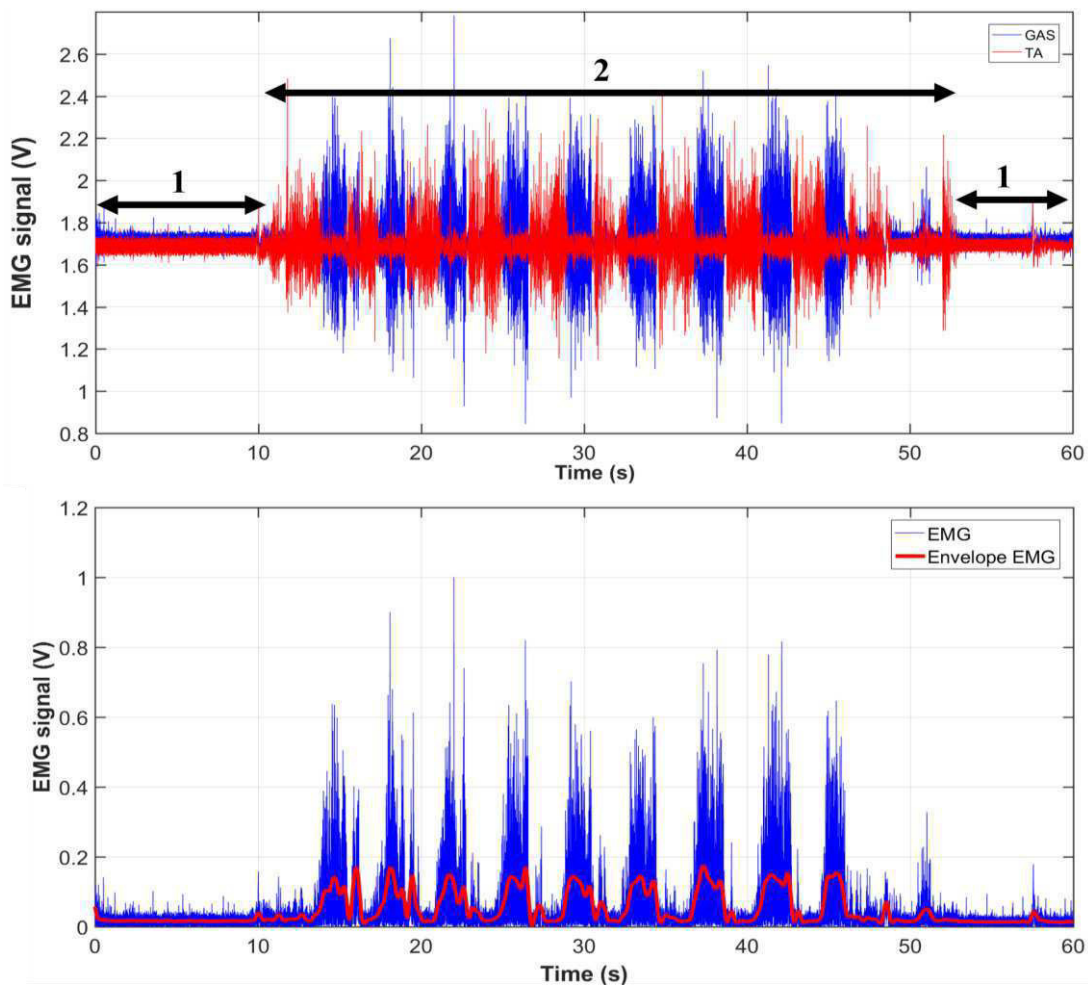
Figure 4.9-Representative EMG signals from one male subject walking at 1 km/h. **Top view**: EMG signals of *gastrocnemius (GAS) and* tibialis anterior (TA) along with gait trial (1: steady-state pose; 2: walking period). **Bottom view**: EMG signal and envelope EMG signal of *GAS.*

The signal-noise ratio of the EMG signals of the tibialis anterior was lower than the one achieved for *gastrocnemius*. Additionally, the muscle activation level of tibialis anterior was inferior to the one measured by *gastrocnemius,* as depicted in Figure 4.9. This finding is

related to the nature of the agonist/antagonist functions of these muscles [195]. Moreover, the real-time **gait analysis tool correctly computed the EMG envelope**, as showed in the bottom view of Figure 4.9. The obtained envelope signal adequately highlights the most significant components of the EMG signal for all considered static and dynamic walking conditions.

In overall, it is possible to outline that the hardware and software of the EMG system were successfully achieved for muscular activity analysis.

Table 4.4-Mean and standard deviation (std) values of signal-noise ratio (SNR), per gait speed, of EMG signals of the *gastrocnemius (GAS) and* tibialis anterior (TA) muscles.

Muscle	Speed (km/h)	SNR (dB)	
		Mean	**Std**
TA	1.0	19.21	0.89
	2.0	17.11	1.22
	3.0	10.31	3.75
GAS	1.0	19.42	0.99
	2.0	18.84	1.13
	3.0	14.71	2.47

MuscLAB

From the experimental validation, it was observed that the proposed system enables a quicker attachment procedure regarding the EMG sensors.

The results of Figure 4.10 indicate that the **MuscLAB** is able to **detect the muscular activity in static and dynamic conditions**. It also states that the MuscLAB can correctly monitor the agonist (concentric contraction) and antagonist (eccentric contraction) motions. However, the benchmarking analysis with the EMG envelope signal tracked by Trigno™ Avanti Sensors points out that there are deviations in the magnitude and timings of muscular activity signal.

The results presented in Table 4.5 point out that the performance of MuscLAB was consistent for both muscles. The RMSE is higher for dynamic motions (mean RSME < 24.6%) than for static ones (mean RSME < 9.57%), and tends to increase as the gait speed increases. The increment of the magnitude-based errors indicates that the effectiveness of MuscLAB is affected by the dynamic nature of walking motions, and likely, improvements in the attachment of FSRs into textile and usability of MuscLAB are needed. On the other hand, the MuscLAB's muscular activity signals become more similar (correlation coefficient increases) to the ones tracked by Avanti Sensors for dynamic conditions than for the static ones.

A **delay** (mean delay ranges from 144.01 to 163 ms) between the **bioelectrical muscle activity and the mechanical muscle activity** (MuscLAB) was observed. Two reasons may explain this delay. The first lies on the biological muscle proprieties considering that the muscle activity started due to the presence of electrical signals, which in turns, activates the muscle, leading to a mechanical muscle contraction. Second, the displacements between the electrodes and the FSRs since both sensors were positioned in different places in the same muscle, may result in different activation times. The last aspect constitutes a limitation for benchmarking analysis related to surface muscle activation analysis.
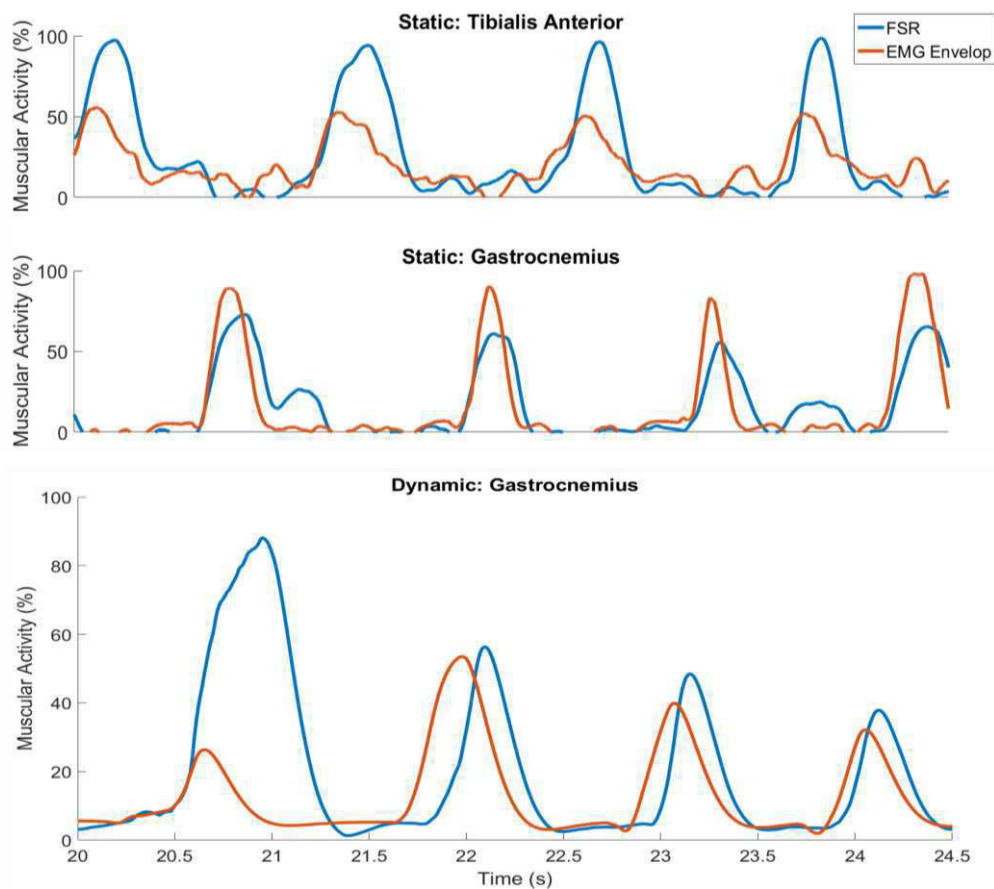
Figure 4.10- Representative muscular activity detected by MuscLAB and Avanti sensors from one female subject. **Top and middle view**: Muscular activity of tibialis anterior and *gastrocnemius* for static motion. **Bottom view**: Muscular activity of *gastrocnemius muscle* for dynamic motion at fast speed.

In overall, the outcomes suggest that the **MuscLAB** has the potential for providing an **evolutive analysis of the muscular activity** across gait training sessions. Nonetheless, the MuscLAB **cannot replace the forecast nature of EMG signals**, that is relevant for user's motion intention recognition and time-effective control purposes.

Table 4.5- A benchmarking analysis of MuscLAB and Avanti sensors for muscular activity. Mean NRMSE, Pearson correlation coefficient (C), delay.

Motion	Speed	Muscle	RMSE (%)	C	Delay (ms)
Static	-	TA	9.18 ± 3.40	0.65 ± 0.05	145.3 ± 35.1
		GAS	9.57 ± 2.66	0.65 ± 0.12	149.0 ± 46.72
Dynamic	Low	TA	18.65 ± 7.48	0.75 ± 0.03	152 ± 41.67
		GAS	18.85 ± 6.76	0.74 ± 0.02	149.01 ± 40.15
Dynamic	Normal	TA	22.78 ± 6.37	0.77 ± 0.05	147.4 ± 51.67
		GAS	23.57 ± 9.29	0.74 ± 0.03	163.02 ± 36.31
Dynamic	Fast	TA	23.68 ± 4.23	0.75 ± 0.02	144.33 ± 50.97
		GAS	24.6 ± 1.35	0.77 ± 0.04	145.63 ± 50.62

4.5. Conclusions

The Wearable Motion Lab integrates a set of quickly and automatically calibrated, low-cost, easily **wearable sensor systems** to cover 10th-to-90th percentile of the male/female population. The sensor systems enable the **all-day monitoring of kinematic or muscular activity** data in dynamic walking scenarios without interfering with the user's motion and with autonomy for at least eight hours of records, as demanded.

The **open-architecture** of the sensor systems contributes to their use as stand-alone and system-cooperative functioning in third-party systems, as SmartOs. The last feature enables providing real-time sensor data and feedback with minimal latency for (i) gait event detection (Chapter 5) (ii) locomotion mode recognition and prediction (Chapter 6), and (iii) assistive control strategies to provide a user-oriented gait training (Chapter 7). Moreover, the monitored kinematic and muscular activity data is being useful as objective outcomes (for computing spatiotemporal measures and kinematic and muscle synergies), and in the development of a tool for post-stroke disability locomotor analysis to support the clinical-based decision.

The benchmarking analysis with commercial systems demonstrates that the developed sensor systems are **purposeful for a user's evolutive gait analysis** in ambulatory scenarios, eliminating the need for high-complex and expensive capture systems.

Chapter 5 – Gait Event Detection

This chapter outlines the relevance of gait event detection for human motion analysis and current challenges considering previous achievements in the literature. Moreover, it presents a novel, real-time, adaptive gait event detection tool (more detail described in [52]) involving inertial data measured by wearable sensors as InertialLAB and GaitShoe (Chapter 4), and its evaluation considering repeated measures from healthy subjects in non-controlled gait conditions varying gait speed and terrain. A comparative analysis of the proposed tool and literature work is presented. The chapter ends with critical analysis and future challenges.

5.1. Introductory Insight

Gait event detection can potentially be applied in the design of personalized gait therapies and playing an integral role in the spatiotemporal gait evaluation. Different motion capture systems have been used to detect gait events. Most commonly, this analysis is conducted in a motion analysis laboratory with non-portable force platforms [39]. Consequently, these systems are not optimal to analyze consecutive gait cycles in free-mobility scenarios [101].

Current research suggests there is a need for assessing human events in non-structured conditions using wearable sensors. **Force-based systems**, such as foot-switches or FSRs, are generally considered the gold standard for detecting gait events [38]. However, these sensors

(i) can be **unreliable** when used in **drop-foot gait** due to their shifting weight during standing [162], [182], [196]–[198], and (ii) do not provide any information regarding the sub-phases of the **swing phase** [182], [196].

To overcome the inherent limitations of force-based sensors, recent studies have explored the potentialities of inertial sensors, particularly isolated accelerometers [37], [197]–[199], isolated gyroscopes [36], [39], [40], [102], [200], [201], and IMUs [35], [101], [161], [188], [196], [202], [203] for real-time gait event detection. According to systematic review of Taborri *et al.* [160], **gyroscopes provide better performance** than other inertial quantities for monitoring human gait. Commonly, gyroscopes placed on the shank [35], [36], [39], [40], [101], [102], [196], [200] and on the foot [101], [161], [197], [198], [201], [202], [204] lead to reliable gait event detection. However, Aung *et al.* [198] demonstrated better performance with the sensor located on the foot rather than ankle or shank.

5.2.Critical Analysis of Related Work

Most of the available computational methods that use measurements from the gyroscope for gait segmentation (Table 5.1) are based on the definition of heuristic thresholds through a rule-based FSM [35], [36], [39], [40], [101], [102], [197]. The threshold-based FSM proposed in [39] was able to detect 98% of HS and TO events performed by healthy children in indoor and outdoor inclined and flat scenarios. Kotiadis *et al.* [203] showed that using the gyroscope and accelerometer data as inputs of the FSM resulted in the proper detection of HS, TO, and HO events on flat surface and staircase walking. Furthermore, Storm *et al.* [35] demonstrated that the threshold-based FSM could accurately segment (accuracy of 100%) the HS and TO events performed by healthy subjects free-walking in an indoor and outdoor urban environment.

The use of **FSM** is mainly explained by its low computational demand and easy application [40]. Nevertheless, it has been reported that its performance can be affected by the high inter-subject [201] and inter-step variability [202]. To surpass the limited generalization when processing new datasets, previous studies [51], [159], [196], [205] introduced an updating layer for tailoring the thresholds endowed in the heuristic rules with the most recent state of the gait pattern.

The assessment of gait events proposed in the literature has been conducted in controlled environments (i.e., trials performed on treadmill or static walkways) and level-ground walking [26], [37], [102], [159], [161], [162], [197], [201]. When applied to real-life situations, previous gait analyses have mostly been restricted to two or three gait events [35]–[40]. Furthermore, evaluations have reported few repeated measures with different subjects, which is a problematic for evaluation of the reproducibility of the proposed computational methods under real-life applications.

There is a need to **find time-effective, inter-subject and inter-step versatile computational solutions** that describe human gait in both **controlled and real-life situations using few wearable sensors** to be easily reproducible in different contexts. The absence of a quantitative computational benchmark for the assessment of human gait events is a concern in the rehabilitation research community.

Table 5.1- Review of human gait segmentation tools only using gyroscope sensor.

Study	Tool	Event /Phase	Body Part	Real-Time	Results*
Sabatini *et al.* [163]	FSM	ST, HO, SW, HS	Foot	Y	H: < 35ms
Catalfamo *et al.* [39]	FSM	HS, TO	Shank	N	H: > 98 % H: < 75 ms
Greene *et al.* [206]	FSM	HS, TO	Foot, Shank	N	H: < 43 ms P: < 99 ms
Lee *et al.* [36]	FSM	HS, TO	Shank	Quasi	H: < 19 ms
Abaid *et al.* [161]	HHM	ST, HO, SW, HS	Foot	N	P: > 92 %
Gouwanda *et al.* [207]	FSM	HO, TO	Shank	Y	H: > 94 %
Mannini *et al.* [201]	HHM	HS, FF, HO, TO	Foot	Y	H: < 45 ms
Bejarano *et al.* [162]	FSM	HS, TO	Shank	Y	H: >99 %

Y: Yes; N: No; H: Healthy subjects; P: Pathological subjects; HHM: Hidden Markov Models
HS: Heel Strike; FF: Flat Foot; HO: Heel-Off; TO: Toe-Off; ST: Stance; SW: Swing;
*Results reported in the studies relative to detection delay (in ms) or detection accuracy (in %)

5.3.Methods

The proposed tool aims to address current challenges in gait event detection. First, the tool consists of an **adaptive FSM** to effectively detect the gait events in different daily locomotion activities, **varying gait speeds and terrains**, which represents a contribution to the current literature. Thus, the tool follows a threshold-based structure where a FSM detects the events and, in parallel, updates the thresholds used in the heuristic decision rules.

Second, the tool was designed to be a versatile tool able to detect **six human gait events** (HS, FF, MMST, HO, TO, and MMSW). It constitutes a state-of-the-art contribution, as previous analyses centered on the detection of HS, TO and MMSW events.

Moreover, the tool only relies on **single-axis of a wearable gyroscope placed on the user's feet** to minimize the number of sensors and to provide a more practical solution. The tool may use the gyroscope embedded on InertialLAB or GaitShoe to measure the foot angular velocity in the sagittal plane at 100 Hz. Through an empiric analysis (Figure 5.1.A), it was verified that the foot angular velocity presents a similar waveform under different terrains (namely, level-ground, inclined surfaces, and staircases). This remark indicates the versatility of this kinematic data for gait detection across different ground surfaces [160].

5.3.1. Adaptive FSM

Definition of Heuristic Decision Rules

For the definition of the heuristic decision rules, the angular velocity signal was segmented into six moments that correspond to the six gait events to be detected. To determine the exact moments of HS, HO and TO events, two FSRs were placed on the heel and toe (Figure 5.3). HO and TO events were set as the decreasing moment (when the FSR signal decreases by 70% relative to its maximum) of the heel and toe FSR signal, respectively, whereas the HS event consisted of the increasing instant (when the FSR signal is 70% higher than its minimum) of the heel FSR. The ground truths for FF, MMST, and MMSW events were based on direct visual inspection of the video-based angular velocity with the IMU angular velocity; both were overlapped and synchronized by overlay tools of an open-source tracker.

Figure 5.1.B depicts each gait event associated with the foot angular velocity signal, that is according to the literature, as follows. For the FF and MMST events, the angular velocity is almost steady at 0 rad/s until the HO event (that occurs after the zero-crossing) [156], [163]. According to [156], [163], [208], the gyroscope signal reaches the global minimum at the TO event. Studies [163], [202], [208] report that during the swing phase, the peak value appearing in the gyroscope signal occurs at the moment of mid-swing (i.e., MMSW event).
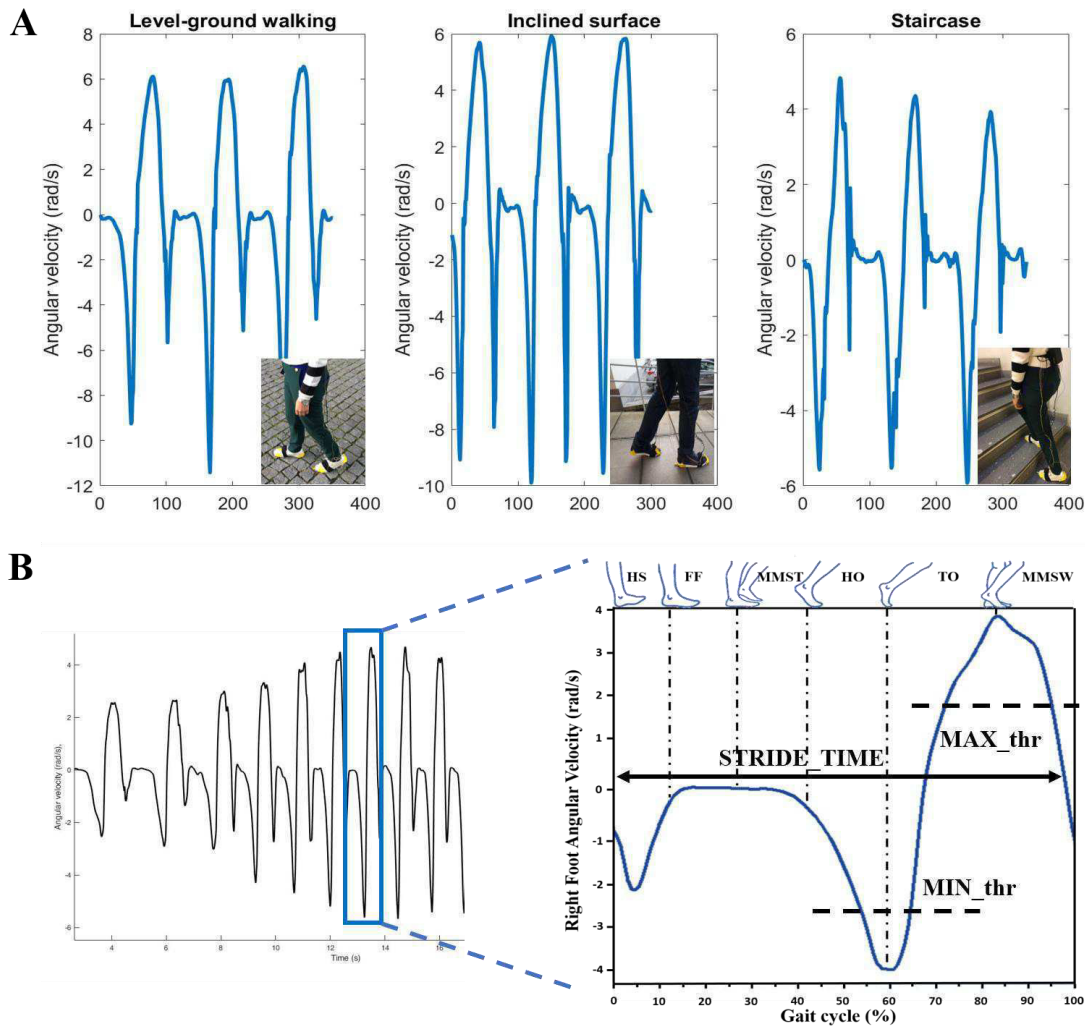
Figure 5.1- A: Foot angular velocity along sagittal plane measured at different ground surfaces: level-ground, inclined surface (10°), and staircase. **B:** Angular velocity of the right foot along the sagittal plane and representation of six human gait events during one gait cycle performed by a healthy subject [52].

Table 5.2 presents the **decision rules** based on **curve tracing techniques,** such as **adaptive thresholds crossing, local extrema detection** (i.e., maximum and minimum angular velocity), and the evaluation of **signal derivatives**. HS was defined as the first instant in which the angular velocity is within a range empirically determined to be close to the null angular velocity ($HS\_thr_{mean} \pm HS\_thr_{std}$ = -0.5 ± 0.05) after the maximum value has occurred. FF was detected when the signal becomes approximately constant (n samples with the 1st derivative almost null) after the detection of the 1st minimum. MMST was defined as n samples after FF occurred (n corresponds to the duration of the last valid MMST). HO was defined as when the velocity becomes negative after a constant period. TO was the 2nd minimum detected by an adaptive threshold (MIN_{thr} in Figure 5.1.B). MMSW was determined as the maximum detected above

95

an adaptive threshold (*MAX_{thr}* in Figure 5.1.B). The rules also have a condition that depends on stride time (*STRIDE_TIME* in Figure 5.1.B), which establishes adaptative intervals where the events shall occur and increases the robustness of the algorithm to changes in gait speed.

Table 5.2- Decision rules with adaptive thresholds in generic form. C indicates condition. [52]

C	Decision Rule	State
1	$(\text{gyro}_n > \text{MAX}_{thr})$ AND $(\text{derivative}_n < 0)$ AND $(\text{derivative}_{n-1} > 0)$ AND $(\text{gyro}_{index} - \text{MAX}_{index} \in [0.7 * \text{STRIDE\_TIME}_{Prev}; 1.3 * \text{STRIDE\_TIME}_{Prev}])$	MAX / MMSW
2	$((\text{HS\_thr}_{mean} - \text{HS\_thr}_{std} < \text{gyro}_n < \text{HS\_thr}_{mean} + \text{HS\_thr}_{std})$ OR 1st_gyro_min) AND 1st_gyro_max AND $(\text{gyro}_{index} - \text{MAX}_{index} \in [0; 0.4 * \text{STRIDE\_TIME}_{Prev}]))$	HS
3	$(\text{derivative}_n \approx 0)$ AND $|\text{derivative}_n| \leq 0.2$ AND 1st_gyro_min AND $(\text{gyro}_{index} - \text{MAX}_{index} \in [0.15 * \text{STRIDE\_TIME}_{Prev}; 1.0 * \text{STRIDE\_TIME}_{Prev}]))$	FF
4	MMST_counter $> (\text{HO}_{indexPrev} - \text{FF}_{indexPrev})/2$	MMST
5	$(\text{gyro}_n < 0)$ AND $(\text{derivative}_n < 0)$ AND $(\text{derivative}_{n-1} < 0)$ AND $(\text{derivative}_n > 0.9 * \text{derivative}_{n-1})$ AND $(\text{gyro}_{index} - \text{MAX}_{index} \in [0.3 * \text{STRIDE\_TIME}_{Prev}; 1.0 * \text{STRIDE\_TIME}_{Prev}]))$	HO
6	$(\text{gyro}_n < \text{MIN}_{thr})$ AND $(\text{derivative}_n = 0)$ AND $(\text{derivative}_{n-1} < 0)$ AND $(\text{gyro}_{index} - \text{MAX}_{index} \in [0.5 * \text{STRIDE\_TIME}_{Prev}; 1.1 * \text{STRIDE\_TIME}_{Prev}])$	TO

Adaptability and Finite State Machine

Adaptability is a pivotal feature for developing a **benchmark tool for gait analysis**. Given gait pattern variability, the proposed tool inspects changes in the duration (using *STRIDE_TIME* adaptive parameter) and amplitude (using adaptive thresholds, *MAXthr* and *MINthr*) of angular velocity since these signal conditions may change with variations in gait speed and terrain. The adaptive parameters were initialized based on an empirical inspection of the angular velocity from distinct gait patterns.

Figure 5.2.A shows the flowchart of the proposed computational tool executed via STM32F4-Discovery in each interaction at 100 Hz. The tool only starts the detection of gait events after the occurrence of the maximum peak of angular velocity.

Since the algorithm uses real-time peak detection, it was necessary to smooth the gyroscope data through a digital 1st order low-pass exponential filter. Posteriorly, the filtered sample was analyzed in 3 different stages to make the FSM adaptable for different real-life walking situations. The **first stage determines the 1st derivative** by detecting when the velocity increases (positive signal), decreases (negative signal) or becomes approximately zero.

A

Run

Signal Acquisiton
gyro(n) = getSample()

Low-Pass Filtering
gyroLP(n) = gyro(n)*K + gyro(n-1)*(1-K)

Derivative Computation
gyroDER(n) = gyroLP(n) - gyroLP(n-1)

Max/Min Detection

STRIDE Calculation

FSM

END

Max/Min (START)

gyroDER(n) < 0 && gyroDER(n-1) > 0? →YES→ Maximum detected

NO

Update Maximum Threshold
MAX_thr = 60%*mean(gyroMAX(n-3:n))

gyroDER(n) > 0 && gyroDER(n-1) < 0? →YES→ Minimum detected

NO

Update MinimumThreshold
MIN_thr = 60%*mean(gyroMIN(n-3:n))

END

STRIDE (START)

gyroLP(n) > 0.4 && gyroLP(n-1) < 0.4 && gyroDER > 0 →YES→ betweenRisesCounter >0.45*STRIDE(n-1) →YES→ Update Stride Duration
Stride = 60%*mean(Strides(n-3:n))

NO

NO

Reset Counter
betweenRisesCounter = 0

Update Adaptive Ranges
(HS range, FF range, MMST range, HO range, TO range, MMSW range)

gyroLP(n) < 0.4 && gyroLP(n-1) > 0.4 && gyroDER < 0 →YES→ betweenFallsCounter >0.45*STRIDE(n-1) →YES→ Update Stride Duration
Stride = 60%*mean(Strides(n-3:n))

NO

NO

Reset Counter
betweenFallsCounter = 0

Update Adaptive Ranges
(HS range, FF range, MMST range, HO range, TO range, MMSW range)

betweenRisesCounter++
betweenFallsCounter++

END

B

HS — 3 → FF

2

1

MAX/ MMSW — 1 → DEF

DEF

MMST

4

5

1

TO — 6 ← HO

R

E

Figure 5.2- A: Flowchart of the proposed adaptive computational method. **B**: FSM, where DEF is default state and R is reset state [52].

The **second stage covers the minimum/maximum calculation**, which is used to detect HS (after maximum), MMSW (maximum), FF (after 1st minimum) and TO (2nd minimum), given their dependency on the local extrema. A maximum angular velocity was only detected when the angular velocity was higher than the adaptive threshold (MAX_{thr}), the previous signal derivative is a positive value and the current signal derivative is negative soon after the signal derivative evaluation (*gyroDER)* is approximately zero (less than 0.01 rad/s – value set empirically to address the signal fluctuations). A similar approach to detect the angular velocity minima was applied using MIN_{thr}. The *Max/Min detection* stage also updates the *MAXthr* and *MINthr* thresholds (initialized as 0.7 rad/s and -2 rad/s, respectively) using the three previous valid strides, as in [52].

The **third stage updates *STRIDE_TIME* parameter** based on the last three valid strides, as described in detail in [52]. Briefly, to compute a valid stride, the tool looks for rising periods where the angular velocity was higher than 0.4 rad/s with a positive derivative, and at this moment a duration at least 45% of the previous stride has passed (*betweenRisesCounter* in Figure 5.2.A). *STRIDE_TIME* is used to establish the adaptive ranges where the events must occur. This strategy **tailors the algorithm to operate at distinct gait speeds properly** and allows the FSM to restart when an event is not detected (exit condition - E).

The **last stage implements the FSM** through the switch statement presented in Figure 5.2.B). The FSM includes six states, one for each gait event (MAX/MMSW, HS, FF, MMST, HO, TO), and two additional states (default state and reset state). The decision rules defined in Table 5.2, and the exit condition (E) are used to trigger the state transitions. The reset state is the first state to run, resetting all variables and setting the initial conditions. Next, the FSM transits to the default state and only leaves this state when rule (1) is true, transiting to MAX state, in the first detection, or to MMSW state, in the remaining situations. Lastly, the developed tool can also address situations in which the user stands for a period without walking. In this case, the algorithm resets after a pre-defined time (at least 5.0* *STRIDE_TIME*).

5.3.2. Experimental Validation

The gait event detection tool was validated using repeated measures of healthy gait patterns recorded in controlled and real-life situations, as depicted in Figure 5.3. The subjects signed a written informed consent to participate in this study.

Figure 5.3- Validation of the gait event detection system under controlled (1) and real-life walking conditions (2-flat and rough level-ground, 3-ramp, 4-stairs). The users wore two IMUs of InertialLAB (instep of the foot) and two FSRs attached to heel and toe by a yellow rubber strap [52].

Controlled walking situations: Participants and Protocol

This validation included 11 healthy volunteers (7 males and 4 females). The subjects presented an average age of 28.27 ± 4.17 years old, the height of 1.70 ± 0.08 m, and body mass of 69 ± 12.02kg. The participants were randomly divided into barefoot (6 subjects) and footwear conditions (5 subjects).

The participants conducted walking experiments on a treadmill at different speeds (1.5, 2.5, 3.5, and 4.5 km/h) and slopes (0%, 5%, and 10%). The subjects were asked to perform 3 trials of 30 seconds per condition. Furthermore, the participants were instructed to conduct walking trials at variable speeds. The subjects walked for 60 seconds and changed gait speed every 20 seconds according to the provided instructions (increasing from 1.5 km/h to 4.5 km/h and decreasing from 4.5 km/h to 2.5km/h).

Real-life walking situations: Participants and Protocol

The algorithm validation was extended to real-life indoor and outdoor environments to evaluate human locomotion in different conditions. For this matter, 9 healthy subjects (6 males and 3 females) were involved, who wore their own sports-shoes. The participants' mean age is 27 ± 7.35 years old, and they presented a height of 1.70 ± 0.12 m and body mass of 62.63 ± 9.39 kg.

Three gait trials were randomly performed in the following scenarios: forward level-ground walking on a 20 m flat surface; forward level-ground walking on a rough surface (urban ground) along 30 m; descending and ascending an inclined ground (10°) and a 10 m rough surface; and climbing a staircase of 8 steps (height of 17 cm, depth of 31 cm, and step width of 110 cm). For each condition, the participants were asked to walk at three self-selected gait speeds: slow, normal, and fast.

Data Collection and Analysis

The detected and reference gait events were collected at 100 Hz. The ground truths of HS, HO, and TO events came from two FSRs placed on the heel and toe (Figure 5.3). The reference FF, MMST, and MMSW events were found through visual inspection and based on the literature information [163], [202], [208].

A total of **5657 steps** from both feet were analyzed through Matlab® (2016a, The Mathworks, Natick, MA, USA). As performance metrics, the **accuracy**, the **percentage of occurrence and duration of delays and advances** were computed to assess the versatility and time-effectiveness of the proposed tool. The time-effectiveness was only inspected for correct detections. Timing errors greater than 100 ms (a critical duration for motor rehabilitation purposes) were considered as a misdetection.

Furthermore, the performance of the proposed tool was compared to a similar state-of-the-art gait event detection algorithm (four-state Hidden Markov model (HMM) [201]) using the same dataset. The comparative analysis was limited to the gait events assessed in [201]; HS, FF, HO and TO events. Note that the two compared methods were tuned using different data collected in healthy subjects from treadmill forward-walking. Further details in [51] and [201].

Lastly, two **statistical analyses** were carried out with a significance level of 5%. The first analysis investigates the accuracy and time-effectiveness of the proposed tool relative to the desired performance, i.e., 100% and zero ms, respectively. The second analysis is centered on the comparative analysis including two statistical tests; first, the accuracy of the proposed algorithm is higher than the one reached by the Mannini's tool; second, the delay and advance times of the proposed algorithm are lower than the one achieved by the Mannini's method.

5.4. Results

5.4.1. Adaptability

The findings indicate that the **algorithm's adaptability provides a proper detection** (orange line in top view of Figure 5.4) even when the foot angular velocity varies with changes in speed from 1.5 km/h to 4.5 km/h (controlled situation) and from 1 ± 0.2 m/s to 2 ± 0.18 m/s (real-life situations).

The increased gait speed results in higher values of angular velocity with shorter stride duration, supporting the need to update the thresholds of MAX_{thr}, MIN_{thr}, and $STRIDE\_TIME$,

respectively. In particular, by analyzing Figure 5.4, it is possible to conclude that the values of the adaptive thresholds (*MAXthr* and *MINthr*) increase or decrease when the magnitude of the maxima and minima are higher or lower, respectively.

Also, the adaptive ranges, which are directly dependent on the value of the *STRIDE_TIME* (blue line in bottom view of Figure 5.4), change in accordance with these values. The algorithm's adaptability can also address changes in the magnitude of the angular velocity, which may result from walking in overground (flat and rough ground) or on staircases.
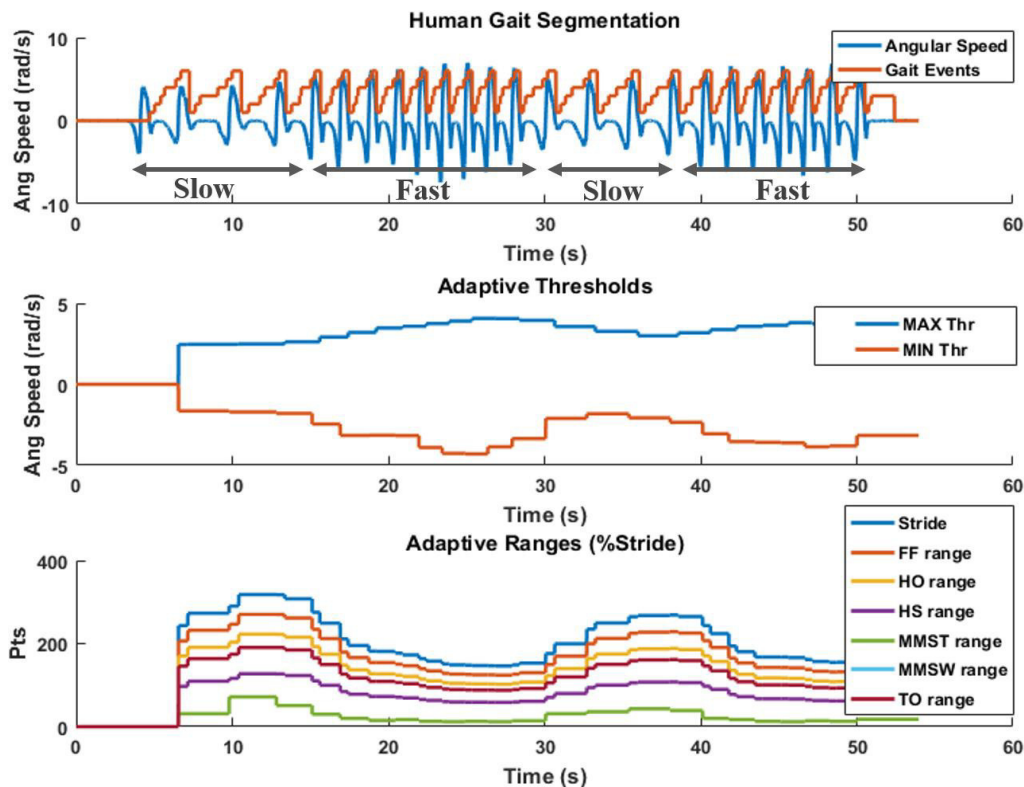
Figure 5.4- Gait detection for one subject (top view), walking at distinct speeds, with representation of adaptive thresholds (middle view) and adaptive ranges (bottom view) changing during the trial. Note that *Ang Speed* indicates angular speed and *Pts* the value of the adaptive thresholds dependent on the *STRIDE_TIME* [52].

5.4.2.Performance Metrics

By analyzing Table 5.3, it was verified that the proposed tool is significantly accurate ($p = 0.0812$) for the detection of all events at distinct conditions (e.g., speed, slope, footwear or barefoot) in the controlled situation (accuracy > 95.06%). **TO and MMSW events exhibited lower accuracy** (accuracies of 95.95% and 95.06 %, respectively) and had a higher occurrence of delayed detections (30.80% and 29.35%, respectively), likely due to the existence of local maxima and minima, respectively. Advanced detections were most observed for HO (18.62 ± 9.63 ms) and TO (14.38 ± 12.83 ms) events.

Table 5.3- Performance of proposed tool and Mannini's tool

	Proposed tool					Mannini's tool				
	ACC (%)	*Delay*		*Advance*		ACC (%)	*Delay*		*Advance*	
		%	ms	%	ms		%	ms	%	ms
CONTROLLED SITUATIONS										
HS	100	12.4	6.28±12.0	11.86	10.25±12.0	95.07	19.71	40.29±8.9	79.98	19.77±18.1
FF	99.37	6.23	4.36±5.1	9.21	9.18±17.8	92.37	9.16	52.76±20.7	90.31	20.84±19.6
MMST	98.78	20.46	30.53±9.9	7.92	15.31±5.5	-	-	-	-	-
HO	99.27	23.78	19.67±16.9	11.02	13.75±9.6	88.27	81.26	61.04±10.8	16.0	24.72±12.0
TO	97.57	8.74	5.82±15.9	18.24	11.13±9.6	90.47	77.49	21.22±12.0	21.93	44.87± 8.5
MMSW	94.71	7.41	4.54±4.3	0.29	1.75±4.5	-	-	-	-	-
REAL-LIFE SITUATIONS: LEVEL-GROUND										
HS	100.0	0.8	1.90±9.1	1.2	4.01±1.9	93.07	25.68	55.23±10.1	74.32	17.80±3.67
FF	99.24	2.8	2.22±8.56	1.6	1.19±9.46	91.32	34.42	46.05±8.65	63.40	23.15±2.56
MMST	91.04	23.5	8.63±12.5	16.7	8.43±4.24	-	-	-	-	-
HO	96.18	30.8	26.39±4.7	0	0.00	86.37	68.11	43.69±6.7	31.40	37.52±5.61
TO	98.64	1.1	4.8±10.56	4.3	3.69±8.95	89.54	71.35	17.34±9.34	28.09	36.80±9.1
MMSW	90.50	4.5	8.40±2.65	0.3	5.3±0.80	-	-	-	-	-
REAL-LIFE SITUATIONS: INCLINED SURFACES										
HS	99.82	0	0.0±0.0	2.3	0.71±2.45	92.57	1.44	61.75±2.4	98.56	11.50±7.60
FF	99.82	0	0.0±0.0	2.7	1.43±1.98	91.10	16.85	23.36±3.21	82.79	19.49±4.78
MMST	91.87	22.7	18.79±3.2	18.67	2.14±0.67	-	-	-	-	-
HO	96.17	28.9	16.43±12.3	1.6	0.71±0.56	85.47	85.89	38.11±6.54	13.80	48.32±4.81
TO	97.13	0	0.0±0.0	5.3	6.43±5.7	88.94	88.11	14.49±4.0	11.58	30.79±3.58
MMSW	90.12	3.7	8.63±2.56	0	0.0±0.0	-	-	-	-	-
REAL-LIFE SITUATIONS: STAIRS										
HS	96.98	0	0.0±0.0	2.56	2.51±1.56	90.46	10.6	44.91±5.2	89.42	18.88±2.45
FF	96.78	0	0.0±0.0	2.4	1.43±1.98	89.43	9.0	58.88±6.71	91.0	23.59±1.45
MMST	92.79	27.41	16.79±1.2	12.67	22.2±0.67	-	-	-	-	-
HO	93.98	24.6	23.6±7.3	0	0.0±0.0	81.67	80.0	67.39±8.92	18.57	52.35±4.67
TO	95.89	0	0.0±0.0	3.3	6.43±5.7	85.47	79.59	24.94±2.60	20.41	45.97±4.60
MMSW	90.79	2.63	2.63±3.16	0	0.0±0.0	-	-	-	-	-

The findings indicate that the proposed tool is significantly **more accurate** ($p > 0.0526$) in **level-ground and inclined surfaces than in staircases** ($p < 0.05$). However, in level-ground surfaces, the timing errors were significantly different than zero ms ($p < 0.05$), in contrast, to ramps ($p > 0.0942$) and staircases ($p > 0.151$).

In the real-life walking situations, the **HS was the most correctly detected event** (accuracy>96.98%). On the other hand, **MMSW** was the **least** correctly detected event (accuracy > 90.12%) due to the existence of local maxima. MMST was the earlier detected event (mean advances < 22.2±067 ms). **HO was the most delayed gait event** (mean delays < 26.39±4.67 ms) due to possible instabilities of the signal during stance (not completely constant). The remaining gait events presented lower timing errors.

Comparatively to Mannini's tool, the **proposed tool showed significantly lower timing errors** ($p = 0.9314$) and a **lower occurrence of misdetection** ($p = 0.9953$) in controlled situations. Moreover, the proposed tool (accuracy>96.98%) is significantly more accurate ($p > 0.9925$) in real-life gait event analysis than was Mannini's tool (accuracy>85.47%). Mannini's tool also demonstrated higher timing errors; delayed detections of HS (61.75 ± 2.4 ms) and HO events (67.39 ± 8.92 ms); advanced detections of the HO event (< 52.35 ± 4.67 ms).

5.5. Discussion

The novelty of the proposed gait event detection tool lies in using a **single kinematic measure to detect six gait events in real-life scenarios**, which include variations in gait speeds and surfaces. Consequently, the algorithm's adaptability proved to be a key feature for the successful application of the proposed tool in real-life situations. Note that the validation only considered straight-line walking.

In comparison with the literature regarding real-time gait event detection based on gyroscope signals, the proposed tool was able to conduct a **more holistic gait segmentation** by detecting six gait events instead of only detecting HS and TO events (the most commonly detected events). Moreover, this tool was more accurate when compared with similar studies [36], [162], [200] conducted in controlled situations and on level-ground surfaces.

So far, there has been no study able to detect the six gait events in both inclined surfaces and staircases. Catalfamo *et al.* [39] reported that their heuristic rules were able to segment the HS and TO events (accuracy of 98%) on inclined surfaces (indoor and outdoor

environments) with a delay of 25 ms and an advance of 75 ms. The presented adaptive method has shown to be **more time-effective** (advance errors lower than 6.43±5.7 ms and no observed delayed timing errors), and **similarly accurate** (accuracy of 99.82% and 97.13% for HS and TO, respectively) on **inclined surfaces**. Moreover, in stair walking, the proposed tool achieved favorable performance in terms of accuracy (HS=96.98% > 95.5%; TO = 95.89% > 93.1%) and time-effectiveness (HS=0.0±0.0 ms < 11±18 ms; TO=6.43±5.7 ms < 35±20 ms) when compared to study [40].

Furthermore, through a comparison with the HMM proposed in [201] using the same dataset, it was verified that the **proposed approach performs advantageously** in the detection of HS (delays of 61.75>6.28 ms; advances of 19.77>10.25ms), FF (delays of 58.88>4.36 ms; advances of 23.59>9.18 ms), HO (delays of 67.39 > 26.39 ms; advances of 52.35>11.02 ms), and TO (delays of 24.94>5.82 ms; advances of 28.09>18.24 ms). This benchmark analysis highlights the benefits of the proposed computational method for the gait event detection field.

5.6. Conclusions

The proposed gait event detection tool has shown to be a **time-effective, wearable strategy attempting for minimal sensing input** to provide a more practical solution for real-time and real-life gait analysis. The **adaptability** introduced provides more accurate gait analysis in different walking conditions, handles with inter-subject and inter-step variability. Moreover, the tool was robust in barefoot and footwear conditions even when different types (size, shape) of shoes were worn. This finding highlights the **versatility** of the proposed tool for different user's foot conditions in opposition to the force-based sensors. Additionally, the inertial sensor-based detection showed to be more accurate when compared to FSR-based detection, as reported in [209], due to the inconsistency response of FSR signals across terrains. Overall, the use of IMUs may be advantageous over FSR for gait event detection.

The gait segmentation plays an important role for user's motion recognition, as described in Chapter 6. Additionally, as the delay presented by the developed tool is lower than the response time of human physiological structures (128 ms [210]), the integration of this tool in real-time control is feasible. The tool has also been useful in the analysis of orthotic-based assisted gait, as considered in Chapter 7.

Chapter 6 – Daily Locomotion Mode Recognition and Prediction

This chapter highlights the potential of the user's motion intention recognition in gait rehabilitation, namely the contribution of recognition and prediction tools to timely classify locomotion modes (LMs) and locomotion mode transitions (LMTs). Moreover, it presents the development and validation of an automatic, versatile, user-independent machine learning-based tool for user's motion intention recognition and prediction of different daily LMs and LMTs, based on minimal kinematic data from wearable sensors, namely InertialLAB described in Chapter 4, and applying the gait segmentation introduced in Chapter 5. The chapter ends with a critical analysis of the effectiveness of the developed gait analysis tool and future directions.

6.1. Introductory Insight

Humans can perform distinct LMs in a variety of conditions and terrains in their daily routine. The **classification of daily LMs and LMTs** can be applied to tune the assistance provided by robotic assistive devices such as AOs according to the patient's LM and to generate smooth transitions, respectively [9]. The recognition and prediction of LMs and LMTs is a requirement

in user-oriented rehabilitation and assistance in daily-life scenarios [211]. For this purpose, it is necessary to develop automatic, user-independent tools capable of recognizing and predicting the LM and LMTs [9].

Multiple efforts have been made to develop automatic LM recognition tools. Part of them tackles pattern-recognition from EMG data [41], [212], [213]. However, EMG sensors present some drawbacks when compared to wearable kinematic sensors, such as the lengthy and expert-based installation, difficulty for keeping them attached during the user's daily locomotion, and the shifting electrodes may change EMG patterns and degrade the classification over time [189], [211], [213]. To avoid these limitations, more cost-effective, wearable kinematic sensors, namely IMUs, have applied.

6.2. Critical Analysis of Related Work

Previous studies [189], [211], [214] have proposed **LM recognition tools driven by IMU sensors** and validated in able-bodied subjects. Jang *et al.* [214] and Li *et al.* [211] applied a threshold-based FSM to recognize three (level-ground walking, and stair ascent and descent) and five (level-ground walking, stair ascent and descent, and ramp ascent and descent) locomotion modes, respectively.

On the other hand, Liu *et al.* [189] and Leuenberger *et al.* [215] employed machine learning approaches, namely the linear discriminant analysis (LDA) and the *k*-nearest neighbors (KNN), to recognize five (level-ground, stair ascent and descent, and ramp ascent and descent) and three (level walking, stair ascent, and stair descent) locomotion modes, respectively. Despite their contribution to accurate recognition tools, these works did not tackle the LM prediction problem, nor LMT classification, both demanded on robotic-based rehabilitation and assistance.

Considering the existing state-of-the-art [41]–[43] on predicting LMs and recognizing LMTs, some methodological drawbacks were observed. Huang's work [41] used LDA and support vector machine (SVM) to recognize five LMTs (level-ground walking to stair ascent, ramp ascent, and stepping over an obstacle and stair descent and ramp descent to level-ground walking). Despite the successful classification, some factors are limiting this work; namely, the tool depends on EMG information, and **transitions were recognized when one of the legs was already on the next terrain type**. This transition assumption, also observed in [42], does not

lead to a genuine user-independent tool since the user is asked to start the terrain transition with a predefined limb and it may interfere with the natural gait flow. In contrast, Chen *et al.* [43] applied LDA for LMT recognition without imposing a predefined leg for performing the transition. Nevertheless, this tool was not prepared to recognize common LMTs between the level-ground and ramp.

There is still a set of challenges to be pursued, as follows. First, to develop a **more versatile tool** for predicting and recognizing more daily LMs and LMTs. Second, to use discriminative sensor data measured by a **minimal number of easily wearable sensors**. Third, to allow the user to choose the leading limb to perform the LMT freely. The last challenge demands less cognitive effort from the user and enabling a more natural walk during daily activities.

6.3. Methods

The proposed tool tackles the challenges mentioned above. It consists of a **versatile, automatic recognition and prediction tool for classifying LMs and LMTs using kinematic data** collected from an easily wearable sensor system, namely the InertialLAB, that fosters a natural gait. The recognition and prediction tool aims at an efficient classification of the LMs commonly encountered in the daily life while covering different **walking directions** (i.e., forward, back, clockwise, and counter-clockwise) along with variations in **gait speed and terrains** (i.e., flat, ascending and descending stairs, climbing up and down ramp, stepping over obstacles). The tool also approaches transitions from/to those terrains using the user's self-selected lower limb. Furthermore, the tool was designed to be user-independent, i.e., it was built including data from different subjects instead of building a tool tuned per subject [42].

To develop the proposed tool, a **machine learning-based framework**, illustrated in Figure 6.1, was designed for enabling the fast and systematic implementation, testing, and comparison of various state-of-the-art algorithms namely, feature selection and pre-processing methods, and machine learning classifiers (DA, KNN, random forest, and SVM) with the same data. The framework, implemented in Matlab® (2017b, The Mathworks, MA, USA), allows the automatic and replicated LM and LMT classification and a benchmark to identify an accurate classification tool for both recognition and prediction purposes. This framework considers the procedures reviewed in [47], which points out the contributions of machine learning classifiers for this application due to their generalization ability to accommodate the environmental and

subject variability and to be accurate for classifying newly available data [47]. Each stage of the proposed framework is explained in the following.
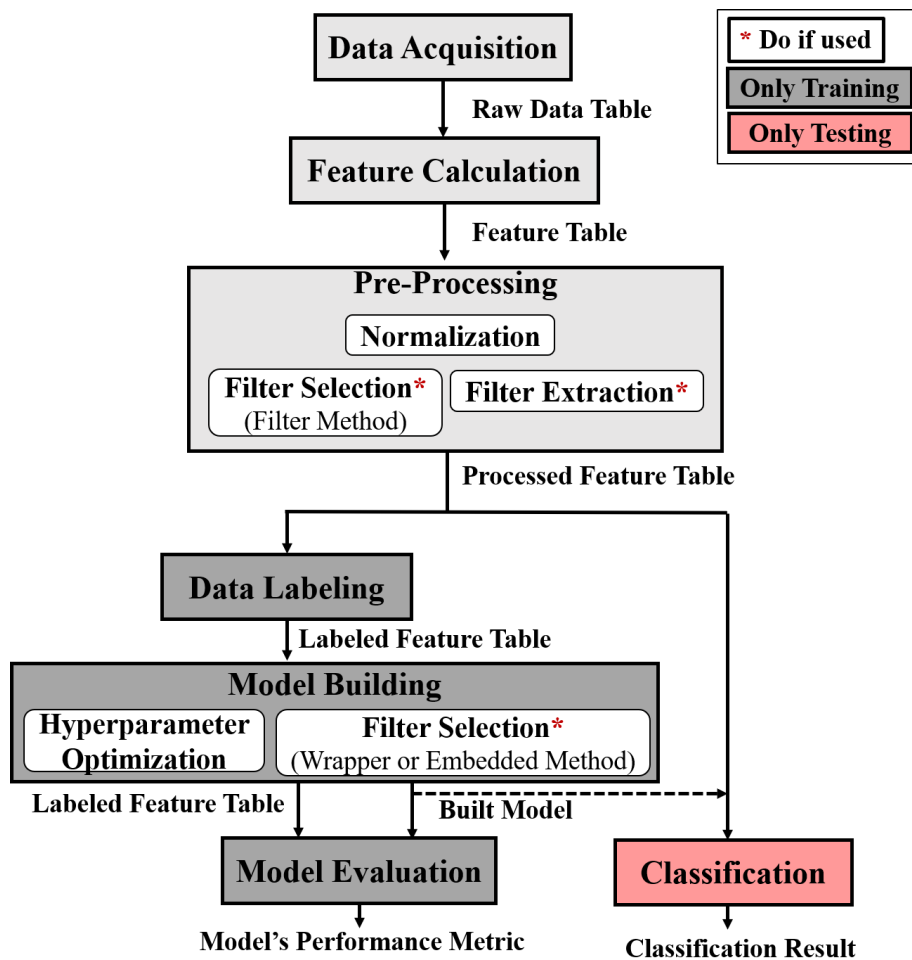
Figure 6.1- Schematic of the machine learning-based framework.

6.3.1.Data Acquisition

The *raw data table* (Figure 6.1) included kinematic data, sampled at 200 Hz, namely the **angle/orientation and angular velocity of lower limb segments'** (thigh, shank, and foot) in the sagittal plane, and the **angle and angular velocity of the torso in the sagittal and axial planes**. For this purpose, the InertialLAB was used considering the IMUs positioning on the outer side of the thighs and shanks, on top of the feet, and one IMU on the torso. Data were filtered by a 1st order low-pass filter (exponential smoothing) with 0.5 as the smoothing factor.

Participants

Ten able-bodied subjects (6 males and 4 females) were included who signed an informed consent form before the trials. The participants' mean age was 27±7.35 years old, with a height of 1.70 ± 0.12 m and body mass of 62.63 ± 9.39 kg.

Protocol

Before data collection, the InertialLAB was calibrated while the subject was in the upright standing position for 5 s. Then, the participants were asked to perform **9 trials per walking direction** (3 trials per gait speed). The trials included different walking directions (forward, backward, clockwise, and counterclockwise) performed on a 10 m level-ground at **3 self-selected gait speeds** (slow, normal, and fast).

Additionally, the subjects conducted **10 trials on four circuits** at a self-selected gait speed. In the first circuit (Figure 6.2.A), they walked 2 m forward on level-ground; ascended the **staircase**; walked forward on level-ground for 2 m and stopped; and descended the staircase back to the starting position. This circuit included 3 LMs (level-ground walking (LW), stair ascent (SA), and stair descent (SD)) and 4 LMTs (LW→SA, SA→LW, LW→SD, SD→LW). The staircase had 8 steps each with 17 cm of height, 31 cm of depth and 110 cm width. On the second circuit, the participants walked 2 m forward on level-ground; ascended a **ramp**; walked forward on level-ground for 2 m and stopped; and descended the ramp back to the starting position. The ramp was 10 m with 10° inclination. This circuit included 3 LMs (LW, ramp ascent (RA), and ramp descent (RD)) and 4 LMTs (LW→RA, RA→LW, LW→RD, RD→LW). On the 2 last circuits, the subjects walked forward 2 m on level-ground, **step over an obstacle** (SO), and walked forward 2 m (Figure 6.2.B). These circuits differ on the obstacle dimension. One circuit included an obstacle with 22 cm in height and 34 cm in depth; whereas, the other circuit involved an obstacle with 34 cm in height and 22 cm in depth. The **subjects could freely perform the LMTs with any leading leg** to enable transition seamlessly between LMs.

During the terrain transition, the participants performed transitional steps, which have a different meaning for recognition and prediction purposes. For recognition, a transitional step refers to the period from the instant that the leading limb left the prior terrain (last foot contact) to the first moment that this limb touched the upcoming terrain (initial foot contact). For prediction, the transitional step is the step that precedes the ongoing transitional step (used in recognition). An experimenter walked alongside the subjects marking the transitional moments (vertical red line in (Figure 6.2) using a digital button, similarly to [42], [216]. A transitional moment is a moment belonging to the transitional step considered for recognition.
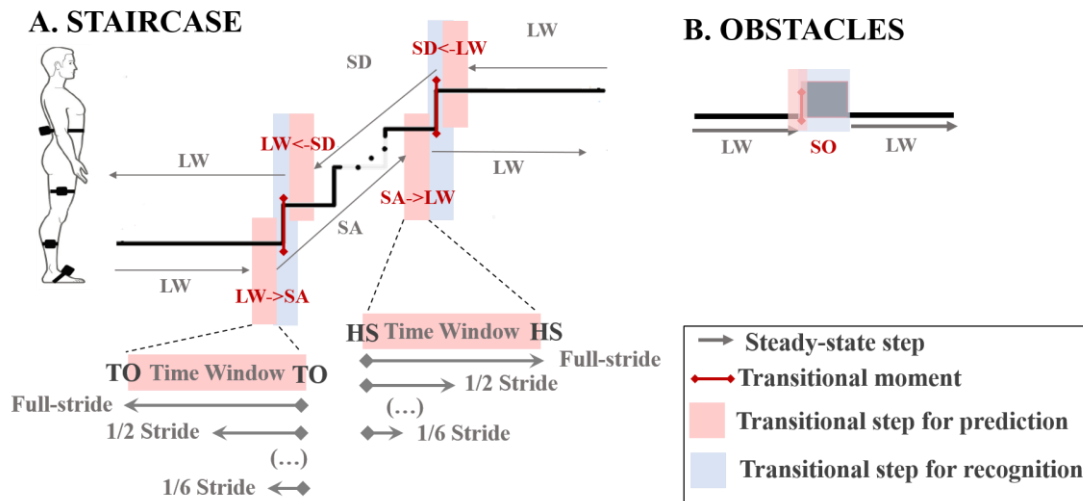
Figure 6.2- Representation of two circuits highlighting the transitional step, the transitional moment, and the explored time window's sizes for recognition and prediction purposes using HS and TO events. **A**: Staircase. **B**: Obstacles.

6.3.2. Feature Calculation

The *Feature Calculation* stage aims to obtain a *feature table* that includes **five types of features** (the **mean value, standard deviation value, range,** and the **values of the first and last positions**) calculated per gait stride for each kinematic data of the *raw data table*, resulting in a total of 80 features. Previous published intent recognition tools have used such features [42], [216], [217]. Figure 6.3 presents the content of the *feature table*.
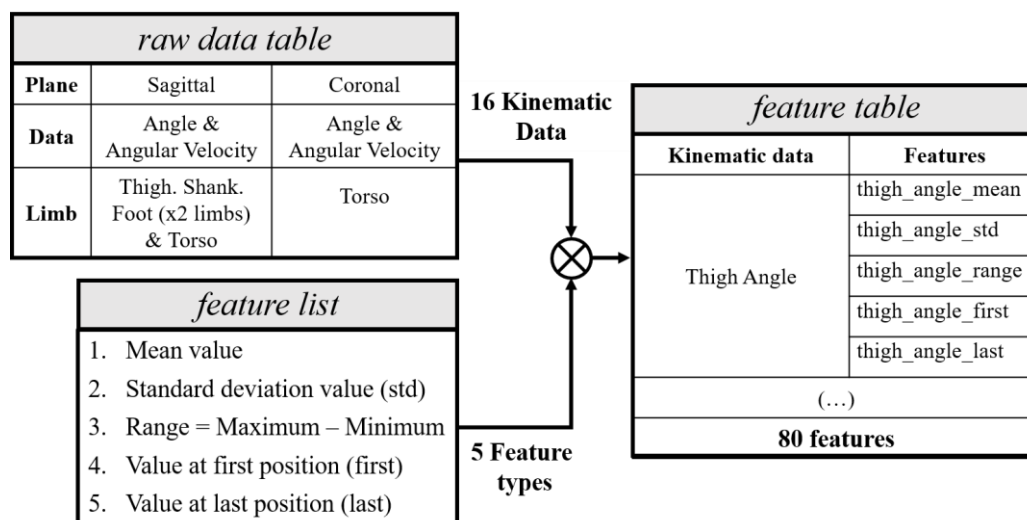
Figure 6.3- Content of the feature table with 5 types of features per kinematic data.

The gait stride's boundaries were defined as the HS and TO events (detected as described in Chapter 5 and in [51]) for recognition and prediction models, respectively, as illustrated in Figure 6.2. The TO was elected for prediction instead of HS event since it is a critical point for

110

transition (i.e., the beginning of the transitional step) [42] and it has achieved low prediction errors [218].

Further, **different time window's sizes** were investigated and established as fractions of the stride (namely, full-stride, 1/2, 1/3, 1/4, 1/5, and 1/6) to identify the most representative window's size for recognition and prediction models. The fractions of the stride were arbitrary selected, as in [218], to explore segmentation approaches less dependent on external tools for gait event detection in an attempt to minimize cumulative errors. As the time window's size is based on fractions of the stride, it adapts automatically to gait speed variations instead of considering a fixed timing size.

As depicted in Figure 6.2, for recognition and prediction models, the features were calculated from a time window that starts with the HS event and ends according to the selected stride's fraction, and from a time window that starts according to the selected stride's fraction and ends with the TO event, respectively.

The *feature table* contains data from both legs [219]. There is evidence that bilateral features improve intent recognition [216] and that walking, especially transitions, requires bilateral coordination of the lower limbs. **Two leg feature approaches were explored** to study the relevance of discriminating the leading and opposite legs. The first approach considers the *leading* and *opposite* leg, whereas the second approach considers the left and right leg.

6.3.3. Pre-Processing

The *Pre-Processing* stage is relevant for improving features using normalization techniques and for identifying discriminative features to build the models.

The features were normalized by the subject's height since the anthropometric scaling features reduce the variability of the *feature table* [47]. Additionally, different **normalization techniques,** namely **centering, *z*-score standardization, and min-max scaling** [220], were implemented and compared.

Furthermore, one filter feature selection method and one feature extraction method were implemented for identifying discriminative features. As the filter method, it was considered the **analysis of variance (ANOVA)-based method** that uses the minimum-redundancy maximum-relevancy (mRMR) algorithm to rank features in descending order according to their relevance [221]. Afterward, the ANOVA, starting on the highest ranked feature, assessed which classes are distinguishable for the feature considering the feature's mean and variance per

class. This procedure was done until there are a set of features that distinguish between all classes.

Regarding the feature extraction method, the **principal component analysis** (PCA) was implemented considering the Horn's Parallel Analysis as a cut-off criterium for extracting the number of components to retain [222]. A component is retained whether the associated eigenvalue is higher than 95th of the distribution of eigenvalues derived from the random data.

6.3.4. Data Labeling

In the *Data Labeling* stage, the *processed feature table* was labeled according to the LM or LMT from whereas it was collected, creating the *labeled feature table*. The labeling process merged a priori knowledge of the feature's origin with the transitional moment recorded during gait trials. During the training, the *labeled feature table* is the ground truth on which the model bases its decisions.

The **framework** was designed and implemented with **8 classification models for both recognition and prediction purposes** (4 models for each one), following the classification scheme depicted in Figure 6.4. The features of the recognition and prediction databases were equally labeled as follows. The ***direction_ft* database** includes features from the trials varying the **walking direction**. This database contains 4 classes (i.e., forward, backward, counterclockwise, and clockwise), and the features were labeled according to these classes.

The ***sts_trs_ft* database** contains two classes; the **steady-state step**, that considers all gait steps associated with the LMs; and **transition step**, that includes the gait steps related to LMTs. The features of the ***steady_state_type_ft* database** were labeled according to the five steady-state classes, one per LM (i.e., LW, SA, SD, RA, and RD). The database ***transition_type_ft*** includes features from transitional steps, which were labeled according to nine classes: LW→SA; SA→LW; LW→SD; SD→LW; LW→RA; RA→LW; LW→RD; RD→LW; and, SO. The period for crossing the obstacle (SO) refers to a transitional step from the first terrain (LW) to the second one (LW).

6.3.5. Model Building

The ***Model Building* stage builds the classification models** for recognition and prediction purposes. It may involve the application of wrapper and embedded feature selection methods and the optimization of the model's hyperparameters.

Two wrapper **feature selection methods** were explored, the **"mRMR plus forward selection"** and **"forward selection plus backward selection"**. When using "mRMR plus forward selection", the features were ranked through the mRMR method and a classification model was built and evaluated using the highest rated feature. A feature was only kept when it increased the performance. This selection was made for every feature or until the classification model reached the maximum performance (Mathew's correlation coefficient equal to 1). When using "forward selection plus backward selection", the feature that improves the performance the most in combination with the already established feature set was added to the set. Afterward, the backward selection was used on the obtained feature set, and the process was inverted; the features were iteratively removed if their absence did not affect the model's performance.

Moreover, **four machine learning classifiers** were implemented and compared; **DA** with linear and quadratic approaches; **KNN**, using both weighted and unweighted (regular) neighbor distances; **random forest**, and **SVM**, using linear, quadratic, cubic and Gaussian kernels. This comparison aims to identify the best-suited classifier for the LM and LMT prediction and recognition, given their prevalence in the literature [47].

The **classifiers' hyperparameters were optimized** for each selected feature dataset. The KNN and random forest were tuned by increasing the number of nearest neighbors (k) and the number of decision trees, respectively, starting with 1 until the performance reached the maximum value or started decreasing. For the SVM, the grid-search strategy ([-10 ; 10] interval) was used to tune the box constraint parameter (C) and the kernel scale parameter (σ) for the Gaussian kernel. DA used the delta threshold set to 0, and gamma regularization set to 1.

This stage produced 4 classification models (Figure 6.4) per recognition and prediction purposes, as follows. The **Direction Classification Model** classified the gait step data according to the walking direction. If a gait step has been classified as forward, then it was classified as a steady-state step or a transitional step by the **Steady-State/Transition Type Classification Model**. If it has been classified as steady-state, the **Steady-State Type Classification Model** was used for the final classification. Otherwise, the final classification used the **Transition Type Classification Model**. This classification sequence was applied to build the recognition and prediction models.
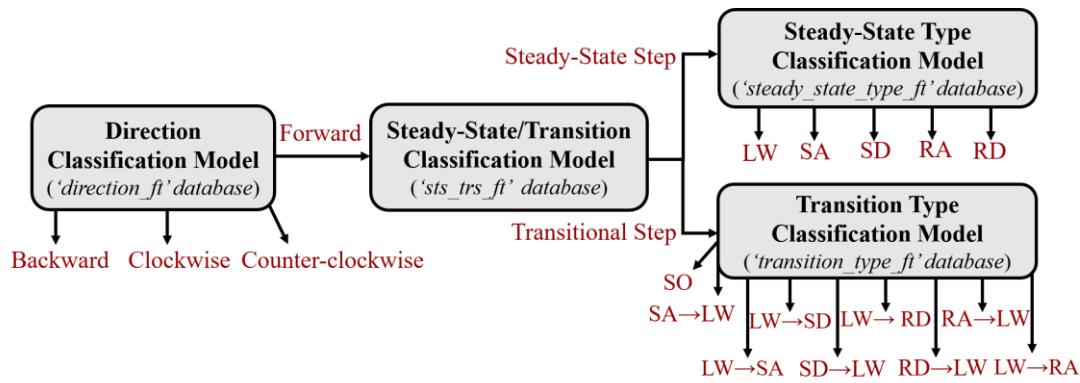
Figure 6.4- Schematic of the classification model's sequence for recognition and prediction purposes. Identification of databases and classes (marked at red).

The **implemented classification scheme** (Figure 6.4) seems to be advantageous compared with the one proposed in [42], [216] since it **demands fewer models**, decreasing the computational load, and allows the easy incorporation of further LMs and LMTs, adding versatility to the framework to act as a benchmark tool.

6.3.6. Model Evaluation

For evaluating the *built model*, **cross-validation methods** were applied following a two-fold applicational goal. The first goal aims the hyperparameter tuning and comparison of the classification models using the different features and pre-processing techniques. In this case, the *Model Evaluation* was performed by 2-fold cross-validation for minimizing the computational burden associated with the exhaustive model's comparison. The second goal aims to evaluate the generalization capability of the final classification models using the leave-one-subject-out cross-validation [47].

As performance metrics, **Mathew's correlation coefficient** (MCC) was used due to its good representative properties of unbalanced classes [223], as considered in this work. The **accuracy** was calculated for comparing the results with the literature's findings [47].

6.4. Results and Discussion

This section presents the results achieved for the final recognition and prediction tool built from the developed machine learning-based framework using the most effective techniques found for each stage. The comparative analysis of the different techniques explored in the framework is detailed in Appendix F. The findings presented in this subchapter allow investigating whether kinematic data is enough to recognize and predict LMs and LMTs.

6.4.1. Evaluation of Recognition Tool

The final recognition models were built using features calculated from a window size covering **full-stride** with the *left/right* **approach** and normalized by **min-max scaling in [-1; 1] interval**, the **"mRMR plus forward selection"** method for feature selection, and the **Gaussian SVM** classifier ($C = 64$, $\sigma = 4$).

Table 6.1 summarizes the results by describing the number of classified steps, the number of selected features by "mRMR plus forward selection" method, and the performance metrics, MCC and accuracy.

Table 6.1- Recognition tool's performance considering mean and standard deviation of MCC and accuracy (ACC)

Recognition Model	Number of steps	Number of selected features	MCC	ACC (%)
Direction	6064	43	0.998 ± 0.001	99.9 ± 0.4
Steady-State/Transition	3170	69	0.817 ± 0.008	96.5 ± 0.12
Transition Type	300	19	0.993 ± 0.011	99.6 ± 0.22
Steady-State Type	2870	53	0.995 ± 0.001	99.8 ± 0.3

As shown in Table 6.1, the **number of used features was variable**. Some features were selected for all recognition models, namely: (i) for left thigh, the last position of the sagittal angle and mean of the angular velocity; (ii) for left shank, the first position of the sagittal angle; (iii) for left foot, standard deviation of the sagittal angle, standard deviation and range of the angular velocity; (iv) for right thigh, mean value of the angular velocity; and (v) for right shank, the mean value of the angular velocity.

In particular, the features collected from the **IMU placed on the back were exclusively used in the recognition models**, as follows: standard deviation of the axial torso angle for Direction Recognition Model; mean of sagittal torso angular velocity for Transition Type Recognition Model; standard deviation of the axial torso angular velocity for Steady-State Type Recognition Model; and, mean, range and first position of the sagittal torso angle, first and last position of the sagittal torso angular velocity, mean and first position of the axial torso angle for Steady-State/Transition Recognition Model. The feature selection for the different models was consistent across subjects and involved features from all 7 IMUs.

The **Direction Recognition Model had near-perfect results** (MCC = 0.998, accuracy = 99.9%) with only few forward steps being classified as counter-clockwise or clockwise. This

model used 43 features from a total of 80. It shows that not all information is necessary for accurate classification of the walking direction.

On the other hand, the **Steady-State/Transition Recognition Model was less effective** (MCC = 0.817, accuracy = 96.5%) even using more features (69 features). Previous studies [42], [218] reported that the inclusion of ramps as an LM introduced some error due to the similarities between ramps and LW. This remark is according to the obtained results since **all misclassifications involved the walking on or transitioning to ramps**. The performance of Steady-State/Transition Recognition Model may affect end-stage classification accuracy, i.e., the performance of the Transition Type Recognition Model and Steady-State Type Recognition Model.

The **Transition Type Recognition Model was accurate** (MCC = 0.993, accuracy = 99.6%), even when it was built with one-tenth of the steps and with the least number of features (19 features) used in other models. This finding shows that it is possible to distinguish transition steps with high accuracy using a small number of kinematic features. The Steady-State Type Recognition Model had near-perfect results (MCC = 0.995, accuracy = 99.8%) using 53 features. Errors were due to the classification of level walking steps as ramp steps and vice-versa.

By comparing with the existing machine learning-based recognition tools based on kinematic data from wearable sensors, the **proposed recognition tool can perform a more versatile classification**. So far, there is still any accurate recognition tool able to classify LMs and LMTs that considers different walking directions in LW (forward, back, clockwise, and counter-clockwise) and terrains (LW, RA, RD, SA, and SD). Chan *et al.* [62] limited the recognition to SA and SD by using a less accurate tool (accuracy = 96.8%) than the one proposed in this work (accuracy = 99.8%). Further, the proposed recognition tool performs better when comparing to the one in [215], which identified the LW, SA, and SD with a sensitivity of 97%, 94%, and 87%, respectively.

The achieved results for recognizing steady-state steps in the LMs (LW, SA, SD, RA, and RD) are consistent with the ones reported in [43] (accuracy = 99.8% and accuracy = 99.7%, respectively), where the lowest recognition accuracy occurred for RA. Nonetheless, this tool [43] did not define transitional steps as their class; instead, they set a boundary between LMs after which the upcoming LM was attributed. In contrast, the **proposed tool recognizes the transitional steps** to allow some time to the robotic assistive device to timely generate smooth LMTs.

Lastly, it was observed that the most effective recognition tools proposed in the literature [41], [42] only recognized a LMT after the leading leg is already on the next terrain. In contrast, the proposed recognition tool **recognizes an LMT before the leading leg reaches the second terrain type**, without demanding any predefined leading leg, allowing a more natural walk in daily activities.

6.4.2.Evaluation of Prediction Tool

The final prediction models were built using features calculated over a window size of **1/4 of the stride** preceding the *leading/opposite* **leg approach**, normalized by **min-max scaling in [-1; 1] interval**, and selected by the **"mRMR plus forward selection"** method. The prediction models were built using **Gaussian SVM** classifier ($C = 64, \sigma = 4$). The findings suggest that the interval from 1/4 stride's fraction to the toe-off event (likely from terminal stance phase to preswing phase) contains relevant information for the user's motion prediction.

Table 6.2 presents the results considering the number of classified steps, the number of selected features by "mRMR plus forward selection" method, and the performance metrics, the MCC and accuracy.

Table 6.2- Prediction tool's performance considering mean and standard deviation of MCC and accuracy (ACC)

Recognition Model	Number of steps	Number of selected features	MCC	ACC (%)
Direction	6070	52	0.989±0.008	99.6±0.3
Steady-State/Transition	3192	64	0.607±0.024	93.3±0.28
Transition Type	316	38	0.887±0.0184	95.9±0.47
Steady-State Type	2876	59	0.986±0.003	99.4±0.8

The prediction models incorporate a different number of features by including features calculated from all IMUs of InertialLAB. This outcome indicates that the **dimensionality reduction did not contribute to reducing the number of wearable sensors**. Around eighteen features (almost 25% of the total) were common to all models. The prediction models used more features than analogous recognition models.

Some features were exclusively used in the prediction models, as follows: mean of the event foot angular velocity for Direction Prediction Model; first and last positions of the sagittal torso angle, and standard deviation of the sagittal torso angular velocity for Steady-State/Transition Prediction Model; mean angular velocity of the opposite shank, range of the

opposite foot angle, range of the sagittal torso angle, last position of the sagittal torso angular velocity for Steady-State Prediction Model. No specific feature was associated exclusively with the Transition Type Prediction Model, and there is no evidence for indicating the critical sensors per prediction model.

The **Direction Prediction Model presented a near-perfect behavior** (MCC = 0.989, accuracy = 99.6%), even when considering variations in gait speed. The misclassifications that occurred when forward steps were classified as counter-clockwise or clockwise and vice-versa, similarly to the recognition models. The model used 52 features from a total of 80 features, showing that there were still quite a few features irrelevant to the model. A previous turn system with IMUs reported results similar to the ones achieved in this work (accuracy> 97% vs. accuracy = 99.6%, respectively) [219].

The **Steady-State/Transition Prediction Model had the worst performance** (MCC = 0.607, accuracy = 93.3%) while using most features (64 features). The use of an unbalanced *sts_trs_ft* database including a higher number of steady-state steps than transitional steps may explain this finding. The **Transition Type Prediction Model was suitable** (MCC = 0.887, accuracy = 95.7%), mainly for SA->LW, SD->LW, RD->LW transitions. Moreover, the **Steady-State Type Prediction Model has shown to be effective** (MCC = 0.9857, accuracy = 99.4%) when using 59 features.

A previous study [42] developed a prediction system based on kinematic data and LDA that was able to classify LW, ramp, and stair steady-states with 99% accuracy. The **proposed prediction tool** (accuracy = 99.4%) also matches this performance, suggesting it is **more versatile** (considers more LM and LMTs) and **similarly effective**, when compared with similar works. Moreover, the proposed tool was in part identical to study [216], by investigating kinematic data from the step that precedes the LMT. However, the presented prediction models are more accurate, more versatile by varying walking direction and speed on LW, and followed a lower complex prediction scheme than the one proposed in [216]. Furthermore, the **developed approach is more practical considering daily application** requirements given the faster time for wearing the IMUs and provided a less intrusive experience than the one reached with the tethered solution proposed in [216].

Other studies [218], [224] have combined EMG with kinematic sensors, addressing a neuromechanical sensor fusion for improving the steady-state and transition prediction. The sensor fusion used in [224] was slightly more effective (accuracy = 0.95) in the transition

prediction problem than the proposed kinematic-based tool (accuracy = 93.3% for Steady-State/Transition Prediction Model and accuracy = 95.9% for Transition Type Prediction Model). On the other hand, the developed transition prediction model was more accurate than the models described in [218] (accuracy = 88%), which used EMG sensors that also reported uncomfortable usability [42].

6.4.3.Limitations

The developed classification scheme requires accurate classification models throughout the classification sequence since classification errors would propagate from the initial to final classification stage. This means that the performance of both the Steady-State Type Classification Model and Transition Type Classification Model depends on the effectiveness of Direction Classification Model and Steady-State/Transition Type Classification Model. In practice, the accuracy of Steady-State Type Classification Models and Transition Type Classification Models is lower than the one presented in Table 6.1 and Table 6.2 since it would be needed to add the classification error of Direction Classification Model and Steady-State/Transition Type Classification Model.

Moreover, the reduced number of transitional steps might be underperformed the Steady-State/Transition Prediction Model.

The validation of the proposed recognition and prediction tool was limited to gait patterns obtained from a set of healthy subjects. The variation of walking direction and gait speed with terrains was not addressed in this thesis.

6.5.Conclusions

The benchmarking analysis using the developed machine learning-based framework concluded that the **min-max normalization within [-1; 1] interval, "mRMR plus forward selection" feature selection method,** and **Gaussian SVM classifier** as the most accurate techniques for building recognition and prediction tool. The findings highlight the following concluding remarks. First, the discrimination of the leading and opposite legs is relevant for prediction. Second, the dimensionality reduction methods that depend on the *built model* outperformed the ones (as ANOVA and PCA) that do consider the classification model. The SVM's ability to define more complex decision boundaries favors the user's motion analysis, as reviewed in [47].

The developed automatic, user-independent recognition and prediction tool tuned with **kinematic patterns correctly classify LMs and LMTs** commonly encountered in daily life. The contribution of this work to the state-of-the-art is manifold; it proposes a **more versatile tool** that classifies several LMs and LMTs while covering different walking directions and terrains; it tackles the transition prediction problem only using kinematic data; and, it allows the **user to self-select the leading limb** for performing the transitional step. There is evidence that **kinematic data are appropriate for predicting** LMs and LMTs one step before their occurrence.

Moreover, the proposed tool was able to achieve generalization for a given set of healthy subjects. It may be applied to establish a recognition and prediction tool for a segment of the population of pathological end-users.

There is still room for improving the decision-making from/to ramp by using environment awareness to infer the interaction between the user and the world [225]. Recent efforts are being made to update the user's motion intention tool of SmartOs considering the forecasting nature of infrared laser sensor data, inspired by the human ability to adapt and transit among LMs considering the visualized upcoming terrain changes. The LM transition prediction tool based on a wearable infrared laser sensor showed in [54] to be accurate and time-effective (prediction time > 0.73 s) for LMTs in different terrains (level-terrain, stairs, and ramps).

Lastly, the ability of the proposed tool for classifying the user's motion intention will be extended for the high-level layer of the control architecture described in Chapter 7.

Chapter 7 – Assistive Control Strategies

This chapter starts with an introductory insight into the assistive control strategies applied in robotic-based gait training. Then, it presents the implemented hierarchical control architecture, detailing the development and validation of the assistive control strategies approached in this thesis. The potential rehabilitation benefits of each assistive strategy are disclosed and discussed. Moreover, this chapter investigates the contributions of Feedback Error Learning (FEL) as a time-effective and adaptive low-level controller for SmartOs system. The chapter ends with a comprehensive concluding insight into the proposed assistive control strategies.

7.1. Introductory Insight

Gait rehabilitation involves a physical and cognitive relearning of how to move to carry out their needs successfully and in a safe manner [11]. AOs should foster such gait rehabilitation by endowing **assistive control strategies** designed to enable **user-oriented** and **intuitive motor learning**. While assisting and enabling long-term recovery of motor abilities, these control strategies have been reducing the burdens placed on short supply of therapies and other health care personnel [9].

121

Previous neuroscience studies have demonstrated that repetition plays a significant role in potentiating **motor relearning and functional reorganization** [11]. Consequently, rehabilitation intervention involving AOs towards **repetitive locomotor movements** for long-term training sessions, mainly when **trajectory assistive strategies** are applied [9], [31]. The trajectory control is a conventional assistive strategy that guides the AOs to move along repetitive and specific movements, based on predefined position or torque trajectories, similar to the way that therapists move patient's legs during manual assistance [11], [29]. New directions include **adjustment of trajectories** according to the users' body conditions and gait speed, approaching the adaptive trajectory control to improve the user's movement coordination and enabling a natural gait pattern recovery [27], [28]. Central pattern generators, applying biological concepts of the human motion control system, can be used for generating adaptive trajectories considering gait speed variations [226].

Motor learning theories have also highlighted the needed for **teaching more functional gait patterns,** which allow neurologically impaired subjects to achieve a certain level of physical independence on daily living [11]. Consequently, assistive control strategies such as **EMG-based control** [33], [227] and reflex-based control using neuromuscular bioinspired models [28], [228] have been proposed to foster user-oriented assistance during **high-challenging and dynamic locomotor tasks**.

There is evidence that the effects' size of robotic-driven gait rehabilitation, such as the functional motor recovery result from the user's voluntary participation, depends on how compliant is the human-robot interaction [31], [229]. **Impedance assistive strategies** have been implemented by modulating the impedance of assistive devices to establish a symbiotic **human-robot interaction**, maintaining the interaction force below safe levels for the user while controlling the limb position according to the desired trajectories for the gait therapy [229].

Additionally, **AAN control strategies**, such as **adaptive impedance control** [29], [230], [231], **AAN EMG-based control** [232], [233], and **energy-based control** (making use of a physiological signal of energy) [234] have been proposed to ensure an energetic-efficient assistance for providing a more **personalized and functional training** [11], [27], [235]. These strategies are able to automatically modify control parameters to tailor the assistance based on the individual user's needs.

Note that different controllers, such as feedback control, model-based control, iterative learning control, and fuzzy control [236], may be used to ensure that the assistive devices track the desired assistance set by these assistive control strategies.

Table 7.1 presents an overview of the assistive control strategies mostly applied in active assistive devices. Each of these strategies may be advantageous in some gait rehabilitation and assistance paradigms depending on the user's disability level and therapeutic purposes.

Table 7.1- Summary of the control strategies applied to active assistive devices. Information obtained from [10], [11], [13], [45], [46], [237].

Control Strategy	Principle	Advantage	Disadvantage	Assistive Device (e.g.)
Predefined Trajectory Control / Adaptive Trajectory Control	Impose repetitive trajectories	- Useful for patients with severe motor pathology; - Increase the leg's natural frequency;	- Not encourage the subject's participation; - Not consider the user's movement intention;	ATLAS; eLEGs; HAL; Mindwalker, SCKAFOS
Impedance control / Adaptive impedance control	Modify the impedance/compliance of the assistance	- Considers human-robot interaction. - Encourage the user's participation; - Considers the user's disabilities;	- Inter/intra-subject difference affects the control modelling;	Knee orthosis by Daachi; Lokomat®; Orthosis by Hussain
EMG-based Control	Follow user's motion intention based on EMG signals	- Considers the user's disabilities; - Tracks patient's rehabilitation progress; - Encourage the user's participation;	- Differences in muscular activity between users and motion tasks; - Requires repeated calibration to deal with muscular activity variation	AAFO by P. Kao, AAFO by Ferris, Sharif Exo-skeleton

Introducing gait training variability improves the overall function motor performance and enables to accommodate the variability of the inter-and intra-subject needs. In this sense, the AOs should approach different assistive control strategies offering a **multi-functional assistive system suitable for distinct kinds of therapies.**

Bioinspired control architectures, following the principles and organization of the human motion-control system, started to emerge [9], to efficiently approach user-oriented and AAN strategies and to provide a seamless and synergetic user-orthosis interaction for increasing brain plasticity [28]. Such architectures comprise the design of low-, mid-, and high-level

controls, distributed hierarchically to accounts with the physical interaction between the user, the environment, and the AO [9], [46].

The design and development of the hierarchical control architecture of SmartOs followed these research directions and the potentialities of each assistive control strategy, as following described in this chapter.

7.2.Hierarchical Control Architecture

SmartOs system endows a **safe, hierarchical, closed-loop control architecture hierarchically structured into three-control levels**, as illustrated in Figure 3.1. Both structure and the fusion of control and sensor feedback systems were bioinspired on the human motion-control system.

The **high-level**, the perception layer, was designed to manage the gait analysis tools for user's motion intention recognition (presented in Chapter 6), gait event detection (described in Chapter 5), gait speed estimation (given in Chapter 4), and user's disability level recognition. It **sets user-oriented gait trajectories**. The **mid-level**, the translation layer, **converts the user-oriented trajectories into AO reference trajectories** tailored by the current gait event and human-orthosis interaction when needed. Lastly, the **low-level layer** uses **tracking controllers** to generate assistive commands such that the AOs' state timely track the desired assistive. Currently, the control architecture endows low-level position-based and torque-based tracking controllers implemented through proportional integral derivative (PID) and FEL.

Concerning the control frequency, the low-level was set to 1 kHz (high-frequency for achieving an effective human-machine tracking control loop) while the high- and mid-level to 100 Hz (enough for human-machine gait analysis). All software routines of the low- and mid-level controllers were implemented in C language in the STM32F407VGT microcontroller, whereas the high-level controllers, implemented in C++ language, are executed in the CCU, the Raspberry Pi 3.

The architecture presents a modular design to be expandable for including further assistive control strategies as required for making SmartOs a multi-functional robotic-based gait training solution.

7.2.1.Overview of Proposed Assistive Control Strategies

Currently, the control architecture includes four user-oriented, closed-loop assistive control strategies, implemented in the high- and mid-level controllers, as follows.

(1) **User-orthosis interaction-based control** that controls the human-orthosis interaction to minimize the mechanical impedance of the AO to act like a passive device and follow the user's motion intentions (chapter 7.3);

(2) **User-oriented trajectory control** that controls the position-based trajectory of the human joint according to user-oriented trajectories (chapter 7.4);

(3) **Adaptive impedance control,** an AAN control strategy that controls and adjusts the impedance of the human-orthosis interaction, providing interactive and compliant training (chapter 7.5);

(4) **EMG-based Control** that controls the assistance level of AOs based on the voluntary muscle contraction of the user, reflecting the user's motion intentions (chapter 7.6).

Figure 7.1 presents an overview of the hierarchical implementation of each control strategy. Throughout this chapter, each assistive control strategy will be presented and validated involving healthy subjects to investigate their usability and time-effectiveness for real-time gait rehabilitation and assistance and to establish guidelines for their application in neurological conditions.
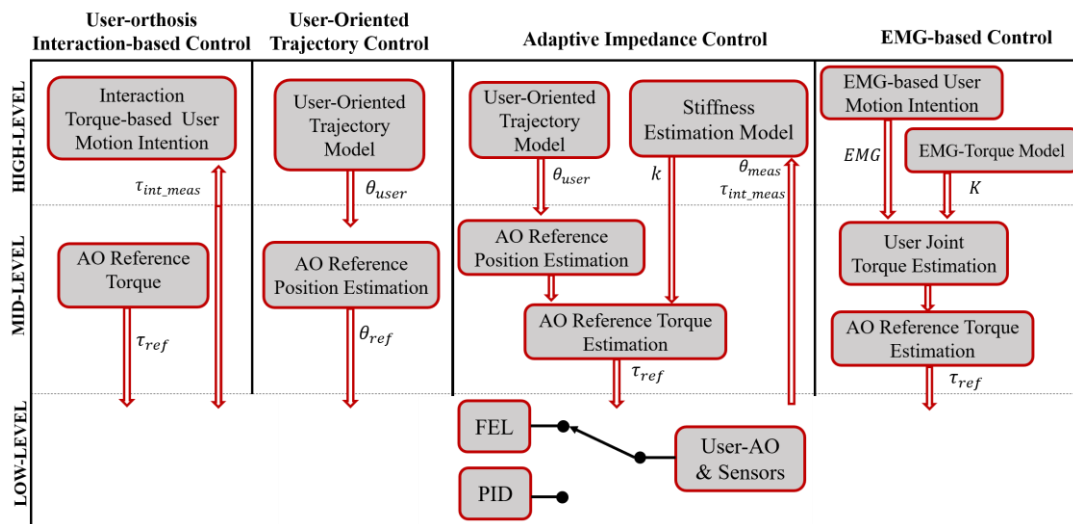
Figure 7.1- User-oriented assistive control strategies implemented in the hierarchical control architecture. τ_{ref}, AO reference torque; τ_{int_meas}, user-AO interaction torque; θ_{user}, user-oriented position trajectory; θ_{ref}, AO reference position trajectory; θ_{meas}, AO measured position trajectory; k, stiffness of the user-orthosis interaction; EMG, EMG envelops; K, EMG-torque user-oriented parameter.

The control strategies were selected considering the therapeutic challenges proposed for SmartOs system in the post-stroke gait training, as listed in Table 7.2. In overall, these strategies make the SmartOs suitable for distinct kinds of therapies to accommodate short- and long-term changes in motor capacities. All strategies enable gait speed variation from 0.5 to 1.6 km/h (considering the mechanical limits of AOs) to enable high-challenging gait training within each strategy.

Table 7.2- Summary of assistive control strategies applied to SmartOs

Assistive control strategy	Low-level Control*	Principle	Therapeutic Purpose
User-Orthosis Interaction-based Control	Torque PID	User's interaction User's motion intentions	- User's active participation encouragement - High-level of muscle strengthening - Familiarization period
User-oriented Trajectory Control	Position PID or FEL	Repetitive movements	- User-oriented repetitive gait training - User's natural gait pattern recovery - More symmetrical gait pattern
Adaptive Impedance Control	Torque PID	User's interaction User's intentions	- User's natural gait pattern recovery - Long-term recovery of functional motor abilities - Energetic-efficient motor recovery - User's active participation encouragement - Increased muscular strength - Assistance level adjustment
EMG-based Control	Torque PID	User's intentions	-Long-term recovery of functional motor abilities - Increased muscular strength - Reduced muscular atrophy - User's active participation encouragement

* Current low-level controllers implemented per assistive control strategy.

7.2.2. Safety Measures and AO's Attachment Methodology

Different **safety measures** were included throughout the control architecture and applied for all assistive control strategies **to safeguard the user and AO integrity**. The first safety measure was regarding the mechanical limits, i.e., the range of motion of the AOs. The range of motion of PKO and PAFO was limited to [5; 98]° and [-18; 18]°, respectively. These intervals are contained within the range of motion of the user's joints so that the AOs do not compromise the users' joints integrity by applying overextension or over-flexion motions.

The control commands were limited to [-2500; 2500], i.e., the maximum values of the AOs' pulse-width modulation, to avoid the controller instabilities. For this purpose, the hierarchical architecture includes a saturator. Additionally, the therapy is interrupted or stopped smoothly and safely when the user is touching on the ground to avoid a fall risk situation.

Lastly, an **adaptable attachment** of the AOs with the user's lower limbs and joints, respectively, was considered **maximizing the AO's usability**. The location of the braces was adjusted according to the user's limb length, and the strap system enables the adjustment of AO to the user's limb width. This attachment methodology makes the AOs suitable for subjects with different anthropometric features to cover 10th-to-90th percentile of the male/female population (height ranging from 1.50 m to 1.90 m and body mass ranging from 45 kg to 100 kg).

A four-strap system was incorporated in the mechanical structure of the PKO, by placing two upper straps on the tight and two lower straps on the shank, as represented in Figure 7.2.A. The PAFO was attached to the human lower limb using a two-strap system placed on the user's shank and a four-strap system built-in the PAFO's outsole placed on the user's feet, as depicted in Figure 7.2.B. This outsole system was used on the non-assisted limb (i.e., limb without the PAFO) to minimize the gait asymmetry due to the height of the outsole placed on the assisted-limb.

Furthermore, the attachment system also aims to improve the **user's joint and AO alignment** and consequently, to minimize the loss of mechanical power without obstruction or resistance to the movement.

Figure 7.2- AOs' attachment system. **A:** Four-strap System (1-4). **B**: Two-strap System (1-2) and four-strap system built-in the PAFO's outsole (3).

7.2.3.Gravity Compensation

The control architecture includes at the low-level layer a gravity compensation component to minimize the gravitational burden of the wearable AOs' mass from the user [238]. The control architecture was designed to provide the gravity compensation torque when a user is wearing the PKO or PAFO.

Methods

Generally, the gravity compensation torques ($G(\theta)$) may be computed through the expression of the potential energy (P), as given in Equation (7.1a), considering the Euler-Lagrange formulation. As the PKO and PAFO are a two-link articulated system (including an upper and lower link, here presented as link$_1$ and link$_2$, respectively), the potential energy (P) of these AOs is described using Equation (7.1b). Consequently, the expression for computing the gravity compensation torques can be written, as given in Equation (7.1c).

$$G(\theta) = \frac{\partial P(\theta)}{\partial \theta} \tag{7.1a}$$

$$P = \sum_{i=1}^{2} P_i \tag{7.1b}$$

$$G(\theta) = \begin{bmatrix} \dfrac{\partial P}{\partial \theta_1} \\ \dfrac{\partial P}{\partial \theta_2} \end{bmatrix} \tag{7.1c}$$

The **gravity compensation is variable along with gait cycle** given its dependency on the AO's joint angle, namely the angle of the upper and lower link, represented as θ_1 and θ_2 in Figure 7.3.A, respectively. For both AOs, the θ_2 was measured by the potentiometer embedded on the AO. The θ_1 was got from IMU-based angle estimation, as described in Chapter 4.2. To monitor θ_1 in PKO, the IMUs were placed on the human center of mass and thigh (IMU1 and IMU2 in Figure 7.3.A, respectively). For PAFO, the IMUs were placed on the thigh and shank (IMU2 and IMU3 in Figure 7.3.A, respectively).

Overall, the gravity compensation torques were computed through Equation (7.2), where m represents the link's mass, l is the link's length, lc represents the length between the center of AO's rotation to the center of mass of the link, θ is the link orientation, and g the gravitational acceleration, 9.8 m/s². As the actuation system is placed on the lower link, the

actuation system of **AO can only generate the $G(\theta_2)$ gravitational torques**. Consequently, the control architecture of SmartOs includes a partial gravitational compensation as it is not able to generate $G(\theta_1)$ torques.

$$G(\theta) = \begin{bmatrix} G(\theta_1) \\ G(\theta_2) \end{bmatrix}$$

$$\begin{bmatrix} G(\theta_1) \\ G(\theta_2) \end{bmatrix} = \begin{bmatrix} m_1 g l c_1 \sin(\theta_1 + \theta_2) \\ m_1 g l_2 \sin(\theta_2) + m_1 g l c_1 \sin(\theta_1 + \theta_2) + m_2 g l_{c2} \sin(\theta_2) \end{bmatrix}$$

(7.2)

As depicted in Figure 7.3.B, the $G(\theta_2)$ torques were converted into a gravity compensation command (u_G) through a proportional gain (k), as proposed in [230]. Subsequently, u_G is summed to the control command (u_c) to determine the total command (u_t) to be provided by the AO's actuation system such that it is able to compensate for the gravitational burden of the wearable AOs' mass and to assist as desired.
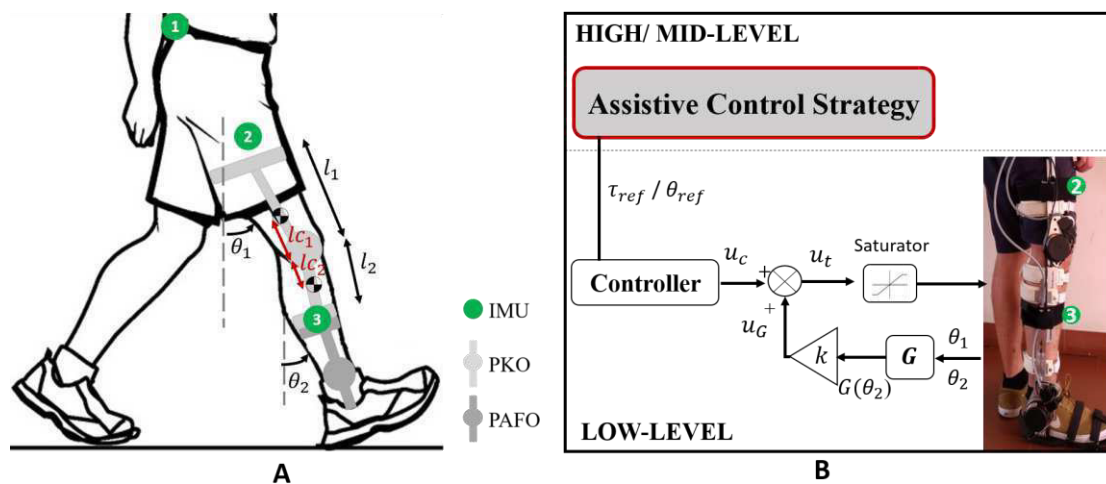
Figure 7.3- A: Gravity compensation strategy, highlighted for PKO. IMU1 and IMU2 were used in PKO for estimating hip angle (θ_1), and IMU2 and IMU3 for determining the knee angle (θ_1) used in PAFO. For both AOs, the θ_2 was measured by potentiometer embedded on AO. **B**: Control architecture considering the gravity compensation strategy ($G(\theta_2)$), with k gain empirically set to 100.

Experimental Validation

The effect of gravity compensation on assisted walking by PKO and PAFO was evaluated assuming that trials without gravity compensation require more effort from the user comparing to those with gravity compensation. Consequently, the **user's physical effort** (evaluated by EMG signals) and the **user's effort perception** was compared in the presence and absence of gravity compensation.

The validation involved 12 healthy subjects (7 males and 5 females), with age of 23.5 ± 1.78 years old, the height of 1.71 ± 0.09 m, and the mass of 69.58 ± 10.23 kg.

The participant started the experimental validation by wearing the AO (PAFO or PKO), two embedded IMUs (required for gravity compensation), and two EMG surface electrodes, the Trigno^TM Avanti Sensors (Delsys, USA). For PAFO, the electrodes were placed on the *tibialis anterior* and *gastrocnemius lateralis* muscles; whereas the *semitendinosus* and *vastus lateralis* muscles were selected for PKO.

Each subject was asked to perform a familiarization trial with the AO walking on the treadmill. Then, he/she stand still for 5 seconds for IMUs' calibration. Subsequently, each participant performed 4 trials of 60 seconds walking at 1.0, 1.3 and 1.6 km/h on a treadmill with the AO configured with the user-orthosis interaction-based control strategy. The gravity compensation was activated on the second and fourth trial without the knowledgeable of the user. At the end of each trial, the participants were asked about the felt effort during walking by answering (with a number of a scale range from one to five, where one is very low, and five is very high) to the following question: *How do you quantify your effort in this trial?.* The protocol was firstly performed for PAFO and posteriorly repeated for PKO.

For evaluating the effects of gravity compensation, the EMG envelope (100 Hz) was computed using EMGWorks (Delsys' software), and normalized within [0, 1] interval across gait speeds for the elected muscles (i.e., *tibialis anterior*, *gastrocnemius lateralis* muscles, *semitendinosus* and *vastus lateralis*). Moreover, the user's perception collected at the end of each trial was analyzed.

Results and Discussion

By analysing the user's muscular activity variation across trials with and without gravity compensation, a **decreased of the user's muscular effort in the presence of the gravity compensation** was noticed. For instance, Figure 7.4 presents the findings achieved for walking trials performed at 1 km/h, where the muscular activation of *tibialis anterior* and *gastrocnemius lateralis* muscles was lower with gravity compensation (trial 4) than without gravity compensation (trial 3). For *gastrocnemius lateralis*, the mean value of maximum muscular activation reduced from 21% to 14%, corresponding to an overall decrement of 33.3% of muscular effort in the presence of gravity compensation. In *tibialis anterior* muscle, a decrease of 37.1%

of the maximum muscle activation was observed when the gravity compensation was acti-vated.
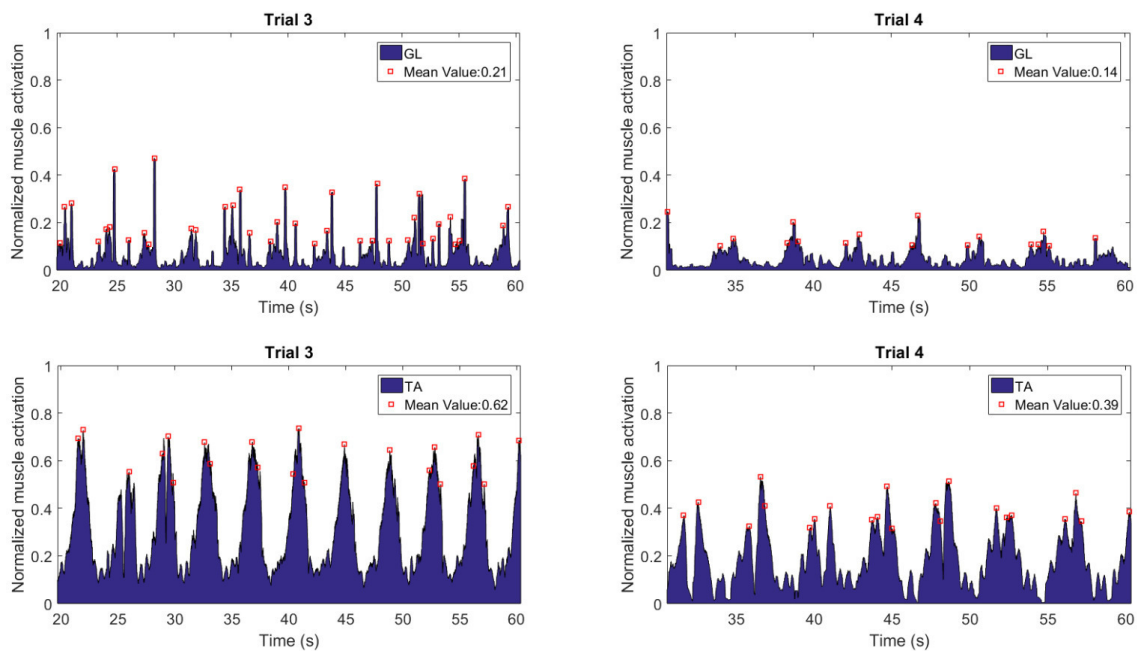
Figure 7.4- Representative outcomes of gravity compensation effect. Normalized EMG envelope of *tibialis anterior* and *gastrocnemius lateralis* muscles from one subject while walking with PAFO at 1.0 km/h. Identification of the maximum muscle activation across gait trials. The gravity compensation is only activated in trial 4.

On the other hand, most of **the participants were not able to differentiate trials with and without gravity compensation** effect, as they considered that the applied effort across the trials was identical ("low-to-reasonable effort" for PAFO, and "reasonable effort" for PKO). This finding may be explained by the lower gravity compensation torques ($G(\theta_2)$) supplied by the AOs (absolute maximum value round 2 Nm), which may be imperceptible by a healthy subject. Even so, three participants correctly perceived the gravity compensation effect by feeling the AO "more lighter".

Overall, the developed computational mechanism to compensate the part of the AOs' mass shown to be relevant for reducing the user's physical effort during walking. Nevertheless, there is still room for improvements through compensation of entire AOs' mass considering a mechanical compensation mechanism.

7.3.User-Orthosis Interaction Based Control

7.3.1.Methods

The **user-orthosis interaction based control** consists of a torque-based control that minimizes the mechanical impedance of the **AO to act as a passive device** (although actuated). Under a research insight, this control strategy was implemented (i) considering a **learning and development phase** ("Teach and Replay") [11], where the trajectories and interaction torque are recorded to be applied in other control strategies posteriorly, (ii) for **comparison purposes** with different assistive control strategies, and (iii) to infer the impact of the robotic device in the user's.

Figure 7.5 depicts the hierarchical control architecture implemented in PKO and PAFO for user-orthosis interaction based control. This control strategy ensures that the AOs follows integrally the **user's motion intentions**, which are processed at the **high-level** in terms of the user-AO interaction torque (τ_{int}) monitored by the strain gauges embedded on PKO and PAFO. Note that the interaction torque values describe the gravitational and inertial components, as well as the torques produced by the user.

The **mid-level sets the AO reference torque** (τ_{ref}) to zero such that the user feels more freedom to move accordingly with his/her intentions and to emulate a passive mode. The **low-level consists of a PID controller** to send a command (u) to the actuation system using the PID control law presented in Equation (7.3), where e_k and e_{k-1} correspond to the current and previous between the reference (τ_{ref}) and the measured interaction torque (τ_{int}).

$$u = K_p e_k + K_i \sum_{n=1}^{k} e_n \Delta t + K_d \frac{e_k - e_{k-1}}{\Delta t} \qquad (7.3)$$

The PID was tuned with the Ziegler-Nichols method, with a similar procedure as was reported in [154]. This tuning considered the practical application of PKO and PAFO in a rehabilitation scenario to avoid abrupt movements that can cause discomfort to the user and to avoid oscillations and overshoot in the actuator's response. The achieved gains were: $K_p = 90$ and $K_i = K_d = 1.5$.
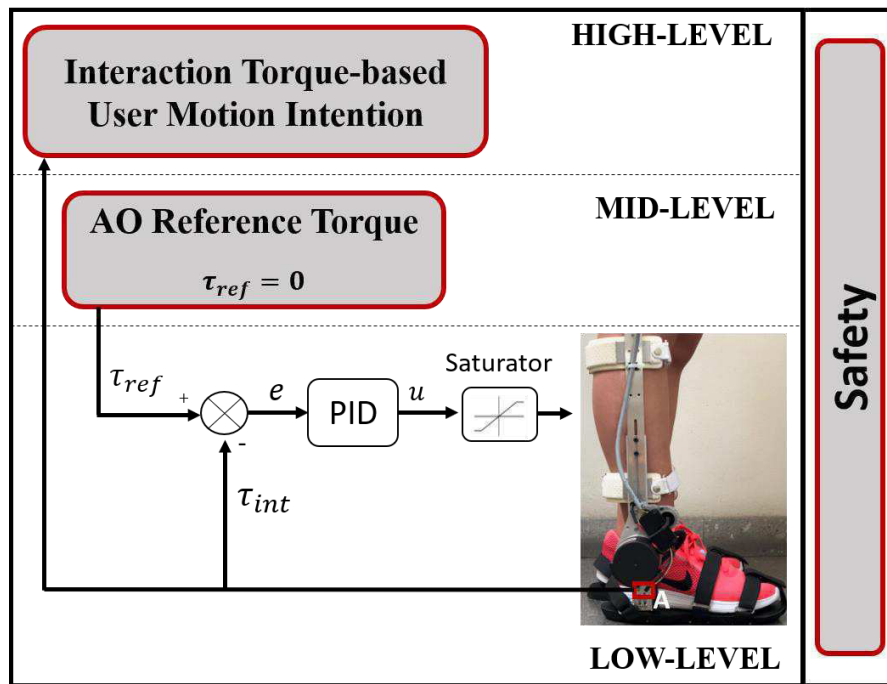
Figure 7.5- Hierarchical control architecture of the user-orthosis interaction based control strategy. A: represents the strain gauge.

7.3.2.Experimental Validation

The experimental validation aimed to (i) test the effectiveness of the user-orthosis interaction based control strategy in PKO and PAFO, (ii) investigate the usability of both AOs, and (iii) collect data for validating the gait event detection tool in assisted gait conditions and for tuning parameters in adaptive impedance control.

Participants

The validation involved 12 healthy subjects (7 males and 5 females), with age of 23.5 ± 1.78 years old, the height of 1.71 ± 0.09 m, and the body mass of 69.58 ± 10.23 kg. The participants gave informed consent to perform the trials and to use the collected data for research purposes.

Protocol

The experimental protocol was applied for both PKO and PAFO, as follows. The participants started by wearing an IMU (embedded IMU of AO) instep of the foot, two FSRs placed on the heel and toe for ground truth in the gait event detection, and the AO (PKO or PAFO) mounted in the right human limb (knee or ankle joint, respectively).

The participants conducted a familiarization walking trial of 2 minutes per AO. The participant started the gait trials in standing position with both knee and ankle joints aligned to round 0°, enabling the IMU calibration. Subsequently, they were asked to perform 3 level-ground walking trials of 2 minutes on a treadmill. These trails were carried out for distinct gait speed: 1.0, 1.3, and 1.6 km/h. The subjects cloud start the trial when they felt comfortable and cloud rest 2 minutes between the trials. Figure 7.6 shows a screenshot of a female subject performing this protocol.
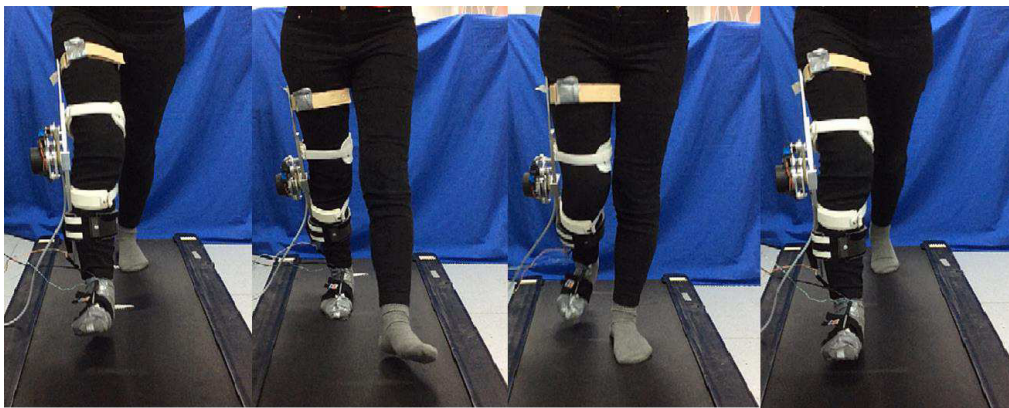
Figure 7.6- Screenshot of a female subject walking at 1.6 km/h. The participant is wearing the PKO at the knee joint, an IMU in the instep of the foot, and two FSRs placed on the heel and toe.

Data Collection and Analysis

The data were collected at 100 Hz and analyzed in Matlab® (2017b, The Mathworks, MA, USA). The sensor information (user-AO interaction torque, joint angle, foot angular velocity, and FSR measure at heel and toe) was monitored, together with the control architecture outputs (reference torque, measured interaction torque, and controller's command). Furthermore, the subjects were asked about the comfort and safety felt during the trials.

7.3.3.Results and Discussion

The performance and effectiveness of the developed user-orthosis interaction based control strategy considered the inspection of the control outputs considering the user's interaction and the feedback provided by the subjects during the trials.

Figure 7.7 provides the control results of PAFO (Figure 7.7.A) and PKO (Figure 7.7.B), namely the reference control variable (reference torque, τ_{ref}), measured control variable (interaction torque, τ_{int}), control command (u), and the AO's angle.
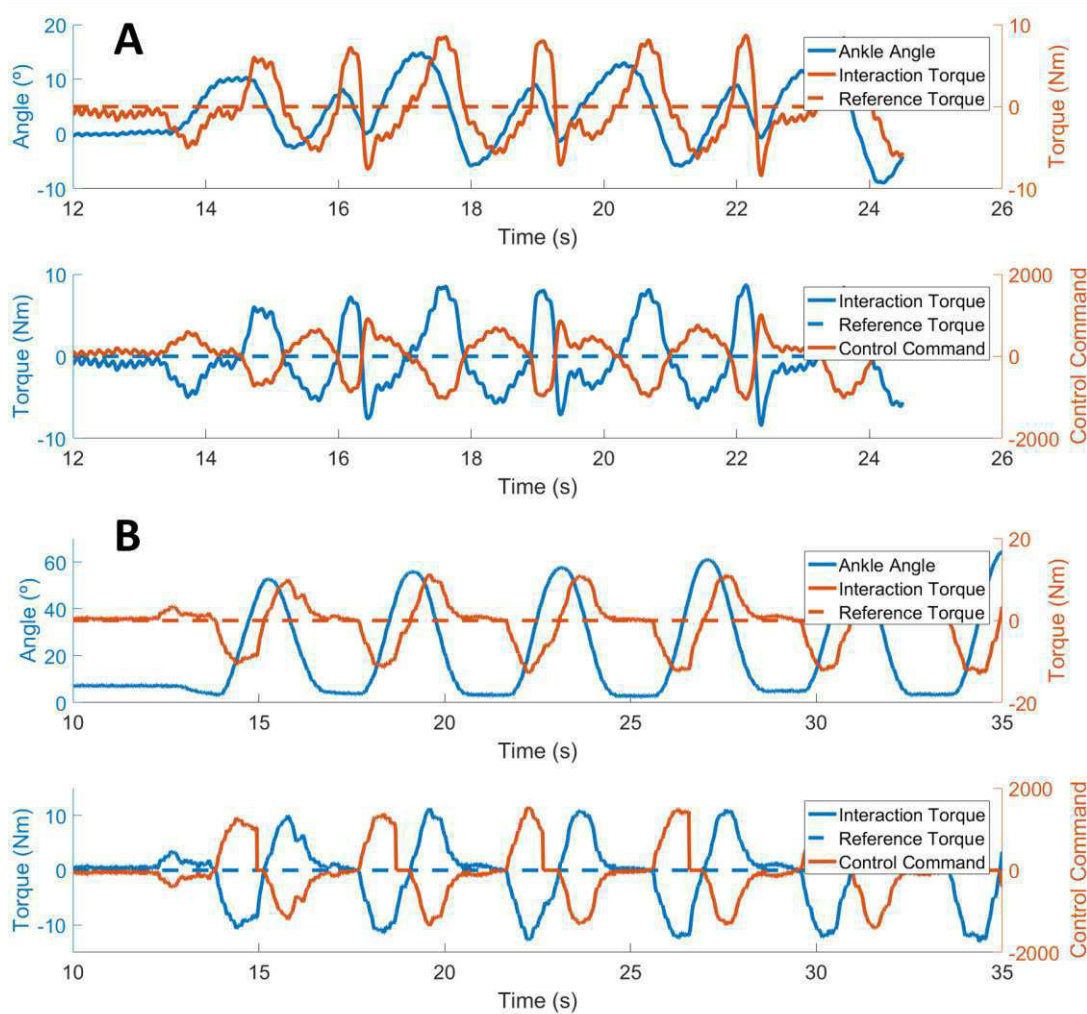
Figure 7.7- Representative outcomes of the user-orthosis interaction based control during walking trials. **A**: Male subject walking with the PAFO at 1.6 km/h. **B**: Male subject walking with PKO at 1.0 km/h.

By analyzing the bottom view of Figure 7.7.A and Figure 7.7.B, it is possible to verify that the output of the control architecture, i.e., the control command time-effectively **follows the user's motion intention** measured by the interaction torque.

Furthermore, it was observed that the **AO's angle trajectory** (i.e., ankle angle and knee angle in Figure 7.7) **is handled by the user-orthosis interaction torque** regarding its magnitude. In the first seconds of the trial (before the participants start the walking trial), the user is not interacting with the AO (interaction torque value near to 0 Nm), and consequently, the angle trajectory keeps approximately constant. On the other hand, the increased user's interaction with the AO (interaction torque varies) results in a variation in the AO's angle trajectory. From the top view of Figure 7.7.A and Figure 7.7.B, it is possible to verify that as higher was the user's interaction, higher was the ROM of AO. The AOs' range of motion was not constant

135

during the trials, indicating that the **subjects had the freedom to move** in the direction of the human-orthosis interaction force, with minimized rigidity offered by the device.

The ankle and knee angle trajectories are similar to the ones reported for healthy subjects[239], and the interaction torque changes following the direction of the movement (increases until maximum flexion and decreases until maximum extension).

Concerning the AO's impact on walking, the participants reported that **both AOs are comfortable to use and easy and safe to wear**. When wearing the PAFO, no misalignments issues were observed. However, the **misalignment of the PKO affected the therapy** (requiring to readjust the PKO's usability across the trials) mainly for shorter subjects. With this assistive strategy, the participants perceived that they could control the AO's trajectory in the direction of his/her motion intentions.

This strategy showed to be suitable for therapies that exclusively approached the user's motion intention, with low rigidity offered by the AOs. Thus, the subjects must present voluntary muscular contractions to interact with the device. The **user's voluntary effort** provides ways to **enhance the muscular strength** and the user's involvement for maintaining the **motor learning function active**. Nonetheless, this strategy does not take into consideration the user's disability level.

Lastly, an analysis on the foot angular velocity at the sagittal plane was performed to investigate whether the walking assisted by AOs modifies the kinematic signal used in the gait event tool (see example in Figure 7.8). This analysis enables to verify that the foot angular velocity signal remains similar in waveform and magnitude to the one measured for non-assisted conditions. This finding indicates that the gait event detection tool described in Chapter 5 may be applied for gait assisted situations.
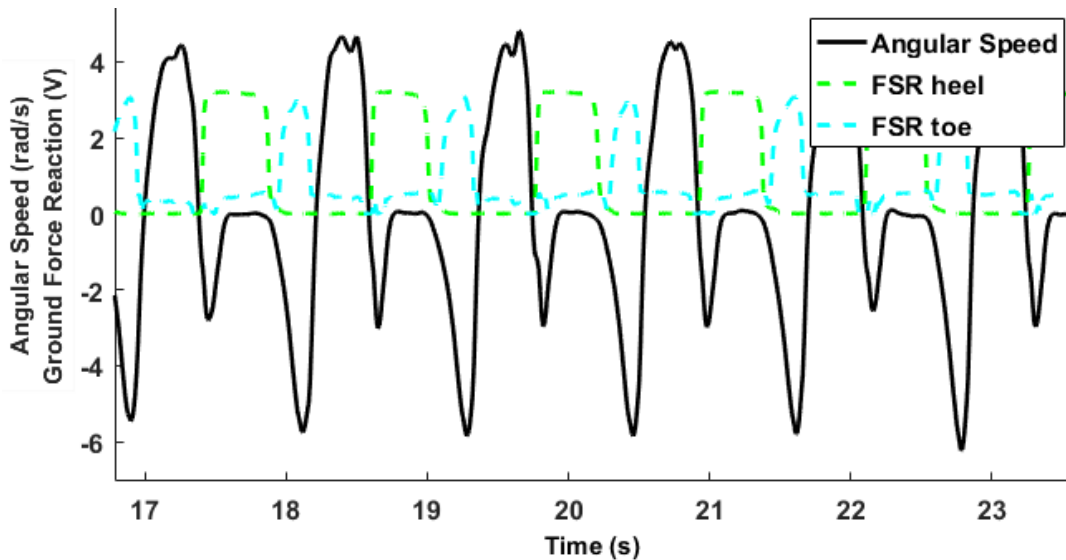
Figure 7.8- Foot angular velocity in the sagittal plane and FSRs (heel and toe) signals recorded from assisted walking with PAFO in the user-orthosis interaction based control at 1.4 km/h.

7.4. User-Oriented Trajectory Control

7.4.1. Methods

The **user-oriented trajectory control strategy** was designed towards the parameterization of **trajectories according to the users' height and gait speed** to enable a natural gait pattern recovery, as depicted in Figure 7.9.
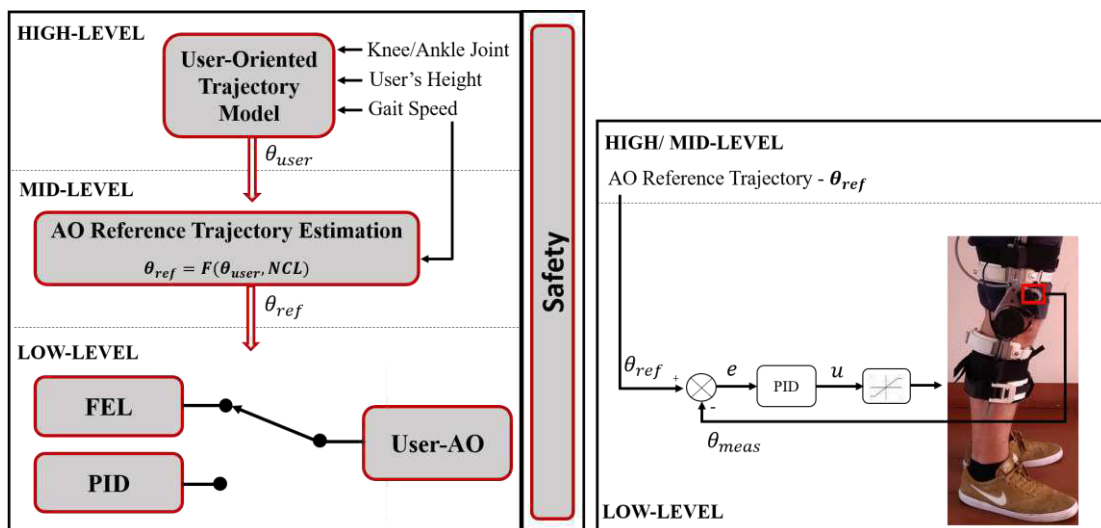
Figure 7.9- Hierarchical control architecture of the user-oriented trajectory control strategy, highlighting the low-level PID controller.

The **high-level** includes an **user-oriented trajectory model** based on a trajectory regression model [240] dependent on the user's height and speed, joint (the knee or ankle) to set an

user-oriented position trajectory (θ_{user}) for the knee and ankle joints. For instance, Figure 7.10 illustrates the variability of knee angle trajectory according to the desired gait speed and user's height.
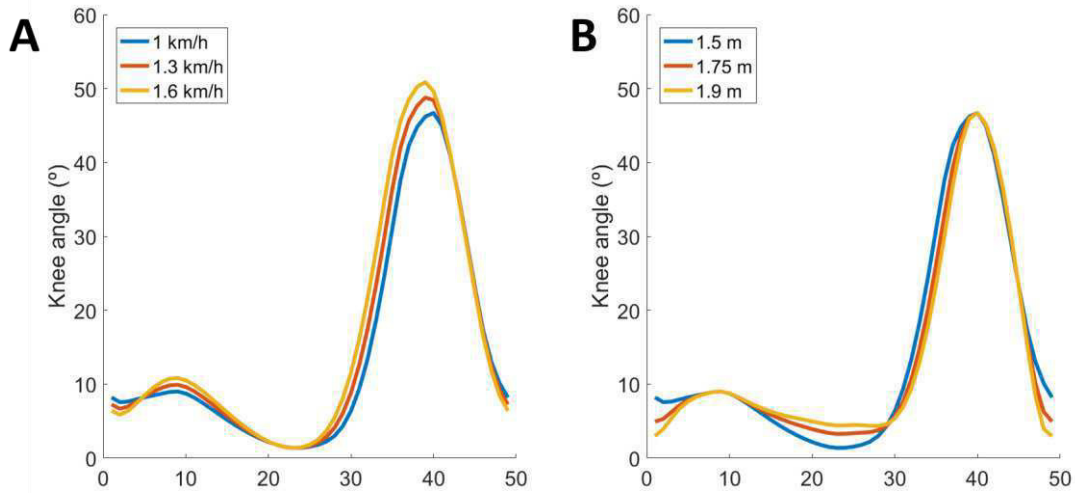
Figure 7.10- Knee trajectories generated by the trajectory model [240] used at the high-level control. **A**: Knee trajectories generated for a subject with 1.5 m for different gait speeds. **B**: Knee trajectories generated for subjects with different heights for 1 km/h.

The **mid-level controller** sets the **AO's reference position trajectory** (θ_{ref}) as the user-oriented position trajectory (θ_{user}) parameterized according to the gait speed. As such, Equation (7.4), empirically found, sets the Number of Control Loops (NCL), each lasting 1 ms, that must occur to update the value of the reference trajectory. This speed-parameterization aims to ensure user-AO coordination.

$$NCL = -34.62 * Gait\ Speed + 107.31 \qquad (7.4)$$

The **low-level controller** covers a position-based control loop to ensure that the AO's angular position matches the user-oriented trajectory. Currently, both **PID** and **FEL controllers** may be applied. The FEL controller is detailed described in Chapter 7.7 as well as a comparative analysis among these low-level controllers. Regarding the PID controller, the used PID gains were: $K_p = 90$ and $K_i = K_d = 1.5$, as described in Chapter 7.3. The PID controller implements the control law presented in Equation (7.3) to compute the PID control command (u), where e_k and e_{k-1} correspond to the current and previous error between the reference (θ_{ref}) and measured (θ_{meas}) angular position by a potentiometer embedded on the AO, as illustrated in Figure 7.9.

The experimental validation centered on investigating the effectiveness of the user-oriented trajectory control strategy in PKO and PAFO by involving the participants and the protocol described in Chapter 7.3. However, in this experiment, the participants only wore PAFO or PKO, as depicted in Figure 7.11.
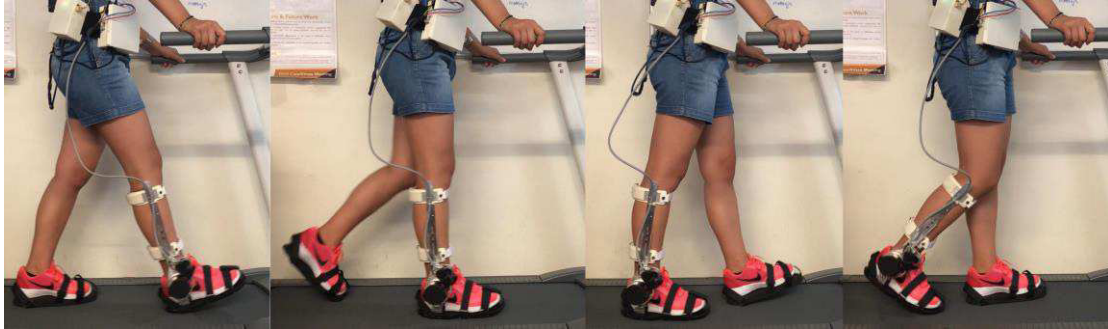
Figure 7.11- Screenshot of a female subject walking at 1.0 km/h. The participant is wearing the PAFO at the ankle joint.

The control architecture outputs (reference trajectory, measured trajectory, and controller's command) were collected at 100 Hz and analyzed in Matlab®. The participants were asked concerning the comfort and safety felt during the walking trials.

7.4.2.Results and Discussion

The **user-oriented trajectory control** was designed for therapies that ensure repetitive movements of the user's lower limbs. The experimental results indicate this strategy successfully foster a **repetitive user-oriented gait trajectory** at the knee and ankle joint, when the participants used the PKO and PAFO, respectively. Figure 7.12 depicts results from one trial with PAFO and PKO, highlighting the repeatability assistance fostered by this assistive strategy since the real knee and ankle angle trajectories followed the same pattern (similar waveform and magnitude) along with gait trial.

Nonetheless, there is a **delay** (PKO: 260 ± 0.46 ms; PAFO: 260 ± 0.27 ms) between the user-oriented trajectory and the real angle trajectory. This delay, approximately constant across the trial, may be caused by the mechanical response of AOs. Consequently, the PAFO to reach to lower extrema nor the PKO to achieve the desired maximum flexion. This delayed assistance was also reported in the literature for this strategy [11]. Consequently, it was necessary to improve the time-effectiveness of the low-level controller of the user-oriented trajectory, as proposed in Chapter 7.7 [104].

The participants rated the assistance as **comfortable and safe**, and they did not perceive the delayed assistance. However, due to the misalignment issues in the PKO, it was necessary to readjust the alignment between the PKO system and the knee joint across the trials.

In general, this assistive strategy demonstrated to be suitable for **therapies involving repetitive movements** with a pre-defined, user-oriented trajectory. This strategy aims to emulate manual assistance therapy while relieving the heavy effort from the therapists [11]. The therapeutic benefits include the improvement in the user's **movement coordination** and **more symmetrical gait**.
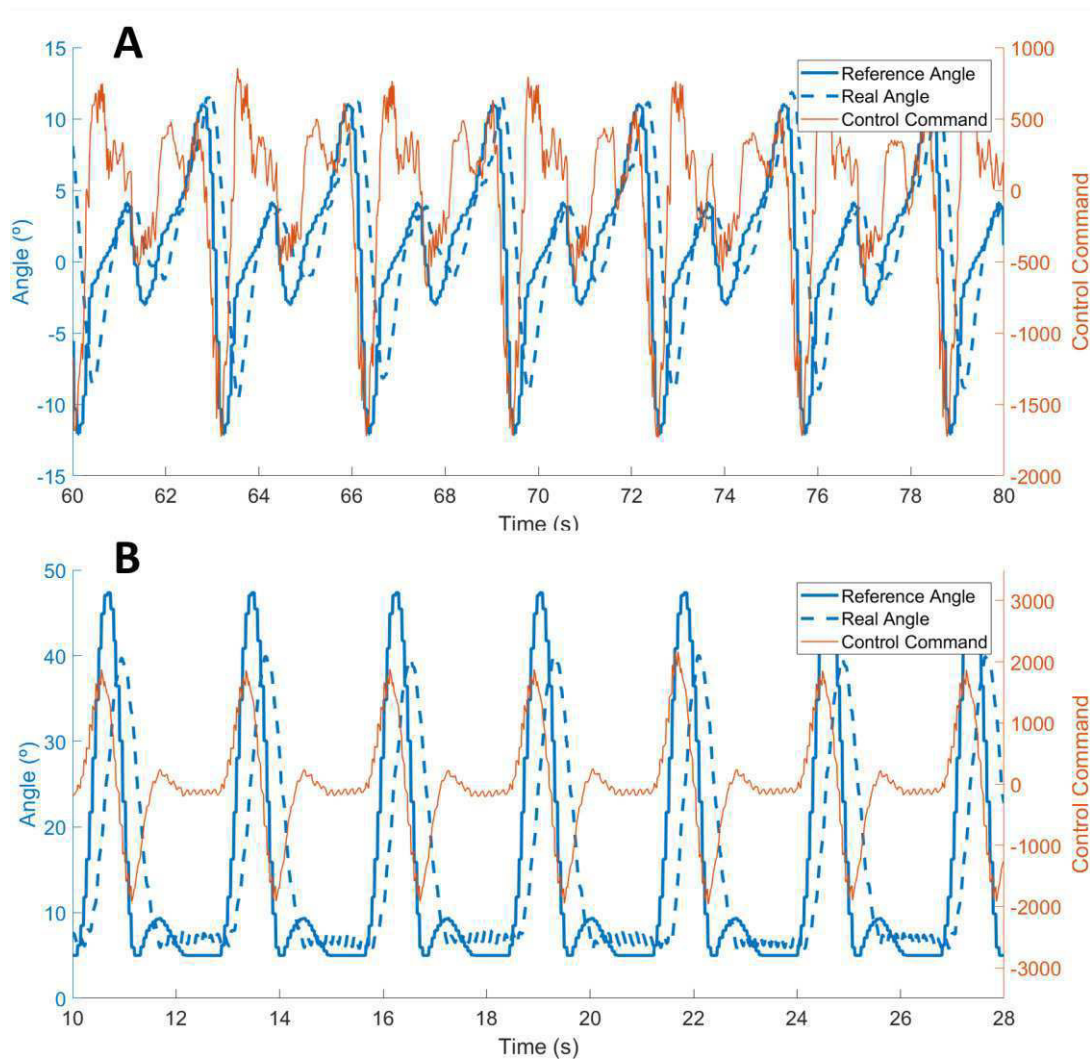
Figure 7.12- Representative outcomes of the user-oriented trajectory control strategy during walking trials. **A**: Female subject with 1.62 m walking with the PAFO at 1.2 km/h. **B**: Male subject with 1.75 m walking with PKO at 1.4 km/h.

Nevertheless, this strategy is not adaptive **nor approaches the AAN strategy**; therefore, it presents some application limitations. First, the user-oriented trajectory does not consider

the variability of the disability level from patient to patient, and also for the same patient in the rehabilitation process [29]. Consequently, this control strategy is being updated to enable the real-time adjustment of the user-oriented trajectory, within a virtual tunnel, according to the user's immediate needs. For this purpose, the user or the therapist can increase or decrease the trajectory by setting commands in the mobile graphical application, as illustrated in Figure 7.13. The high-level controller handlers these commands in as percentual gains that adjust the initially set trajectory.

Second, this strategy does not provide ways for the user to interact with the devices. The inclusion of the biofeedback system may play an important role to ensure active participation of the patients in therapies. These limitations were also reported in the literature [11], [29], [241].
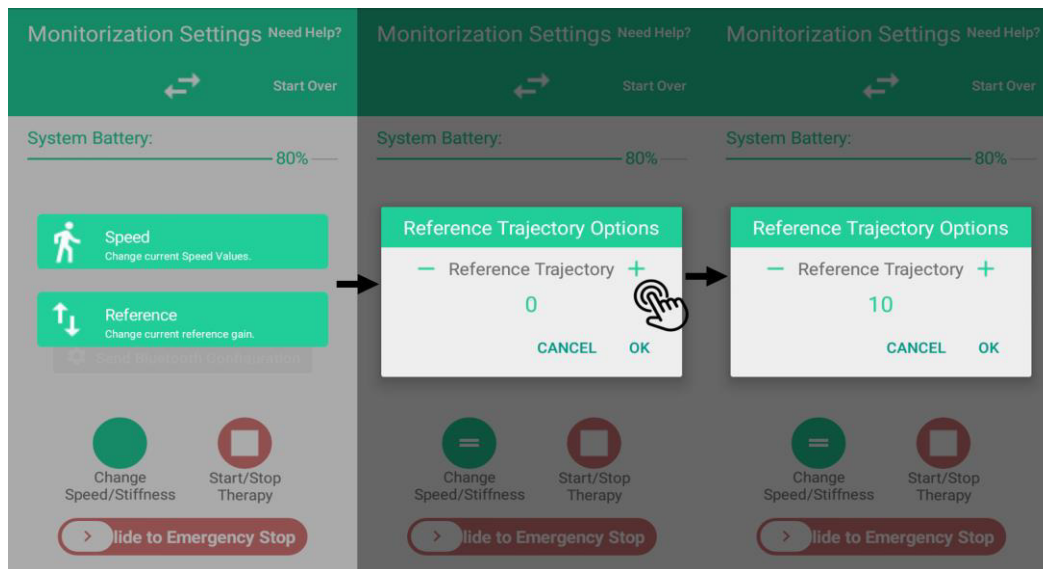
Figure 7.13- Menu of mobile graphical application to adjust the user-oriented trajectory.

7.5.Adaptive Impedance Control

7.5.1.Related Work

Cooperative and AAN gait therapies demand flexible interaction between the human and the assistive device. AAN strategies may endow controllers capable of modulating the **impedance of AOs** to allow patient's natural variability, **promote a compliant human-robot interaction**, and to **encourage the user's active participation** [31]. These strategies are able to resemble the manual assistance provided by a therapist, which is compliant and adaptive to the needs of the patients [29], [241].

Recent studies have proposed **adaptive impedance control** as an effective AAN strategy [11], [29]. The control relies on tailoring the robot's dynamic properties (stiffness and/or damping) based on individuals' active joint torque [29], [242]. The adaptive impedance control was firstly applied in the AAN robotic gait training through Lokomat®[238]. Moreover, Hussain *et al.* [29] implemented this control strategy in the powered orthosis using the interaction torque as an indication of the subject's effort. Similar approaches were introduced in [230], [231]; however, these studies did not validate the proposed strategy in the real environment.

7.5.2.Methods

This chapter presents the development of the **adaptive impedance control** strategy for PKO, as detailed described in [55]. This AAN strategy was implemented in a hierarchical control architecture (illustrated in Figure 7.14) to tailor the impedance behavior, namely the **stiffness of the human-orthosis interaction** throughout the **gait cycle and speed**. The stiffness of the human-orthosis interaction was virtually modulated without introducing mechanical apparatus, such as spring, reducing mechanical issues for PKO.
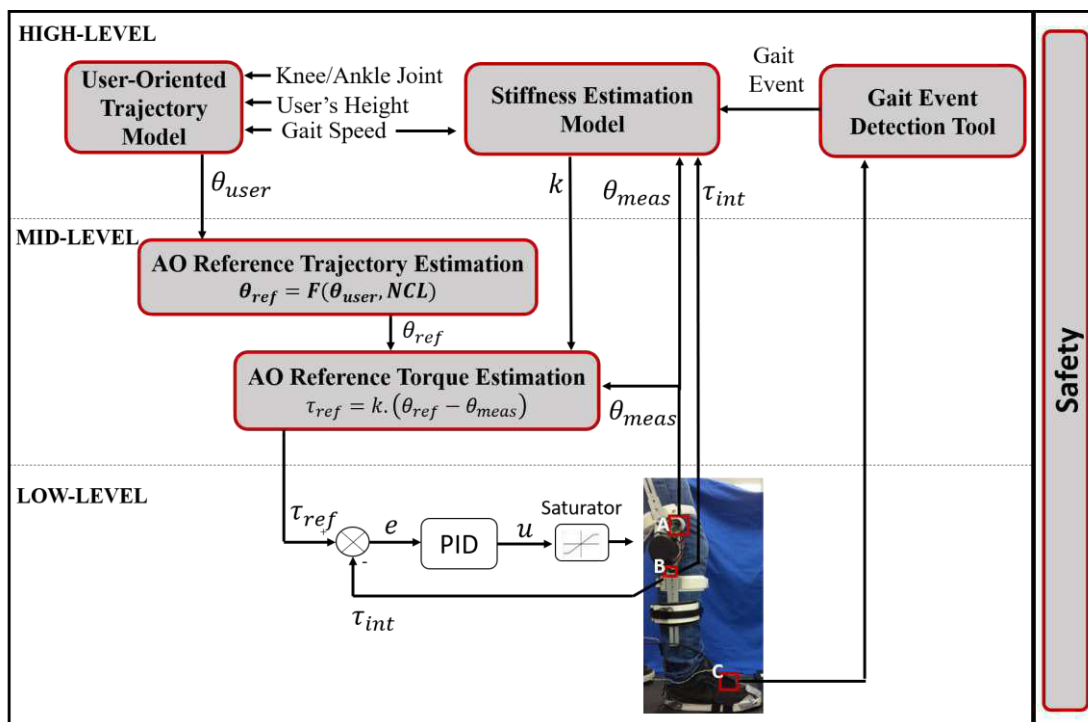
Figure 7.14- Hierarchical control architecture of the adaptive impedance control. A- Potentiometer used to measure the real knee joint angle (θ_{meas}), B- Strain gauge measured the user-orthosis interaction torque (τ_{int}), C-IMU measured the foot angular velocity for gait event detection tool.

The stiffness of the human-orthosis interaction was investigated instated of AO's stiffness to make the AO more compliant and **cooperative to the user's motion intention** (considering the strain gauges' measures), **encouraging the user's participation and the intuitiveness of interaction.** In wearable assistive devices, direct interaction with humans still is a critical concern [243].

Stiffness Estimation

The **stiffness of the human-orthosis interaction** was estimated as the slope of the linear regression of the human-orthosis interaction torque *versus* angle at the knee joint. This approach is based on the concept of quasi-stiffness, explored in [135].

For that matter, healthy participants performed gait trials at different gait speeds wearing the PKO in user-orthosis interaction based control strategy, as described in Chapter 7.3.2. With this control strategy, there is no contribution of the orthosis' actuation system in the locomotion, limiting the actuation of the mechanical properties.

By applying the linear regression to the curve that relates the angle with the human-orthosis interaction torque, the stiffness values and the gait events in which they should be tailored in the adaptive impedance control strategy were determined. The estimated stiffness values were normalized to [0; 1] interval through the participant-specific percentage of the maximum stiffness due to operating limits of the actuation technology empirically observed for stiffness values higher than 1.5 Nm.

Hierarchical Control Architecture

Figure 7.14 illustrates the hierarchical control architecture implemented for the adaptive impedance control strategy. The **high-level defines the user-oriented trajectory** (θ_{user}) accordantly the user's height and gait speed, as described in Chapter 7.4.1. Furthermore, this control level estimates the **stiffness of the user-AO interaction** (k) as the slope of the linear regression of the joint angle (θ_{meas}) and user-AO interaction torque (τ_{int}), through the stiffness estimation model. The stiffness is adaptively modulated for each user according to the configured gait speed and detected gait event (using the detection tool presented in Chapter 5). The stiffness adjustment takes into considering the user's intention and participation through τ_{int}.

The **mid-level** starts by **setting the AO's reference position trajectory** (θ_{ref}) as the user-oriented position trajectory (θ_{user}) parameterized according to the gait speed, as indicated in (7.4). Subsequently, it defines the **AO's reference torque** (τ_{ref}) through the used impedance control law (Equation (7.5)), with reference and real position trajectory of AO (θ_{ref} and θ_{meas}, respectively) and the adaptable stiffness (k) along gait cycle (damping and inertial moment were not considered in this scope). The potentiometer measured the real knee joint angle (θ_{meas}).

$$\tau_{ref} = k.(\theta_{ref} - \theta_{meas}) \qquad\qquad (7.5)$$

At the **low-level**, the tuned **PID controller** was applied to guide the human-orthosis interaction torque in the direction of the desired torque (τ_{ref}). This level relies on the interaction torque values (τ_{int}) between the AO and the human, measured by the strain gauges embedded in AO, to compute the torque errors (e) that feed the PID controller.

7.5.3.Experimental Validation

The experimental validation aimed to test the effectiveness of adaptive impedance control. This control strategy was compared to user-oriented trajectory control to establish the benefits of an AAN strategy for gait training regarding a non-AAN strategy.

Participants

Five healthy subjects (2 females and 3 males) with no history of neurologic disorders gave informed consent and participated in the study. The demographic characteristics of the involved subjects are 26.80 ± 2.78 years old, the height of 1.68 ± 0.07 m, and the body mass of 64.60 ± 8.5 Kg.

Protocol

The participants started by wearing the embedded IMU instep of the right foot and PKO. The subjects performed 3 level-ground walking trials of 2 minutes on a treadmill while wearing the PKO in the user-orthosis interaction based control to estimate the stiffness. The trials were carried out at different gait speeds: 1, 1.3, and 1.6 km/h.

Regarding the comparative analysis of control strategies, the participants performed 3 level-ground walking trials on a treadmill at different gait speeds: 1, 1.3, 1.6 km/h. In each

trial, the participant walked 5 minutes in an assistive mode delivered by one control strategy, resting 2 minutes, and restarting the assisted walking with the other control strategy for 5 minutes. The participants were randomly involved in both assistive modes not to influence their perception regarding the effects introduced per control strategy. During these experiments, the subjects were encouraged to interact with the orthotic system, by following and opposing the reference trajectory. Figure 7.15 shows a screenshot of male subjects performing this protocol.
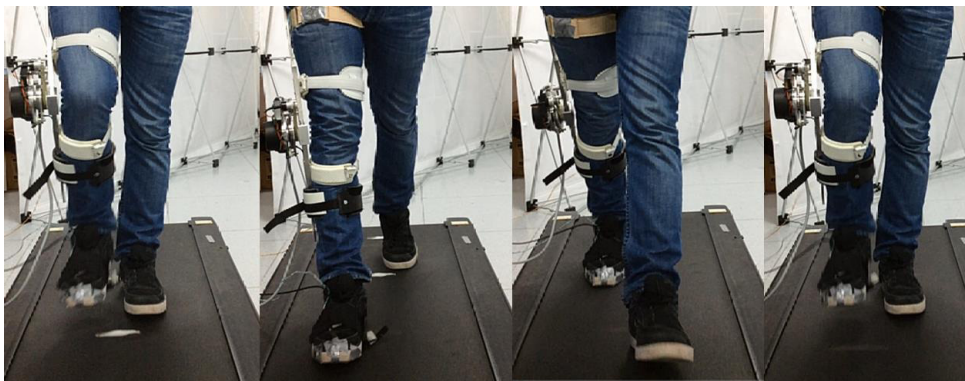
Figure 7.15- Screenshot of an experiment conducted at 1.3 km/h with a male subject, wearing the PKO, assisted by adaptive impedance control, and an IMU placed on the right foot for gait event detection.

Data Collection and Analysis

Data from the strain gauges (user-PKO interaction torque), potentiometers (real knee angle), and the control architecture values (user's oriented trajectory, reference torque, measured torque, and controller's command) were collected at 100 Hz and analyzed in Matlab®.

Additionally, at the end of experiments, each subject reported his/her perception regarding both control strategies considering: (i) freedom of movement, (ii) possibility or not to deviate from the imposed trajectory, and (iii) effort demanded during walking. Once more, the patients also indicated their insights concerning the applied attachment system, comfort, and safety felt during the experiments.

7.5.4. Results and Discussion

This subchapter firstly presents the estimated stiffness. Then, it provides the results achieved with the adaptive impedance control strategy and the comparison with user-oriented trajectory control.

Estimated Stiffness

Figure 7.16 provides the interaction torque *vs.* knee angle curve along three trials and the obtained linear regression (black lines). With the linear regression, different slopes were observed in the curves related to the interaction torque *versus* the knee angle. These results indicate that the **human-orthosis interaction stiffness** varies through the **gait cycle**, mainly in **four gait periods**: (i) from HO to TO; (ii) from TO to MMSW; (iii) from MMSW to TS; and, (iv) from terminal swing (TS) to HO.
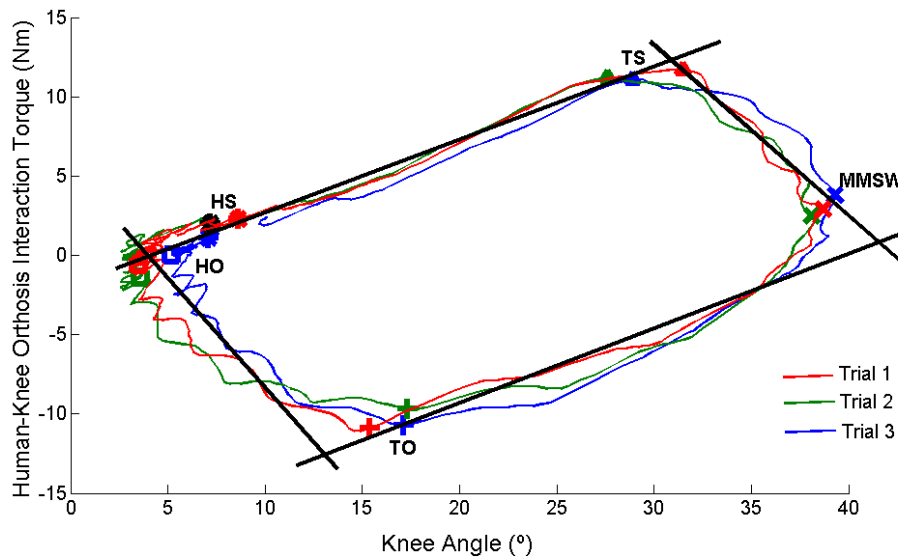
Figure 7.16-Representative curve of the human-knee orthosis interaction torque *vs* knee angle of 3 gait trials of a male subject walking at 1.3 km/h on the treadmill. Black lines represent the linear regression on the curve, which changes for the identified gait events (TS - Terminal Swing) [55].

Table 7.3 presents the mean and standard deviation values of the estimated stiffness across the subjects, per gait speed and gait period, and the stiffness values normalized per user's body mass and in [0; 1] interval.

Figure 7.17 illustrates the module of the stiffness values to provide a better interpretation of their variability with the gait speed and gait period. By analyzing Figure 7.17, it was observed the similarity of the stiffness values in HO→TO and MMSW→TS periods, and TO→MMSW and TS→HO. This finding indicates that the human-orthosis interaction should be **stiffer** (higher impedance) to perform the **HO event** (start preparing the foot to swing phase) and **MMSW event** (change the limb's excursion from the flexion to extension).

Table 7.3- Module of the mean and standard deviation (std) values of the estimated stiffness, normalized in [0; 1] interval.

Gait speed (km/h)	Gait Period	Stiffness (N.m/°kg)		Stiffness Normalized in [0;1]
		Mean	*Std*	
1	HO → TO	0.012	0.003	1.0
	TO → MMSW	0.0085	0.001	0.71
	MMSW→ TS	0.012	0.003	1.0
	TS → HO	0.008	0.002	0.71
1.3	HO → TO	0.020	0.005	0.95
	TO → MMSW	0.008	0.001	0.38
	MMSW→TS	0.021	0.004	1.0
	TS → HO	0.008	0.003	0.38
1.6	HO →TO	0.024	0.004	1.0
	TO → MMSW	0.008	0.001	0.33
	MMSW→ TS	0.023	0.004	0.96
	TS →HO	0.007	0.0005	0.29
1.8	HO → TO	0.036	0.002	0.92
	TO → MMSW	0.007	0.003	0.18
	MMSW→TS	0.039	0.004	1.0
	TS → HO	0.009	0.002	0.23

On the other hand, the results indicate that the PKO should be **compliant** from the **initial to middle-swing phase**, and from the **terminal swing to middle-stance phase** given the low human-orthosis interaction values to achieve a high knee ROM.

Furthermore, the results presented in Figure 7.17 show that the **stiffness** of the human-orthosis interaction varies positively with the **gait speed**, i.e., higher gait speed requires more stiff behaviors. The stiffness's dependency on speed was more evident in moments that involve high stiffness values (HO→TO and MMSW→TS).
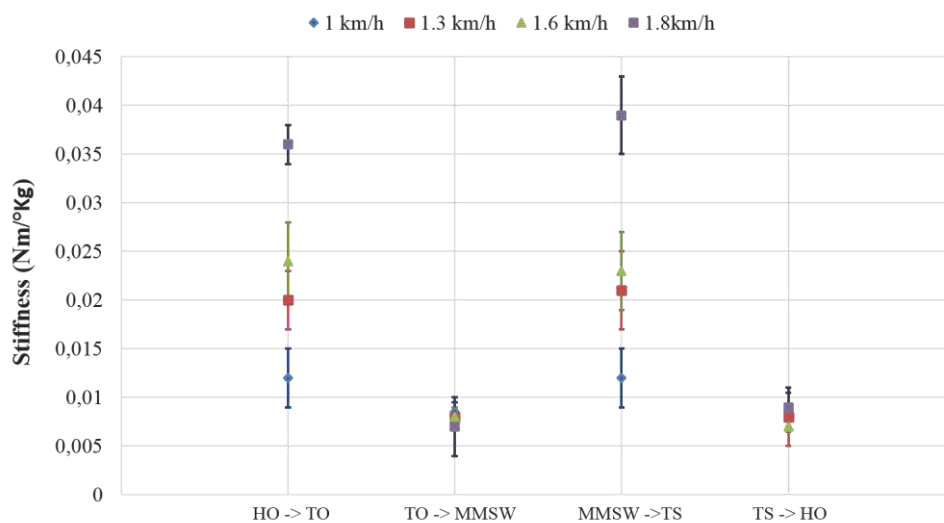
Figure 7.17-Module of the mean and standard deviation values of the estimated stiffness throughout gait cycle for different gait speeds [55].

So far, no work has investigated the variation of the stiffness of the human-orthosis interaction throughout the gait cycle and speed. Previous studies focused on the investigation of the stiffness of the human joint to define how the mechanical systems (e.g., springs) attached to the orthosis have to emulate the dynamic properties of a healthy joint [111], [135], [244]. Nevertheless, the obtained findings are according to the ones presented in the literature regarding the stiffness variation with the gait speed (positively correlated) and gait cycle [30], [135], [245].

Adaptive Impedance Control *vs.* User-Oriented Trajectory Control

Figure 7.18 depicts representative outcomes of the adaptive impedance control and the user-oriented trajectory control.

For the adaptive impedance control, as illustrated in Figure 7.18.A and Figure 7.18.B, the **increase of the interaction torque leads to an augment of the real knee trajectory**. Consequently, the real knee trajectory may exceed the ROM of the reference trajectory with maximum values around 70°; however, it never exceeds the imposed limits for PKO's range of motion due to the applied safety measures. The **flexibility for deviating from the desired knee trajectories** creates a **"virtual tunnel"** along the desired trajectory in the sagittal plane, as disclosed in [242].

Additionally, Figure 7.18 shows the adaptability of the stiffness along the gait cycle, and that the **user has more freedom** to move when the user-PKO interface is less stiff (low stiffness values). As the adaptive impedance control takes input in the form of human-orthosis interaction torque, it can adjust the PKO's assistance to meet the needs of individual subjects based on their voluntary participation and stage of gait rehabilitation. Hussain *et al.* [29] investigated a similar AAN gait training based on human-orthosis interaction; however, they involved a predefined position trajectory for all participants instated of a user-oriented position trajectory.

On the other hand, the results of the user-oriented trajectory control (for instance, Figure 7.18.C in the timing interval from 48 to 53 s) indicate that the real knee trajectory is not affected by the human-orthosis interaction torque independently of its magnitude. This finding suggests that the user-oriented trajectory control does not deliver an AAN gait training nor considers the user's participation in gait.
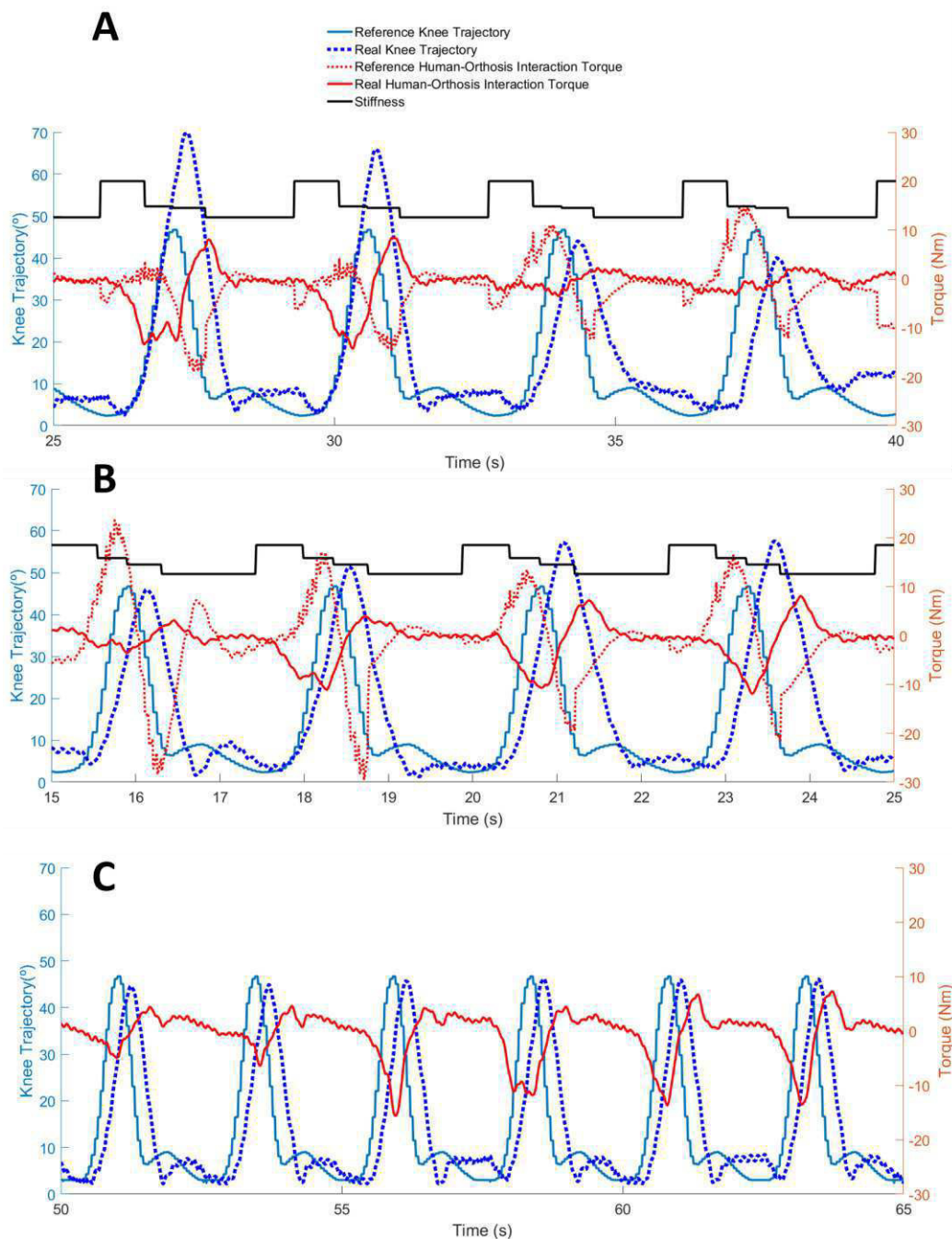
Figure 7.18- Representative control outcomes of the gait trials assisted with PKO. **A**: Adaptive impedance control at 1 km/h. **B**: Adaptive impedance control at 1.6 km/h. **C**: User-oriented trajectory control at 1.6 km/h.

The feedback provided by the participants followed the evidence presented above. In all cases, they reported that the **adaptive impedance control** delivers a more **comfortable and natural motion**, and also possibilities the deviation from the reference trajectory. As expected, the **increasing freedom of movement was more pronounced when low stiffness values** were involved in the adaptive impedance control, since the rigidity of the device is lower.

Moreover, the participants straightforwardly perceived that the impedance control allows more interaction comparatively to user-oriented trajectory control since, in this case, they could not deviate their limb from the set trajectory, and they felt the orthosis stiffer.

The overall findings enhance the suitability of the **adaptive impedance control as an AAN strategy** for applications focused on guiding the user's lower limb through user-oriented gait patterns while considering the user's muscle effort and motion intention [11], [29]. Furthermore, this strategy favors the user's active physical participation.

The possibility of adjusting and modulating the stiffness provides a way to **tune the assistance level** in gait therapies in favor of the **user's needs** and **disability level** [29]. The stiffness was adjusted to decrease the human effort required for ensuring a successful knee joint movement during walking. This evidence was reported in [29]. The cooperative user-orthosis interaction aligned with assistance's adaptability is a major step forward for the **long-term recovery of functional motor abilities**.

Nonetheless, the implementation of the proposed adaptive impedance control presents two main limitations. It depends two times on the precision of the position and torque sensors. The impedance modulation was limited to stiffness, not considering the effect of damping nor inertia.

7.6. EMG-based Control

7.6.1. Related Work

User-oriented assistive strategies could take into account the body condition of the user with information from biomedical sensors, namely EMG signals [246], [227], [247]. The major advantage of **EMG-based control strategy is its ability to predict the user's motion intention**, as long as the muscles are not paralyzed or too weak to perform the movements. This assistive strategy provides a **functional gait training** to encourage the **user's muscular effort**, and thus, avoid muscle atrophy [248].

The EMG-based assistive strategies involve a **user's joint torque estimation method** based on the acquired EMG signals from superficial muscles. Subsequently, the torque of the AO's actuator should timely track the estimated user's joint torque. Most studies have applied a complex musculoskeletal model for joint torque estimation. Fleisher *et al.* [227] and Hassani

et al. [33] used the modified Hill-type muscle model. However, it requires complex methods and several calibration procedures to determine several parameters.

On the other hand, more straightforward approaches based on the **proportional method** have been approached. Kawamoto *et al.* [249] proposed a simple calibration method that only requires the **tuning of two proportional gains** (one for flexion and one for extension) that relate the EMG signals with the torque generated at the knee joint by the flexion and extension muscles, respectively. This method stands, in the field of gait rehabilitation, for its simplicity and real-time effectiveness.

7.6.2. Methods

This subchapter presents the EMG-based hierarchical control architecture implemented and validated with the PKO. Figure 7.19 provides an overview of the procedure carried out to achieve the EMG-based control, detailed described in [56].
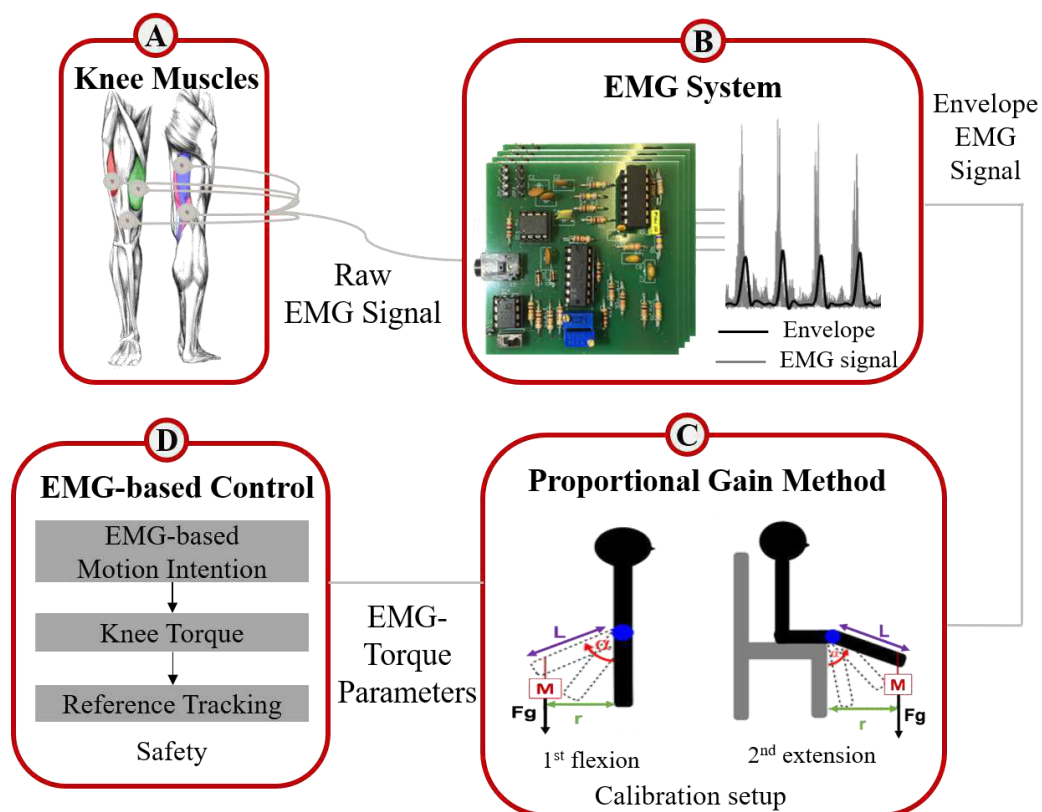
Figure 7.19- System Overview. **A**: Chosen muscles to acquire EMG signals (*vastus lateralis* and *vastus medialis* marked with red and green, and *semitendinosus* and *semimembranosus* marked with purple and pink, respectively). **B**: EMG system used to obtain the EMG envelope. **C**: Proportional method implemented to find EMG-torque parameters from a calibration routine for the user's knee torque estimation. **D**: Hierarchical EMG-based control architecture.

First, the **most significant muscles** for controlling the knee motion were selected, considering a trade-off between performance and simplicity of the control strategy. Throughout a literature analysis, it was verified that **two flexors** (*Semitendinosus* and *Semimembranosus*) and **two extensors** (*Vastus Lateralis* and *Vastus Medialis*) contribute more to the knee joint movement during gait [32].

Second, the **EMG system** detailed in Chapter 4.4 was used in the 4-channel configuration to obtain the EMG envelope signals for the four selected muscles. Third, the EMG envelope signals are then used to estimate the user's knee joint torque (i.e., the torque generated at the knee joint by the knee flexion and extension muscles) through the **proportional gain method**. This stage endows an experimental calibration procedure to find the parameters able to convert the EMG envelope into the user's knee joint torque.

Lastly, **EMG-based control** is executed such that torque of the AO's actuator should track the estimated user's knee torque. Details regarding the knee torque estimation and EMG-based control are disclosed below.

Proportional Gain Method

The **proportional gain method** [14] was implemented for estimating the user's knee torque, given its simplicity for clinical applications, and it has a straightforward calibration procedure when compared to the musculoskeletal model-based methods.

The proportional gain method aims to find **two parameters** (K_{fl} and K_{ex}) that directly maps the EMG signals into knee torque values. The knee torque was estimated ($\hat{\tau}_{Knee}$) using Equation (7.6), where $E_{fl}(t)$ and $E_{ex}(t)$ represent the EMG envelope obtained from the flexor and extensor muscles, respectively; K_{fl} and K_{ex} are the parameters responsible for relating the envelope EMG signals from flexor and extensor muscle, respectively, to the knee torque; $\hat{\tau}_{fl}(t)$ is the estimated flexor torque; and, $\hat{\tau}_{ex}(t)$ is the estimated extensor torque.

$$\hat{\tau}_{Knee} = K_{fl}E_{fl}(t) - K_{ex}E_{ex}(t)$$

$$\Leftrightarrow \hat{\tau}_{Knee} = \hat{\tau}_{fl}(t) - \hat{\tau}_{ex}(t)$$

(7.6)

The determination of K_{fl} parameter assumed that torque being generated by the PKO's actuator (τ_{meas}) matches the flexor torque generated by the user ($\tau_{fl}(t)$), represented in Equation (7.7a). Further, it considers that the estimated torque provided by the flexor muscle

$(\hat{\tau}_{fl}(t))$ attempts to match the torque being generated by the actuator (τ_{meas}), as given in Equation (7.7b). Then, the error between the actuator's torque and the estimated flexor torque can be calculated using Equation (7.7c).

$$\tau_{meas}(t) = \tau_{fl}(t) \tag{7.7a}$$

$$\hat{\tau}_{fl}(t) \approx \tau_{meas}(t) \tag{7.7b}$$

$$e(k) = \tau_{fl}(k) - \hat{\tau}_{fl}(k) = \tau_{meas}(k) - \hat{\tau}_{fl}(k) \tag{7.7c}$$

Equation (7.8a) provides a way to define a performance function based on the error. Equation (7.8a) can be minimized by setting its derivative concerning K_{fl} equal to zero, as shown in Equation (7.8b). Thus, K_{fl} can be determined by the least square method, given in Equation (7.8c).

$$J = e^2(k) = \sum_{k=0} (\tau_{meas}(k) - \hat{\tau}_{fl}(k))^2 = \sum_{k=0} (\tau_{meas}(k) - K_{fl}E_{fl}(k))^2 \tag{7.8a}$$

$$\frac{dJ}{dK_{fl}} = -2 \sum \tau_{meas}(k)E_{fl}(k) + 2 K_{fl} \sum E_{fl}^2(k) = 0 \tag{7.8b}$$

$$K_{fl} = \frac{\sum \tau_{meas}(k)E_{fl}(k)}{\sum E_{fl}^2(k)} \tag{7.8c}$$

The Equation (7.8c) can be rewritten considering Equation (7.7a), and consequently, the K_{fl} parameter was computed through Equation (7.9).

$$K_{fl} = \frac{\sum \tau_{fl}(k)E_{fl}(k)}{\sum E_{fl}^2(k)} \tag{7.9}$$

The same procedure was applied to determine K_{ex} parameter. The determination of **K_{fl} and K_{ex} parameters** required an experimental calibration procedure, as reported in [14]. However, a new **calibration method** was endowed due to the mechanical instability of PKO while performing the calibration described in [14]. The proposed calibration considers general physical principles and the operating range of the PKO's torque values. This method computes the torque produced by the user's knee (τ_{Knee}) to support a known mass $(m = \text{constant})$ at a known knee angle (α), as generally stated in Equation (7.10), where r is the knee moment-arm F_{Knee} represents the applied force by the user's knee at a given acceleration (a).

$$\tau_{Knee} = F_{Knee} * r = m * a * r \tag{7.10}$$

Consequently, during calibration, the user's knee torque was computed by Equation (7.11), considering that the user's knee kept still at a known angle ($\alpha =$ constant), that only exists the gravitational acceleration (9.8 m/s^2), and known the length of the user's leg from the hip to the ground (L).

$$\tau_{Knee} = m * 9.8 * r = \text{ m} * 9.8 * \text{L} * \sin\alpha \qquad (7.11)$$

The calibration method was implemented in two stages, as illustrated in Figure 7.19.C. In the first stage, the user was standing with the knee flexed so only the flexion torque is considered (τ_{fl}) and in the second stage, the user was seated in a chair with the knee extended, so only extension torque is considered (τ_{ex}). For both stages, the expected user's knee torque is known since the user has to keep the knee still at a known angle with a known mass attached to the foot. Surface electrodes were placed on the selected muscles to measure the EMG signals that produced the user's knee torque. When the desired torque was achieved, the envelope EMG signals from the flexor and extensor muscles were recorded, enabling the determination of the K_{fl} and K_{ex} **parameters through Equation (7.9).** Subsequently, the **user's knee torque was estimated by Equation (7.6).**

EMG-Based Control

Figure 7.20 presents the architecture control architecture implemented for EMG-based control. The **high-level** control infers the **user's motion intention** from EMG envelope signals ($E_{fl}(t)$, $E_{ex}(t)$) and computes user-oriented flexion (K_{fl}) and extension (K_{ex}) parameters during the calibration phase, to be applied in the knee joint torque estimation posteriorly.

The **mid-level control estimates the knee joint torque** using the proportional gain method law, presented in Equation (7.6). For this purpose, it uses the EMG envelopes and the calibrated parameters K_{fl} and K_{ex}. Subsequently, this level **sets the reference PKO torque** (τ_{ref}) equal to the estimated knee joint torque ($\hat{\tau}_{Knee}$) to ensure that PKO follows the user's motion intention. The **low-level** implements a **torque control through a PID controller law** to track the error (e_k) between the reference knee torque (τ_{ref}) and real torque at the PKO's actuator (τ_{meas}), as given in Equation (7.3).
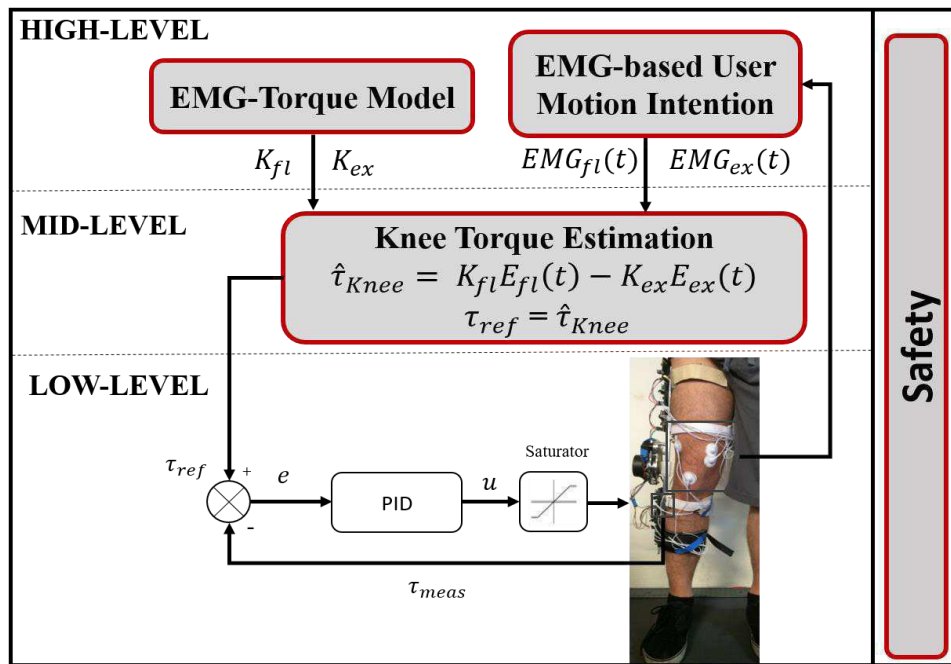
Figure 7.20- Hierarchical control architecture of the EMG-based control strategy [56].

7.6.3.Experimental Validation

The effectiveness of EMG-based assistive strategy was inspected and compared with other implemented intention-based strategy, the user-PKO interaction based control strategy.

Participants

Two healthy users (a male and a female) with demographic characteristics of 24.0 ± 0.0 years old, the height of 1.685 ± 0.0919 m, and the body mass of 63.5 ± 14.8492 kg were included. The participants gave informed consent to participate in the study and to use the collected data for research purposes.

Protocol

The experiment started with the placement of the surface electrodes on the selected muscles, *Semitendinosus*, *Semimembranosus*, *Vastus Medialis,* and *Vastus Lateralis,* following standard recommendations for surface electrodes assessment [193]. This procedure assures the repeatability of the sensor's placement and minimizes intra-subjects and intra-trials variability. Three surface electrodes were used per muscle. One is a reference electrode that was placed on the center of the knee joint, which is an electrically neutral tissue [194]. The other two electrodes were placed on the muscle motor point, separated by about 2 cm from each other [194]. The gain of the EMG system was tuned regarding the level of muscular activity

presented in the user's muscles. The overall validation of the EMG-based strategy covers three phases, as presented in Figure 7.21.
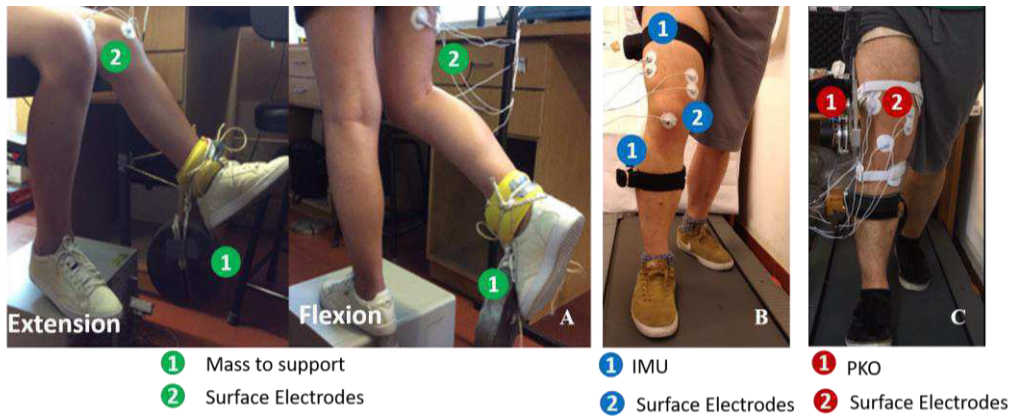
Figure 7.21- Experimental validation. **A**: Validation of calibration method. **B**: Validation of knee torque estimation method. **C**: Validation of EMG-based control [56].

First, the proposed calibration method (to compute K_{fl} and K_{ex}) was validated, considering the set-up presented in Figure 7.19.C and Figure 7.21.A. The participants were asked to perform isometric contractions during 5 s (for flexion and extension motions), that enabled to acquire the EMG signals. The isometric movements were performed at different knee angles (α), as indicated in Table 7.4. By varying the knee angle (α), it was possible to achieve the desired torques (τ_{fl} and τ_{ex}) at the user's knee joint, i.e., 8, 16, 24, and 32 Nm, as these torque values are within the range of PKO's actuator. Table 7.4 shows the knee angles covered to match the desired knee torque for a constant mass and knee force during the calibration procedure.

Table 7.4- Biomechanical values used in the calibration procedure.

Knee Joint Angle (α, [°])	Moment-arm (r, [m])	Mass (m, [Kg])	Force (F_{Knee}, [N])	Desired torque (τ_{fl}/τ_{ex}, [Nm])
10.9	0.07			8
22.4	0.15	10.7	104.86	16
34.9	0.22			24
49.7	0.30			32

The second phase aims to evaluate the performance of the proportional gain method in knee torque estimation. The subjects were asked to walk on the treadmill at different speeds (1, 1.3 and 1.6 km/h) for 3 minutes, as shown in Figure 7.21.B. Each participant performed 3 trials per gait speed. Two IMUs, placed on the human shank and thigh, were used as ground

truth to investigate if the muscles were activated properly through the gait cycle, with the emphasis in the knee flexion and extension.

The third phase covers the validation of the EMG-based control using the PKO (Figure 7.21.C). The participants walked 3 minutes on the treadmill at different speeds (1, 1.3 and 1.6 km/h), performing 3 trials per speed. Moreover, the participants conducted the same procedure wearing the PKO in user-PKO interaction based control.

Data collection

The desired and real user's knee torque, knee joint angle (α), estimated torque ($\hat{\tau}_{Knee}$), PKO's actuators torque (τ_{meas}), and the EMG signals ($E_{fl}(t)$, $E_{ex}(t)$) were collected. The NRMSE and phase delay between the reference torque (τ_{ref}) and measured torque (τ_{meas}) were inspected. Furthermore, during the EMG-based control, the users were asked if the PKO follows their intention to move.

7.6.4. Results and Discussion

Estimated K_{fl} and K_{ex} Parameters

The K_{fl} and K_{ex} parameters were computed by applying Equation (7.9) and considering the data collected during the experimental procedure proposed for the calibration method. The K_{fl} and K_{ex} parameters for the male subject were 24.3 and 46.7, respectively, and for the female subject, 27.9 and 25.26, respectively. The **differences in the parameters highlight the needed for a user-specific calibration** in an attempt to effectively address a user-oriented assistive strategy.

Estimated Knee Torque

The values of the estimated knee torques were similar to the expected ones, as observed in Figure 7.22.A. The results depicted in Figure 7.22.B also indicate that the knee joint torque was estimated properly, i.e., the knee flexion occurs when positive torques are estimated, and the knee extension occurs when negative torque values are estimated [250]. When there is an inversion of the limb's excursion (i.e., from flexion to extension, and vice-versa), the estimated torque becomes zero at that moment (as illustrated in Figure 7.22.B as moment reversal).

These findings indicate that the implemented **proportional gain method** and the proposed **calibration procedure were effective for the knee torque estimation** and relevant to deal with different user's physical conditions (different parameters found for subjects, who differ in body mass and height).
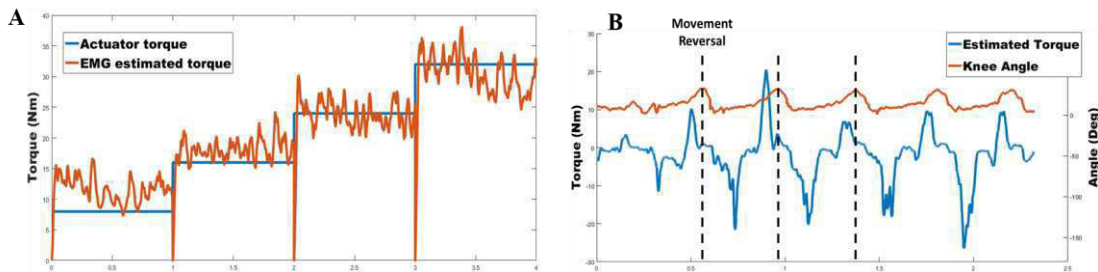
Figure 7.22- Representative results of the estimated knee torque for the male subject. **A**: Estimated knee torque *vs.* desired torque (actuator torque) during isometric contractions. **B**: Estimated knee torque and estimated knee angle by IMUs from a subject walking on the treadmill at 1.6 km/h [56].

EMG-Based Control

The EMG-based control achieved a mean NRMSE of 12% and a mean phase delay of 22 ms in a gait cycle ranging from 2.5 to 3.5 s (depends on gait speed), between the reference (τ_{ref}) and measured (τ_{meas}) torque. These results indicate that the implemented hierarchical control **has the potential to track the user's motion intentions with minimal delay.** Furthermore, the subjects reported that their intentions were followed, allowing them to move forward freely.

Figure 7.23 presents the results for both control strategies based on the user's motion intentions. The **participants applied higher muscle activation in user-orthosis interaction based control,** as indicated by the higher EMG measures of the flexor and extensor muscles (0.54 V and 0.35 V, respectively). The flexor and extension muscles activation is 52% and 31% higher in the user-orthosis interaction based control.

On the other hand, the **EMG-based control requires less effort from the user** (EMG measure of the flexors and extensors was 0.26 V and 0.24 V, respectively) while correctly generating the gait pattern based on the user's motion intention. Nonetheless, this evidence was limited to a set of gait patterns from two participants.
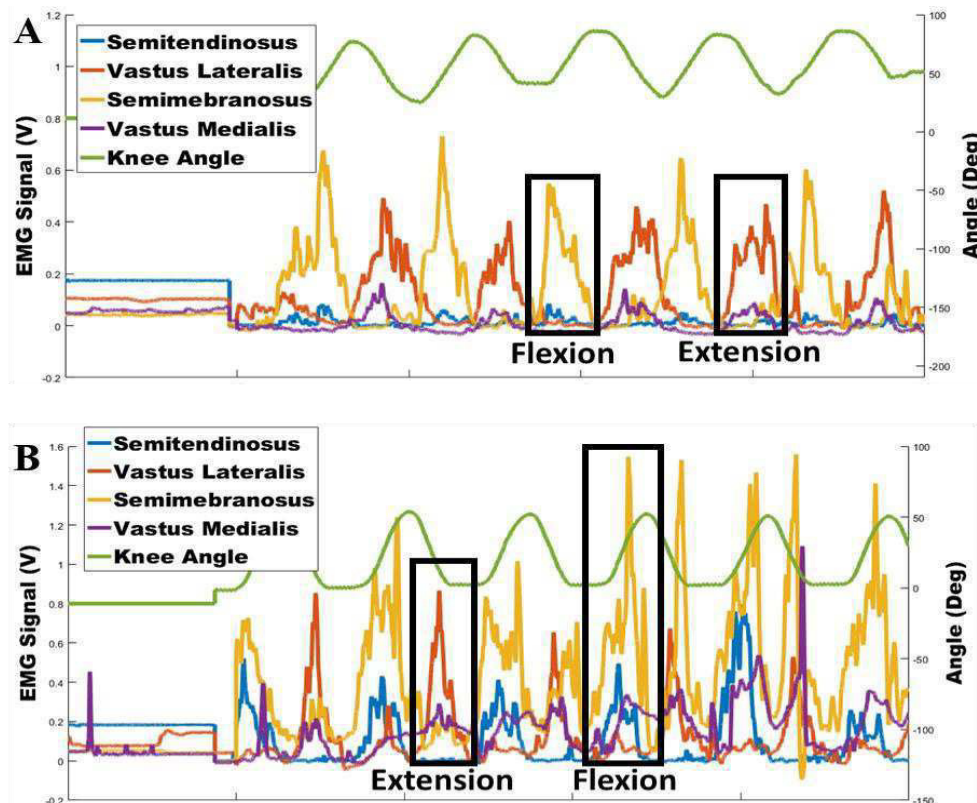
Figure 7.23- Representative results of control strategies of walking experiments in a treadmill at 1 km/h. A: EMG-based control. B: User-PKO interaction based control [56].

The finding suggests that the **EMG-based control** strategy is more suitable for subjects with a moderate level of impaired gait function than the user-orthosis interaction based strategy, **favoring therapies based on the user's intention**. This strategy may be applied for gait therapies that aim to **enhance the muscular strength and functional motor ability**. Furthermore, the user's active participation in the gait therapy will maintain active both the motor relearning and control of the learned gait pattern.

7.7.Low-Level Control Strategies

7.7.1.Related Work

Feedback and feedforward controllers play an important role in the low-level layer of the hierarchical control architectures. Feedback controllers, such as the PID, are the low-level controllers mostly applied in AOs due to their feasibility and mathematical straightforwardness [10], [237], [251]. Nevertheless, the development of **time-effective low-level controllers** for AOs capable of providing **low steady-state errors**, emphasizing **adaptiveness** to different

walking scenarios without requiring system modeling (as in optimal and robust controls), becomes imperative.

FEL control [252] has been applied to address these features. FEL, bioinspired on the learning process of the human motor cortex, is a hybrid control combining a feedback controller with a feedforward controller capable of learning the inverse dynamics of the AO using the feedback control command as the error signal for the learning (feedback error). The feedforward controller usually includes regression techniques to simplify and shorten the learning of the inverse dynamics for real-time and medical applications [253], [254]. The overall performance of FEL beneficiates from the adaptive and anticipatory features of the **feedforward control to adapt to changes in AOs' dynamics** and enable **time-effective** fast movements while the **feedback controller can compensate for disturbances** [254].

7.7.2.Methods

Considering the potentialities of FEL controller comparatively to the solo PID, this chapter presents the real-time implementation of FEL control into the low-level layer of the hierarchical control architecture of SmartOs. In the scope of this thesis, the FEL was implemented and validated as a **position-based control loop** considering the user-oriented trajectory assistive strategy. As a low-level controller, the FEL runs at 1 kHz.

FEL implies a feedback and a feedforward controller to command the AO in the desired way, as depicted in Figure 7.24. The **PID feedback controller** (previously presented) provides control commands and guarantees stability during the **real-time learning of the AOs' inverse dynamics model** and **compensates disturbances** when the learning phase is completed.

An **artificial neural network** (ANN) was implemented as the **feedforward controller** [252] to learn the inverse dynamics of the AO taking the output of a PID command (feedback controller) as an error signal [252], [253], [255]. The ANN was elected due to its proper estimation performance, good generalization, and its capability to map non-linearities [256]. Note that two inverse models were designed and implemented, one for PKO and one for PAFO.

The ANN was implemented with Multi-Layer Perceptron structure and trained in real-time following a supervised learning method. As illustrated in Figure 7.24.B, each **ANN has 3 layers** as follows: the input layer with 3 neurons for the 3 inputs, the **reference position** (θ_{ref}), **speed** ($\dot{\theta}_{ref}$) and **acceleration** ($\ddot{\theta}_{ref}$); the hidden layer with 4 and 5 neurons for PKO and PAFO, respectively; and, the output layer with 1 neuron, i.e., the feedforward command (u_{ff}). Bias

160

nodes were included in the hidden and output layers to increase the flexibility of the ANN to fit the input data.

A
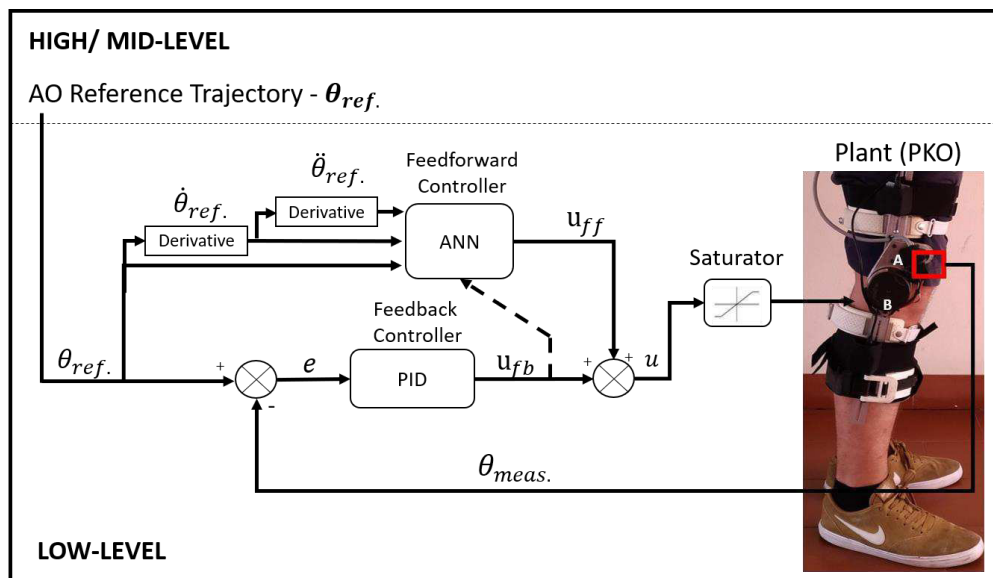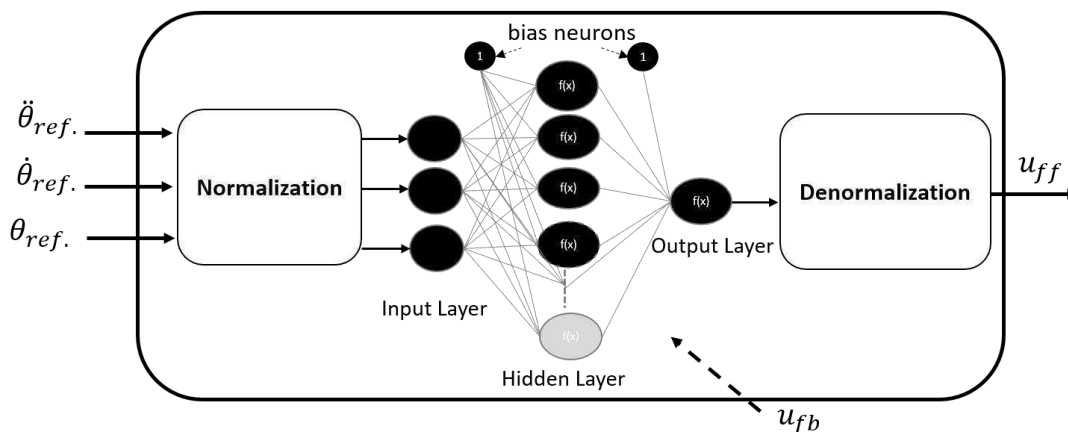
B

Figure 7.24- FEL control. **A**: FEL control loop for PKO. θ_{ref} is the reference angle; $\dot{\theta}_{ref}$ is the reference angular velocity; $\ddot{\theta}_{ref}$ is the reference angular acceleration θ_{meas} is the measured angular position; e is the position error; u_{fb} is the feedback command; u_{ff} is the feedforward command; u is the final control command; A is the potentiometer and B is the actuator. **B**: ANN-based feedback controller.

The backpropagation algorithm that includes a forward and a backward phase was used as a learning method. The forward phase predicts feedforward commands (u_{ff}) for the given inputs and based on the current weights. The backward phase updates the weights based on the gradient descent of the current feedback command (u_{fb}) concerning the network's weights change. The stochastic gradient descent approach was implemented such that the

weights are updated based on inputs presented in a random order [257]. The Adaptive Moment Estimation optimizer [258] was applied to enable the stochastic gradient descent implementation in real-time and to meet the temporal requirement of 1 ms (1 kHz). This optimization used adaptive learning rates per weight connection, providing adaptability to the ANN training and decreasing the training time.

Table 7.5 presents the empirically found set-up for training the ANN for PKO and PAFO. These parameters' setting resulted from a trade-off between the ANN performance and the real-time temporal requirements (1 kHz). For finding the ANN set-up for training phase, an empiric study was performed, varying the ANN's conditions as follows: (i) the number of hidden neurons ranged from 3 to 20; (ii) the initial weights in the hidden (w_{hid}) and output (w_{out}) layers were modified through Equation (7.12) [259], where L is the input neuron length, M is the hidden neuron length, and $\alpha = \{1, 10, 100\}$; and, (iii) the learning rate ranged from 0.001 to 0.00001.

$$-\frac{1}{\alpha\sqrt{L}} \leq w_{hid} \leq \frac{1}{\alpha\sqrt{L}}$$
$$-\frac{1}{\alpha\sqrt{M}} \leq w_{out} \leq \frac{1}{\alpha\sqrt{M}}$$

(7.12)

Table 7.5- ANN's setup for training phase, namely the number of neurons in the hidden layer, the maximum learning rate, and the initial weights in the hidden (w_{hid}) and output (w_{out}) layers.

AO	Hidden Neurons	Initial Weights	Learning Rate
PKO	4	$-0.058 \leq w_{hid} \leq 0.058$	Adaptive
		$-0.05 \leq w_{out} \leq 0.05$	(≤0.0001)
PAFO	5	$-0.058 \leq w_{hid} \leq 0.058$	Adaptive
		$-0.045 \leq w_{out} \leq 0.045$	(≤0.00001)

For both training and recall phases, the **input signals of ANN** (θ_{ref}, $\dot{\theta}_{ref}$, $\ddot{\theta}_{ref}$) **were normalized between** [-1; 1] to provide adaptability and versatility to the ANN. Moreover, it reduces the estimation error and accelerates the training phase [260]. As presented in Figure 7.24.B, the predicted output of the ANN (u_{ff}) was denormalized to the maximum operating magnitude of the control commands, experimentally set to [-2500; 2500], i.e., to the maximum values of the AOs' pulse-width modulation.

Moreover, in both training and recall phases, the computed feedback (u_{fb}) and feedforward (u_{ff}) commands are summed to get the total control command (u) to be applied to the AOs. The total command was limited to [-2500; 2500] with a saturator (Figure 7.24.B) to protect the operability of AOs. When three gait cycles are performed, the contribution of the feedback control command ($u_{fb}(\%)$) to the total control command (u) is estimated, as given by Equation (7.13), considering $\overline{u_{ff}^2}$ as the mean squared feedforward contribution.

$$u_{fb}(\%) = 100\% \times \frac{\overline{u_{ff}^2}}{u} \qquad (7.13)$$

The **training phase ends when the contribution of the feedback controller is equal or lower to 5%** ($u_{fb} \leq 5\%$) of the total control command since we empirically verified that the feedback contribution did not reach much lower than 5% of the total control command. Then, the recall phase starts, and the learned inverse dynamics models of PKO and PAFO are able to predict time-effective control commands to timely track the reference trajectory (θ_{ref}) while the feedback controller is released from this task to compensate for disturbances. Details of the FEL tuning, i.e., the real-time training of the ANN are presented in Appendix G.

7.7.3.Experimental Validation

FEL control was validated in PKO and PAKO regarding its time-effectiveness and repeatability along the time in order to investigate the possible inclusion of FEL as a low-level controller in SmartOs. Moreover, the presented validation considers the user-AO interaction to investigate the FEL adaptability to changes in the dynamics due to the interaction with the user.

Participants

Two healthy subjects (a male and a female) with 25.5 ± 0.71 years old, the height of 1.69 ± 0.1 m, and the body mass of 64.50 ± 14.84 kg. They gave their informed consent to take part in the experiment.

Protocol

The participants were asked to walk at 0.8, 1.0, and 1.2 km/h in level-ground on a treadmill with the PKO and PAFO. Each participant performed 3 trials with a duration of 5 minutes. Moreover, under the same conditions, the subjects were informed and asked to counteract the PKO and PAFO in the terminal stance and the initial stance phase, respectively, preventing

both AOs from increasing their position. The participants performed the disturbances in self-selected gait cycles. These disturbances were selected since they are commonly prevalent during a gait therapy to study the FEL response to external perturbations to the user-AO interaction.

Data Collection and Analysis

To evaluate the FEL performance while comparing with the single PID controller, the position trajectory measured by the potentiometer (θ_{meas}), the feedback (u_{fb}) and feedforward commands (u_{ff}), for PKO and PAFO, were collected. All signals were sampled at 100 Hz. The control commands were reported as AOs' pulse-width modulation values. Performance metrics as the phase delay (ms), the angular position error (°) and its normalized root mean square error (NRMSE (%)), and the feedback command contribution ($u_{fb}(\%)$), were computed in Matlab.

7.7.4.Results and Discussion

The findings of FEL tuning indicate that the designed ANN was capable of correctly learning the inverse dynamics for both AOs. When the learning phase finished, the ANN can timely track the reference trajectory, discharging the feedback controller for this task. The **learning phase lasted 90 s** (approximately 25 gait cycles) and **315 s** (approximately 70 gait cycles) for **PKO and PAFO**, respectively. These temporal differences are due to the different learning rates used in both cases (Table 7.5).

Additionally, the running time of the FEL control loop (0.25 ms) is lower than the one required by the bioinspired control architecture of SmartOs (1 ms). These temporal findings suggest that the techniques applied for approaching a real-time implementation were effective to **avoid long-time periods in the training phase**.

FEL Evaluation in PAFO

Table 7.6 presents the results of FEL performance, considering the user-PAFO interaction. It was observed a mean NRMSE of 6.51%, a mean phase delay of 25 ms and a mean contribution of 5.8% of the feedback controller to the total control command.

Table 7.6- Results (mean and std) of FEL and PID controllers achieved in gait trials with PAFO and PKO

	Speed (km/h)	Control	NRMSE (%)	Delay (ms)	u_{fb} (%)
PAFO	0.8	PID	22.28±0.14	250±0.28	-
		FEL	6.95±0.008	30±0.01	6.2±0.01
	1.0	PID	24.28±0.18	260±0.27	-
		FEL	5.99±0.002	20±0.001	6.9±0.3
	1.2	PID	26.99±0.17	250±0.28	-
		FEL	6.58±0.004	25±0.007	4.84±1.9
PKO	0.8	PID	21.58±0.17	260±0.046	-
		FEL	5.55±0.04	15±0.007	6.94±0.67
	1.0	PID	22.33±0.16	210±0.024	-
		FEL	5.69±0.04	1±0.004	6.1±0.95
	1.2	PID	22.0±0.16	230±0.05	-
		FEL	6.37±0.013	22.5±0.004	6.52±0.23

Figure 7.25 shows the consistency of FEL performance, presenting **low position error and delay**, and repetitive time-effective feedforward commands even when considering the user-PAFO interaction under different gait speeds. The findings show that **FEL can be used as an adaptive controller** to deal with dynamics changes due to interaction with the user. It also yielded **time-effective commands** since the AO's position achieves the reference position at least 40 ms before the reference position is updated (every 65 ms for 1.2 km/h, the more demanding condition).
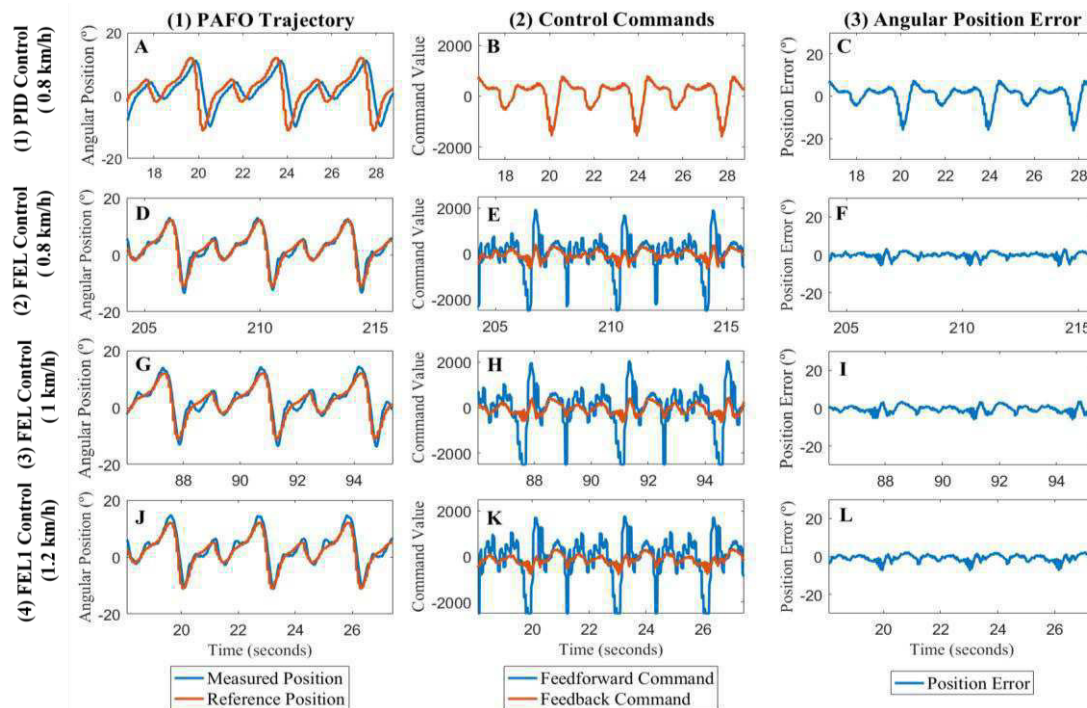
Figure 7.25- Representative results of PID control (A-C) at 0.8 km/h and FEL control (D-L) in the recall phase considering the user-PAFO interaction for 0.8, 1 and 1.2 km/h gait speeds.

Furthermore, the FEL performance was assessed in the presence of external disturbances (as marked in Figure 7.26 between 116 and 118 s). Such disturbances increased the position error due to the displacement between the reference and measured position. In response to this disturbance, the FEL control augments the feedback controller contribution (increases the PID command) while the feedforward command stayed periodic since the PAFO dynamics did not change. These outcomes demonstrate that the **feedback control** is charged to compensate for **disturbances** while the **feedforward control** is charged to **drive the desired movement**.
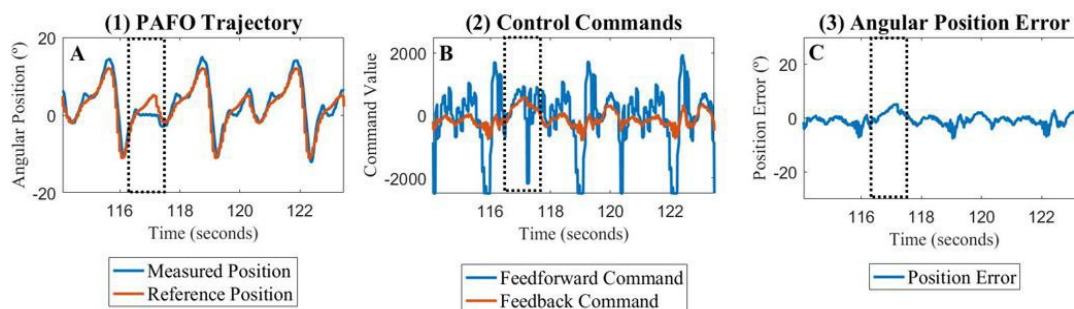
Figure 7.26- Results of FEL control to external disturbances (marked at the dashed box) for 1 km/h.

FEL Evaluation in PKO

Regarding the validation of the user-PKO interaction, a mean NRMSE of 5.87%, a mean phase delay of 12.5 ms, and a mean contribution of 6.52% of the feedback controller were yielded. Moreover, Figure 7.27 shows that the feedback command increases once the position error grows (Figure 7.27.C) due to the external disturbance caused by the user to the normal gait pattern of the user-PKO interaction. The increased contribution of the feedback control aimed to prevent the FEL control from falling into an instability state. On the other hand, the feedforward controller command stayed periodic (Figure 7.27.B), as the reference signals and the learned inverse dynamics model did not change.
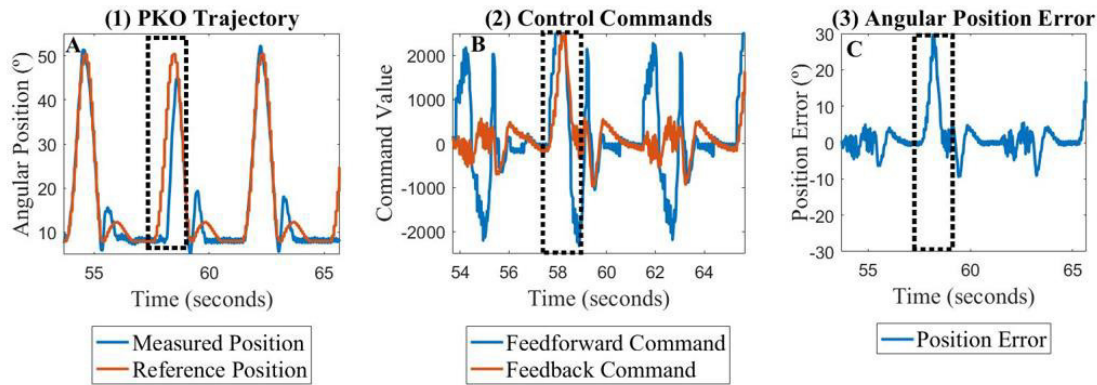
Figure 7.27- Results of FEL control to external disturbances (marked by the dashed box) to the user-PKO interaction for 1 km/h.

Comparative Analysis to PID

The FEL performance was compared with the low-level controller available in SmartOs system. For the assistance provided by the **PKO** under all tested speeds, the PID control achieved a NRMSE around 22% and a phase delay of 230 ms. Consequently, it was verified that the **FEL control decreased the NRMSE and phase delay in 16.5% and 93%,** respectively. In the ankle-foot assistance by **PAFO**, the PID achieved a mean NRMSE of 24% and a phase delay of 250 ms for all speeds. For PAFO, the **FEL control decreased by 17.5% and 90.7% the NRMSE and delay**, respectively.

The application of the **FEL controller** in AOs for gait rehabilitation constitutes an **innovate research point**. So far, the FEL's use in real robotic assistive devices has been limited to upper limbs' assistance by functional electrical stimulation [254] and neuroprosthetics [253].

In overall, the **FEL control can provide more accurate and time-effective assistance**, with lower position error and phase delay than single PID control, which is relevant for the correct application of the user-oriented trajectory strategy in repetitive gait training. FEL control time-effectively adapts the AOs' responses to the changes in the dynamics due to the nonlinear effects that arise from the user interaction with the device and compensated for random disturbances. Therefore, FEL control is an adaptive and time-effective low-level controller for the AOs embedded in SmartOs, which may yield to an efficient gait rehabilitation.

Nevertheless, more extended validation involving more subjects and assistive control strategies is required to strengthen the robustness and the evidence of FEL low-level controller

considering subject-specific effects and control dynamic variability. Lastly, a benchmarking comparison with a hybrid controller should be approached.

7.8.Conclusions

The developed control architecture includes four different assistive control strategies, which approached different therapeutic goals to make the **SmartOs a multi-functional assistive system** to accommodate for the variability of the inter-and intra-subject needs. The control architecture enables the inclusion of further assistive strategies to rise the SmartOs' applicability and expandability for distinct kinds of therapies.

Note that the performance of these assistive control strategies is determined by the (i) precision of the sensors, (ii) the actuator's torque precision and bandwidth, (iii) AO's mechanical response, and (iv) time-effectiveness of the low-level controller.

The reduced number of participants and explored AOs limit the effect size of the proposed assistive control strategies.

Chapter 8 – Conclusions

This chapter provides concluding remarks and main contributions by putting the results of the previous chapters into perspective. The future directions to increase the technological and clinical value of SmartOs system, as well as opportunities for further technical improvement, are also presented.

8.1. Concluding Remarks and Main contributions

This Ph.D. thesis proposes a **smart, wearable active lower limb orthotic system**, SmartOs system, to meet current challenges in gait rehabilitation and assistance towards a **user-oriented and repetitive gait training** while fostering a real-time and **objective assessment** of the user's motor condition. SmartOs system was designed, developed, and **experimentally validated to function as a personalized assistive solution** for stroke survivors that present impaired gait function and spastic gait.

The conducted investigation and development actions, together with the obtained promising results through benchmarking analyses, contributed to the accomplishment of the ultimate goal of this Ph.D. thesis, as follows.

An user-centered design approach, considering the end-users' reports and clinicians' expertise, was applied throughout the SmartOs' system design and development (Objective 2).

In this sense, it is expected that the pathological end-users report positive acceptability and usability with SmartOs assistance.

Chapter 3 disclosed that SmartOs combines in an innovative and interoperable manner wearable sensor systems, gait analysis tools, assistive control strategies into AOs such that they are able to time-effectively adapt the assistance according to real-time evaluation of the user's needs and motion intention. The **modules combination was successfully established through a modular, deterministic framework** (Objective 2), which demonstrated well-functioning and met the real-time constraints. The framework endows a hierarchical combination of SmartOs' modules to boost the reliability of personalized assistance and cooperation between the end-user, devices, and environment, as handled by the human motion-control system, and thus, contributing to **smart action of SmartOs.**

Moreover, the modular architecture (Objective 2) confers easy **technological scalability** that allows **extending the SmartOs' clinical perspectives** for novel therapeutic goals, different neurologically impaired end-user's, elderly assistance, and even introducing neuroprosthesis to explore the physiological and cognitive opportunities that hybrid electrical and mechanical assistance may offer.

In Chapter 4, a **wearable motion lab** with four stand-alone, self-calibrated, low-cost, wearable sensor systems was **successfully developed**. These sensor systems include real-time gait analysis tools for estimating biomechanical and muscular outcome measures (Objective 3), given their relevance in post-stroke gait recovery assessment according to International Classification of Functioning, Disability and Health (ICF). The **benchmarking analysis** with commercial systems outlined that the developed **sensor systems are purposeful for all-day monitoring in real-world walking scenarios**. Experimental findings indicate that the MuscLAB is an objective and easily applied method for providing an evolutive analysis of the muscular activity across gait therapies. However, the MuscLAB's outputs do not endow the forecast nature of muscular electrical activity measured through EMG system, which plays a relevant role in prediction and control domains.

The **open-architecture** approached in these sensor systems allows their application as stand-alone or combined into third-party systems with an **extendable potential for a versatile ambulatory human gait analysis** in healthy, pathological, and robotic-assisted conditions. This research initiative goes forward the orthosis domain, allowing the real-time and objective

evaluation of the user's motor condition to support the clinical-based motor diagnosis with more accurate information and to investigate the clinical evidence of AO-driven assistance.

Furthermore, Chapter 5 presented a **real-time gait event detection tool** through an FSM that showed to be **accurate to handle with inter-subject and inter-step variability** when varying gait speed, slope, climbing staircases, barefoot and footwear conditions (Objective 4). Features as **lower computational load**, **simple usage** (only using a small, wearable sensor from InertialLAB or GaitShoe), **more holistic gait segmentation** (up to six gait events) when compared with literature, together with the improved performance, makes the proposed detection system suitable as a benchmark for real-time assessing human gait events.

The research activities of this thesis also contributed with an **automatic, user-independent machine learning-based recognition and prediction tool** that accurately classified daily performed LMs and LMTs (Objective 5), as stated in Chapter 6. This tool advances the state-of-the-art by demonstrating that the **exclusive use of kinematic data** successfully allows (i) tackling the transition prediction problem, (iii) **predicting** LMs and LMTs one step before their occurrence, and (iii) performing a **more versatile classification** while covering different walking directions (forward, back, clockwise, and counter-clockwise) with variations in gait speed and terrains (flat, ascending and descending stairs and ramp, stepping over obstacles). This finding suggests that the user's motion intention may be successfully achieved using more practical sensors for daily locomotion than EMG sensors.

In Chapter 7, a **hierarchical, closed-loop control architecture**, prioritizing safety measures, **was successfully achieved** such that AO's assistive commands are based on the sensor feedback, that tracks the user's motor condition and his/her interaction with AO, and high-level gait analysis tool for decoding user's needs and intention inspection. This control architecture demonstrated a reliable performance for executing different user-oriented assistive control strategies in real-time when attempting to the user's motion intention and participation, as experimentally inspected. This research action transforms the SmartOs into a multi-functional assistive system within the healthcare domain to attain for the variability of the inter-and intra-subject needs and to offer distinct kinds of therapies for post-stroke gait rehabilitation (Objective 6).

Regarding the performance of these assistive strategies, the overall findings outline several concluding remarks that may guide the clinical therapies. The **user-oriented trajectory strategy** is suitable for **repetitive gait training** with user-oriented movements (mainly when using

FEL controller). Consequently, it contributes to augment the user's **movement coordination, motor sequence relearning**, and potentiating the user's natural locomotor pattern recovery given the user-oriented trajectories. As relearning motor skills after a stroke requires a person to practice movements by repetition [261], this assistive strategy potentially addresses **patients** in an **initial stage of gait therapy** or with a **high-to-moderate degree of disability.** The inclusion of wearable biofeedback systems should be approached in gait therapies since this assistive strategy does not provide any mechanism to consider or boost the user's participation.

Moreover, SmartOs covers **AAN gait training** through **adaptive impedance control** that tailors the stiffness of the human-orthosis interaction, innovatively investigated to make the AO more cooperative to the user's motion intention. The stiffness adjustment enables permanent **adaptability of the assistance level** and thus the **strength** of **motor memory** over time. This strategy contributes to **long-term efficient movements and functional motor ability**.

Furthermore, the **user-orthosis interaction-based control** and **EMG-based strategy** favour **high-challenging motor therapies** that involve the user's motion intention and physical effort. The EMG-based control strategy is more suitable for subjects with a high-to-moderate level of impaired gait function since it requires lower physical effort from the user than the user-orthosis interaction-based strategy. The findings pointed out that these strategies contribute to augment **muscular strength,** and **improve functional locomotor ability**. Nonetheless, these assistive strategies do not tailor the assistance according to the user's disability level.

The adaptive impedance control, user-orthosis interaction-based control, and EMG-based strategy showed to be featured by the **user's active and voluntary participation in the therapy**. The **involvement of cognitive processes** results in beneficial **effects on the control of learned motor behavior** and **muscle memory skills** [262]. Further, it may accelerate the motor recovery.

As the **user-orthosis interaction-based control** minimizes the mechanical impedance of the AO to act as a passive device, it was elected, in collaboration with clinicians, to be applied under spastic conditions.

The reliability and time-effectiveness of these assistive control strategies is determined by the efficacy of the low-level controller. The promising results of the **FEL** controller highlight the potential of a hybrid low-level controller to **more accurate and time-effective assistance with enough adaptability to the dynamic changes** that arise from the user interaction, when

compared to the single feedback control, PID controller. Therefore, AOs should attempt to hybrid controllers as FEL.

The overall results obtained during experimental and technical validation, proved the well-functioning of the SmartOs system, reaching the Technology Readiness Level 4 "Technology validated in lab". At this level, **SmartOs is functionally operative** and is **ready to be validated in the clinical environment**, and a protocol has already been proposed, although not described in this thesis. This clinical validation is itself innovative. The SmartOs-driven gait rehabilitation will contribute to a long-term biomechanical and functional gait recovery, augmenting the movement coordination, muscular strength, energetic efficiency locomotion, cognitive motor abilities, and general user's wellbeing. The cognitive advances may be assessed through neuroimaging.

8.2. Research Questions

The research initiatives conducted in this thesis allow answering to the following RQs.

- **RQ1:** *Which are the key outcome measures to evaluate the functional motor recovery of stroke survivors upon orthotic-based gait rehabilitation?*

This RQ was answered in Chapter 2. There is evidence to apply **outcome measures** from the Activity ICF category, including **spatiotemporal** (mainly, gait speed, step length, stride duration), **kinematic** (flexion/extension of hip, knee, and ankle at different stages of the gait cycle, and range of motion), and **functional** (mainly, Time-Up-Go Test, 10 Meter Walking Test, and Berg Balance Scale) outcomes.

- **RQ2:** *What are the main assistive potentialities and scientific challenges to consider in the design of a wearable active orthotic system for robotic-based gait rehabilitation?*

This RQ was tackled in Chapter 2. When compared with manual gait rehabilitation and passive orthotic assistance, the main **assistive potentialities of wearable AOs** are: (i) provide an intensive, repetitive therapeutic training according to a real-time evaluation of the user's needs (AAN approach); (ii) tailor the assistance to different motor activities and gait speed variations; (iii) incorporate the patient-active mode and the voluntary effort; (iv) long-term functional

motor recovery and enhanced motor learning; and, (vi) continuous and objective gait monitoring.

Challenges in wearable AOs include the integration of the following technologies: (i) time-effective assistive control strategies tailored according to the current user's needs to deliver a personalized assistance, (ii) unobtrusive wearable biofeedback system approaching less-cognitive effort to actively encourage the user's participation, (iii) wearable sensor systems and easy to apply methodologies for real-time monitoring of the neuro-biomechanical user's motor condition, and (iv) tools for the recognition of user's motion intention and current patient's disability level.

Clinical challenges include the accomplishment of more clinical experiments with (i) a significant number of participants, particularly patients that exhibit spasticity, (ii) repetitive functional motor activities daily performed, and (iii) long-term AO's evidence evaluation with quantitative outcome measures.

- **RQ3:** *Can a single kinematic measure enable a time-effective detection of several gait events under distinct walking conditions?*

This RQ was tackled in Chapter 5. Experimental evidence demonstrated the exclusive use of **foot angular velocity signal at the sagittal plane provided a time-effectiveness detection** of six gait events in controlled and non-controlled gait conditions, varying gait speed and slopes, climbing staircases, and attending to inter-subject and inter-step variability.

- **RQ4:** *Is it possible to recognize and predict daily performed locomotion modes and locomotion mode transitions using a machine learning tool that exclusively deploys kinematic data?*

This RQ was answered in Chapter 6. The promising findings support the **potential of using only the trunk and lower limb kinematic data** (angular velocity and angle) to accurately recognize and predict daily performed locomotion modes and locomotion mode transitions.

- **RQ5**: *Which set of assistive control strategies will yield a multi-functional assistive system addressing different gait therapies?*

Chapter 7 approached these RQs though the design and validation of distinct control strategies. It was verified that (i) **user-oriented trajectory control** is indicated for **repetitive training** with user-oriented movements, potentially addressing the initial stage of gait therapy; (ii)

adaptive impedance control enables a promising **AAN gait training** with adaptive assistance level; and, (iii) **EMG-based control and user-orthosis interaction-based control** are promising for therapies driven by the user's motion intentions aiming **physical high-challenging gait therapies**.

- **RQ6**: *Can feedback-error learning control, a low-level controller, provide proper real-time performance to an active assistive lower-limb device?*

The findings outline that **FEL is a time-effective low-level controller for AOs** that beneficiates from the anticipatory and time-effective performance of the feedforward control in the cyclic task of walking while the feedback controller is suited to compensate for uncertain dynamics of the human-robot system.

8.3. Future Directions

In this section, some of the scientific and technical improvement opportunities that could be explored are highlighted.

Future directions for **technical improvements** include: (i) **Integrating** the **wearable bio-feedback systems** under development to encourage the high-intensity user's physical participation into the therapy to boost the overall motor recovery. (ii) **Enhancing aesthetic and ergonomic issues** in the Wearable Motion Lab by upgrading sensor systems with wireless technology and attenuating sensors' misalignments. (iii) **Extending the validation of GaitShoe and MuscLAB** to further non-structured walking scenarios such as climbing stairs and slopes to investigate measurement repeatability under these daily locomotor tasks. (iv) Exploring the MuscLAB's response to the use of a force sensor array rather than a single sensor to deal with attachment problems and delayed muscular activity measurement. (v) **Improving the joint angle estimation**, by merging fusion-based methods with gait event resetting-based approaches to deal with the bias errors. (vi) **Improving** the overall performance of the **user's motion intention recognition and prediction tool** by including more participants and more transitional steps to increase the user-independent character and accuracy of Steady-State/Transition Classification Model, respectively. (vii) **Combining variable walking direction and gait speed across different terrains**; otherwise, the Direction Classification Model is only useful for level-ground. (viii) Utilizing **FEL low-level controller with all assistive control**

strategies and optimizing the AOs' mechanical response to achieve overall purposeful assistance. (ix) Conducting more exhaustive validation of overall hierarchical control architecture focused on the potentialities of each assistive control strategy. (x) Developing a user-custom made attachment system for **mitigating the misalignments** between the user's and AOs, mainly for PKO system to effectively obtain a user-centered device, making it more attractive.

Future scientific challenges were also pointed out during the conducted research activities, as follows. (i) **Investigate which type of biofeedback system**, vibrotactile or visual, fosters a more intuitive and cooperative user-AO interface during assisted walking conditions. (ii) Study the effectiveness of **MuscLAB** as an easily and quickly applied methodology for **assessing muscle fatigue**. (iii) Explore the affordability of tools for **gait event prediction** to tune the AO's assistance when needed. (iv) Employ the machine learning-based framework presented in Chapter 6 for achieving a **disability analysis tool** supporting the clinical-based decision in post-stroke conditions using kinematic and muscular activity data (e.g., spatiotemporal measures and kinematic and muscle synergies). (v) Complement the **hierarchical control architecture with machine learning-based tools** for incipient risk detection and user's motion intention recognition and prediction for achieving a smooth movement transition and comfortable assistance for end-users. (vi) **Include recurrent NN** into the machine learning-based framework given the ability of this NN to storage the temporal sequence of human gait that is embedded in the time-series of kinematic data. (vii) **Advance the motion prediction** problematic fusing kinematic motion data **with environment aware data**. (viii) Update current achievements of assistive control strategies, by introducing **real-time adjustment of the user-oriented trajectory** in user-oriented trajectory strategy, **AAN strategy in EMG-based control**, and damping and inertia modulation in the adaptive impedance control. (ix) Explore energy-based control strategy considering the evaluation of the user's energetic effort.

Innovative aspects cover the evaluation of the reliability, through benchmark outcomes, of the **SmartOs system** and individual modules in **clinical environment with stroke survivors**. A wide-ranging analysis of the locomotor ability of the pathological users will be tackled for creating an **open-source database with meaningful motion data** for enabling the offline building and testing of gait analysis tools and control strategies.

Lastly, long-term technical improvements aim to enable the SmartOs application in daily assistance and will strong-up the motor ability and offer the patients an adequate level of independence to perform daily locomotor activities and raise the user's confidence.

References

[1]   M. Whittle, *Gait analysis: an introduction*, 4 th. Heidi Harrison, 2007.

[2]   J. Perry, *Gait Analysis: Normal and Pathological Function*. Thorofare: SLACK Incorporated, 1992.

[3]   I. N. de E. INE, "Projeções de População Residente: 2015-2080," 2017.

[4]   World Health Organization (WHO), "Global burden of stroke," *atlas Hear. Dis. stroke*, vol. 15, pp. 50–51, 2014.

[5]   W. Johnson, O. Onuma, and S. Sachdev, "Stroke: a global response is needed," 2016.

[6]   A. Martin, S. Abogunrin, H. Kurth, and J. Dinet, "Epidemiological, humanistic, and economic burden of illness of lower limb spasticity in adults: A systematic review," *Neuropsychiatr. Dis. Treat.*, vol. 10, pp. 111–122, 2014.

[7]   J. Bae *et al.*, "A Soft Exosuit for Patients with Stroke: Feasibility Study with a Mobile Off-Board Actuation Unit," *IEEE Int. Conf. Rehabil. Robot.*, vol. 2015–Septe, pp. 131–138, 2015.

[8]   Y. Béjot, H. Bailly, J. Durier, and M. Giroud, "Epidemiology of stroke in Europe and trends for the 21st century," *Presse Med.*, vol. 45, no. 12, pp. 391–398, 2016.

[9]   M. R. Tucker *et al.*, "Control Strategies for Active Lower Extremity Prosthetics and Orthotics: A Review.," *J. Neuroeng. Rehabil.*, vol. 12, no. 1, p. 1, Jan. 2015.

[10]   S. Viteckova, P. Kutilek, and M. Jirina, "Wearable lower limb robotics: A review," *Biocybern. Biomed. Eng.*, vol. 33, no. 2, pp. 96–105, Jan. 2013.

[11]   J. Cao, S. Q. Xie, R. Das, and G. L. Zhu, "Control strategies for effective robot assisted gait rehabilitation: the state of art and future prospects.," *Med. Eng. Phys.*, vol. 36, no. 12, pp. 1555–66, 2014.

[12]   Y. Yang, C. Yang, K. M. Lee, and H. Yu, "Model-based fuzzy adaptation for control of a lower extremity rehabilitation exoskeleton," *IEEE/ASME Int. Conf. Adv. Intell. Mechatronics, AIM*, pp. 350–355, 2009.

[13]   H. Herr, "Exoskeletons and orthoses: classification, design challenges and future directions.," *J. Neuroeng. Rehabil.*, vol. 6, p. 21, 2009.

[14]   A. Pennycott, D. Wyss, H. Vallery, V. Klamroth-Marganska, and R. Riener, "Towards more effective robotic gait training for stroke rehabilitation: a review," *J. Neuroeng. Rehabil.*, vol. 9, no. 1, p. 65, 2012.

[15]   J. Bergmann, C. Krewer, F. Muller, A. Koenig, and R. Riener, "Virtual Reality to control active participation in a subacute stroke patient during robot-assisted gait training," *IEEE Int Conf Rehabil Robot*, vol. 2011, p. 5975407, 2011.

[16]   A. M. Dollar and H. Herr, "Lower Extremity Exoskeletons and Active Orthoses:Challenges and State-of-the-Art," *IEEE Trans. Robot.*, vol. 24, no. 1, pp. 144–158, Feb. 2008.

[17]   K. A. Shorter, J. Xia, E. T. Hsiao-Wecksler, W. K. Durfee, and G. F. Kogler, "Technologies for powered ankle-foot orthotic systems: Possibilities and challenges," *IEEE/ASME Trans. Mechatronics*, vol. 18, no. 1, pp. 337–347, 2013.

[18]   A. W. Boehler, K. W. Hollander, T. G. Sugar, and D. Shin, "Design, Implementation and Test Results of a Robust Control Method for a Powered Ankle Foot Orthosis (AFO)," in *IEEE International Conference on Robotics and Automation*, 2008, pp. 2025–2030.

[19]   J. Ward, T. Sugar, A. Boehler, J. Standeven, and J. R. Engsberg, "Stroke survivors' gait adaptations to a powered ankle-foot orthosis," *Adv. Robot.*, vol. 25, no. 15, pp. 1879–

References

1901, 2011.

[20] E. T. Hsiao-Wecksler *et al.*, "A pneumatic power harvesting ankle-foot orthosis to prevent foot-drop.," *J. Neuroeng. Rehabil.*, vol. 6, no. January 2016, p. 19, 2009.

[21] D. P. Ferris and C. L. Lewis, "Robotic lower limb exoskeletons using proportional myoelectric control," *Proc. 31st Annu. Int. Conf. IEEE Eng. Med. Biol. Soc. Eng. Futur. Biomed. EMBC 2009*, pp. 2119–2124, 2009.

[22] J. a Blaya and H. Herr, "Adaptive control of a variable-impedance ankle-foot orthosis to assist drop-foot gait.," *IEEE Trans. Neural Syst. Rehabil. Eng.*, vol. 12, no. 1, pp. 24–31, Mar. 2004.

[23] J. Lorentzen *et al.*, "Assessment of a portable device for the quantitative measurement of ankle joint stiffness in spastic individuals," *Clin. Neurophysiol.*, vol. 123, no. 7, pp. 1371–1382, 2012.

[24] E. L. Santos, M. C. Santos, E. Krueger, G. N. Neto-Nogueira, and P. Nohama, "Mechanomyography Signals in Spastic Muscle and the Correlation with the Modified Ashworth Scale," *38th Annu. Int. Conf. IEEE Eng. Med. Biol. Soc.*, 2016.

[25] S. Crea, M. Donati, S. M. M. De Rossi, C. M. Oddo, and N. Vitiello, "A wireless flexible sensorized insole for gait analysis.," *Sensors*, vol. 14, no. 1, pp. 1073–1093, 2014.

[26] I. González, J. Fontecha, R. Hervás, and J. Bravo, "An Ambulatory System for Gait Monitoring Based on Wireless Sensorized Insoles," *Sensors*, vol. 15, no. 7, pp. 16589–16613, 2015.

[27] Y. Huang, B. Vanderborght, R. Van Ham, and Q. Wang, "Torque–stiffness-controlled dynamic walking with central pattern generators," *Biol. Cybern.*, vol. 108, no. 6, pp. 803–823, 2014.

[28] A. R. Wu, F. Dzeladini, T. J. H. Brug, and F. Tamburella, "An Adaptive Neuromuscular Controller for Assistive Lower-Limb Exoskeletons : A Preliminary Study on Subjects with Spinal Cord Injury," *Front. Neurorobot.*, vol. 11, no. June, pp. 1–14, 2017.

[29] S. Hussain, S. Q. Xie, S. Member, and P. K. Jamwal, "Adaptive Impedance Control of a Robotic Orthosis for Gait Rehabilitation," vol. 43, no. 3, pp. 1025–1034, 2013.

[30] K. Shamaei, G. S. Sawicki, and A. M. Dollar, "Estimation of Quasi-Stiffness of the Human Knee in the Stance Phase of Walking," *PLoS One*, vol. 8, no. 12, 2013.

[31] W. Meng, Q. Liu, Z. Zhou, Q. Ai, B. Sheng, and S. (Shane) Xie, "Recent development of mechanisms and control strategies for robot-assisted lower limb rehabilitation," *Mechatronics*, vol. 31, pp. 132–145, 2015.

[32] C. Fleischer, "Controlling Exoskeletons with EMG signals and a Biomechanical Body Model," 2007.

[33] W. Hassani, S. Mohammed, H. Rifa, and Y. Amirat, "EMG Based Approach for Wearer-centered Control of a Knee Joint Actuated Orthosis," *Int. Conf. Intell. Robot. Syst.*, pp. 990–995, 2013.

[34] G. Chen *et al.*, "Adaptive Control Strategy for Gait Rehabilitation Robot to Assist-When-Needed," *2018 IEEE Int. Conf. Real-time Comput. Robot.*, pp. 538–543, 2018.

[35] F. A. Storm, C. J. Buckley, and C. Mazzà, "Gait event detection in laboratory and real life settings: Accuracy of ankle and waist sensor based methods," *Gait Posture*, vol. 50, pp. 42–46, 2016.

[36] J. K. Lee and E. J. Park, "Quasi real-time gait event detection using shank-attached gyroscopes," *Med. Biol. Eng. Comput.*, vol. 49, pp. 707–712, 2011.

[37] S. Khandelwal and N. Wickström, "Evaluation of the performance of accelerometer-based gait event detection algorithms in different real-world scenarios using the

MAREA gait database," *Gait Posture*, vol. 51, pp. 84–90, 2017.

[38]   M. Hanlon and R. Anderson, "Real-time gait event detection using wearable sensors.," *Gait Posture*, vol. 30, no. 4, pp. 523–7, Nov. 2009.

[39]   P. Catalfamo *et al.*, "Gait Event Detection on Level Ground and Incline Walking Using a Rate Gyroscope," *Sensors*, vol. 10, no. Ic, pp. 5683–5702, 2011.

[40]   P. C. Formento, R. Acevedo, S. Ghoussayni, and D. Ewins, "Gait event detection during stair walking using a rate gyroscope," *Sensors*, vol. 14, no. 3, pp. 5470–5485, 2014.

[41]   H. Huang, F. Zhang, L. J. Hargrove, Z. Dou, D. R. Rogers, and K. B. Englehart, "Continuous locomotion-mode identification for prosthetic legs based on neuromuscular - Mechanical fusion," *IEEE Trans. Biomed. Eng.*, vol. 58, no. 10, pp. 2867–2875, 2011.

[42]   A. J. Young and L. J. Hargrove, "A Classification Method for User-Independent Intent Recognition for Transfemoral Amputees Using Powered Lower Limb Prostheses," *IEEE Trans. Neural Syst. Rehabil. Eng.*, vol. 24, no. 2, pp. 217–225, 2016.

[43]   B. Chen, E. Zheng, and Q. Wang, "A locomotion intent prediction system based on multi-sensor fusion," *Sensors*, vol. 14, no. 7, pp. 12349–12369, 2014.

[44]   P. L. Butler and J. P. Jones, "A Modular Control Architecture for Real-Time Synchronous and Asynchronous Systems," in *SPIE 1964, Applications of Artificial Intelligence 1993: Machine Vision and Robotics*, 1993, vol. 1964, pp. 287–298.

[45]   R. Jiménez-Fabián and O. Verlinden, "Review of control algorithms for robotic ankle systems in lower-limb orthoses, prostheses, and exoskeletons," *Med. Eng. Phys.*, vol. 34, no. 4, pp. 397–408, 2012.

[46]   K. Anam and A. A. Al-Jumaily, "Active exoskeleton control systems: State of the art," *Procedia Eng.*, vol. 41, no. Iris, pp. 988–994, 2012.

[47]   J. Figueiredo, C. P. Santos, J. C. Moreno, J. L. Pons, J. C. Moreno, and J. C. M. Joana Figueiredo, Cristina P. Santos, Jose L. Pons, "Automatic recognition of gait patterns in human motor disorders using machine learning: A review," *Med. Eng. Phys.*, vol. 53, pp. 1–12, 2018.

[48]   P. Felix, J. Figueiredo, C. P. Santos, and J. C. Moreno, "Eletronic Design and Validation of Powered Knee Orthosis System with Werable Sensors," *17th Int. Conf. Auton. Robot Syst. Compet. (ICARSC 2017)*, 2017.

[49]   P. Félix, J. Figueiredo, C. P. Santos, and J. C. Moreno, "Powered Knee Orthosis for Human Gait Rehabilitation : First Advances," in *IEEE 5th Portuguese Meeting on Bioengineering (ENBENG)*, 2017, pp. 1–4.

[50]   J. Figueiredo, C. Ferreira, L. Costa, L. P. Reis, J. C. Moreno, and C. P. Santos, "Instrumented Insole System for Ambulatory and Robotic Walking Assistance : First Advances," in *IEEE International Conference on Autonomous Robot Systems and Competitions (ICARSC 2017)*, 2017.

[51]   P. Félix, J. Figueiredo, C. P. Santos, and J. C. Moreno, "Adaptive real-time tool for human gait event detection using a wearable gyroscope," *20th Int. Conf. Climbing Walk. Robot. Support Technol. Mob. Mach. (CLAWAR 2017)*, pp. 1–9, 2017.

[52]   J. Figueiredo, P. Felix, L. Costa, J. C. Moreno, and C. P. Santos, "Gait Event Detection in Controlled and Real-life Situations: Repeated Measures from Healthy Subjects," *IEEE Trans. Neural Syst. Rehabil. Eng.*, vol. 26, no. 10, pp. 1945–1956, 2018.

[53]   J. Figueiredo, D. Gonçalves, J. C. Moreno, and C. P. Santos, "Automatic and Real-Time Locomotion Mode Recognition of a Humanoid Robot," *20th Int. Conf. Climbing Walk. Robot. Support Technol. Mob. Mach. (CLAWAR 2017)*, pp. 1–8, 2017.

[54]   S. Carvalho, J. Figueiredo, and C. P. Santos, "Environment-Aware Locomotion Mode

References

Transition Prediction System," in *19th IEEE International Conference on Autonomous Robot Systems and Competitions (ICARSC)*, 2019.

[55] J. Figueiredo, P. Félix, C. P. Santos, and J. C. Moreno, "Towards human-knee orthosis interaction based on adaptive impedance control through stiffness adjustment," *IEEE Int. Conf. Rehabil. Robot.*, pp. 406–411, 2017.

[56] P. N. Fernandes *et al.*, "EMG-based Motion Intention Recognition for Controlling a Powered Knee Orthosis," in *19th IEEE International Conference on Autonomous Robot Systems and Competitions (ICARSC)*, 2019.

[57] P. N. Fernandes, J. Figueiredo, J. C. Moreno, and C. P. Santos, "Feedback - Error Learning for Gait Rehabilitation Using a Powered Knee Orthosis : First Advances," in *6th IEEE Portuguese Meeting on Bioengineering (ENBENG 2019)*, 2019.

[58] H. Y. Lee, J. H. Lee, and K. Kim, "Changes in angular kinematics of the paretic lower limb at different orthotic angles of plantar flexion limitation of an ankle-foot-orthosis for stroke patients.," *J. Phys. Ther. Sci.*, vol. 27, no. 3, pp. 825–8, 2015.

[59] S. Farina *et al.*, "Combined effects of botulinum toxin and casting treatments on lower limb spasticity after stroke," *Funct. Neurol.*, vol. 23, no. 2, pp. 87–91, 2008.

[60] E. S. Park, D. wook Rha, J. K. Yoo, S. M. Kim, W. H. Chang, and S. H. Song, "Short-term effects of combined serial casting and botulinum toxin injection for spastic equinus in ambulatory children with cerebral palsy," *Yonsei Med. J.*, vol. 51, no. 4, pp. 579–584, 2010.

[61] J. Y. Choi, S. Jung, D. W. Rha, and E. S. Park, "Botulinum toxin type a injection for spastic equinovarus foot in children with spastic cerebral palsy: Effects on gait and foot pressure distribution," *Yonsei Med. J.*, vol. 57, no. 2, pp. 496–504, 2016.

[62] H. Chan *et al.*, "Assessing Gait Patterns of Healthy Adults Climbing Stairs Employing Machine Learning Techniques," *Int. J. Intell. Syst.*, vol. 29, no. 2, pp. 495–524, Mar. 2014.

[63] M. Bryant, A. Pourmoghaddam, and A. Trasher, "Gait Changes with Walking Devices in Persons with Parkinson's Disease," *Disabil. Rehabil. Assist. Technol.*, vol. 7, no. 2, pp. 149–152, 2012.

[64] O. Bello, J. A. Sanchez, and M. Fernandez-del-Olmo, "Treadmill walking in Parkinson's disease patients: adaptation and generalization effect.," *Mov. Disord.*, vol. 23, no. 9, pp. 1243–9, Jul. 2008.

[65] S. L. Patterson, "Effect of treadmill exercise training on spatial and temporal gait parameters in subjects with chronic stroke: A preliminary report," *J. Rehabil. Res. Dev.*, vol. 45, no. 2, pp. 221–228, Dec. 2008.

[66] T. Herman, N. Giladi, L. Gruendlinger, and J. M. Hausdorff, "Six weeks of intensive treadmill training improves gait and quality of life in patients with Parkinson's disease: a pilot study.," *Arch. Phys. Med. Rehabil.*, vol. 88, no. 9, pp. 1154–8, Sep. 2007.

[67] K. Hase, E. Suzuki, M. Matsumoto, T. Fujiwara, and M. Liu, "Effects of therapeutic gait training using a prosthesis and a treadmill for ambulatory patients with hemiparesis.," *Arch. Phys. Med. Rehabil.*, vol. 92, no. 12, pp. 1961–6, Dec. 2011.

[68] A. Koenig *et al.*, "Psychological state estimation from physiological recordings during robot-assisted gait rehabilitation," *J. Rehabil. Res. Dev.*, vol. 48, no. 4, pp. 367–386, 2011.

[69] W. Huo, S. Mohammed, J. C. Moreno, and Y. Amirat, "Lower Limb Wearable Robots for Assistance and Rehabilitation: A State of the Art," *IEEE Syst. J.*, vol. 10, no. 3, pp. 1068–1081, 2014.

[70]   J. L. Pons, *Wearable Robots: Biomechatronic Exoskeletons*. New York, USA: John Wiley & Sons, Ltd, 2008.

[71]   C. Bushnell *et al.*, "Chronic Stroke Outcome Measures for Motor Function Intervention Trials: Expert Panel Recommendations," *Circ Cardiovasc Qual Outcomes*, vol. 8, pp. 1–13, 2017.

[72]   R. Salter, Katherine; Campbell, Nerissa; Richardson, Marina; Mehta, Swati; Jutai, Jeffrey; Zettler, Laura; Moses, Matthew; McClure, Andrew; Mays, Rachel; Foley, Norine; Teasell, "Outcome measures in stroke rehabilitation," *Evidence-Based Rev. Stroke Rehabil.*, vol. 110, pp. 1–144, 2013.

[73]   D. Moher, A. Liberati, J. Tetzlaff, D. G. Altman, and P. Grp, "Preferred Reporting Items for Systematic Reviews and Meta-Analyses: The PRISMA Statement (Reprinted from Annals of Internal Medicine)," *Phys. Ther.*, vol. 89, no. 9, pp. 873–880, 2009.

[74]   Cochrane, "Cochrane Handbook for Systematic Reviews of Interventions," 2017.

[75]   S. Portnoy, A. Frechtel, E. Raveh, and I. Schwartz, "Prevention of Genu Recurvatum in Poststroke Patients Using a Hinged Soft Knee Orthosis," *PM R*, vol. 7, no. 10, pp. 1042–1051, 2015.

[76]   C. K. Wong, L. Bishop, and J. Stein, "A wearable robotic knee orthosis for gait training: A case-series of hemiparetic stroke survivors," *Prosthet. Orthot. Int.*, vol. 36, no. 1, pp. 113–120, 2012.

[77]   K. Shihomi, O. Koji, T. Tadao, S. Yuichi, and H. Yoshiyuki, "Development of new rehabilitation robot device that can be attached to the conventional Knee-Ankle-Foot-Orthosis for controlling the knee in individuals after stroke," *IEEE Int. Conf. Rehabil. Robot.*, pp. 304–307, 2017.

[78]   J. Kim, S. Hwang, R. Sohn, Y. Lee, and Y. Kim, "Development of an active ankle foot orthosis to prevent foot drop and toe drag in hemiplegic patients: A preliminary study," *Appl. Bionics Biomech.*, vol. 8, no. 3–4, pp. 377–384, 2011.

[79]   S. Iida *et al.*, "Exercise using a robotic knee orthosis in stroke patients with hemiplegia," *J. Phys. Ther. Sci.*, pp. 1920–1924, 2017.

[80]   A. Pourghasem, I. E. Takamjani, M. T. Karimi, M. Kamali, M. Jannesari, and I. Salafian, "The effect of a powered ankle foot orthosis on walking in a stroke subject: a case study." *J. Phys. Ther. Sci.*, vol. 28, no. 11, pp. 3236–3240, 2016.

[81]   E. S. Kim, Y. S. Yoon, M. K. Sohn, S. H. Kwak, J. H. Choi, and J. S. Oh, "Effect of pneumatic compressing powered orthosis in stroke patients: Preliminary study," *Ann. Rehabil. Med.*, vol. 39, no. 2, pp. 226–233, 2015.

[82]   P. W. Duncan, H. S. Jorgensen, and D. T. Wade, "Outcome measures in acute stroke trials: A systematic review and some recommendations to improve practice," *Stroke*, vol. 31, no. 6, 2000.

[83]   C. Geroin *et al.*, "Systematic review of outcome measures of walking training using electromechanical and robotic devices in patients with stroke," *J. Rehabil. Med.*, vol. 45, no. 10, pp. 987–996, 2013.

[84]   T. J. Quinn, J. Dawson, M. R. Walters, and K. R. Lees, "Functional outcome measures in contemporary stroke trials." *Int. J. Stroke*, vol. 4, no. 3, pp. 200–205, 2009.

[85]   M. A. Gatti *et al.*, "Effects of ankle foot orthosis in stiff knee gait in adults with hemiplegia," *J. Biomech.*, vol. 45, no. 15, pp. 2658–2661, 2012.

[86]   B. Carse, R. Bowers, B. C. Meadows, and P. Rowe, "The immediate effects of fitting and tuning solid ankle-foot orthoses in early stroke rehabilitation." *Prosthet. Orthot. Int.*, p. 0309364614538090-, 2014.

References

[87] N. Rao *et al.*, "Gait assessment during the initial fitting of an ankle foot orthosis in individuals with stroke.," *Disabil. Rehabil. Assist. Technol.*, vol. 3, no. 4, pp. 201–207, Jul. 2008.

[88] B. Carse, R. J. Bowers, B. C. Meadows, and P. J. Rowe, "Visualisation to enhance biomechanical tuning of ankle-foot orthoses (AFOs) in stroke: study protocol for a randomised controlled trial," *Trials*, vol. 12, pp. 1–8, 2011.

[89] C. C. K. Chen *et al.*, "Kinematic features of rear-foot motion using anterior and posterior ankle-foot orthoses in stroke patients with hemiplegic gait," *Arch. Phys. Med. Rehabil.*, vol. 91, no. 12, pp. 1862–1868, 2010.

[90] C. Lairamore, M. K. Garrison, W. Bandy, and R. Zabel, "Comparison of tibialis anterior muscle electromyography, ankle angle, and velocity when individuals post stroke walk with different orthoses," *Prosthet. Orthot. Int.*, vol. 35, no. 4, pp. 402–410, 2011.

[91] F. Farmani, M. A. Mohseni-Bandpei, M. Bahramizadeh, G. Aminian, A. Abdoli, and M. Sadeghi-Goghari, "The Influence of Rocker Bar Ankle Foot Orthosis on Gait in Patients with Chronic Hemiplegia," *J. Stroke Cerebrovasc. Dis.*, vol. 25, no. 8, pp. 2078–2082, 2016.

[92] K. J. Nolan and M. Yarossi, "Preservation of the first rocker is related to increases in gait speed in individuals with hemiplegia and AFO," *Clin. Biomech.*, vol. 26, no. 6, pp. 655–660, 2011.

[93] L. Zollo *et al.*, "Comparative analysis and quantitative evaluation of ankle-foot orthoses for foot drop in chronic hemiparetic patients," *Eur. J. Phys. Rehabil. Med.*, vol. 51, no. 2, pp. 185–196, 2015.

[94] A. Zissimopoulos, S. Fatone, and S. Gard, "Effects of ankle-foot orthoses on mediolateral foot-placement ability during post-stroke gait.," *Prosthet. Orthot. Int.*, 2014.

[95] C. D. M. Simons, E. H. F. van Asseldonk, H. van der Kooij, A. C. H. Geurts, and J. H. Buurke, "Ankle-foot orthoses in stroke: Effects on functional balance, weight-bearing asymmetry and the contribution of each lower limb to balance control," *Clin. Biomech.*, vol. 24, no. 9, pp. 769–775, 2009.

[96] C. L. Chen, Y. L. Teng, S. Z. Lou, H. Y. Chang, F. F. Chen, and K. T. Yeung, "Effects of an anterior ankle-foot orthosis on walking mobility in stroke patients: Get up and go and stair walking," *Arch. Phys. Med. Rehabil.*, vol. 95, no. 11, pp. 2167–2171, 2014.

[97] E. Cakar, O. Durmus, L. Tekin, U. Dincer, and M. Z. Kiralp, "The ankle-foot orthosis improves balance and reduces fall risk of chronic spastic hemiparetic patients," *Eur. J. Phys. Rehabil. Med.*, vol. 46, no. 4, pp. 363–368, 2010.

[98] C. D. Nikamp, J. H. Buurke, J. van der Palen, H. J. Hermens, and J. S. Rietman, "Early or delayed provision of an ankle-foot orthosis in patients with acute and subacute stroke: A randomized controlled trial," *Clin. Rehabil.*, 2016.

[99] A. J. Pavlik, "The effect of long-term ankle-foot orthosis use on gait in the poststroke population," *J. Prosthetics Orthot.*, vol. 20, no. 2, p. 49–52 4p, 2008.

[100] A. Peaco, E. Halsne, and B. J. Hafner, "Assessing Satisfaction With Orthotic Devices and Services: A Systematic Literature Review," *JPO J. Prosthetics Orthot.*, vol. 23, no. 2, pp. 95–105, 2011.

[101] A. U. Alahakone, S. M. N. A. Senanayake, and C. M. Senanayake, "Smart wearable device for real time gait event detection during running," *IEEE Asia-Pacific Conf. Circuits Syst. Proceedings, APCCAS*, pp. 612–615, 2010.

[102] M. A. Azhar, D. Gouwanda, and A. A. Gopalai, "Development of an Intelligent Real - time Heuristic - based Algorithm to Identify Human Gait Events," pp. 573–576, 2014.

[103] D. C. M. de Wit, J. H. Buurke, J. M. M. Nijlant, M. J. Ijzerman, and H. J. Hermens, "The effect of an ankle-foot orthosis on walking ability in chronic stroke patients: a randomized controlled trial," *Clin. Rehabil.*, vol. 18, no. 5, pp. 550–557, Aug. 2004.

[104] J. Boudarham *et al.*, "Effects of a knee-ankle-foot orthosis on gait biomechanical characteristics of paretic and non-paretic limbs in hemiplegic patients with genu recurvatum," *Clin. Biomech.*, vol. 28, no. 1, pp. 73–78, 2013.

[105] J. Boudarham, D. Pradon, N. Roche, D. Bensmail, and R. Zory, "Effects of a dynamic-ankle-foot orthosis (Liberté) on kinematics and electromyographic activity during gait in hemiplegic patients with spastic foot equinus," *NeuroRehabilitation*, vol. 35, no. 3, pp. 369–379, 2014.

[106] S. Erel, F. Uygur, I. Engin Simsek, and Y. Yakut, "The effects of dynamic ankle-foot orthoses in chronic stroke patients at three-month follow-up: a randomized controlled trial.," *Clin. Rehabil.*, vol. 25, no. 6, pp. 515–523, 2011.

[107] D. G. Everaert *et al.*, "Effect of a foot-drop stimulator and ankle-foot orthosis on walking performance after stroke: a multicenter randomized controlled trial.," *Neurorehabil. Neural Repair*, vol. 27, no. 7, pp. 579–591, 2013.

[108] S. Fatone, S. A. Gard, and B. S. Malas, "Effect of Ankle-Foot Orthosis Alignment and Foot-Plate Length on the Gait of Adults With Poststroke Hemiplegia," *Arch. Phys. Med. Rehabil.*, vol. 90, no. 5, pp. 810–818, 2009.

[109] R.-Y. Wang, L.-L. Yen, C.-C. Lee, P.-Y. Lin, M.-F. Wang, and Y.-R. Yang, "Effects of an ankle-foot orthosis on balance performance in patients with hemiparesis of different durations.," *Clin Rehabil*, vol. 19, no. 1, pp. 37–44, 2005.

[110] L. R. Sheffler, S. N. Bailey, and J. Chae, "Spatiotemporal and Kinematic Effect of Peroneal Nerve Stimulation Versus an Ankle-Foot Orthosis in Patients With Multiple Sclerosis: A Case Series," *PM R*, vol. 1, no. 7, pp. 604–611, 2009.

[111] Y. L. Kerkum, A. I. Buizer, J. C. Van Den Noort, J. G. Becher, J. Harlaar, and M. A. Brehm, "The effects of varying ankle foot orthosis stiffness on gait in children with spastic cerebral palsy who walk with excessive knee flexion," *PLoS One*, vol. 10, no. 11, 2015.

[112] Y. L. Kerkum, J. Harlaar, A. I. Buizer, J. C. Van Den Noort, J. G. Becher, and M. A. Brehm, "An individual approach for optimizing ankle-foot orthoses to improve mobility in children with spastic cerebral palsy walking with excessive knee flexion," *Gait Posture*, vol. 46, pp. 104–111, 2016.

[113] P. M. Kluding *et al.*, "Foot drop stimulation versus ankle foot orthosis after stroke: 30-week outcomes," *Stroke*, vol. 44, no. 6, pp. 1660–1669, Jun. 2013.

[114] M.-P. de Seze *et al.*, "Effect of early compensation of distal motor deficiency by the Chignon ankle-foot orthosis on gait in hemiplegic patients: a randomized pilot study," *Clin. Rehabil.*, vol. 25, no. 11, pp. 989–998, 2011.

[115] F. Bethoux *et al.*, "The Effects of Peroneal Nerve Functional Electrical Stimulation Versus Ankle-Foot Orthosis in Patients With Chronic Stroke: A Randomized Controlled Trial.," *Neurorehabil. Neural Repair*, vol. 28, no. 7, pp. 688–697, 2014.

[116] A. Esquenazi, D. Ofluoglu, B. Hirai, and S. Kim, "The effect of an ankle-foot orthosis on temporal spatial parameters and asymmetry of gait in hemiparetic patients.," *PM R*, vol. 1, no. 11, pp. 1014–8, Nov. 2009.

[117] G. S. Sawicki and D. P. Ferris, "A pneumatically powered knee-ankle-foot orthosis (KAFO) with myoelectric activation and inhibition.," *J. Neuroeng. Rehabil.*, vol. 6, p. 23, Jan. 2009.

[118] C. Krishnan, D. Kotsapouikis, Y. Y. Dhaher, and W. Z. Rymer, "Reducing robotic guidance

References

during robot-assisted gait training improves gait function: A case report on a stroke survivor," *Arch. Phys. Med. Rehabil.*, vol. 94, no. 6, pp. 1202–1206, 2013.

[119] T. G. Hornby, C. R. Kinnaird, C. L. Holleran, M. R. Rafferty, K. S. Rodriguez, and J. B. Cain, "Kinematic, Muscular, and Metabolic Responses During Exoskeletal-, Elliptical-, or Therapist-Assisted Stepping in People With Incomplete Spinal Cord Injury," *Phys. Ther.*, vol. 92, pp. 1278–1295, 2012.

[120] L. Marchal-crespo and D. J. Reinkensmeyer, "Review of control strategies for robotic movement training after neurologic injury.," *J. Neuroeng. Rehabil.*, vol. 6, no. 1, p. 20, 2009.

[121] C. Krishnan, R. Ranganathan, Y. Y. Dhaher, and W. Z. Rymer, "A Pilot Study on the Feasibility of Robot-Aided Leg Motor Training to Facilitate Active Participation," *PLoS One*, vol. 8, no. 10, 2013.

[122] A. Koenig *et al.*, "Controlling patient participation during robot-assisted gait training.," *J. Neuroeng. Rehabil.*, vol. 8, no. 1, p. 14, 2011.

[123] M. L. Singer, T. Kobayashi, L. S. Lincoln, M. S. Orendurff, and K. B. Foreman, "The effect of ankle-foot orthosis plantarflexion stiffness on ankle and knee joint kinematics and kinetics during first and second rockers of gait in individuals with stroke," *Clin. Biomech.*, vol. 29, no. 9, pp. 1077–1080, 2014.

[124] Ottobock: Advanced Orthotics, "The new C-Brace," 2018.

[125] G. S. Sawicki, A. Domingo, and D. P. Ferris, "The effects of powered ankle-foot orthoses on joint kinematics and muscle activation during walking in individuals with incomplete spinal cord injury.," *J. Neuroeng. Rehabil.*, vol. 3, p. 3, 2006.

[126] M. Arazpour, A. Chitsazan, M. A. Bani, G. Rouhi, F. T. Ghomshe, and S. W. Hutchins, "The effect of a knee ankle foot orthosis incorporating an active knee mechanism on gait of a person with poliomyelitis," *Int. Soc. PROSTHETICS Orthot.*, vol. 37, no. 5, pp. 2013–2016, 2015.

[127] R. W. Horst, "A Bio-Robotic Leg Orthosis for Rehabilitation and Mobility Enhancement," in *31st Annual International Conference of the IEEE Engineering in Medicine and Biology Society*, 2009, vol. 94035, pp. 5030–5033.

[128] C. Meijneke, W. Van Dijk, and H. Van Der Kooij, "Achilles : An Autonomous Lightweight Ankle Exoskeleton to Provide Push-Off Power," pp. 5–10, 2014.

[129] R. J. Farris, H. A. Quintero, and M. Goldfarb, "Preliminary Evaluation of a Powered Lower Limb Orthosis to Aid Walking in Paraplegic Individuals," in *IEEE TRANSACTIONS ON NEURAL SYSTEMS AND REHABILITATION ENGINEERING*, 2011, vol. 19, no. 6, pp. 652–659.

[130] H. Arnez-Paniagua, Victor Rifai, S. Mohammed, and Y. Amirat, "Adaptive Control of an Actuated Ankle Foot Adaptive Control of an Actuated Ankle Foot Adaptive Control Ankle Foot Correction Orthosis for Foot-Drop Correction Orthosis for Foot-Drop," in *International Federation of Automatic Control: IFAC Conference*, 2017, vol. 50, no. 1, pp. 1384–1389.

[131] D. P. Ferris, K. E. Gordon, G. S. Sawicki, and A. Peethambaran, "An improved powered ankle-foot orthosis using proportional myoelectric control," *Gait Posture*, vol. 23, no. 4, pp. 425–428, 2006.

[132] K. A. Shorter, Y. Li, T. Bretl, and E. T. Hsiao-Wecksler, "Modeling, control, and analysis of a robotic assist device," *Mechatronics*, vol. 22, no. 8, pp. 1067–1077, 2012.

[133] K. A. Shorter, Y. Li, E. A. Morris, G. F. Kogler, and E. T. Hsiao-Wecksler, "Experimental evaluation of a portable powered ankle-foot orthosis," *Proc. Annu. Int. Conf. IEEE Eng.*

Med. Biol. Soc. EMBS, no. January 2016, pp. 624–627, 2011.

[134] A. Polinkovsky, R. J. Bachmann, N. I. Kern, and R. D. Quinn, "An Ankle Foot Orthosis with Insertion Point Eccentricity Control," in *IEEE/RSJ International Conference on Intelligent Robots and Systems*, 2012, pp. 1603–1608.

[135] G. M. Gu, S. Kyeong, D. S. Park, and J. Kim, "SMAFO: Stiffness modulated Ankle Foot Orthosis for a patient with foot drop," *IEEE Int. Conf. Rehabil. Robot.*, vol. 2015–Septe, pp. 543–548, 2015.

[136] M. Cestari, D. Sanz-Merodio, J. C. Arevalo, and E. Garcia, "An adjustable compliant joint for lower-limb exoskeletons," *IEEE/ASME Trans. Mechatronics*, vol. 20, no. 2, pp. 889–898, 2015.

[137] A. J. Veale and S. Q. Xie, "Towards compliant and wearable robotic orthoses: A review of current and emerging actuator technologies," *Med. Eng. Phys.*, vol. 38, no. 4, pp. 317–325, 2016.

[138] A. B. Zoss, H. Kazerooni, and A. Chu, "Biomechanical Design of the Berkeley Lower Extremity Exoskleton (BLEEX)," in *IEEE/ASME TRANSACTIONS ON MECHATRONICS*, 2006, vol. 11, no. 2, pp. 128–138.

[139] M. Sugisaka, J. Wang, H. Tsumura, and M. Kataoka, "A control method of ankle foot orthosis (AFO) with artificial muscle," *2008 SICE Annu. Conf.*, pp. 2013–2017, 2008.

[140] K. Bharadwaj, T. G. Sugar, J. B. Koeneman, and E. J. Koeneman, "Design of a Robotic Gait Trainer using Spring Over Muscle Actuators for Ankle Stroke Rehabilitation," *J. Biomech. Eng.*, vol. 127, no. 6, 2005.

[141] M. Noël, B. Cantin, S. Lambert, C. M. Gosselin, and L. J. Bouyer, "An electrohydraulic actuated ankle foot orthosis to generate force fields and to test proprioceptive reflexes during human walking," *IEEE Trans. Neural Syst. Rehabil. Eng.*, vol. 16, no. 4, pp. 390–399, 2008.

[142] D. P. Ferris, G. S. Sawicki, and M. a. Daley, "a Physiologist'S Perspective on Robotic Exoskeletons for Human Locomotion," *Int. J. Humanoid Robot.*, vol. 04, no. 03, pp. 507–528, 2007.

[143] M. Moltedo, T. Bacek, T. Verstraten, C. Rodriguez-Guerrero, B. Vanderborght, and D. Lefeber, "Powered ankle-foot orthoses : the effects of the assistance on healthy and impaired users while walking," *J. ofNeuroEngineering Rehabil.*, vol. 15, no. 86, pp. 1–25, 2018.

[144] P. Lopez-Meyer, G. D. Fulk, and E. S. Sazonov, "Automatic detection of temporal gait parameters in poststroke individuals," *IEEE Trans. Inf. Technol. Biomed.*, vol. 15, no. 4, pp. 594–601, 2011.

[145] K. Yasuda, K. Saichi, N. Kaibuki, H. Harashima, and H. Iwata, "Haptic-based perception-empathy biofeedback system for balance rehabilitation in patients with chronic stroke: Concepts and initial feasibility study," *Gait Posture*, vol. 62, pp. 484–489, May 2018.

[146] M. R. Afzal, M. K. Oh, C. H. Lee, Y. S. Park, and J. Yoon, "A Portable Gait Asymmetry Rehabilitation System for Individuals with Stroke Using a Vibrotactile Feedback," *Biomed Res. Int.*, vol. 2015, pp. 1–16, 2015.

[147] I. H. Khoo, P. Marayong, V. Krishnan, M. Balagtas, O. Rojas, and K. Leyba, "Real-time biofeedback device for gait rehabilitation of post-stroke patients," *Biomed. Eng. Lett.*, vol. 7, no. 4, pp. 287–298, Nov. 2017.

[148] L. Lünenburger, G. Colombo, and R. Riener, "Biofeedback for robotic gait rehabilitation," *J. Neuroeng. Rehabil.*, vol. 4, no. 1, pp. 1–11, Dec. 2007.

[149] J. Olver, A. Esquenazi, V. S. C. Fung, B. J. Singer, and A. B. Ward, "Botulinum toxin

References

assessment, intervention and aftercare for lower limb disorders of movement and muscle tone in adults: International consensus statement," *Eur. J. Neurol.*, vol. 17, no. SUPPL. 2, pp. 57–73, 2010.

[150] D. Rossi *et al.*, "Multi-joint Actuation Platform for Lower Extremity Soft Exosuits," pp. 1327–1334, 2014.

[151] A. T. Asbeck, S. M. M. De Rossi, K. G. Holt, and C. J. Walsh, "A biologically inspired soft exosuit for walking assistance," *Int. J. Rob. Res.*, vol. 34, no. 6, pp. 744–762, 2015.

[152] D. R. Louie and J. J. Eng, "Powered robotic exoskeletons in post- stroke rehabilitation of gait : a scoping review," *J. Neuroeng. Rehabil.*, vol. 13, no. 53, pp. 1–10, 2016.

[153] S. Corrigan, "Introduction to the controller area network (CAN)," 2002.

[154] M. Bortole, "Robotic Exoskeleton With an Assist-as-Needed Control for Gait Rehabilitation After Stroke," 2014.

[155] T. Lima, "Development of intuitive graphical applications for interaction with a smart wearable orthotic system," University of Minho, 2018.

[156] I. P. I. Pappas, T. Keller, S. Mangold, M. R. Popovic, V. Dietz, and M. Morari, "A Reliable Gyroscope-Based Gait-Phase Detection Sensor Embedded in a Shoe Insole," *IEEE Sens. J.*, vol. 4, no. 2, pp. 268–274, 2004.

[157] G. De Luca, "Fundamental Concepts in EMG Signal Acquisition," 2003.

[158] W. Tao, T. Liu, R. Zheng, and H. Feng, "Gait analysis using wearable sensors," *Sensors*, vol. 12, no. 2, pp. 2255–2283, 2012.

[159] S. Lambrecht, A. Harutyunyan, K. Tanghe, M. Afschrift, J. De Schutter, and I. Jonkers, "Real-time gait event detection based on kinematic data coupled to a biomechanical model," *Sensors (Switzerland)*, vol. 17, no. 4, 2017.

[160] J. Taborri, E. Palermo, S. Rossi, and P. Cappa, "Gait partitioning methods: A systematic review," *Sensors (Switzerland)*, vol. 16, no. 1, pp. 40–42, 2016.

[161] N. Abaid, P. Cappa, E. Palermo, M. Petrarca, and M. Porfiri, "Gait Detection in Children with and without Hemiplegia Using Single-Axis Wearable Gyroscopes," *PLoS One*, vol. 8, no. 9, pp. 1–8, 2013.

[162] N. C. Bejarano, E. Ambrosini, a. Pedrocchi, G. Ferrigno, M. Monticone, and S. Ferrante, "An adaptive real-time algorithm to detect gait events using inertial sensors," *IFMBE Proc.*, vol. 41, pp. 1799–1802, 2014.

[163] A. M. Sabatini, C. Martelloni, S. Scapellato, and F. Cavallo, "Assessment of walking features from foot inertial sensing," *IEEE Trans. Biomed. Eng.*, vol. 52, no. 3, pp. 486–494, 2005.

[164] T. Liu, Y. Inoue, and K. Shibata, "Development of a wearable sensor system for quantitative gait analysis," *Measurement*, vol. 42, no. 7, pp. 978–988, 2009.

[165] T. Seel, J. Raisch, and T. Schauer, "IMU-based joint angle measurement for gait analysis," *Sensors (Switzerland)*, vol. 14, no. 4, pp. 6891–6909, 2014.

[166] M. D. Djuric-Jovicic, N. S. Jovicic, and D. B. Popovic, "Kinematics of gait: New method for angle estimation based on accelerometers," *Sensors*, vol. 11, no. 11, pp. 10571–10585, 2011.

[167] S. Tadano, R. Takeda, and H. Miyagawa, "Three dimensional gait analysis using wearable acceleration and gyro sensors based on quaternion calculations.," *Sensors (Basel).*, vol. 13, no. 7, pp. 9321–9343, 2013.

[168] A. Muro-de-la-Herran, B. García-Zapirain, and A. Méndez-Zorrilla, "Gait analysis methods: An overview of wearable and non-wearable systems, highlighting clinical applications," *Sensors (Switzerland)*, vol. 14, no. 2, pp. 3362–3394, 2014.

[169] L. Ambrožič, M. Gorišič, S. Šlajpah, R. Kamnik, and M. Munih, "Wearable sensory system for robotic prosthesis," *Int. J. Mech. Control*, vol. 15, no. 1, pp. 53–59, 2014.

[170] S. Yang and Q. Li, "Inertial sensor-based methods in walking speed estimation: A systematic review," *Sensors*, vol. 12, no. 5, pp. 6102–6116, 2012.

[171] N. F. Ribeiro, L. Rocha, and C. P. Santos, "Improvement and Validation of an Inertial System," *under Rev.*, 2018.

[172] R. E. Kalman, "A New Approach to Linear Filtering and Prediction Problems 1," *J. Fluids Eng.*, vol. 82, no. Series D, pp. 35–45, 1960.

[173] Xsens Technologies, "MVN BIOMECH system: 3D Human Motion Tracking Using Miniature Inertial Sensors.," 2013.

[174] M. Al-Amri, K. Nicholas, K. Button, V. Sparkes, L. Sheeran, and J. L. Davies, "Inertial measurement units for clinical movement analysis: Reliability and concurrent validity," *Sensors (Switzerland)*, vol. 18, no. 3, pp. 1–29, 2018.

[175] J. T. Zhang, A. C. Novak, B. Brouwer, and Q. Li, "Concurrent validation of Xsens MVN measurement of lower limb joint angular kinematics," *Physiol. Meas.*, vol. 34, no. 8, 2013.

[176] D. Graurock, T. Schauer, and T. Seel, "User-Adaptive Inertial Sensor Network for Feedback-Controlled Gait Support Systems," *Int. Funct. Electr. Stimul. Soc.*, 2016.

[177] M. Memedi, S. Aghanavesi, and J. Westin, "A method for measuring Parkinson's disease related temporal irregularity in spiral drawings," *3rd IEEE EMBS Int. Conf. Biomed. Heal. Informatics, BHI 2016*, vol. 0, pp. 410–413, 2016.

[178] T. Beravs, P. Rebersek, D. Novak, J. Podobnik, and M. Munih, "Development and validation of a wearable inertial measurement system for use with lower limb exoskeletons," *IEEE-RAS Int. Conf. Humanoid Robot.*, pp. 212–217, 2011.

[179] P. Félix, J. Figueiredo, C. P. Santos, and J. C. Moreno, "Electronic design and validation of powred knee orthosis system embedded with wearable sensors," *17th Int. Conf. Auton. Robot Syst. Compet.*, pp. 110–115, 2017.

[180] A. M. Howell, T. Kobayashi, T. R. Chou, W. Daly, M. Orendurff, and S. J. M. Bamberg, "A laboratory insole for analysis of sensor placement to determine ground reaction force and ankle moment in patients with stroke," *Proc. Annu. Int. Conf. IEEE Eng. Med. Biol. Soc. EMBS*, pp. 6394–6397, 2012.

[181] S. J. M. Bamberg, A. Y. Benbasat, D. M. Scarborough, D. E. Krebs, and J. a Paradiso, "Gait analysis using a shoe-integrated wireless sensor system.," *IEEE Trans. Inf. Technol. Biomed.*, vol. 12, no. 4, pp. 413–23, 2008.

[182] I. Pappas, M. Popovic, T. Keller, V. Dietz, and M. Morari, "A reliable gait phase detection system," *IEEE Trans. Neural Syst. Rehabil. Eng.*, vol. 9, no. 2, pp. 113–125, 2001.

[183] Nordic Semiconductor, "nRF24L01+ Single chip 2.4 GHz transceiver preliminary product specification v1.0," 2008.

[184] S. Tanaka, K. Motoi, M. Nogawa, and K. Yamakoshi, "A new portable device for ambulatory monitoring of human posture and walking velocity using miniature accelerometers and gyroscope," *26th Annu. Int. Conf. IEEE Eng. Med. Biol. Soc.*, vol. 3, pp. 2283–2286, 2004.

[185] J. C. Alvarez, R. C. González, D. Alvarez, A. M. López, and J. Rodríguez-uría, "Multisensor Approach to Walking Distance Estimation with Foot Inertial Sensing," in *29th Annual International Conference of the IEEE EMBS*, 2007, vol. 3, no. 2, pp. 5719–5722.

[186] C. Huang, Z. Liao, and L. Zhao, "Synergism of INS and PDR in Self-Contained Pedestrian Tracking With a Miniature Sensor Module," *IEEE Sens. J.*, vol. 10, no. 8, pp. 1349–1359,

2010.

[187] D. A. Winter, *Biomechanics and Motor Control of Human Movement*, 4 th., vol. 2nd. 2009.

[188] M. Goršič *et al.*, "Online phase detection using wearable sensors for walking with a robotic prosthesis," *Sensors*, vol. 14, no. 2, pp. 2776–2794, 2014.

[189] M. Liu, D. Wang, and H. Helen Huang, "Development of an Environment-Aware Locomotion Mode Recognition System for Powered Lower Limb Prostheses," *IEEE Trans. Neural Syst. Rehabil. Eng.*, vol. 24, no. 4, pp. 434–443, 2016.

[190] K. S. Turker, "Electromyography: Some methodological problems and issues," *Phys. Ther.*, vol. 73, no. 10, pp. 698–710, 1993.

[191] P. Lukowicz, F. Hanser, C. Szubski, and W. Sehobersberger, "Detecting and interpreting muscle activity with wearable force sensors," *Lect. Notes Comput. Sci.*, vol. 3968 LNCS, pp. 101–116, 2006.

[192] M. Kreil, G. Ogris, and P. Lukowicz, "Muscle Activity Evaluation using Force Sensitive Resistors," pp. 107–110, 2008.

[193] S. Project, "Recommendations for sensor locations on individual muscles," *SENIAM*, 2006. [Online]. Available: http://www.seniam.org/.

[194] C. J. De Luca, "Surface Electromyography: Detection and Recording," 2002.

[195] R. R. Neptune, D. J. Clark, and S. a Kautz, "Modular control of human walking: a simulation study.," *J. Biomech.*, vol. 42, no. 9, pp. 1282–7, Jun. 2009.

[196] N. C. Bejarano, E. Ambrosini, A. Pedrocchi, G. Ferrigno, M. Monticone, and S. Ferrante, "A novel adaptive, real-time algorithm to detect gait events from wearable sensors," *IEEE Trans. Neural Syst. Rehabil. Eng.*, vol. 23, no. 3, pp. 413–422, 2015.

[197] J. Rueterbories, E. G. Spaich, and O. K. Andersen, "Gait event detection for use in FES rehabilitation by radial and tangential foot accelerations," *Med. Eng. Phys.*, vol. 36, no. 4, pp. 502–508, 2014.

[198] M. S. H. Aung *et al.*, "Automated detection of instantaneous gait events using time frequency analysis and manifold embedding," *IEEE Trans. Neural Syst. Rehabil. Eng.*, vol. 21, no. 6, pp. 908–916, 2013.

[199] R. C. González, A. M. López, J. Rodriguez-Uría, D. Álvarez, and J. C. Alvarez, "Real-time gait event detection for normal subjects from lower trunk accelerations," *Gait Posture*, vol. 31, pp. 322–325, 2010.

[200] D. Gouwanda and A. A. Gopalai, "A robust real-time gait event detection using wireless gyroscope and its application on normal and altered gaits," *Med. Eng. Phys.*, vol. 37, pp. 219–225, 2015.

[201] A. Mannini, V. Genovese, A. M. Sabatini, and S. Member, "Online Decoding of Hidden Markov Models for Gait Event Detection Using Foot-Mounted Gyroscopes," *IEEE J. Biomed. Heal. INFORMATICS*, vol. 18, no. 4, pp. 1122–1130, 2014.

[202] J. Barth *et al.*, "Stride segmentation during free walk movements using multi-dimensional subsequence dynamic time warping on inertial sensor data," *Sensors (Switzerland)*, vol. 15, no. 3, pp. 6419–6440, 2015.

[203] D. Kotiadis, H. J. Hermens, and P. H. Veltink, "Inertial Gait Phase Detection for control of a drop foot stimulator. Inertial sensing for gait phase detection.," *Med. Eng. Phys.*, vol. 32, no. 4, pp. 287–297, 2010.

[204] T. Seel, "Learning Control and Inertial Realtime Gait Analysis in Biomedical Applications," Technischen Universität Berlin, 2016.

[205] J. Figueiredo, C. Ferreira, C. P. Santos, J. C. Moreno, and L. P. Reis, "Real-Time Gait

Events Detection During Walking of Biped Model and Humanoid Robot Through Adaptive Thresholds," *IEEE Int. Conf. Auton. Robot Syst. Compet.*, pp. 1–6, 2016.

[206] B. R. Greene, D. McGrath, R. O'Neill, K. J. O'Donovan, A. Burns, and B. Caulfield, "An adaptive gyroscope-based algorithm for temporal gait analysis," *Med. Biol. Eng. Comput.*, vol. 48, no. 12, pp. 1251–1260, 2010.

[207] D. Gouwanda and A. A. Gopalai, "A robustreal-time gaiteventdetection using wirelessgyroscope and itsapplication on normal and alteredgaits," *Med. Eng. Phys.*, vol. 37, no. 2, pp. 219–225, 2015.

[208] A. Ferrari, P. Ginis, M. Hardegger, F. Casamassima, L. Rocchi, and L. Chiari, "A Mobile Kalman-Filter Based Solution for the Real-Time Estimation of Spatio-Temporal Gait Parameters," *IEEE Trans. Neural Syst. Rehabil. Eng.*, vol. 24, no. 7, pp. 764–773, 2016.

[209] L. Costa, "Wearable Sensory Systems for Real-time Human Gait Analysis," University of Minho, 2018.

[210] B. L. Day *et al.*, "Delay in the execution of voluntary movement by electrical or magnetic brain stimulation in intact man.," *Brain*, vol. 112, pp. 649–663, 1989.

[211] Y. David Li and E. T. Hsiao-Wecksler, "Gait mode recognition and control for a portable-powered ankle-foot orthosis," in *IEEE International Conference on Rehabilitation Robotics*, 2013, pp. 1–8.

[212] S. Au, M. Berniker, and H. Herr, "Powered ankle-foot prosthesis to assist level-ground and stair-descent gaits," *Neural Networks*, vol. 21, pp. 654–666, 2008.

[213] A. J. Young, T. A. Kuiken, and L. J. Hargrove, "Analysis of using EMG and mechanical sensors to enhance intent recognition in powered lower limb prostheses," *J. Neural Eng.*, vol. 11, no. 5, pp. 1–12, 2014.

[214] J. Jang, K. Kim, J. Lee, B. Lim, and Y. Shim, "Online gait task recognition algorithm for hip exoskeleton," *IEEE Int. Conf. Intell. Robot. Syst.*, vol. 2015–Decem, pp. 5327–5332, 2015.

[215] K. Leuenberger, R. Gonzenbach, E. Wiedmer, A. Luft, and R. Gassert, "Classification of stair ascent and descent in stroke patients," *Proc. - 11th Int. Conf. Wearable Implant. Body Sens. Networks Work. BSN Work. 2014*, pp. 11–16, 2014.

[216] B. Hu, E. Rouse, L. Hargrove, and B. Hu, "Fusion of Bilateral Lower-Limb Neuromechanical Signals Improves Prediction of Locomotor Activities," *Front. Robot. AI*, vol. 5, no. June, pp. 1–16, 2018.

[217] H. A. Varol, F. Sup, and M. Goldfarb, "Multiclass real-time intent recognition of a powered lower limb prosthesis," *IEEE Trans. Biomed. Eng.*, vol. 57, no. 3, pp. 542–551, 2010.

[218] D. C. Tkach and L. J. Hargrove, "Neuromechanical sensor fusion yields highest accuracies in predicting ambulation mode transitions for trans-tibial amputees," *Proc. Annu. Int. Conf. IEEE Eng. Med. Biol. Soc. EMBS*, pp. 3074–3077, 2013.

[219] D. Novak, M. Goršič, J. Podobnik, and M. Munih, "Toward Real-Time Automated Detection of Turns during Gait Using Wearable Inertial Measurement Units.," *Sensors (Basel).*, vol. 14, no. 10, pp. 18800–18822, Jan. 2014.

[220] J. Zhang, T. E. Lockhart, and R. Soangra, "Classifying lower extremity muscle fatigue during walking using machine learning and inertial sensors.," *Ann. Biomed. Eng.*, vol. 42, no. 3, pp. 600–12, Mar. 2014.

[221] Y. Zhang, C. Ding, and T. Li, "Gene selection algorithm by combining reliefF and mRMR.," *BMC Genomics*, vol. 9 Suppl 2, p. S27, 2008.

[222] R. D. Ledesma, C. Universidad, N. De Mar, P. Valero-mora, and U. De Valencia,

References

"Determining the Number of Factors to Retain in EFA: an easy-to-use computer program for carrying out Parallel Analysis," *Pract. Assessment, Res. Eval.*, vol. 12, no. 2, pp. 2–11, 2007.

[223] G. Jurman, S. Riccadonna, and C. Furlanello, "A comparison of MCC and CEN error measures in multi-class prediction," *PLoS One*, vol. 7, no. 8, pp. 1–8, 2012.

[224] F. Zhang and H. Huang, "Source selection for real-time user intent recognition toward volitional control of artificial legs," *IEEE J. Biomed. Heal. Informatics*, vol. 17, no. 5, pp. 907–914, 2013.

[225] T. Yan, Y. Sun, T. Liu, C.-H. Chcung, and M. Q.-H. Meng, "A Locomotion Recognition System Using Depth Images," *2018 IEEE Int. Conf. Robot. Autom.*, pp. 6766–6772, 2018.

[226] F. Dzeladini, J. Van Den Kieboom, and A. Ijspeert, "The contribution of a central pattern generator in a reflex-based neuromuscular model," *Front. Hum. Neurosci.*, vol. 8, no. June, pp. 1–18, 2014.

[227] C. Fleischer and G.Hommel, "Calibration of an EMG-Based Body Model with six Muscles to control a Leg Exoskeleton," *IEEE Int. Conf. Robot. Autom.*, pp. 10–14, 2007.

[228] H. Geyer and H. Herr, "A Muscle-reflex model that encodes principles of legged mechanics produces human walking dynamics and muscle activities," *IEEE Trans. Neural Syst. Rehabil. Eng.*, vol. 18, pp. 263–273, 2010.

[229] J. C. P. Ibarra and A. A. G. Siqueira, "Impedance control of rehabilitation robots for lower limbs. Review," *Proc. - 2nd SBR Brazilian Robot. Symp. 11th LARS Lat. Am. Robot. Symp. 6th Rob. Work. Appl. Robot. Autom. SBR LARS Rob. 2014 - Part Jt. Conf. Robot. Intell. Syst.* , pp. 235–240, 2015.

[230] G. Aguirre-Ollinger, J. E. Colgate, M. A. Peshkin, and A. Goswami, "Active-impedance control of a lower-limb assistive exoskeleton," *2007 IEEE 10th Int. Conf. Rehabil. Robot. ICORR'07*, vol. 00, no. c, pp. 188–195, 2007.

[231] W. M. Dos Santos and A. A. G. Siqueira, "Optimal impedance control for robot-Aided rehabilitation of walking based on estimation of patient behavior," *Proc. IEEE RAS EMBS Int. Conf. Biomed. Robot. Biomechatronics*, vol. 2016–July, pp. 1023–1028, 2016.

[232] V. Adhikari, A. Majidrad, Y. Yihun, and J. Desai, "Assist-as-Needed Controller to a Task-based Knee Rehabilitation Exoskeleton," pp. 3212–3215.

[233] A. G. Noughaby, "The Control of an Exoskeleton and The Reduction of Interaction Force Using Human Intent Detection by EMG Signals and Torque Estimation," *2018 6th RSI Int. Conf. Robot. Mechatronics*, no. IcRoM, pp. 536–541, 2018.

[234] J. Zhang *et al.*, "Human-in-the-loop optimization of exoskeleton assistance during walking," *Robotics*, vol. 1284, no. June, pp. 1280–1284, 2017.

[235] H. Rifaï, W. Hassani, S. Mohammed, and Y. Amirat, "Bounded control of an actuated lower limb orthosis," *Proc. IEEE Conf. Decis. Control*, pp. 873–878, 2011.

[236] J. Zhang, C. C. Cheah, and S. H. Collins, "Experimental comparison of torque control methods on an ankle exoskeleton during human walking," *2015 IEEE Int. Conf. Robot. Autom.*, pp. 5584–5589, 2015.

[237] T. Yan, M. Cempini, C. M. Oddo, N. Vitiello, C. Maria, and N. Vitiello, "Review of assistive strategies in powered lower-limb orthoses and exoskeletons," *Rob. Auton. Syst.*, vol. 64, pp. 120–136, 2015.

[238] R. Riener, L. Lünenburger, S. Jezernik, M. Anderschitz, G. Colombo, and V. Dietz, "Patient-cooperative strategies for robot-aided treadmill training: First experimental results," *IEEE Trans. Neural Syst. Rehabil. Eng.*, vol. 13, no. 3, pp. 380–394, 2005.

[239] D. A. Winter, A. J. Fuglevand, and S. E. Archer, "Crosstalk in surface electromyography:

Theoretical and practical estimates," *J. Electromyogr. Kinesiol.*, vol. 4, no. 1, pp. 15–26, 1994.

[240] B. Koopman, E. H. F. van Asseldonk, and H. Van der Kooij, "Speed-dependent reference joint trajectory generation for robotic gait support," *J. Biomech.*, vol. 47, no. 6, pp. 1447–1458, 2014.

[241] B. M. Fleerkotte, B. Koopman, J. H. Buurke, E. H. F. van Asseldonk, H. van der Kooij, and J. S. Rietman, "The effect of impedance-controlled robotic gait training on walking ability and quality in individuals with chronic incomplete spinal cord injury: an explorative study.," *J. Neuroeng. Rehabil.*, vol. 11, p. 26, Jan. 2014.

[242] M. Bortole *et al.*, "The H2 robotic exoskeleton for gait rehabilitation after stroke: early findings from a clinical study," *J. Neuroeng. Rehabil.*, vol. 12, no. 1, p. 54, 2015.

[243] C. Guo, S. Guo, J. Ji, and F. Xi, "Iterative Learning Impedance for Lower Limb Rehabilitation Robot," vol. 2017, 2017.

[244] K. Shamaei, M. Cenciarini, A. A. Adams, K. N. Gregorczyk, J. M. Schiffman, and A. M. Dollar, "Design and evaluation of a quasi-passive knee exoskeleton for investigation of motor adaptation in lower extremity joints," *IEEE Trans. Biomed. Eng.*, vol. 61, no. 6, pp. 1809–1821, 2014.

[245] S. Pfeifer, R. Riener, and H. Vallery, "Knee stiffness estimation in physiological gait," *Conf. Proc. … Annu. Int. Conf. IEEE Eng. Med. Biol. Soc. IEEE Eng. Med. Biol. Soc. Annu. Conf.*, vol. 2014, no. October 2016, pp. 1607–1610, 2014.

[246] W. Hassani, Mohammed, and S. Y. Amirat, "Real-Time EMG driven Lower Limb Actuated Orthosis for Assistance As Needed Movement Strategy," *Robot. Sci. Syst.*, 2013.

[247] H. Kawamoto and Y. Sankai, "Power Assist System HAL-3 for Gait Disorder Person," *Comput. Help. people with Spec. needs*, pp. 196–203, 2002.

[248] C. Fleischer, C. Reinicke, and G. Hommel, "Predicting the Intended Motion with EMG Signals for an Exoskeleton Orthosis Controller," *Intell. Robot. Syst.*, 2005.

[249] H. Kawamoto and Y. Sankai, "Power Assist System HAL-3 for Gait Disorder Person," *Int. Conf. Comput. Handicap. Pers.*, pp. 196–203, 2002.

[250] A. M. El-sayed, N. A. Hamzaid, N. Azuan, and A. Osman, "Technology Efficacy in Active Prosthetic Knees for Transfemoral Amputees : A Technology Quantitative Evaluation," *Sci. World J.*, no. July, p. 17, 2014.

[251] K. Anam and A. A. Al-jumaily, "Active Exoskeleton Control Systems : State of the Art," *Int. Symp. Robot. Intell. Sensors*, pp. 988–994, 2012.

[252] M. Kawato, "Feedback-error-learning neural network for supervised motor learning," *Adv. neural Comput.*, vol. 6, pp. 365–372, 1990.

[253] F. Resquín, J. Gonzalez-vargas, J. Ibáñez, F. Brunetti, and J. L. Pons, "Feedback error learning controller for functional electrical stimulation assistance in a hybrid robotic system for reaching rehabilitation," *Eur. J. Transl. Myol.*, vol. 26, no. 3, pp. 255–261, 2016.

[254] K. Kurosawa, R. Futami, T. Watanabe, and N. Hoshimiya, "Joint Angle Control by FES Using a Feedback," *IEEE Trans. NEURAL Syst. Rehabil. Eng.*, vol. 13, no. 3, pp. 359–371, 2005.

[255] H. Miyamoto, M. Kawato, T. Setoyama, and R. Suzuki, "Feedback-Error-Learning Neural Network fot Trajectory Control of a Robotic Manipulator," *Neural Networks*, no. 1, pp. 251–265.

[256] A. P. E. Meireles Magali RG, "A comprehensive review for industrial applicability of ANNs.," *IEEE Trans Ind Electron*, vol. 50, no. 3, pp. 585–601, 2003.

References

[257] S. Ruder, "An overview of gradient descent optimization," pp. 1–14, 2016.

[258] D. Kingma and J. L. Ba, "ADAM: A METHOD FOR STOCHASTIC OPTIMIZATION," in *International Conference on Learning Representations (ICLR)*, 2015, pp. 1–15.

[259] S. Marsland, *Machnine Learning: An Algorithmic Perspective*, 2nd ed. Boca Raton, Florida: CRC Press, 2015.

[260] J. Sola and J. Sevilla, "Importance of input data normalization for the application of neural networks to complex industrial problems," *IEEE Trans. Nucl. Sci.*, vol. 44, no. 3 PART 3, pp. 1464–1468, 1997.

[261] H. Masaki and W. Sommer, "Cognitive neuroscience of motor learning and motor control," vol. 1, no. 3, pp. 369–380, 2012.

[262] B. Thon, "Neuropsychology of gesture (SNLF-SOFMER)," *Ann. Phys. Rehabil. Med.*, vol. 58, 2015.

[263] Q. Li, M. Young, V. Naing, and J. M. Donelan, "Walking speed estimation using a shank-mounted inertial measurement unit," *J. Biomech.*, vol. 43, no. 8, pp. 1640–1643, 2010.

[264] D. Novak *et al.*, "Automated detection of gait initiation and termination using wearable sensors.," *Med. Eng. Phys.*, vol. 35, no. 12, pp. 1713–20, Dec. 2013.

[265] R. Begg and J. Kamruzzaman, "A machine learning approach for automated recognition of movement patterns using basic, kinetic and kinematic gait data.," *J. Biomech.*, vol. 38, no. 3, pp. 401–8, Mar. 2005.

[266] F. J. Badesa, R. Morales, N. Garcia-Aracil, J. M. Sabater, A. Casals, and L. Zollo, "Auto-adaptive robot-aided therapy using machine learning techniques.," *Comput. Methods Programs Biomed.*, vol. 116, no. 2, pp. 123–30, Sep. 2014.

Appendix A- Methodologic Quality Assessment

This appendix provides information on the methodologic quality assessment of each included study in Chapter 2.2 (see Appendix A.1) and Chapter 2.3 (see Appendix A.2) using the Cochrane risk-of-bias tool [74].

Appendix A.1

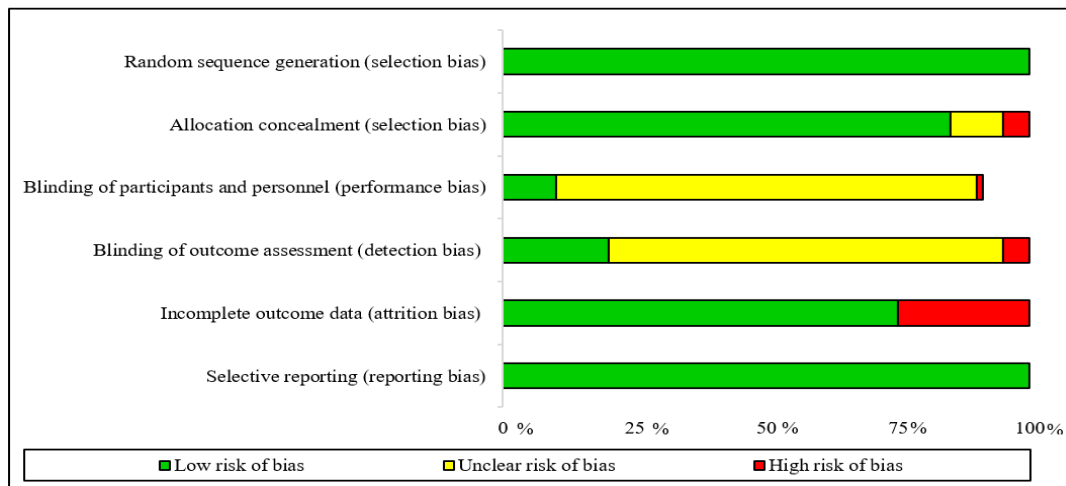Risk of bias assessment of the studies discussed in Chapter 2.2 using the Cochrane tool

Figure A.1.1- Risk of bias graph.

	Random sequence generation (selection bias)	Allocation concealment (selection bias)	Blinding of participants and personnel (performance)	Blinding of outcome assessment (detection bias)	Incomplete outcome data (attrition bias)	Selective reporting (reporting bias)
Simons 2009	+	+	?	?	–	+
Chen 2014	+	+	+	?	+	+
Portnoy 2015	+	+	?	?	–	+
Cakar 2010	+	?	?	?	+	+
Gatti 2012	+	?	–	+	+	+
de Wit 2004	+	+	?	?	+	+
Nikamp 2016	+	+	+	–	–	+
Pavlik 2008	+	+	?	?	+	+
Carse 2014	+	+	?	?	+	+
Zissimopoulos 2014	+	+	?	?	–	+
Rao 2008	+	–	?	?	+	+
Carse 2011	+	+	–	+	+	+
Chen 2010	+	+	?	?	+	+
Farmani 2016	+	+	?	?	+	+
Lairamore 2011	+	+	?	+	+	+
Nolan 2011	+	+	?	?	–	+

Zollo 2015

Wong 2012

+ Low risk of bias

? Unclear risk of bias

− High risk of bias

Figure A.1.2- Risk of bias summary.

Appendix A.2

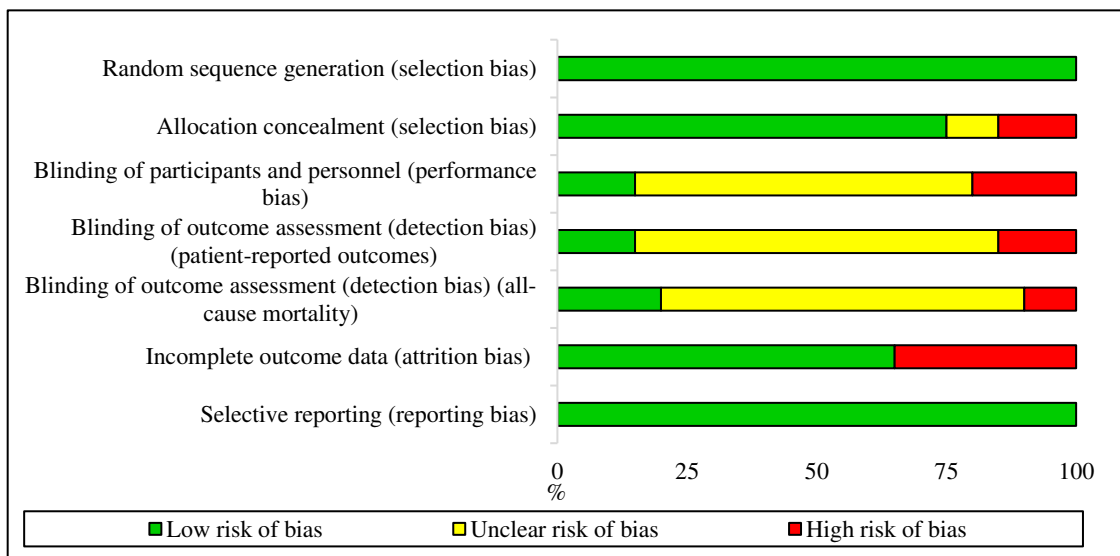Risk of bias assessment of the studies discussed in Chapter 2.3 using the Cochrane tool

Figure A.2.1- Risk of bias graph.

	Pavlik 2008	Everaert 2013	Nikamp 2016	de Wit 2004	Gatti 2012	de Sèze 2011	Erel 2011	Cakar 2010	Portnoy 2015	Boudarham 2013	Chen 2014	Boudarham 2014	Simons 2009
Random sequence generation (selection bias)	+	+	+	+	+	+	+	+	+	+	+	+	+
Allocation concealment (selection bias)	+	+	+	+	?	+	+	?	+	–	+	–	+
Blinding of participants and personnel (performance bias)	?	?	+	?	–	–	–	?	?	?	+	?	?
Blinding of outcome assessment (detection bias) (patients-reported	?	?	–	?	+	?	+	?	?	?	?	?	?
Blinding of outcome assessment (detection bias) (all-cause mortality)	?	?	–	?	+	?	+	?	?	?	?	?	?
Incomplete outcome data (attrition bias)	+	–	–	+	+	+	–	+	–	+	+	+	–
Selective reporting (reporting bias)	+	+	+	+	+	+	+	+	+	+	+	+	+

196

Figure A.2.2- Risk of bias summary.

Appendix B- Outcomes Measures in Post-stroke Gait Rehabilitation

This appendix provides additional information on outcome measures, categorized per ICF category, used in post-stroke orthotic-based rehabilitation, which were presented in Chapter 2.2.

Table B.1- Assessment protocol (goal, outcome measures, motion capture systems, and timing for assessment) in post-stroke orthotic-based rehabilitation. N/A means not available and (*) indicates the primary outcome.

Study	Assessment goal	Disease stage	Orthosis	Outcome measures		Motion capture system	Timing for assessment
				ICF category	Description		
[95]	Functional and dynamic balance	Chronic	Conventional AFO and metal AFO	Activity	-Functional metrics: TUG, 10MWT, FAC, BBS. -Balance metrics: Weight-bearing asymmetry, timed balance test.	6 DOFs motion platform (MOTEK, Netherlands), Vicon system (Vicon, UK)	End of treatment: 35 months
[96]	Walking ability	Chronic	Anterior AFO	Body impairment	-Impairment metrics: MAS.	N/A	N/A
				Activity	-Functional metrics: TUG, TUDS, BBS.		
[75]	Gait pattern and symmetry	Acute	Hinged knee orthosis	Body function	-Muscle activity: electromyography.	4-camera system (Basler Scout, Basler AG, Germany), telemetric EMG device (Zebris Medical GmbH, Germany)	-Baseline; -End of treatment: 4 weeks
				Activity	-Spatiotemporal parameters: gait velocity, cadence, step length, base width, stance, swing and double-support duration, and symmetry index. -Functional metrics: 6MWT, 10MWT (*), TUG, BBS.		
				Participation	- Participation metrics: satisfaction questionnaire with 9 questions concerned the orthotic fit, weight, durability, appearance, the effect on clothes and skin, the difficulty of donning, and related pain.		
[97]	Balance and fall risk mitigation	Chronic	Conventional AFO	Activity	-Functional metrics: BBS. -Balance metric: postural stability measured by Biodex system.	Biodex System (USA), movable balance platform	End of treatment: 1 week
[85]	Knee joint ability	Chronic	Conventional AFO	Activity	-Spatiotemporal parameters: gait speed, step length. -Kinematic metrics of paretic limb: knee flexion and peak knee flexion angle.	ELITE (BTS Bioengineering, Italy) with 8 infrared cameras	End of treatment: 6 trials

Study	Assessment goal	Disease stage	Orthosis	Outcome measures		Motion capture system	Timing for assessment
				ICF category	Description		
[103]	Walking ability	Chronic	Conventional AFO	Activity	- Functional metrics: TUG, TUDS, FAC.	2 infra-red beams	End of treatment: 9 months
[98]	Balance and walking ability	Acute	Conventional AFO	Activity	-Functional metrics: 10MWT (*), 6MWT, TUG, TUDS, FAC, BI, BBS.	N/A	-Baseline; -End of treatment: 2, 9 and 11 weeks
[99]	Long-term effect of walking ability	Chronic	Conventional AFO	Activity	-Functional metrics: 10MWT, TUG.	Footprints	N/A
				Participation	- Participation metrics: perceived exertion scale (ranges from 6 to 20) to assess the activity intensity of each trial for each test.		
[86]	Immediate biomechanical ability	Acute	Conventional AFO	Activity	-Spatiotemporal parameters: walking velocity (*), step length symmetry ratio, average step length, cadence. -Kinematics: thigh-to-vertical angle, shank-vertical angle, maximum thigh-to-vertical angle of paretic limb, knee flexion of paretic limb.	8-camera Vicon 612 system (Oxford Metrics, UK), 2 AMTI BP400600 force platforms	-Baseline; -End of treatment: 7 days
				Participation	- Participation metric: EuroQol EQ-5D-5L29 quality of life questionnaire.		
[94]	Mediolateral foot-placement ability	Chronic	Non-rigid AFO	Activity	- Spatial metrics: mediolateral foot-placement between the ankle and the target line (0%, 15%, 30%, 45% subject's leg length) for each step; circumduction. - Kinematic metrics: hip abduction/adduction angle, peak pelvic angle.	8-camera digital motion capture system	-Baseline; -End of treatment: 6 trials
[87]	Initial effects on gait pattern	Acute, chronic	Conventional AFO	Activity	-Spatiotemporal parameters: gait speed; cadence; step length of paretic and non-paretic limb; stance duration of paretic and non-paretic	GAITRite1 system	End of treatment: 1 month

Study	Assessment goal	Disease stage	Orthosis	Outcome measures		Motion capture system	Timing for assessment
				ICF category	Description		
[88]	Biomechanical ability	Chronic	Conventional AFO	Activity	-Spatiotemporal parameters: walking velocity (*), step length, symmetry ratio based on step length. -Kinematic parameters: thigh and shank orientations. -Kinetic indicators: knee and hip flexion/extension moments.	3D motion analysis	-Baseline measures -End of treatment: 3 months -Follow-up: 6 months
				Body structure	- Impairment metrics: MAS, Modified Rivermead Mobility Index.		
				Participation	- Participation measures: EuroQol (EQ-5D); interviews to the clinicians and patients before and after their participation in the study.		
[89]	Rear-foot motion gait	Acute	Anterior and posterior AFOs	Body impairment	- Impairment metrics: Brunnstrom scale, MAS.	Vicon system (Vicon, UK)	End of treatment: 3 trials
				Activity	-Spatiotemporal parameters: walking speed, step length, cycle time. -Kinematic metrics: angles of the rear-foot joint in three planes.		
[91]	Biomechanical ability	Chronic	Conventional AFO	Activity	-Spatiotemporal parameters: step length normalized to body height, cadence, gait velocity (*), stance and pre-swing time. -Kinematic metrics: hip extension and knee flexion at toe-off.	2 force platforms (Kistler, Switzerland), Vicon system (Oxford Metrics, UK)	End of treatment: 3 trials
[90]	Biomechanical and muscular ability	Acute	Conventional AFO and dynamic AFO	Body function	-Muscular activity: EMG from tibialis anterior muscle.	Myopac EMG unit (Myopac), force plates, Vicon System (Oxford Metrics, UK)	End of treatment: 3 trials
				Activity	-Temporal metric: gait velocity. - Kinematic metrics: ankle angle at initial contact		

Study	Assessment goal	Disease stage	Orthosis	Outcome measures		Motion capture system	Timing for assessment
				ICF category	Description		
[92]	Double support changes related to gait speed	Chronic	Conventional AFO	Activity	-Temporal metrics (*): gait speed; duration of stride initial double support, single support, and terminal double support. -Kinetic metrics (*): mean force, and impulse (bodyweight*seconds) in the wholefoot, hindfoot, forefoot, and toe during initial double support.	Wheel, wireless force platform (pedar®)	End of treatment: 10 trials
[93]	Biomechanical and muscular ability	Chronic	Conventional AFO and dynamic AFO	Body function	-Muscle activity: co-activation index of gastrocnemius, tibialis anterior, biceps femoris, rectus femoris muscles.	Stereo-photogrammetric system (BTS Smart), infrared cameras, miniaturized EMG device (BTS FREEEMG 300)	End of treatment: 3 trials
				Activity	-Spatiotemporal metrics: stride time, cadence, step length, stride length, percentage of swing phase and double stance phase; -Kinematic metrics: angle at initial contact, ROM, dorsiflexion peak during swing phase for ankle; knee flexion/extension ROM; and flexion/extension ROM, flexion peak during swing phase, and pelvic frontal ROM for hip.		
[76]	Overground balance and walking ability	Chronic	Knee orthosis	Activity	-Functional metrics: 10MWT, 6MWT, BBS, five-time sit-to-stand test (5TSST), and Emory Functional Ambulation Profile (EFAP).	N/A	-Baseline; End of treatment: 6 weeks; -Follow-up: 3months

Appendix C- Clinical Protocol on Post-Stroke Rehabilitation

This appendix presents additional information on the results of the systematic review related to post-stroke orthotic-based rehabilitation and presented in Chapter 2.3, namely the inclusion and exclusion criteria and the clinical protocol.

Table C.1- Inclusion and exclusion criteria, and protocol outlined in the studies with post-stroke patients.

Study	Inclusion criteria	Exclusion criteria	Protocol
[95]	- Over 18 years of age. -Have a single unilateral ischemic or hemorrhagic stroke at least 3 months leading to hemiparesis. -Able to walk for 10 m with or without orthosis. -Able to maintain independent unsupported stance with and without an AFO for at least 90 s. -Daily using of AFO for at least 2 months. -Able to follow simple verbal instructions.	N/A	-Randomized cross-over trials. -Patients performed the posture-graphic test and functional tests, with and without AFO, while all subjects were wearing their own shoes. - The static test aimed to assess weight-bearing asymmetry while the subjects were instructed to stand on the force plate for 90 seconds. -Subjects performed 3 dynamic trials lasting 90 seconds, in which they were instructed to maintain balance without moving their feet. -Functional tests consisted on: BBS, TUG test, 10MWT, and FAC.
105]	-Over 18 years old. - Stroke at least 6 months (chronic-phase). -Spasticity of the *gastrocnemius* and *soleus* muscles rated between 1 and 3 on the MAS, leading to foot-drop.	N/A	- 2 sessions of gait analysis at their self-selected gait speed without and with the use of the AFO and shoes, with a 10 minutes rest period. -Each condition was carried out in a 10 meters gait corridor, where the participants performed at least 8 successive gait cycles. -6 trials were carried out for each condition.
[96]	-Unilateral hemiplegic stroke patients capable of following simple verbal instructions. -Ability to walk on a level surface and to walk up and down stairs with or without assistive devices and without wearing an AAFO. -No systemic or local medical problems, other than stroke, that might affect walking mobility.	-Clinically significant visual impairment. -Ability to voluntarily dorsiflex the ankle against gravity, i.e., MRC scale ≥ 3, since the AFO is indicated for the weakness of the ankle dorsiflexor.	-Experiments were randomly performed with and without AAFO. - Participants who already had an AAFO were allowed to use the device. - Participants were requested to complete the TUG and TUDS tests. - During the testing process, 2 individuals stood by the participants, 1 on each side, to prevent falls. - Participants could rest, generally 5 to 10 minutes, between each test. Total testing time ranged from 30 minutes to 1 h.
[75]	-Stroke at least 3 months. -Presence of paresis of leg muscles and/or a spasticity pattern resulting in knee hyperextension. -Ability to walk independently with or without a walking aid.	-Cognitive disorders preventing the understanding. -Ankle or foot contracture or limited ROM, or orthopaedic injury to the paretic or non-paretic limbs.	-8-week prospective, randomized, controlled study with 2 groups. -First group received the orthosis during 4 weeks, and then, 4 weeks without using the orthosis. Second group only received orthosis after 4 weeks for personal use for a 4-week period. -Measures were recorded at baseline, 4 and 8 weeks.
[97]	-Have spasticity at *gastrocnemius* and *soleus*. -Ability to walk safely without an assistive device.	N/A	- Patients were assessed with AFO and without AFO. -All assessments were made with footwear.

Study	Inclusion criteria	Exclusion criteria	Protocol
104]	-Over 18 years old. -Have hemiplegia following a stroke at least 6 months (chronic-phase). -Spasticity or weakness of quadriceps. -Knee hyperextension during the stance phase. -Ability to walk 10 meters without walking aids. -Prescription of a carbon KAFO in last 6 months.	N/A	-Patients performed 2 gait tests successively with (KAFO condition) and without orthosis (control condition) at their preferred walking speed, with a 10 minutes rest period. -Each condition was carried out in 10 meters for 6 trials.
[106]	-Over 18 years of age. - Had a stroke at least 6 months. -Maximum spasticity level of 3 in MAS. - Have FAC ranging 3 to 5. -Range of passive dorsiflexion up to at least 90°. -Have cognitive level to give informed consent, to understand and follow the directions of protocols.	- Have comorbidities, orthopaedic or postural problems that could confound the outcomes. -Have used a dynamic AFO before.	-Randomized controlled trials with (study condition) or without AFO (control), both with shoes. -All subjects underwent TUG test and TUDS test during 3-month follow-up.
[114]	- Spasticity of *gastrocnemius* and *soleus* muscles less than 3 on MAS. -Ankle passive dorsiflexion >5º with the knee flexed to 90º.	- Cannot stand for 10 seconds. -Motor or cardiovascular disease that might impair locomotion or other cognitive alteration that limits the participation in study.	-Multicentre randomized controlled study over 90 days with 2 walking conditions: Chignon AFO (study group) or the standard AFO (control). - Participants underwent to 10MWT. -Standardized assessments were performed at the initial wearing time and at 30 and 90 days of follow-up.
[85]	- Over 18 years old. -Walk at least 10 meters. - No limitation in the ROM in lower limbs. - Plantarflexor spasticity MAS between 1 and 3.	-Gait speed was higher than 1m/s. -Unable to give informed consent. -Significant cardiorespiratory or metabolic disease.	- Patients were asked to walk with AFO or barefoot. - Subjects walked a distance of 10 meters to complete 2 gait cycles. - 6 trials were performed for each condition: 3 without the orthosis and 3 with the orthosis/ footwear combination.
103]	- Aged 40 and 75 years old. -Have a first unilateral ischaemic or hemorrhagic stroke from the middle cerebral artery. - Ability to walk independently with shoes with and without orthosis. - Wearing an AFO for at least 6 months.	N/A	-Tests were randomly carried out with and without their AFO while the participants were wearing shoes, lasting 5 weeks to 6 months. - Patients walked the 10-meter walkway 3 times (comfortable speed). - Participants underwent TUG test, where was permitted to use a walking aid, but no physical help. The TUG was measured three times. -Subjects performed the TUDS test 3 times.

Study	Inclusion criteria	Exclusion criteria	Protocol
[98]	-Over 18 years of age. - Hemiplegia following a unilateral ischemic or hemorrhagic stroke at least 6 months. -Able to follow simple verbal instructions.	-Suffering from severe comprehensive aphasia or neglect. -Present a complicated medical history, as cardiac, pulmonary, or orthopaedic disorders, that could interfere with testing.	- Randomized controlled trial. - Effects were assessed 2 weeks after provision (baseline). Patients from early group were observed from week 3 while subjects from delayed group were analysed week 11. -Patients performed functional walk tests: 10MWT, 6MWT, TUG, TUDS, and they could use their usual assistive device.
[99]	-At least 6 months post-stroke. -Have an initial infarct within the past 10 years. -Patients wearing a thermoplastic AFO for at least 6 months.	N/A	-Randomized crossover trials. -Trials with wearing and not wearing their AFO. -Patient walked on a 10 meters walkway and performed the TUG test.
[107]	- No prior experience with an AFO. -Have no expected change in medications for at least 6 months. -Have adequate stability at the ankle during stance. -Have a Functional Independence Measure score ≥4 for ambulation. -Can ambulate at least 10 meters with or without an assistive device.	-Have history of falling more than once a week prior to the stroke. - Have fixed ankle contractures of 10° of plantarflexion. -Gait speed greater than 1.2 m/s. -Morbid obesity. -Present conditions as myocardial infarction, congestive heart failure, demand pacemaker.	-Randomized controlled trial, since 2005 to 2008, with 2 conditions: with and without a device. -Trials consisted of 2 consecutive phases of 6 weeks intervention. -During each visit, walking performance was tested at 0, 3, 6, 9, and 12 weeks.
[86]	-Over 16 years old. -Have to be within 1 to 12 months after stroke; -Be able to walk with assistance but have difficulty flexing knee and extending hip during gait.	N/A	- Randomized controlled trial study. - Patients undergone a tri-dimensional gait analysis that was taken on two occasions: one before the AFO was fitted walking with shoes only (baseline session), and another 7 days later immediately after the AFO was fitted and tuned (tuning session). - Patients worn basic training shoes (rigid sole) for tuning session. -Were collected 10 trials at baseline and 7 immediately AFO tuning.
[115]	- Subjects ambulating faster than 0.8 m/s. -Subjects that needs physical assistance or external support.	N/A	-Randomized trials. -Subjects were followed for 6 months, and assessed relatively to functionality with activities of daily living, balance, and quality of life.

Study	Inclusion criteria	Exclusion criteria	Protocol
[108]	-Age 40 to 70 years. -A minimum of 24 months post-stroke. -Presence of hemiplegia after stroke. | -Currently wearing or had an articulated AFO. -No major involvement of the contralateral limb.	N/A	-Subjects walked with standardized footwear in 4 conditions: i) shoes only; ii) conventionally AFO; iii) the same AFO realigned with the tibia vertical in the shoe-heel-height compensated AFO; and iv) the same AFO with ¾ length foot-plate -¾. - Data were collected from the walking in a 10 m-walkway at their normal self-selected walking speed with a minimum of 3 walking trials for each condition and speed, each lasting approximately 2 hours. - Subjects were instructed that they could rest as necessary.
[94]	- Over 18 years of age. - At least 1-year post-stroke. -Able to walk without any assistive device. -Currently using a non-rigid AFO. - Able to understand instructions.	N/A	-Randomized across trials. -Subjects performed 6 trials, walking back and forth across 10MWT. -Subjects were tested at the following randomized step widths: 0%, 15%, 30%, and 45% subject's leg length to assess the presence or no of the circumduction. Participants should walk at a comfortable speed.
[87]	-Diagnosis of hemiparesis secondary to cerebrovascular accident with the duration of symptoms less than 6 weeks (Group 1) or more than 6 weeks (Group 2). -Ability to walk for 10 meters with or without assistive devices. -Ability to follow simple instructions.	-Stroke with more than one hemisphere involvement. -Have a score of spasticity higher 2 in MAS. -History of significant orthopaedic problems that would interfere with performing a gait analysis.	- Randomized trials with 2 groups, Group 1 (acute) and Group 2 (chronic), under 2 conditions (without and with AFO). - A patient could start walking 2 meters prior to stepping on the GAITRite carpet, and to continue walking 2 meters past the end of carpet. - Participants were walked toward the end of the GAITRite at a self-selected comfortable speed, with rest periods of 2 minutes.
[109]	-Diagnosis of unilateral hemiparesis from the stroke at 6 months or more than 12 months. -Ability to stand without support for at least 1 min. -Ability to walk for 10 meters with or without assisted device. -No history of significant orthopedic problems. -Ability to follow instructions.	N/A	-Randomized trials, in which subjects were placed into two groups according to the duration of hemiparesis. -Patients performed measurement tests, both wearing and not wearing an AFO on the affected foot.

Appendix D- SmartOs Framework: Software Interfaces

This appendix provides additional information on the software interfaces of the framework implemented for SmartOs' modules integration, as described in Chapter 3.3.

The **CCU** interfaces all SmartOs' modules and graphical applications and implements the high-level methods, running the Ubuntu Mate OS. Given the complexity of distributed systems, the CCU was implemented in C++ language, which allows: (i) object-oriented programming; (ii) complete control over memory management; and (iii) scalability to expand the system following a modular and standard software design. The POSIX Pthread Libraries were used that (i) allow for spawning a new concurrent process flow, (ii) are effective for a multi-core system, such as the Raspberry Pi 3, where the process flow can be scheduled to run on another processor thus gaining speed through parallel and distributed programming, and (iii) provide less operating system overhead.

The software architecture of CCU was organized into five main software modules (classes), namely *ExternalDevice*, *CentralController*, *HLController*, *SmartGaitAnalysis*, and *Log*, described in Table D.1. A task was assigned to each module such that when a new entry is added to the target queue, the task will wake to execute the module's process. Additionality, it was implemented a queue per external device (i.e., graphical applications, LLOS, WML) of the CCU for handling with the messages exchange between CCU and its external devices.

The temporal flow of processes occurs as follows. As the CCU is turned on, the main program setups the hardware interfaces and activates the task of the *CentralController*. Subsequently, the *CentralController* activates the task of mobile graphical application, which is waiting for messages from Bluetooth communication. The received messages are processed in the *CentralController*, which setups and activates the tasks of the selected modules in the mobile graphical application for running the configured therapy. The therapy starts and stops according to start and stop command messages, respectively, sent from the mobile graphical application.

Table D.1- Description of the main software modules of CCU

Module	Description
External Device	- Base class for communication with external devices to CCU; Bluetooth for Mobile Graphical Application, Wi-Fi for Desktop Graphical Application, and serial communication for LLOS and WML. - Handle the communication with the external devices using *handler_Msg* task. - Contain tasks to handle with input (*inMsg* queue including command message) and output (*outMsg* queue including status and data messages) messages of the CCU.
Central Controller	- Process the messages from/to Mobile Graphical Application by *process_BTMsg* task. - Setup and initialize all configurable modules according to the command messages. - Start and stop the therapy including the controllers, gait tools and gait monitoring.
Smart Gait Analysis	- Setup all gait analysis tools (i.e., gait event detection, speed estimation, user's motion intention recognition, risk analysis, disability level recognition). - Executes all gait analysis tools using *SmartGaitAnalysis* timer. - Each gait analysis tool must inherit *GaitAlgorithm* base class. - Each gait analysis tool is also a base class that includes a set of derived classes (e.g., *GaitEventDetection_FSM_InertialLAB* and *GaitEventDetection_FSM_GaitShoe* are derived classes that inherit from *GaitEventDetection_FSM* base class).
HLController	- Setup and manage the assistive control strategy using *AssistiveStrategy* task. - Runs the high-level controller using the *AssistiveStrategy* timer. - Stop the assistive control strategy, ensuring safety in *isExitSafe* class.
Log	- Base class for data logging in JSON file and Desktop Graphical Application. - Handle the communication with the Desktop Graphical Application, LLOS and WML. - Setup JSON file for local data storage in CCU memory. - Get all data from therapy (LLOS, WML, *HLController*, *SmartGaitAnalysis*) to store in JSON file and send externally for Desktop Graphical Application using *Log* task. - Monitor the battery status using *batteryMonitor* timer.

The software framework of LLOS and WML followed the same design and was divided into three main software layers upon the hardware layer. First, the middleware layer incorporates the freeRTOS [147] real-time operating system and HAL libraries, namely STM32Fx HAL drivers (e.g., CAN, ADC, I^{2}C, and SPI drivers). The freeRTOS provides the facilities for multitasking, concurrent programming towards the development of an effective framework and a set of libraries that allow easy definition and use of tasks, queues, and semaphores. The second layer, the application programming interface (API), provides the software interfaces (e.g., routines for initialization, configuration, runtime control, and data acquisition) for controlling and accessing to the SmartOs' modules aiming to create a software application. Lastly, the application layer centered on setting the timers, FreeRTOS tasks, and using the APIs for the easy integration of SmartOs' modules. The programming language selected was C language.

The software architecture of LLOS and WML was organized into four and three main software modules, respectively. Figure 3.6 illustrates the main software modules and the flow of SmartOs' messages through these modules. In the *External Communication* module, incoming data and status messages from other modules (i.e., *Embedded IMU Sensor*, *Orthotic System*, or *Wearable Sensor System*) are sent to the CCU, and the command messages from the CCU are handled in the *Management Unit* module by *Message_Handler* task and sent to the *Setup* tasks (i.e., *Control_Setup*, *IMU_Setup*, *Orth_Setup* or *SensorSystems_Setup*). Two queues were implemented for the external communication with the CCU; one for the transmission of data (from *Run* callback functions) and status (from *Setup* tasks) messages to the CCU; and the other for receiving command messages from CCU to *Setup* tasks. All *Setup* tasks, *Start* and *Stop* functions act upon the reception of command messages. The *Setup* tasks specify intrinsic aspects of each module such as the number of sensors, type of sensor system, type of mid- and low-level controller, calibration routine time, among other aspects. The *Start* functions turn the hardware timer assigned to each module. Subsequently, all functionalities such as *Control_Run, IMU_Run, Orth_Run,* and *SensorSystems_Run* are periodically executed and handled by a specific hardware timer ISR to accurately meet the real-time requirements. The *IMU_Run* and *SensorSystems_Run* callback functions include both sensor data acquisition and processing. The *Control_Run* callback function executes the mid- and low-level controls while acquires data from the embedded sensors on the AO. Additionality, the hardware timer assigned to each module is charged for activating the semaphore of the *SendExternal* tasks. Furthermore, the priority of the real-time software interfaces was adjusted such that the hardware timers were configured to meet the hard-real-time requirements of LLOS and WML.

The temporal flow of processes occurs as follows. When the development board of LLOS or WML is turned on, the main program setup and initializes all the configured hardware interfaces (e.g., system clock, CAN, I^2C, ADC, UART), the *External Communication* and the *Management Unit* modules. Subsequently, the *Embedded IMU Sensor*, *Orthotic System*, and *Wearable Sensor* modules are configured and run in accordance with the command messages from CCU received in the *Receive_Message* task and processed in *Message_Handler* task. Additionally, the LLOS architecture receives real-time data messages from the high-level control loop (*HLController* module in CCU) during the therapy.

Appendix E- Software-in-the-loop: Inertial-LAB and GaitShoe

This appendix provides additional information on the software routines implemented in the InertialLAB and GaitShoe systems, both described in Chapter 4.

Appendix E.1-InertialLAB

As indicated in Figure E.1, the program starts by initializing the I2C communication to wake up the available IMUs. In the subsequent 10 seconds, several I2C readings are performed for conducting the calibration routine. Posteriorly, the real-time data acquisition starts using an interrupt service routine (Timer 2). It ensures the data reading and writing to a linked list every 5 milliseconds (considering the maximum sampling frequency of 200 Hz). In the main program, the offsets are subtracted to the new angular velocity values, and the accelerometer readings are normalized according to the values found in the calibration routine. Then, the angle estimation tool is executed. Lastly, the sample time, the gyroscope and accelerometer data of each IMU, and the estimated angles are stored in the USB flash drive, and these data is removed from the linked list.
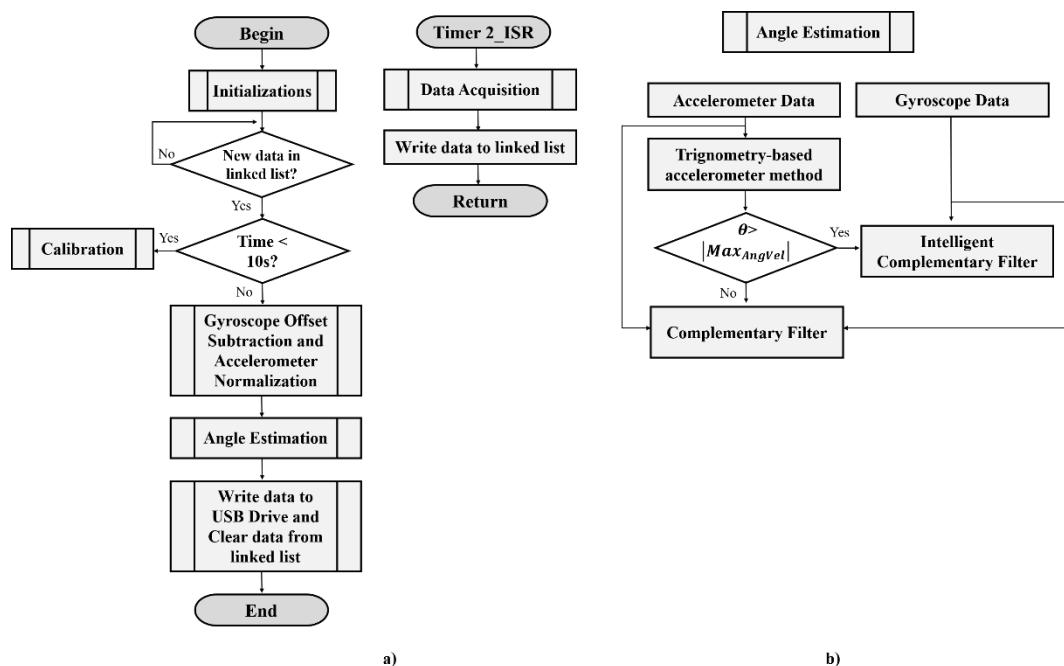

Figure E.1- Flow chart of the software routines implemented in InertialLab, highlighting in (b) the sub-routine of angle estimation.

Appendix E.2-GaitShoe

To easily manage the operating mode of GaitShoe, we designed and implemented a graphical interface in Android studio, which communicates with the master interface through the Bluetooth communication. When master interface receives a "start" command, the interruption service routine embedded on each NRF24L01+ is triggered to synchronously start the data reception from the slave interfaces every 10 ms. The RF communication protocol and the operating mode of slave interfaces end when a "stop" command is configured in the graphical interface. Additionally, according to the commands selected in the graphical interface, the received information from both slaves can be stored in the SD card or transmitted to the interface for real-time visualization.

For each slave, as depicted in the flowchart of Figure E.2, the program starts by initializing the required system's configuration for data acquisition and transmission. When the wireless communication starts, as configured in the graphical interface, the software routines are activated. In the subsequent 10 seconds (overflow controlled by Timer 1), the ADC and I2C readings performed every 10 ms (ensured through the Timer 2) are used to calibrate the FSRs and the IMU. Afterward, the new sensory measures are adjusted according to the information found in the calibration routine; FSRs' measures are adjusted using a scalar multiplication, the gyroscope offsets are corrected, and the accelerations are normalized. Subsequently, the foot angle is estimated using the angular velocity integration with gait cycle-based reset method [263] dependent on FF event. This angle estimation is required for the gait speed determination. Posteriorly, we implemented a gait event detection tool based on a single-axis, foot-mounted gyroscope and FSRs. If the FF event is detected, the gait speed is estimated, and the values of speed and angle are reset. Lastly, the recorded and computed information is organized in a 25-byte wireless packet frame to be transmitted to the master interface at 100 Hz (ensured by Timer 2) using an NRF24L01+ RF module. This process ends as wireless communication is stopped.
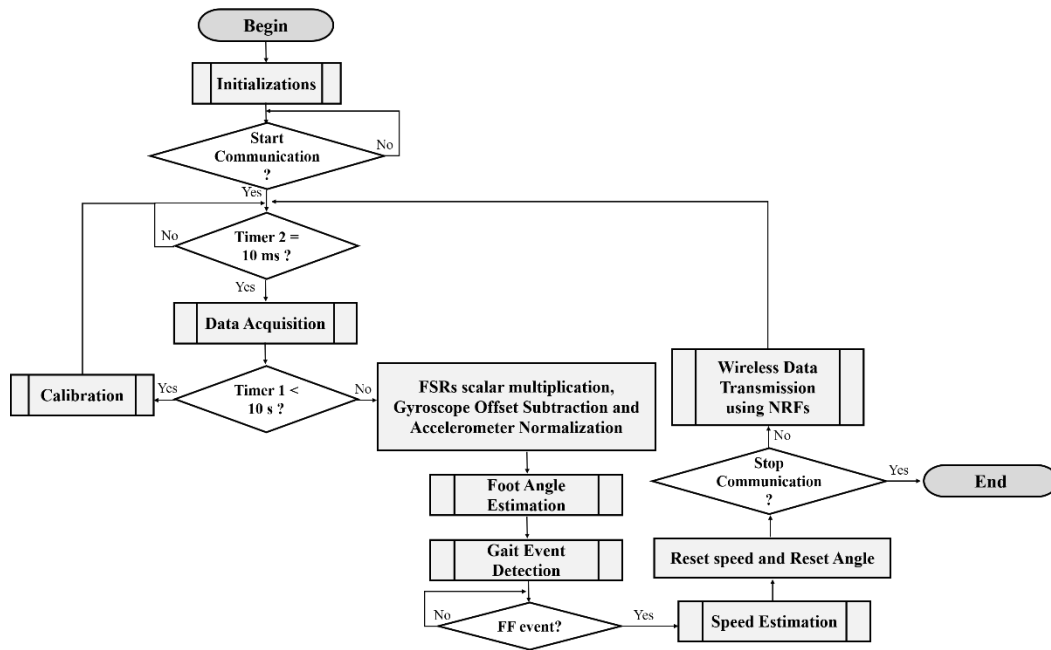
Figure E.2- Flow chart of the software routines implemented in the slave interfaces of GaitShoe.

Appendix F- Performance Analysis of Machine Learning-Based Framework

This appendix presents information related to the comparative analysis of the different techniques explored in some stages of the machine learning-based framework. Table F.1 summarizes the purpose and conditions considered in the comparative analysis.

Table F.1- Experimental comparison of techniques from framework's stages

Stage	Purpose	Condition
Feature Calculation	Window's sizes (full-stride, 1/2, 1/3, 1/4, 1/5,1/6)	KNN classifier (k=1)[a] using all features
	Feature leg approaches (*left/right* or *leading/opposite*)	
Pre-Processing (Feature normalization)	Normalization techniques (centering, *z*-score standardizing min-max scaling with [0; 1] interval, min-max scaling with [-1; 1] interval)	KNN classifier (k=1)[a] using all features
Pre-Processing (Feature selection and extraction)	1 feature extraction (PCA) and 3 feature selection methods (ANOVA-based method with mRMR, "mRMR plus forward selection", "forward selection plus backward selection")	KNN classifier (k=1)[a] using features normalized by min-max scaling in [-1; 1] interval [b]
Model Building	9 machine learning classifiers (RF, linear and dynamic DA, regular and weighted KNN, SVM with linear, quadratic, cubic, and RBF kernels)	Classifiers with all features normalized by min-max scaling in [-1; 1] interval

[a] Only KNN classifier was used given its fast training with reliable results
[b] Previously reported as the best normalization technique

Feature Calculation

Results of the recognition models (Figure F.1) show that using the full- stride fraction with *left/right* approach outperforms (MCC = 0.907) all the other cases by a significant margin (MCC < 0.808). On the other hand, for prediction, the *leading/opposite* approach and 1/4 fraction of gait stride yielded the best results (MCC = 0.857). The findings suggest that both the feature leg approach and the time window size affect the model's performance, but these parameters depend on whether it is a recognition or prediction model.
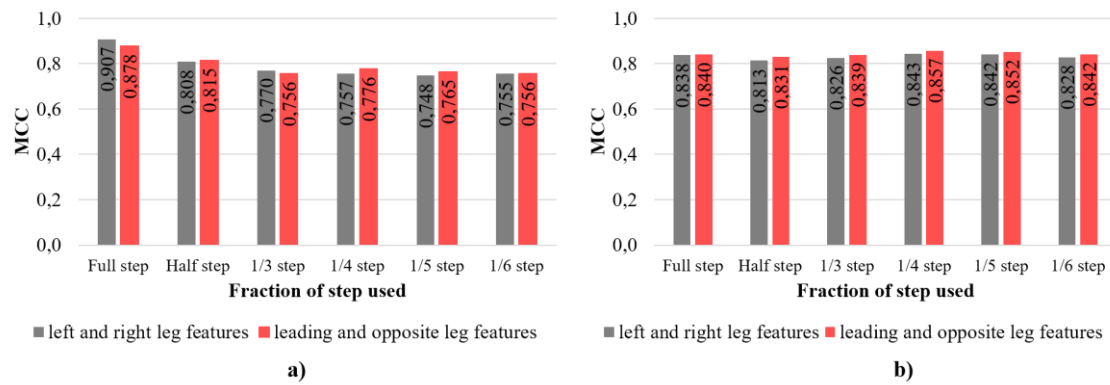
Figure F.1- Average performance of the procedures explored for the Feature Calculation in a) recognition and b) prediction models.

Feature Normalization

Figure F.2 shows that the min-max scaling with the interval [-1;1] yielded the best results for recognition (MCC = 0.852) and prediction (MCC = 0.728). It was chosen for the remaining analyses, as proposed in [264]. Overall, the normalization had a more positive effect in recognition models (MCC > 0.711) than in the prediction ones (MCC > 0.630).
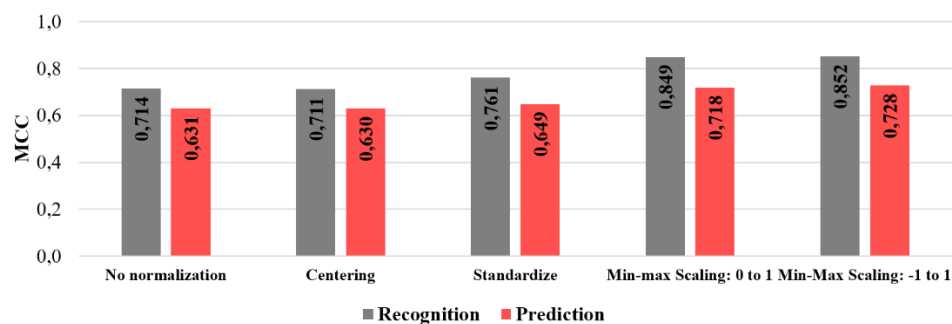

Figure F.2- Average performance per feature normalization technique.

Feature Selection and Extraction

Figure F.3 shows that the feature selection and extraction methods performed better in recognition models (0.677 < MCC < 0.96) than in the prediction ones (0.589 < MCC < 0.87).

The application of an adequate dimensionality reduction method improved the effectiveness of the classifier compared to the inclusion of the entire dataset. This finding is according to the literature [47] since it results from the ability to create a compact set of uncorrelated features that still characterize the original data without redundancy. Using the "mRMR plus forward selection" method (MCC > 0.8483) or "forward selection plus backward selection" (MCC > 0.8696), both feature selection methods, yielded similar results. However, the former is less computationally intensive, and while it selects a larger number of features than the

latter method (20 and 13 features, respectively), it was the selected method allowing a feature reduction of 75% from a total of 80 features. These sequential selection and ranking-based methods were used in [62], [215], [224]. In particular, the findings are consistent with [224], who concluded that the mRMR was faster and more effective than the "forward selection" and "backward selection" methods.

On the other hand, the ANOVA was less effective (MCC < 0.677) due to the low number of features that were chosen (2 to 3 features) to discern between the classes.
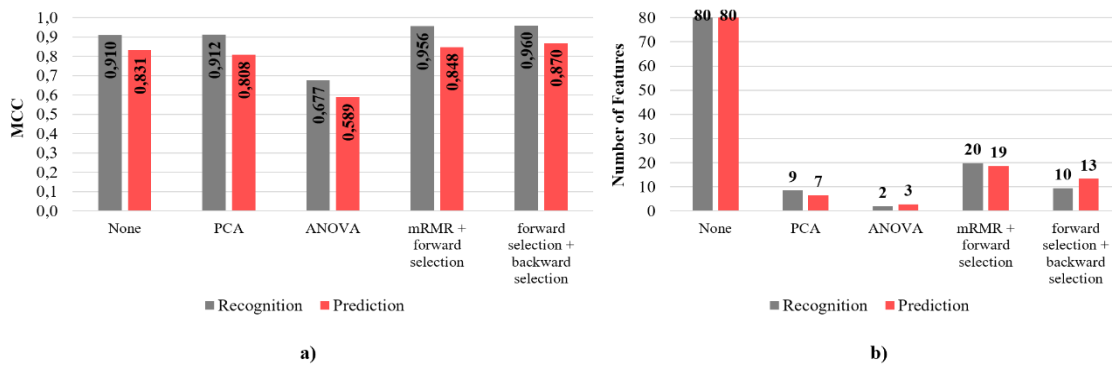

Figure F.3- Feature selection/extraction techniques: a) Average model performance per feature selection technique; b) Number of selected features by feature selection technique.

Model Building

Figure F.4 shows that the SVM classifier with the Gaussian kernel performed better than other classifiers for both prediction (MCC = 0.839) and recognition (MCC = 0.934). The SVM's ability to define more complex decision boundaries by applying optimization instead of probabilities, and its inherent flexibility to suit the data may explain this finding [47]. Previous literature indicates this classifier as the best, mainly when the Gaussian kernel is involved. Begg *et al*. [265] concluded that SVM performs better than ANN. Badesa *et al*. [266] noted that the SVM is more appropriate than LR, LDA, QDA, NB or KNN methods. Huang *et al.* [41] reported that SVM yielded better results than LDA to recognize six LMs and predict five LMTs.

On the other hand, both DA models produced the worst classification performance (MCC < 0.733), in contrast to [216] where the LDA performance was comparable to the SVM. Three reasons can explain this finding: LDA does not work well if the design is not balanced, such as the one in this study; LDA is not suitable for non-linear data, such as the kinematic data; and, LDA simplicity was perhaps not sufficient to discriminate the LMs and LMTs using the calculated features.

Due to the increased complexity of SVM, the *built model* took almost the double time to classify data comparing to other algorithms (Figure F.4). The KNN models took less time to classify data (< 6.5 ms) while presenting similar effectiveness (MCC > 0.807) to the Gaussian SVM (MCC > 0.839). This finding suggests that KNN models can potentially also be applied.
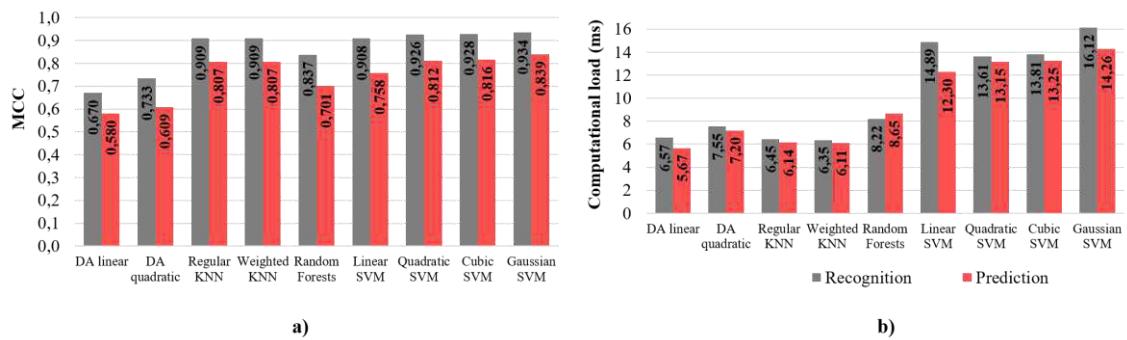

Figure F.4- Average performance for each machine learning classifier across every database and subject: a) MCC; b) computational load (ms).

Appendix G- FEL Control Tuning

This appendix provides information related to the tuning of the FEL low-level controller, introduced in Chapter 7.7, namely the experimental procedure and the controller evolution during FEL tuning.

FEL Tuning: Experimental Procedure

The tuning of FEL control focused on the feedforward controller. No tuning was made in the feedback controller since we used the already tuned PID control. The tuning of the feedforward controller consisted of the real-time training of the ANN by considering the normalized inputs randomly presented to the ANN (SGD approach) and the actual PID commands as the feedback error to be minimized. This procedure was separately performed for the PKO and PAFO with the respective reference trajectories adjusted with NCL for 1 km/h and 0.8 km/h (speeds randomly selected), respectively.

During the real-time training of the feedforward controller, the ANN is trying to learn the AOs' inverse dynamics models. Consequently, the feedforward commands that contribute to the final command (u) could lead the AOs to exceed their mechanical limits and compromising their integrity. Therefore, for the first training phase of the ANN, we decided to modify the original reference position trajectory. An offset of 15º was added to the original knee reference trajectory and smoothed the original ankle reference trajectory with an attenuation gain of 40 % and 4º of offset. With this procedure, it is was possible to get the inverse dynamics models of PKO and PAFO while operating far from their mechanical limits.

As illustrated in Figure G.1, the trajectory modification was possible since the normalized signals of the original and modified trajectory are equal. This finding shows that the ANN would receive equal inputs in both situations. Note that the initial AOs' angular position was set close to the first value of the non-normalized input signals.

The pre-trained ANNs were subsequently retrained using the original reference trajectories to get the final configuration for the ANNs. The pre-trained state is an important advantage to the clinical application once it may decrease the training time for new user-oriented trajectories, as reported in [254].
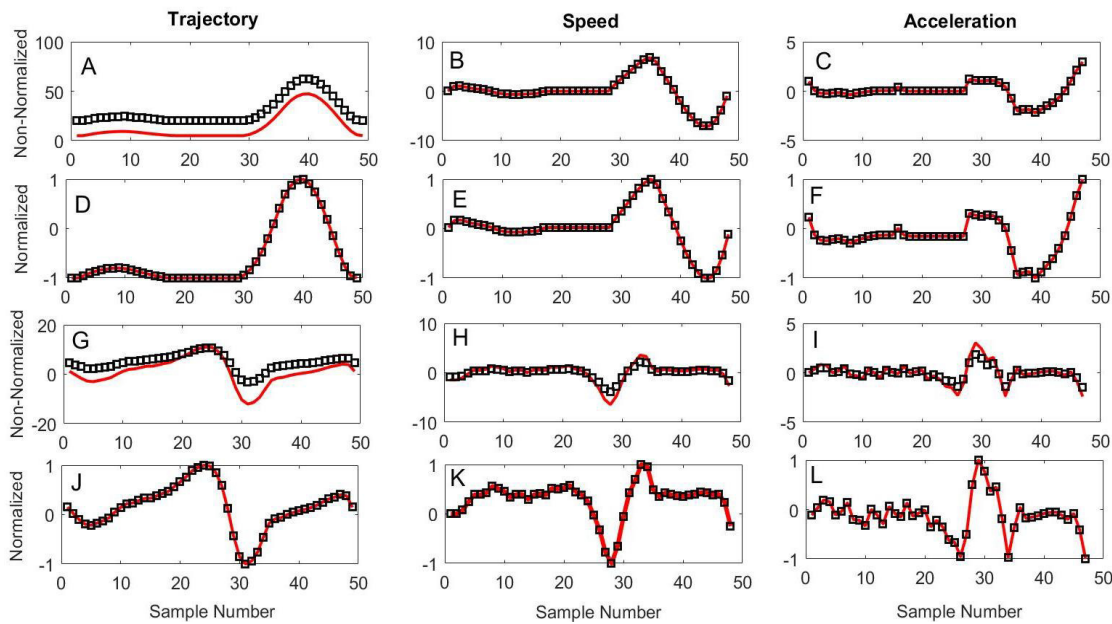
Figure G.1- Original (red) and modified (black) input signals for PKO (A-C non-normalized signals, D-F normalized signals) and PAFO (G-I non-normalized signals, J-L normalized signals).

FEL Tuning: Results and Discussion

AOs' state during FEL tuning was evaluated considering the measured position trajectory, the control commands, and the angular position error. For instance, Figure G.2 presents the results achieved during the ANN training using the modified trajectory for the PKO at 1 km/h under three different periods of FEL control: Initial Phase, Middle Phase, and Final Phase.

During the Initial Phase (first 11 seconds), the feedforward controller is starting to tune its ANN. Consequently, feedforward contribution to the final control command is not significant, being the PID control responsible for trucking the reference trajectory (Figure G.2.B). It is possible to see in Figure G.2.A that the measured trajectory is delayed 210 ms comparatively to the reference one. Hence, the angular position error varies from -20º to 20º, as demonstrated in Figure G.2.C.

In the Middle Phase (after 40 s), the FEL controller is learning the inverse dynamics model of the PKO. Therefore, the measured trajectory starts to decrease its phase difference to the reference signal to a mean value of 6 ms (considering three gait cycles presented in Figure G.2.D). To correct this delay, the feedforward controller produces commands that when summed with PID commands lead the PKO to perform a trajectory with 10º more than the reference trajectory, as illustrated in Figure G.2.D. This happens because the ANN has not learned the inverse dynamics model with the best performance yet. Figure G.2.E highlights an

increase and decrease in the feedforward command and the PID command, respectively, relative to the Initial Phase. As depicted in Figure G.2.F, the position error decreased, varying from -20° to 10°.

For the Final Phase (past 90 s), when the ANN already learned the inverse dynamics of the PKO, we verified that the FEL control has successfully aligned the PKO trajectory with the reference one (Figure G.2.G) and corrected the amplitude divergence previous observed. The position error decreased by 75% compared to the Initial Phase. In this phase, the feedback controller contribution was 4.4% (Figure G.2.K). At this time, the ANN is not able to start a new learning phase after the recall phase is reached.
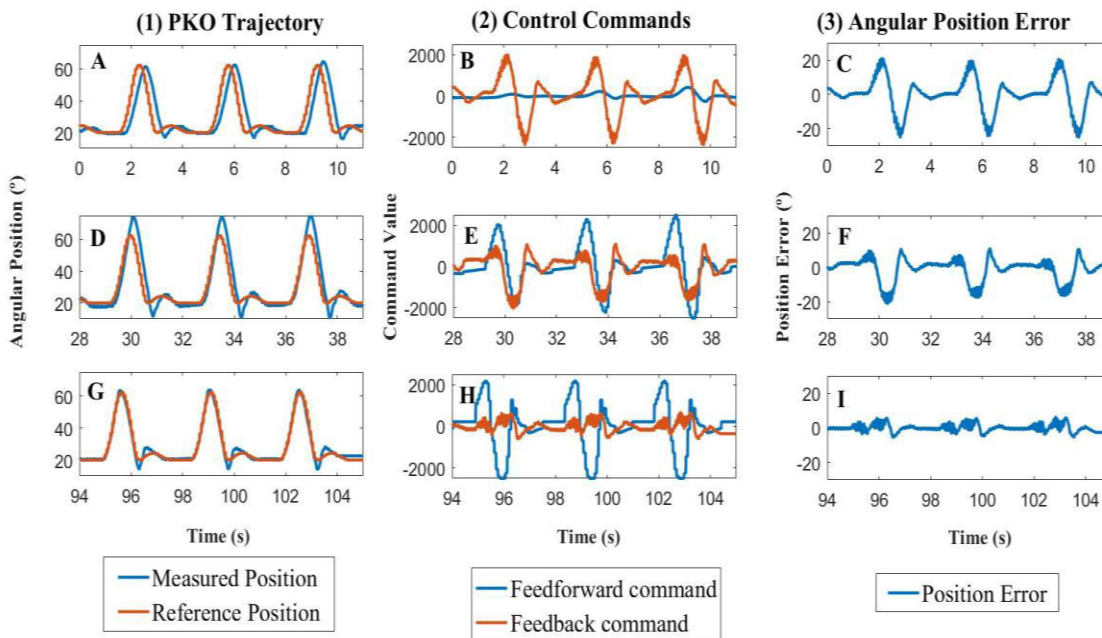

Figure G.2- FEL tuning over three periods: Initial Phase (A-C), Middle Phase (D-F), and Final Phase (G-I). Random example for PKO using the modified trajectory tuned for 1 km/h.

In overall, the findings of FEL tuning indicate that the designed ANN was capable of correctly learning the inverse dynamics for both AOs. When the learning phase finished, the ANN can timely track the reference trajectory, discharging the feedback controller for this task. We observed that the learning phase lasted 90 s (approximately 25 gait cycles) and 315 s (approximately 70 gait cycles) for PKO and PAFO, respectively.

Additionally, it was verified that the run time of the FEL control loop (0.25 ms) is lower than the one required by the bioinspired control architecture of SmartOs (1 ms). These temporal findings suggest that the techniques applied for approaching a real-time implementation were

effective to avoid long-time periods in the training phase. Furthermore, few iterations were required to tune the pre-trained ANN.

It is important mentioning that the modification made in the reference trajectory for the first learning moment protected the AOs. Figure G.2.D shows a practical situation, during the Middle Phase, where a 10°-deviation would put the device out of its lower operating limit (3°). The 10°-deviation did not damage the PKO since the added 15°-offset was enough to deviate the PKO from its lower mechanical limit (3°). A similar effect was observed in PAFO for the lower and upper limits.